Mechanochemistry II

Edited by José G. Hernández

Mechanistic understanding

Synthetic chemistry methodology

Future impact

Imprint

Mechanochemistry II

José G. Hernández

Since the publication of the first thematic issue on mechanochemistry in the *Beilstein Journal of Organic Chemistry* in 2017 [1], the global interest in the field of mechanochemistry has continued exponentially growing. Thus, leading to the implementation of mechanochemical techniques across different areas of science. Such tremendous growth has established mechanochemistry as a sustainable strategy for the future of chemical synthesis. In fact, the potential of mechanochemistry in various domains of research, industry and in commercial entities has been recently recognized by the IUPAC after the inclusion of mechanochemistry among the ten chemical innovations that will change our world [2]. Therefore, once again, the *Beilstein Journal of Organic Chemistry* is contributing to the dissemination of mechanochemistry in the field of organic chemistry through a new thematic issue Mechanochemistry II.

In this new collection of works, the readership of the *Beilstein Journal of Organic Chemistry* will find contributions from renowned global experts in the field of mechanochemistry spanning areas from organic mechanochemistry, supramolecular mechanochemistry to polymer mechanochemistry. Moreover, findings reported in this current thematic issue also contribute to the expansion of synthetic chemistry methodology by mechanochemistry. Importantly, such rapid advancement in applied mechanochemistry is supported by investigations focused on better understanding the fundamental aspects governing mechanochemical transformations.

Therefore, I hope the joint efforts made by the authors of these contributions (review articles, letters, and full research papers), and the *Beilstein Journal of Organic Chemistry* could augment the consolidation of mechanochemistry as an alternative to continue with the development of chemical processes in a more efficient manner.

José G. Hernández

Aachen, June 2019

ORCID® iDs

José G. Hernández - https://orcid.org/0000-0001-9064-4456

References

1. Hernández, J. G. *Beilstein J. Org. Chem.* **2017,** *13,* 2372–2373. doi:10.3762/bjoc.13.234
2. Gomollón-Bel, F. *Chem. Int.* **2019,** *41* (2), 12–17. doi:10.1515/ci-2019-0203

Synthesis of acylglycerol derivatives by mechanochemistry

Karen J. Ardila-Fierro[1], Andrij Pich[2,3,4], Marc Spehr[5], José G. Hernández[*1] and Carsten Bolm[*1]

Abstract

In recent times, many biologically relevant building blocks such as amino acids, peptides, saccharides, nucleotides and nucleosides, etc. have been prepared by mechanochemical synthesis. However, mechanosynthesis of lipids by ball milling techniques has remained essentially unexplored. In this work, a multistep synthetic route to access mono- and diacylglycerol derivatives by mechanochemistry has been realized, including the synthesis of diacylglycerol-coumarin conjugates.

Introduction

In addition to being guided by chemical signals, cells respond to mechanical cues by sensing and transducing external mechanical inputs into biochemical and electrical signals [1]. Consequently, every time a cell is subjected to mechanical loads, the biomolecules that constitute the cell do also experience the effects of the mechanical forces. For example, from the moment a nascent peptide begins growing in the ribosome, such peptide experiences mechanical signals that regulate the speed of protein synthesis [2]. Not surprisingly, the natural ability of peptides to endure mechanical stress in nature has allured scientists to evaluate the mechanical stability of proteins by using single-molecule nanomechanical techniques (e.g., magnetic and optical tweezers or atomic force microscopy) [3,4]. Additionally, the resilience of the peptide bond to mechanical loads has led to mechanoenzymatic transformations [5-7], and to synthesize amino acid derivatives [8-10] and peptides [11-13] by ball milling and extrusion techniques. Similarly, mechanochemical derivatizations of sugars and sugar derivatives such as cyclo-

dextrins (CDs) have proven compatible with the use of ball mills. These reports showed advantages such as higher selectivity by ball milling compared to classic solution methods and the possibility to effectively react CDs and reactants of different solubility profiles [14-17]. The compatibility of synthesizing biologically relevant building blocks with mechanochemistry has further been shown by the recent mechanochemical protocols to transform nucleoside and nucleotide substrates (Figure 1) [18,19].

On the other hand, reports on mechanochemical protocols for the synthesis or derivatization of lipids are scarce [20,21]. Among the variety of amphipathic or hydrophobic small molecules that exhibit a lipid structure, diacylglycerols (DAGs) are important due to their signaling functions in cells (DAG signaling) [22-24]. Structurally, DAGs are glycerolipids containing two fatty acids esterified to the alcohol glycerol (Figure 2).

Biological routes that lead to the formation of DAGs include enzymatic degradation of glycerophospholipids and lipolysis of triacylglycerols (TAGs) [22,25]. However, due to the structural diversity of fatty acids present in acylglycerols and to the small structural differences among these fatty acids (e.g., chain length, degree of unsaturation, double bond position or stereochemistry), the access to pure DAGs and TAGs from natural sources by extraction is cumbersome. Alternatively, protected DAGs **5** can be chemically synthesized starting from glycerol [26] or glycidol [27], but either synthetic alternative involves multiple preparative steps in organic solvents (e.g., CH_2Cl_2, THF, Et_2O). These considerations led us to explore a mechano-chemical multistep route for the synthesis of protected DAGs **5** starting from glycidol (**1**) through the installation of a hydroxy protecting group, followed by epoxide ring-opening and esterification reactions with fatty acids **3** (Scheme 1).

If successful, developing a multistep approach to prepare DAGs would contribute to the expansion of synthetic mechanochemical methodologies in ball mills [28-31], which are often limited to single-step transformations. Additionally, synthesizing lipid structures mechanochemically would complement the preparation of biologically relevant building blocks (amino acids, peptides, saccharides, nucleosides, etc.) by mechanochemistry, thereby highlighting the importance of mechanical forces in the chemistry of life.

Figure 1: Biologically relevant molecules made, used or derivatized by mechanochemistry.

Figure 2: Isomeric diacyl-*sn*-glycerols (DAGs).
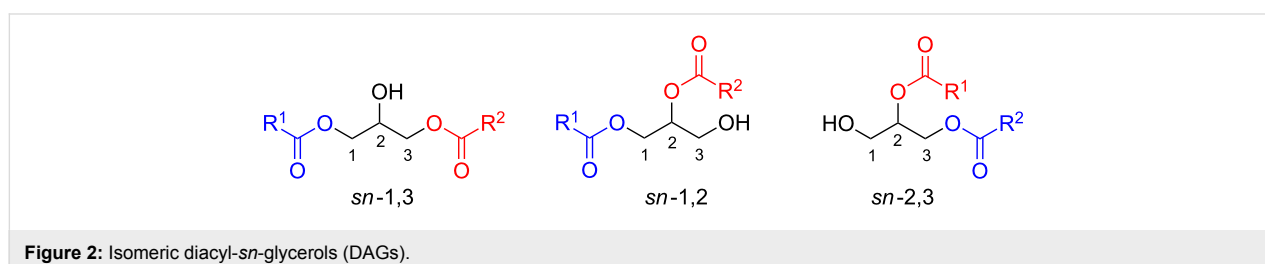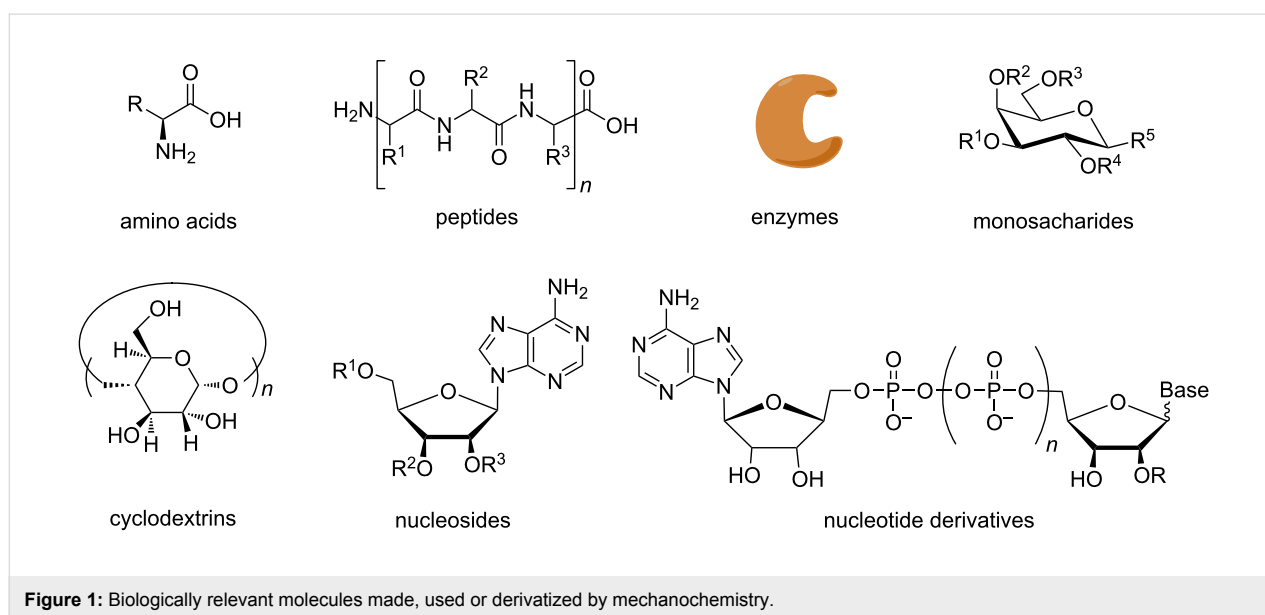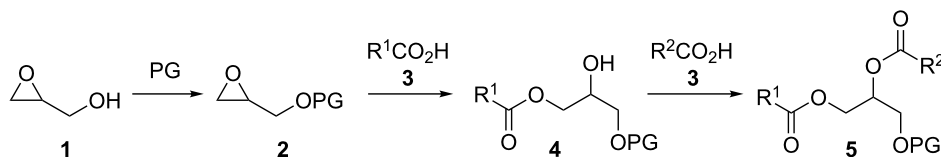
Scheme 1: Synthetic route to access protected DAGs; PG = protecting group.

Results and Discussion

To commence, we focused on the synthesis of *tert*-butyl-dimethylsilyl glycidyl ether (**2**) by reacting glycidol (**1**; 0.67 mmol) and *tert*-butyldimethylsilyl chloride (TBDMSCl) in the presence of imidazole in a mixer mill (MM, Scheme 2) [32].
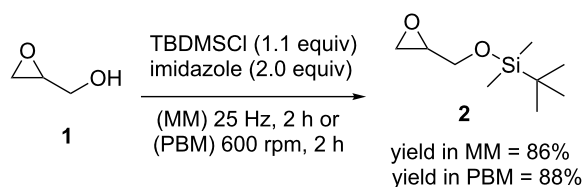
Scheme 2: Protection of glycidol (**1**) with TBDMSCl in the ball mill. MM = mixer mill, PBM = planetary ball mill.

After 2 h of milling at 25 Hz full consumption of the starting materials was observed by thin-layer chromatography (TLC), with exclusive formation of the corresponding silyl ether **2**. However, the high volatility of **2** during posterior vacuum drying processes prevented the isolation of the TBDMS-protected glycidol **2** in higher yields after separation by column chromatography. A 5-fold scaled up version of the reaction using 3.37 mmol of **1** was carried out in a planetary ball mill (PBM) using 45 mL milling containers at 600 rpm, under otherwise identical conditions to afford product **2** in a similar yield.

With TBDMS-protected glycidol **2** in our hands, a selective epoxide ring-opening reaction with fatty acids **3** leading to the formation of the corresponding *sn*-1,3-protected monoacylglycerols (MAGs **4**) was attempted (Scheme 3). Initially, commonly used solution-based protocols were tested in the ball mill [33]. For example, **2** was reacted with stearic acid (**3a**) in the presence of amines such as pyridine or tributylamine. However, the analysis of the reaction mixture only showed unreacted starting materials. In previous work, an acceleration of the oxirane ring-opening reaction with carboxylic acids [34] or alcohols [35] by using Lewis acid catalysts such as iron(III) chloride or bismuth(III) triflate was reported. However, the implementation of these protocols in the ball mill only led to trace amounts (less than 5% yield) of the protected monoacylglycerol **4a**. Finally, one of the well-established Jacobsen catalysts for the epoxide ring-opening reaction of **2** with stearic acid (**3a**) was evaluated (Scheme 3a).
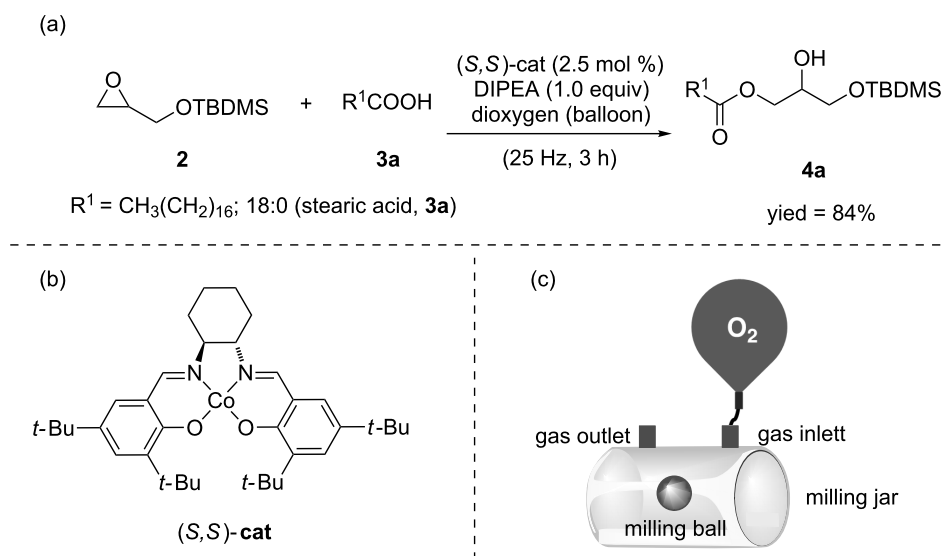
Scheme 3: Cobalt-catalyzed epoxide ring-opening in the ball mill.

Specifically, we focused on the use of Jacobsen cobalt(II)-salen complex (*S*,*S*)-**cat** (Scheme 3b), since similar salen complexes had originally been reported to facilitate epoxide ring-opening reactions with carboxylic acids as nucleophiles [36]. Moreover, salen complexes endure mechanochemical conditions, as proven during their preparation in ball mills [37]. In addition, various related Jacobsen salen complexes have shown catalytic activity under solvent-free conditions [38]. Collectively, these precedents made this synthetic route a promising one to mechanochemically access MAGs by ball milling.

Experimentally, we attempted the cobalt-catalyzed epoxide ring-opening reaction by milling **2** with stearic acid (**3a**) in the presence of (*S*,*S*)-**cat** (2.5 mol %) and *N*,*N*-diisopropylethylamine (DIPEA; 1.0 equiv, Scheme 3a). Mechanistically, it is known that Co(II) complex (*S*,*S*)-**cat** is catalytically inactive and its oxidation is required to facilitate the reaction [39]. Aware of this, we began by relying on the atmospheric dioxygen inside the milling container to oxidize complex (*S*,*S*)-**cat**. This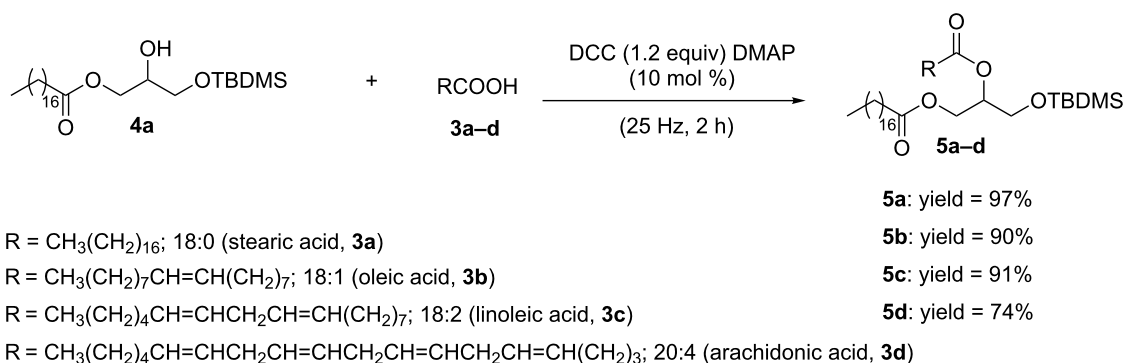 approach has been applied before in the mechanochemical synthesis of Cu–carbene complexes from *N*,*N*-diarylimidazolium salts, dioxygen and metallic copper [40], which involved a mechanochemical reaction with gaseous reagents [41]. Pleasingly, this time the reaction afforded product **4a**, although the yield remained low (59%), even after three hours of milling. In order to improve the yield, we carried out the activation of the Co(II) complex (*S*,*S*)-**cat** by milling under a balloon pressure of dioxygen. Now, the yield of **4a** was boosted up to 84% yield (for a representation of the set up used and experimental details, see Scheme 3c and Supporting Information File 1). Analysis of the reaction mixture by ^{1}H NMR revealed that the epoxide ring-opening had occurred preferentially to give *sn*-1,3-protected monoacylglycerol **4a** over its regioisomer counterpart *sn*-2,3-protected monoacylglycerol **4a'** (**4a**/**4a'** 3.6:1; for details, see Supporting Information File 1). However, purification of **4a** by column chromatography on SiO$_2$ favored acyl migration in **4a**, thereby dropping the yield of

4a by increasing the amount of the isomeric *sn*-2,3-protected monoacylglycerol **4a'** (Figure 2) [42]. Typically, cobalt complex (*S*,*S*)-**cat** has been used for kinetic resolution of racemic epoxides, for which the maximum theoretical yield of the reaction is 50%. Here, however, the yield of the *sn*-1,3-protected monoacylglycerol was high, and consequently we expected the enantiomeric excess of the product to be low. This, assumption was confirmed by analysis of the sample by high-performance liquid chromatography-chiral stationary phase (CSP-HPLC, for more details, see Supporting Information File 1). Access to enantiopure MAGs could be achieved under similar reaction conditions by starting from optically active commercially available silyl-protected glycidol derivatives [27,43].

Next, we targeted the mechanosynthesis of the DAGs by reacting MAG **4a** and fatty acids **3** in the ball mill. Such esterifications required the activation of **3** with *N*,*N*'-dicyclohexylcarbodiimide (DCC), thereby complementing other recently developed solvent-free carboxylic acid activations towards amidation or esterification reactions by ball milling [44]. In practice, we milled a mixture of MAG **4a**, stearic acid (**3a**), DCC and 4-dimethylaminopyridine (DMAP) at 25 Hz for 2 h in a mixer mill. Separation of the product by column chromatography gave DAG **5a** in 97% yield (Scheme 4).

Alternatively, **5a** could be prepared following a one-pot two-step approach in the ball mill by beginning with the cobalt-catalyzed epoxide-ring opening of **2** with **3a**, followed immediately by the esterification of the corresponding MAG **4a** with stearic acid (**3a**), DCC and DMAP. Although successful, this strategy led to DAG **5a** in lower yield (50%). Then, in order to expand the library of DAGs, other fatty acids containing various degrees of unsaturation and chain length were tested. For instance, esterification of MAG **4a** with oleic acid (**3b**), linoleic acid (**3c**), and arachidonic acid (**3d**) underwent smoothly in the ball mill affording DAGs **5b–d** in yields up to 91% (Scheme 4). Particularly interesting was the formation of DAG (18:0/20:4)

R = CH$_3$(CH$_2$)$_{16}$; 18:0 (stearic acid, **3a**)

R = CH$_3$(CH$_2$)$_7$CH=CH(CH$_2$)$_7$; 18:1 (oleic acid, **3b**)

R = CH$_3$(CH$_2$)$_4$CH=CHCH$_2$CH=CH(CH$_2$)$_7$; 18:2 (linoleic acid, **3c**)

R = CH$_3$(CH$_2$)$_4$CH=CHCH$_2$CH=CHCH$_2$CH=CHCH$_2$CH=CH(CH$_2$)$_3$; 20:4 (arachidonic acid, **3d**)

5a: yield = 97%

5b: yield = 90%

5c: yield = 91%

5d: yield = 74%

Scheme 4: Mechanosynthesis of DAGs **5**.

5d, an important lipidic backbone present in the biologically relevant phosphatidylinositol 4,5-bisphosphate (PIP2) [22]. In fact, diacylglycerols have proven to play vital roles in regulation of lipid bilayer and in the catalytic action of various membrane-related enzymes, such as protein kinase C (PKC) isoforms [45]. Therefore, the development of strategies for visualization of acylglycerols in cellular environments by their fusion with fluorescent molecular labels is in high demand [46]. As a result, once the mechanosynthesis of DAGs **5** was established, we turned our efforts towards the conjugation of DAG **5a** with 7-hydroxycoumarin (**9**) (Scheme 5).

Initially, removal of the TBDMS protecting group of **5a** was attempted by milling. However, reacting DAG **5a** with a mixture of $BF_3 \cdot CH_3CN$ and silica gel followed by an aqueous work-up gave DAG **6a** in only 31% yield, together with concomitant acyl migration of the corresponding *sn*-1,2-diacylglycerol **6a** into *sn*-1,3-diacylglycerol **6a'**. Therefore, the desilylation reaction was carried out by stirring **5a** and $BF_3 \cdot CH_3CN$ (Scheme 5a). Next, DAG **6a** was reacted with 4-nitrophenyl chloroformate (**7**) and triethylamine in the ball mill to form the activated DAG anhydride derivative **8a** (Scheme 5b). Analysis by ^{1}H NMR spectroscopy of the reaction mixture revealed the presence of DAG **8a** along with its isomeric DAG **8a'**. Formation of the latter compound could have been facilitated through

acyl migration of **6a** under the basic milling conditions. Subsequently, the reaction mixture containing **8a** and **8a'** was milled with 7-hydroxycoumarin (**9**) and triethylamine to achieve the conjugation of the DAGs **8** in 53% yield after two steps (Scheme 5c). A mixture of **10a** and **10a'** (**10a/10a'** 72:28) was separated from the unreacted starting materials, and analyzed by UV–vis spectroscopy (Figure 3). Comparison of the UV–vis spectra of **6a** and **10a/10a'** showed the successful conjugation of the DAG with the coumarin moiety [47].

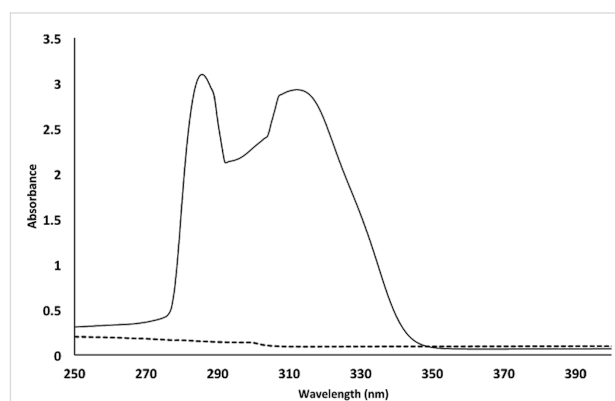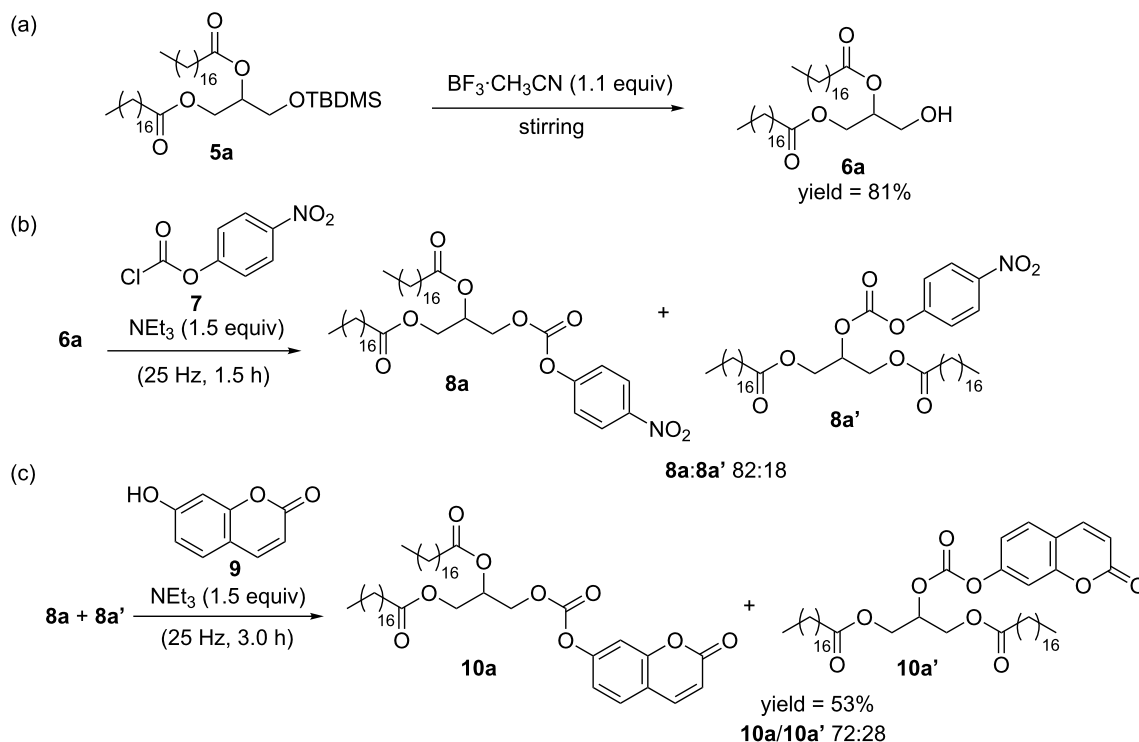**Figure 3:** UV–vis spectra of DAG **6a** (dotted line) and conjugated DAGs **10a** and **10a'** as a mixture (**10a/10a'** 72:28) in toluene at a concentration of 0.5 µM.

Scheme 5: Conjugation of DAG **5a** with 7-hydroxycoumarin (**9**).

Conclusion

The implementation of ball milling techniques has provided the opportunity to extend the applicability of mechanochemistry to the synthesis of architecturally complex targets, such as mono- and diacylglycerols. Altogether, the mechanosynthesis of lipids and lipid derivatives complements the current systematic work towards the synthesis of other biologically relevant molecules under environments of high mechanical stress. Specifically, the synthesis of mono- and diacylglycerols required first, the application of solventless functional group protection chemistry in ball mills, second, the implementation of metal-catalyzed epoxide-ring opening, and third, the development of solvent-free ester formation between monoacylglycerols and fatty acids to afford DAGs. Moreover, the synthesis of conjugated DAGs **10** represents a step forward towards the establishment of mechanochemical conjugation reactions for linking fluorescent materials to lipids at the proof-of-concept level.

Supporting Information

Supporting Information File 1

Experimental procedures, set-ups and characterization data.
[https://www.beilstein-journals.org/bjoc/content/supplementary/1860-5397-15-78-S1.pdf]

Acknowledgements

ORCID® iDs

Karen J. Ardila-Fierro - https://orcid.org/0000-0002-5801-5534
Andrij Pich - https://orcid.org/0000-0003-1825-7798
Marc Spehr - https://orcid.org/0000-0001-6616-4196
José G. Hernández - https://orcid.org/0000-0001-9064-4456
Carsten Bolm - https://orcid.org/0000-0001-9415-9917

References

1. Petridou, N. I.; Spiró, Z.; Heisenberg, C.-P. *Nat. Cell Biol.* **2017**, *19*, 581–588. doi:10.1038/ncb3524
2. Fritch, B.; Kosolapov, A.; Hudson, P.; Nissley, D. A.; Woodcock, H. L.; Deutsch, C.; O'Brien, E. P. *J. Am. Chem. Soc.* **2018**, *140*, 5077–5087. doi:10.1021/jacs.7b11044
3. Garcia-Manyes, S.; Beedle, A. E. M. *Nat. Rev. Chem.* **2017**, *1*, 0083. doi:10.1038/s41570-017-0083
4. Schönfelder, J.; Alonso-Caballero, A.; De Sancho, D.; Perez-Jimenez, R. *Chem. Soc. Rev.* **2018**, *47*, 3558–3573. doi:10.1039/c7cs00820a
5. Bolm, C.; Hernández, J. G. *ChemSusChem* **2018**, *11*, 1410–1420. doi:10.1002/cssc.201800113
6. Ardila-Fierro, K. J.; Crawford, D. E.; Körner, A.; James, S. L.; Bolm, C.; Hernández, J. G. *Green Chem.* **2018**, *20*, 1262–1269. doi:10.1039/c7gc03205f
7. Hernández, J. G.; Ardila-Fierro, K. J.; Crawford, D.; James, S. L.; Bolm, C. *Green Chem.* **2017**, *19*, 2620–2625. doi:10.1039/c7gc00615b
8. Bolm, C.; Mocci, R.; Schumacher, C.; Turberg, M.; Puccetti, F.; Hernández, J. G. *Angew. Chem., Int. Ed.* **2018**, *57*, 2423–2426. doi:10.1002/anie.201713109
9. Jörres, M.; Aceña, J. L.; Soloshonok, V. A.; Bolm, C. *ChemCatChem* **2015**, *7*, 1265–1269. doi:10.1002/cctc.201500102
10. Baron, A.; Martinez, J.; Lamaty, F. *Tetrahedron Lett.* **2010**, *51*, 6246–6249. doi:10.1016/j.tetlet.2010.09.069
11. Métro, T.-X.; Colacino, E.; Martinez, J.; Lamaty, F. Amino Acids and Peptides in Ball Milling. *Ball Milling Towards Green Synthesis: Applications, Projects, Challenges;* Green Chemistry Series; Royal Society of Chemistry: Cambridge, United Kingdom; pp 114–150. doi:10.1039/9781782621980-00114
12. Maurin, O.; Verdié, P.; Subra, G.; Lamaty, F.; Martinez, J.; Métro, T.-X. *Beilstein J. Org. Chem.* **2017**, *13*, 2087–2093. doi:10.3762/bjoc.13.206
13. Yeboue, Y.; Gallard, B.; Le Moigne, N.; Jean, M.; Lamaty, F.; Martinez, J.; Métro, T.-X. *ACS Sustainable Chem. Eng.* **2018**, *6*, 16001–16004. doi:10.1021/acssuschemeng.8b04509
14. Kumar, V.; Taxak, N.; Jangir, R.; Bharatam, P. V.; Kartha, K. P. R. *J. Org. Chem.* **2014**, *79*, 3427–3439. doi:10.1021/jo5001753
15. Menuel, S.; Doumert, B.; Saitzek, S.; Ponchel, A.; Delevoye, L.; Monflier, E.; Hapiot, F. *J. Org. Chem.* **2015**, *80*, 6259–6266. doi:10.1021/acs.joc.5b00697
16. Jicsinszky, L.; Caporaso, M.; Martina, K.; Calcio Gaudino, E.; Cravotto, G. *Beilstein J. Org. Chem.* **2016**, *12*, 2364–2371. doi:10.3762/bjoc.12.230
17. Jicsinszky, L.; Caporaso, M.; Tuza, K.; Martina, K.; Calcio Gaudino, E.; Cravotto, G. *ACS Sustainable Chem. Eng.* **2016**, *4*, 919–929. doi:10.1021/acssuschemeng.5b01006
18. Eguaogie, O.; Vyle, J. S.; Conlon, P. F.; Gîlea, M. A.; Liang, Y. *Beilstein J. Org. Chem.* **2018**, *14*, 955–970. doi:10.3762/bjoc.14.81
19. Appy, L.; Depaix, A.; Bantreil, X.; Lamaty, F.; Peyrottes, S.; Roy, B. *Chem. – Eur. J.* **2019**, *25*, 2477–2481. doi:10.1002/chem.201805924
20. Tyagi, M.; Kartha, K. P. R. *Carbohydr. Res.* **2015**, *413*, 85–92. doi:10.1016/j.carres.2015.04.008
21. Hu, H.; Li, H.; Zhang, Y.; Chen, Y.; Huang, Z.; Huang, A.; Zhu, Y.; Qin, X.; Lin, B. *RSC Adv.* **2015**, *5*, 20656–20662. doi:10.1039/c5ra02393a
22. Eichmann, T. O.; Lass, A. *Cell. Mol. Life Sci.* **2015**, *72*, 3931–3952. doi:10.1007/s00018-015-1982-3
23. Yang, C.; Kazanietz, M. G. *Trends Pharmacol. Sci.* **2003**, *24*, 602–608. doi:10.1016/j.tips.2003.09.003
24. Brose, N.; Betz, A.; Wegmeyer, H. *Curr. Opin. Neurobiol.* **2004**, *14*, 328–340. doi:10.1016/j.conb.2004.05.006
25. Storck, E. M.; Özbalci, C.; Eggert, U. S. *Annu. Rev. Biochem.* **2018**, *87*, 839–869. doi:10.1146/annurev-biochem-062917-012448
26. Martin, S. F.; Josey, J. A.; Wong, Y.-L.; Dean, D. W. *J. Org. Chem.* **1994**, *59*, 4805–4820. doi:10.1021/jo00096a023
27. Fodran, P.; Minnaard, A. J. *Org. Biomol. Chem.* **2013**, *11*, 6919–6928. doi:10.1039/c3ob41483c

28. Bonnamour, J.; Métro, T.-X.; Martinez, J.; Lamaty, F. *Green Chem.*
2013, *15,* 1116–1120. doi:10.1039/c3gc40302e

29. Hernández, J. G.; Butler, I. S.; Friščić, T. *Chem. Sci.* **2014,** *5,*
3576–3582. doi:10.1039/c4sc01252f

30. Beillard, A.; Golliard, E.; Gillet, V.; Bantreil, X.; Métro, T.-X.;
Martinez, J.; Lamaty, F. *Chem. – Eur. J.* **2015,** *21,* 17614–17617.
doi:10.1002/chem.201503472

31. Crawford, D. E.; Miskimmin, C. K.; Cahir, J.; James, S. L.
Chem. Commun. **2017,** *53,* 13067–13070. doi:10.1039/c7cc06010f

32. Giri, N.; Bowen, C.; Vyle, J. S.; James, S. L. *Green Chem.* **2008,** *10,*
627–628. doi:10.1039/b801455h

33. Rytczak, P.; Drzazga, A.; Gendaszewska-Darmach, E.; Okruszek, A.
Bioorg. Med. Chem. Lett. **2013,** *23,* 6794–6798.
doi:10.1016/j.bmcl.2013.10.020

34. Zhao, Y.; Wang, W.; Li, J.; Wang, F.; Zheng, X.; Yun, H.; Zhao, W.;
Dong, X. *Tetrahedron Lett.* **2013,** *54,* 5849–5852.
doi:10.1016/j.tetlet.2013.08.074

35. Cucciniello, R.; Ricciardi, M.; Vitiello, R.; Di Serio, M.; Proto, A.;
Capacchione, C. *ChemSusChem* **2016,** *9,* 3272–3275.
doi:10.1002/cssc.201600989

36. Tokunaga, M.; Larrow, J. F.; Kakiuchi, F.; Jacobsen, E. N. *Science*
1997, *277,* 936–938. doi:10.1126/science.277.5328.936

37. Ferguson, M.; Giri, N.; Huang, X.; Apperley, D.; James, S. L.
Green Chem. **2014,** *16,* 1374–1382. doi:10.1039/c3gc42141d

38. Jacobsen, E. N. *Acc. Chem. Res.* **2000,** *33,* 421–431.
doi:10.1021/ar960061v

39. Schaus, S. E.; Brandes, B. D.; Larrow, J. F.; Tokunaga, M.;
Hansen, K. B.; Gould, A. E.; Furrow, M. E.; Jacobsen, E. N.
J. Am. Chem. Soc. **2002,** *124,* 1307–1315. doi:10.1021/ja016737l

40. Beillard, A.; Métro, T.-X.; Bantreil, X.; Martinez, J.; Lamaty, F.
Chem. Sci. **2017,** *8,* 1086–1089. doi:10.1039/c6sc03182j

41. Bolm, C.; Hernández, J. G. *Angew. Chem., Int. Ed.* **2019,** *58,*
3285–3299. doi:10.1002/anie.201810902

42. Laszlo, J. A.; Compton, D. L.; Vermillion, K. E. *J. Am. Oil Chem. Soc.*
2008, *85,* 307–312. doi:10.1007/s11746-008-1202-5

43. Fodran, P.; Das, N. J. L. C.; Eisink, N. N. H. M.; Welleman, I. M.;
Kloek, W.; Minnaard, A. J. *Eur. J. Lipid Sci. Technol.* **2016,** *118,*
1768–1774. doi:10.1002/ejlt.201500547

44. Métro, T.-X.; Bonnamour, J.; Reidon, T.; Duprez, A.; Sarpoulet, J.;
Martinez, J.; Lamaty, F. *Chem. – Eur. J.* **2015,** *21,* 12787–12796.
doi:10.1002/chem.201501325

45. Sprong, H.; van der Sluijs, P.; van Meer, G. *Nat. Rev. Mol. Cell Biol.*
2001, *2,* 504–513. doi:10.1038/35080071

46. Cai, X.; Mao, D.; Wang, C.; Kong, D.; Cheng, X.; Liu, B.
Angew. Chem., Int. Ed. **2018,** *57,* 16396–16400.
doi:10.1002/anie.201809641

47. Taniguchi, M.; Lindsey, J. S. *Photochem. Photobiol.* **2018,** *94,*
290–327. doi:10.1111/php.12860

Mechanochemistry of supramolecules

Anima Bose and Prasenjit Mal[*]

Abstract

The urge to use alternative energy sources has gained significant attention in the eye of chemists in recent years. Solution-based traditional syntheses are extremely useful, although they are often associated with certain disadvantages like generation of waste as by-products, use of large quantities of solvents which causes environmental hazard, etc. Contrastingly, achieving syntheses through mechanochemical methods are generally time-saving, environmentally friendly and more economical. This review is written to shed some light on supramolecular chemistry and the synthesis of various supramolecules through mechanochemistry.

Introduction

In living systems an important aspect is to create complex functional molecules from simpler units by following biomolecular mechanisms [1]. The biological assemblies for living beings are developed from processes of spontaneous self-assembly with a high degree of compartmentalization [2]. In addition, the same building units are often used across an enormous number of structures in a reversible fashion through thermodynamic control [3]. Conversely, small-molecule synthesis is generally performed under kinetically controlled reaction conditions through covalent approaches. By using common synthetic methodologies chemists are able to proficiently synthesize a variety of both natural and unnatural molecular scaffolds [4-6].

The era of supramolecular chemistry began with the introduction of coordination theory by Alfred Werner in 1893 [7] fol-

lowed by the lock-and-key concept of Emil Fischer in 1894 [8]. Weak or non-covalent interactions had been used systematically in the early 1960s by Lehn, Cram and Pederson to create targeted supramolecular architectures [9]. Small molecules, anions or cations could be assembled spontaneously to form supramolecular structures through self-assembly processes by exploiting the weak or non-covalent interactions [10]. Self-assembly is a kinetically reversible process which is more efficient than traditional stepwise synthesis concerning large molecules. Some recent developments in supramolecular chemistry are dynamic combinatorial chemistry [11], subcomponent self-assembly approach [12-14], and systems chemistry [15-18], etc.

There also has been growing interest towards exploration of nontraditional energy sources like visible light [19,20], micro-

wave [21], mechanochemical mixing [22,23], ultrasound [24], etc. as alternative energy sources to replace common laboratory techniques [25]. Among them, especially mechanochemical synthesis [26-29] has gained popularity due to its advantage over conventional solution-based methods [30]. The process is highly beneficial as the solvent-free condition may make traditional workup superfluous [31,32]. Also, mechanochemical methods have high impact in ecology and economy as they save time [33]. Mechanochemical syntheses benefit from high to quantitative conversions, minimized steps for purification and diminished liberation of undesired byproducts [34,35]. In literature, classical small organic molecules' synthesis has been well explored which includes multistep synthesis [36-39]. However, the concept of supramolecular chemistry under mechano-milling conditions only has limited number of examples [40-42].

Review
Self-assembly
During a metal-directed self-assembly process, the coordination geometry and coordination number at the metal center plays a central role in creating a self-assembled system. In 1962, Busch and coworker first demonstrated the concept of the template effect by choosing a suitable metal ion to control a self-assembly process [43,44]. The template enforces the assembly of the smaller units around it in a distinct and organized way favoring the formation of a particular product from a mixture with multiple possibilities [45]. Therefore, the concept

of selection of appropriate metal ion(s) and ligand(s) has been demonstrated in various reports [46-49]. In Figure 1, a comprehensive framework is shown in which nanoscale architectures are built from various monodentate (pyridine; Figure 1a), bidentate (bipyridine, phenanthroline; Figure 1b) and tridentate (terpyridines; Figure 1c) ligands [49]. The model systems depicted in Figure 1 are constructed using metals like Pd(II) or Pt(II) ions for square planar geometry, Cu(I) or Ag(I) ions for tetrahedral geometry and Co(II)/Cu(II)/Fe(II)/Zn(II)/Hg(II) for octahedral organization [50].

In Figure 2, Busch's first example of a metal-directed self-assembly is shown [44]. The mixing of diacetyl and 2-amino-ethanethiol led to a dynamic mixture of products including **1**. The square-planar directing metal ion nickel(II) induces the formation of cyclic product **2** through a process called self-sorting [51-53]. Subsequently, compound **2** underwent substitution with α,α'-dibromo-*o*-xylene to create the nickel(II) complex **3** [54].

In 2014, James and co-workers reported a one-pot two-step mechanochemical synthesis of metal complexes **7** (Figure 3). First, the salen-type ligand **6** was synthesized from *o*-hydroxy-benzaldehyde (**4**) and ethylenediamine (**5**). Subsequently, to the same pot appropriate metals were added to obtain the respective complexes **7** [55].

In 2002, Otera and co-workers reported the formation of some supramolecular self-assembled structures which was found to

Figure 1: A generalized overview of coordination-driven self-assembly.

Figure 2: Examples of self-assembly or self-sorting and subsequent substitution.

Figure 3: Synthesis of salen-type ligand followed by metal-complex formation in the same pot [55].
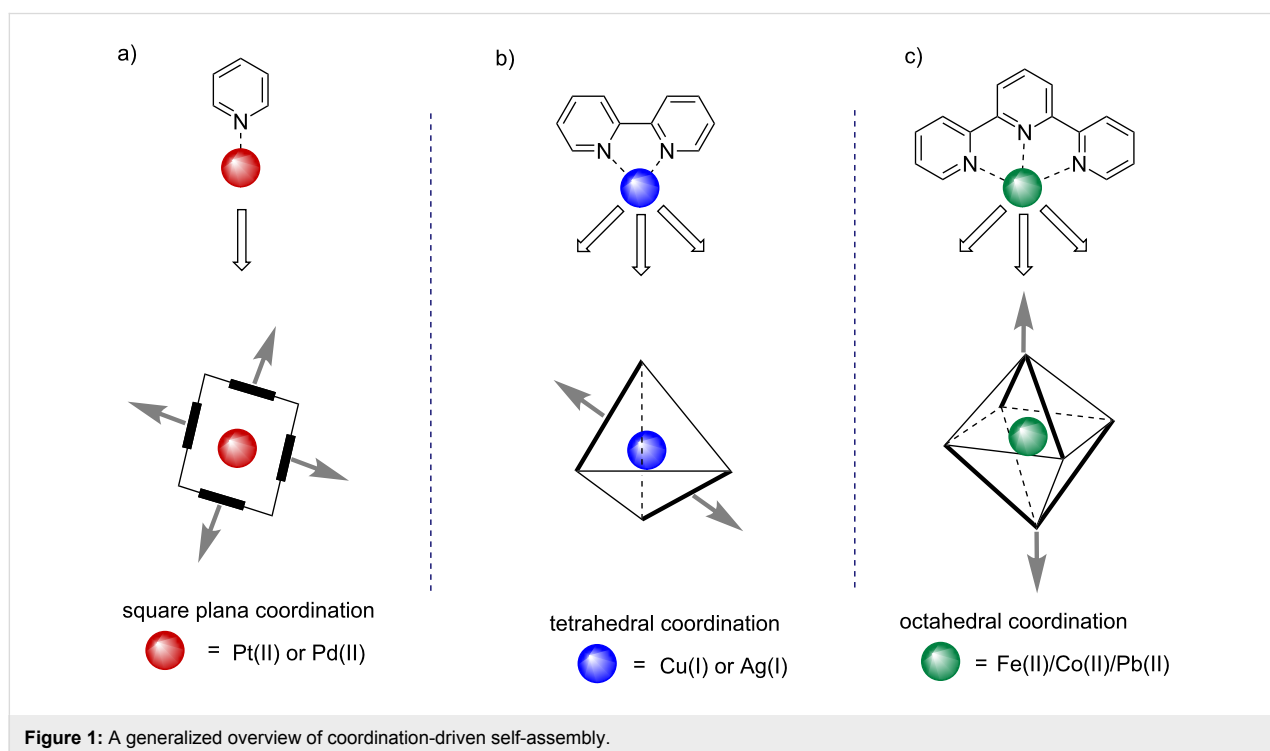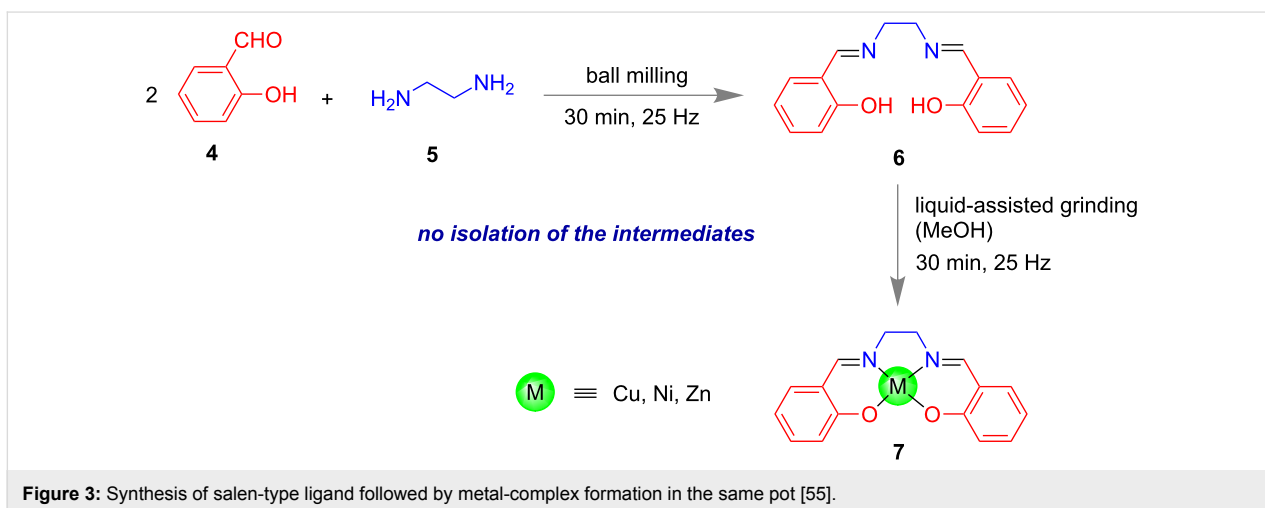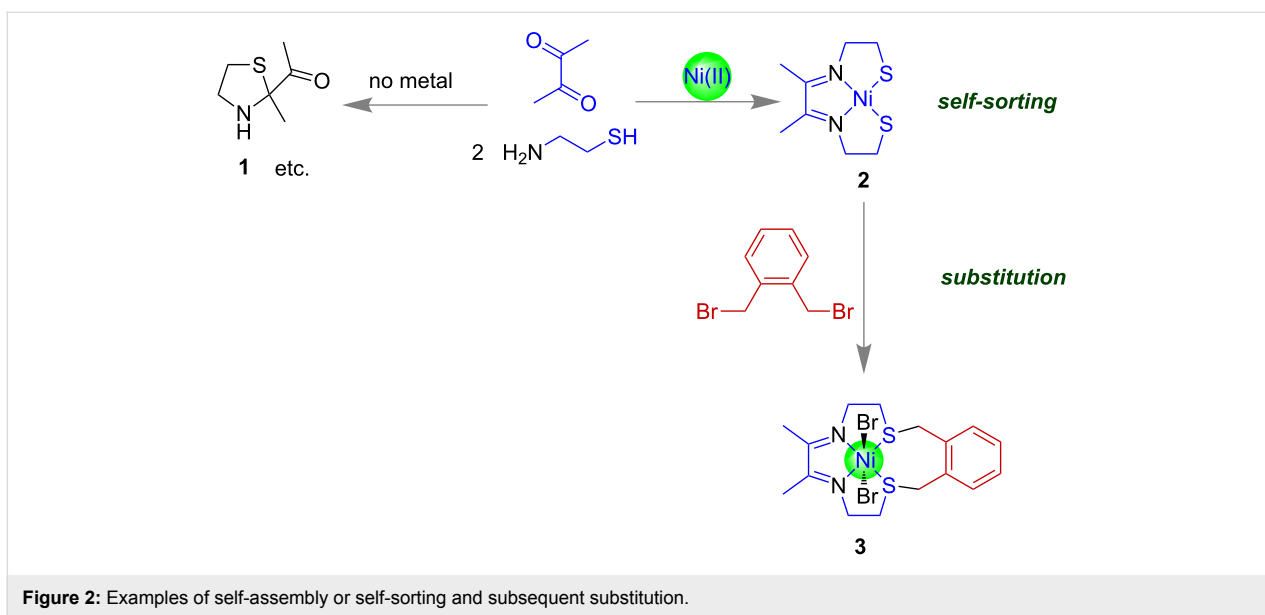
be faster under solvent-free mechanochemical condition than in aqueous media [56]. When a 1:1 mixture of the platinum salt [(en)PtNO₃)₂] and 4,4'-bipyridine were grinded in a mortar and pestle for 10 min, an NMR yield of 76% was found for the formation of molecular square **8** (Figure 4a). Similar structures were reported by Fujita's group [57] in which the formation of a Pt-based supramolecular square took more than four weeks at 100 °C. Using a similar approach, Otera's group also demonstrated for the formation of a bowl-shaped assembly **9** in 90% yield upon grinding for 10 min 2,4,6-tri(pyridin-3-yl)-1,3,5-triazine and palladium ((en)Pd(NO₃)₂, Figure 4b). Contrastingly, in solution the same synthesis took 4 h at 70 °C to isolate complex **9** in 56% yield.

Ćurić and co-workers prepared cyclopalladated complexes such as **10** by a grinding method and were the first to confirm a

mechanochemical C–H bond activation of an unsymmetrically substituted azobenzene [58]. The cyclopalladation process was proved to be a highly regioselective process and the observed palladation rate was faster compared to the conventional solution-phase method. An equimolar amount of 4'-(*N,N*-dimethyl-amino)-4-nitroazobenzene and Pd(OAc)₂ in the presence of 25 μL of glacial acetic acid (for liquid-assisted grinding, LAG) led to the regioselective C–H activation (Figure 5) [58].

In 2008, the mechanochemical synthesis of both [2]- and [4]rotaxanes was reported by Chiu and co-workers. The reactions led to high yields of the products **12** and **13** under solvent-free conditions at a milling frequency of 22.5 Hz (Figure 6b) [59]. The stoppers were constructed in situ with 1,8-diaminon-aphthalene through the formation of an imine via dehydration of the amine and aldehyde.
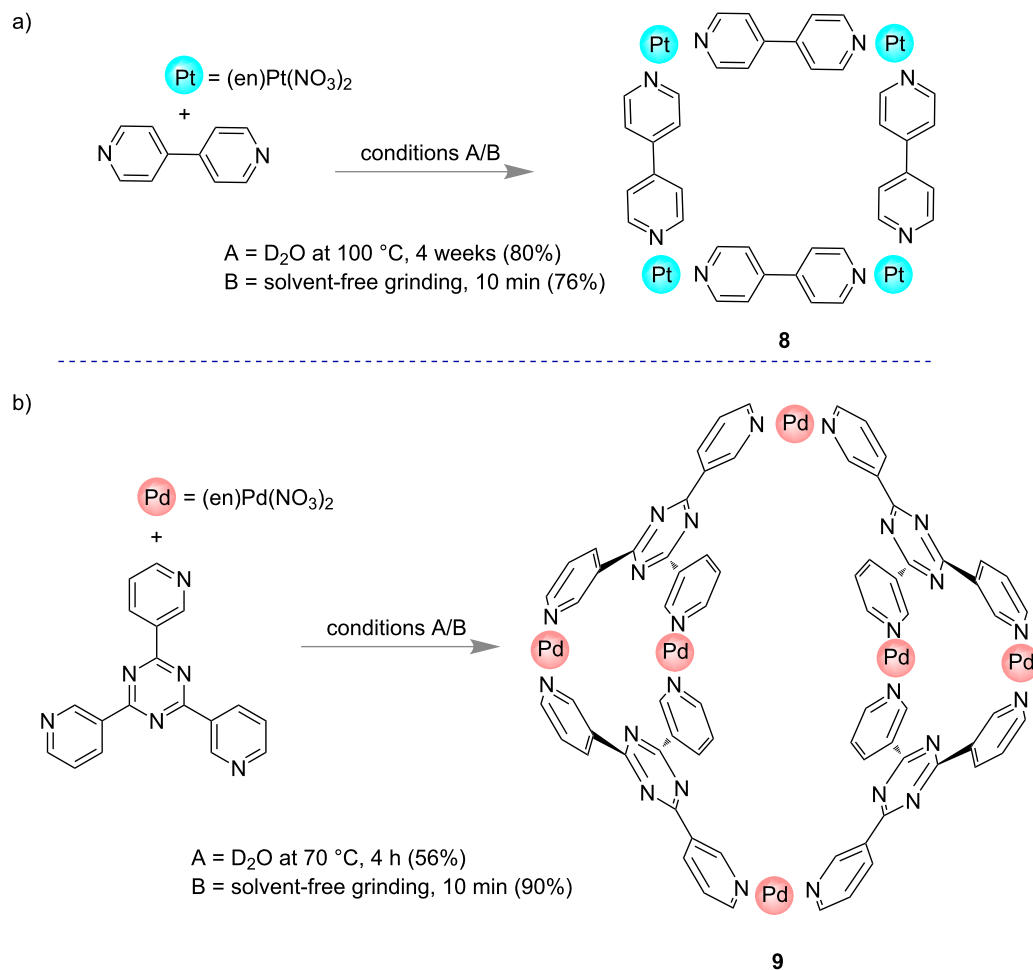
Figure 4: Otera's solvent-free approach by which the formation of self-assembled supramolecules could be accelerated [56].
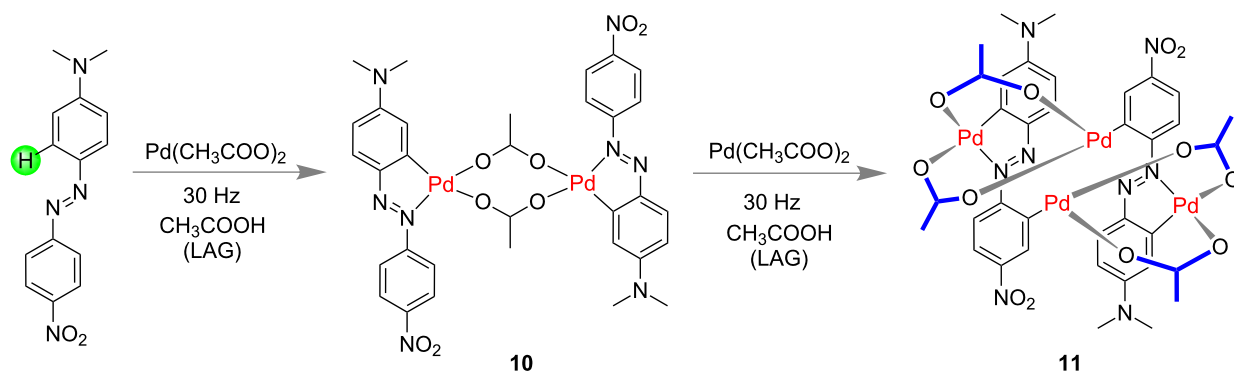
Figure 5: Synthesis of a Pd-based metalla-supramolecular assembly through mechanochemical activation for C–H-bond activation of unsymmetrically substituted azobenzene [58].

Interestingly, a synthesis of the smallest [2]rotaxane also has been demonstrated by the same group [60]. They applied a Diels–Alder reaction of 1,2,4,5-tetrazine with a terminal alkyne unit in a 21-crown-7-based [2]pseudorotaxane **14**. The [2]rotaxane **15** was produced in 81% yield having pyridazine groups as stoppers (Figure 7).

Figure 6: a) Schematic representation for the construction of a [2]rotaxane. b) Chiu's ball-milling approach for the synthesis of [2]rotaxanes.

Figure 7: Mechanochemical synthesis of the smallest [2]rotaxane.
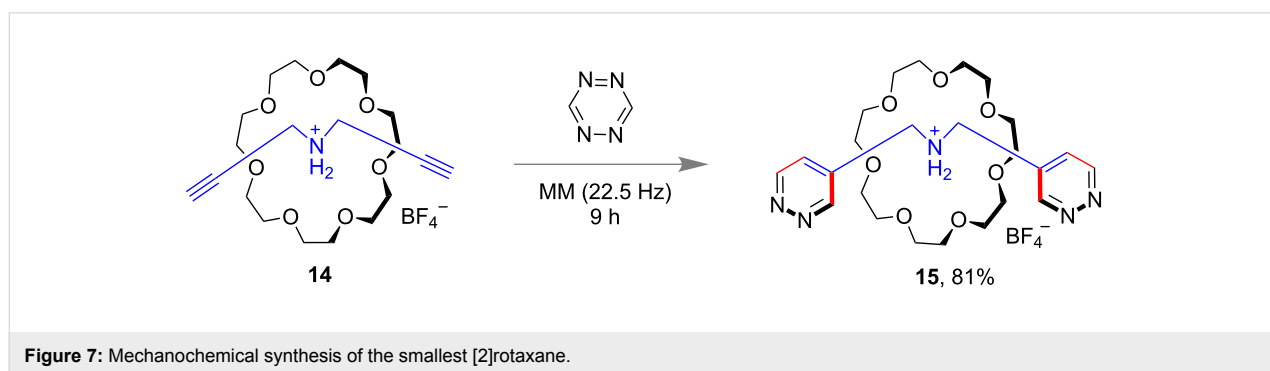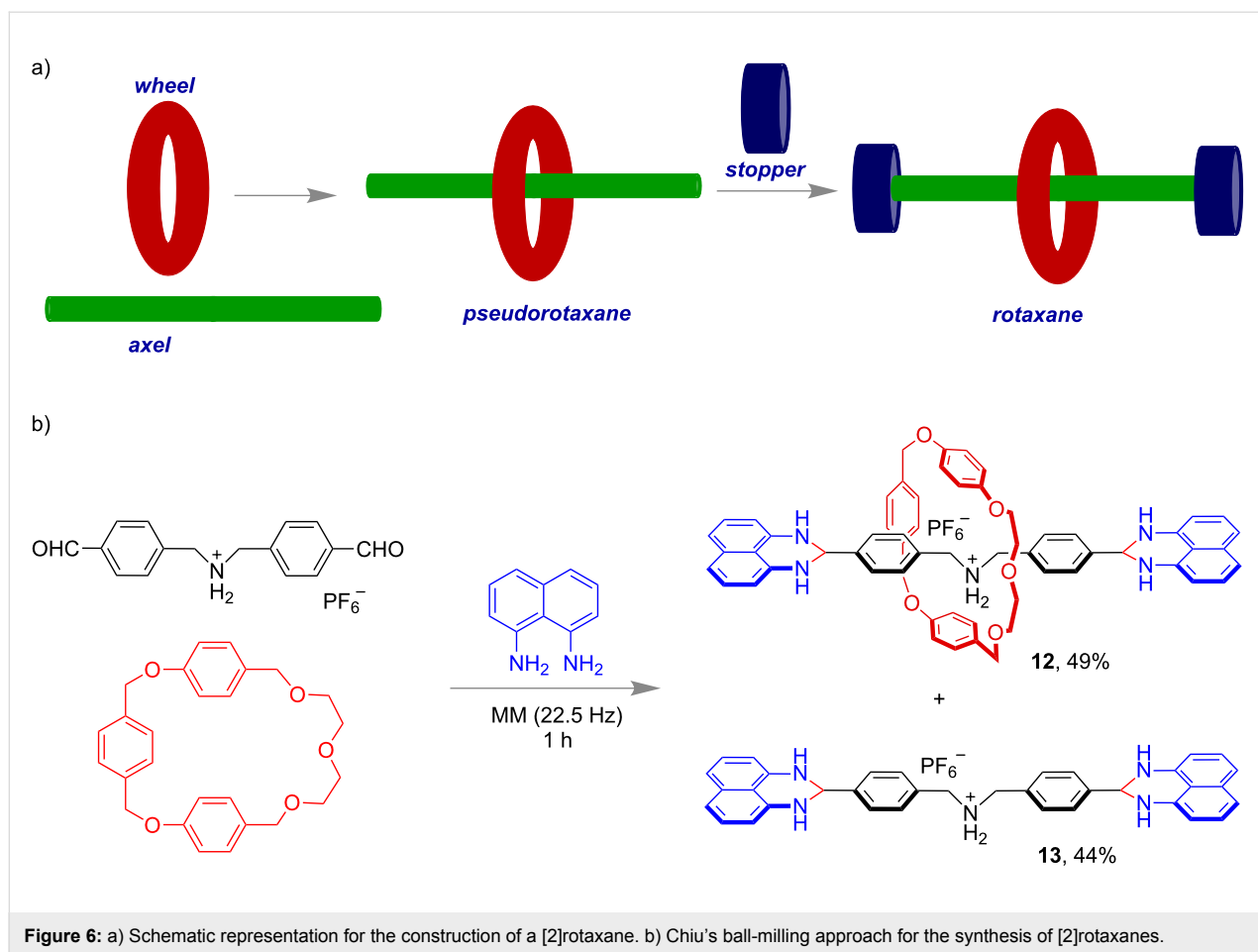
Very recently, Nierengarten and co-workers reported a solvent-free mechanochemical synthesis of pillar[5]arene-containing [2]rotaxanes (Figure 8). Mixing a 2:1 ratio of pillar[5]arene (wheel) with dodecanedioyl dichloride (axle) in CHCl₃ resulted in the formation of pseudorotaxane **16** which was further treated with different amines (stopper) in a stainless-steel jar with 4 steel balls under milling conditions (30 Hz for 1–2 h). When for example, *N*-methyl-1,1,-diphenylmethanamine was used as one of the stoppers, diamido [2]rotaxane **17** was obtained with high yield (ca. 87%) [61] (Figure 8).

In 2017, Wang and co-workers reported an efficient method for the synthesis of neutral donor–acceptor [2]rotaxanes such as **19** through liquid-assisted mechanochemical milling (Figure 9). The donor–acceptor interaction between the electron-deficient naphthalene diimide moiety and the electron-rich naphthalene moieties embedded in the macrocyclic polyethers played the vital role for the construction of the rotaxane system via pseudorotaxane **18**. A shorter reaction time, use of small amounts of solvent and the high yield were the advantages over the solvent-mediated synthesis [62].
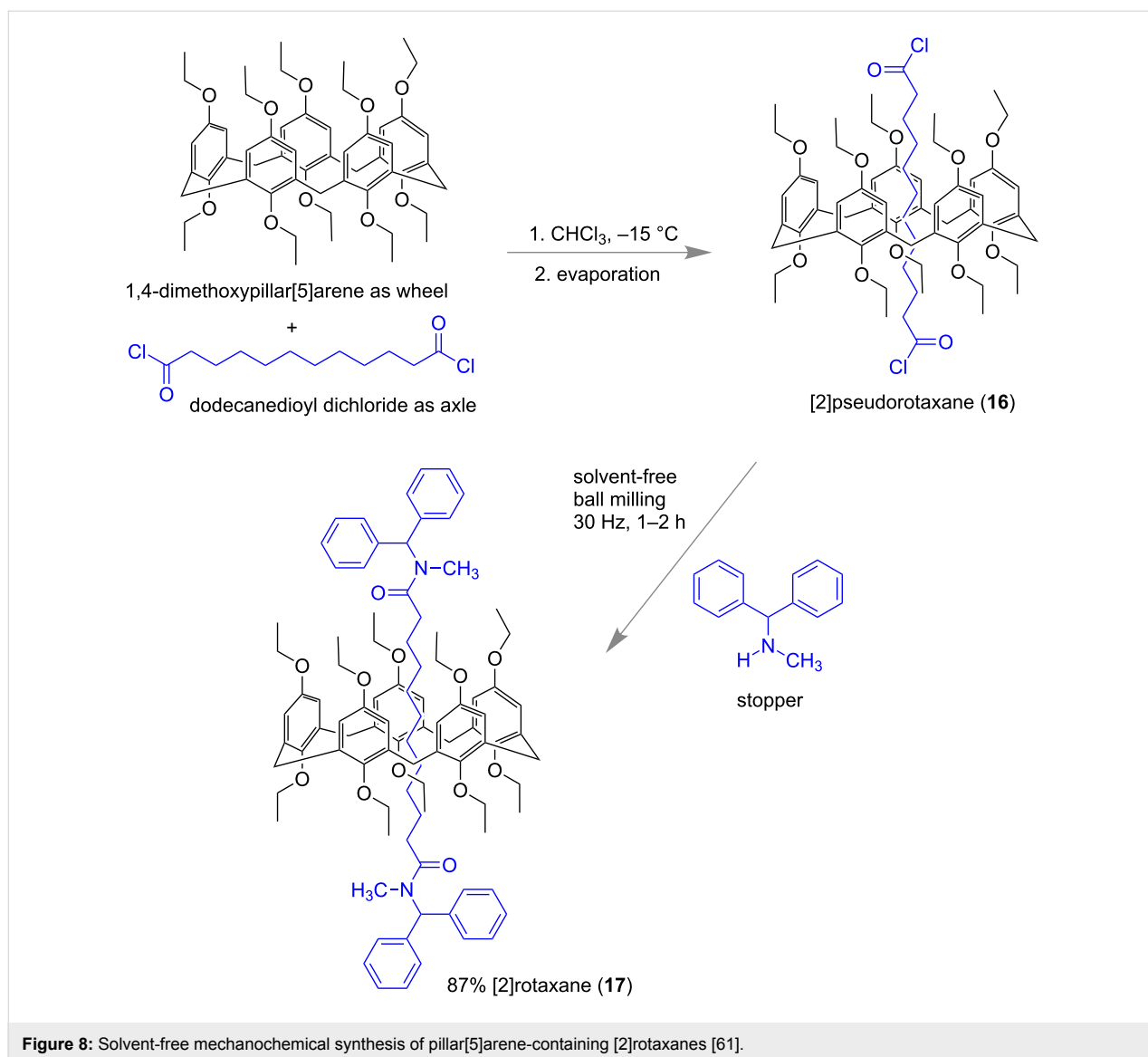
Figure 8: Solvent-free mechanochemical synthesis of pillar[5]arene-containing [2]rotaxanes [61].

Macrocycle synthesis

The mechanochemical synthesis of sphere-like nanostructures was reported by Severin and co-workers (Figure 10). Under ball-milling conditions (20 Hz), the condensation of 4-formyl-phenylboronic acid, pentaerythritol and 1,3,5-tri(aminomethyl)-2,4,6-triethylbenzene afforded 94% of sphere-like compound **21** in 1 h [63].

In 2018, Wang and co-workers also demonstrated the synthesis of boronic ester cages under high-speed vibration milling (HSVM) conditions. The condensation of pentaerythritol and triboronic acid at 58 Hz for 40 min led to the formation of cage structure **22** (Figure 11) with nearly 96% yield [64]. The authors also reported that the cage compounds such as **22** had high thermal stabilities by exhibiting a decomposition temperature up to 320 °C.

In 2013, Severin and co-workers reported the mechanochemical synthesis of large macrocycles with borasiloxane and imine links using a ball mill (Figure 12). In a polycondensation reaction using diamines, 4-formylbenzeneboronic acid and *t*-Bu$_2$Si(OH)$_2$, borasiloxane-based macrocycle **23** was obtained in >90% yield after 2 × 45 min of grinding [65].

In 2017, Xu and his group developed the first method towards the synthesis of 2-dimensional aromatic polyamides (2DAPAs) under solvent-free ball-milling conditions [66]. Reacting 1,3,5-benzenetricarbonyl chloride and 1,4-phenylenediamine in a ball mill afforded 75% of the desired 2D polymer **24** within 15 min (Figure 13). When using 4,4'-diaminobiphenyl in place of 1,4-phenylenediamine the analogous 2D structure comprising biphenylene units was obtained within the same time albeit with a lower yield (≈65%).
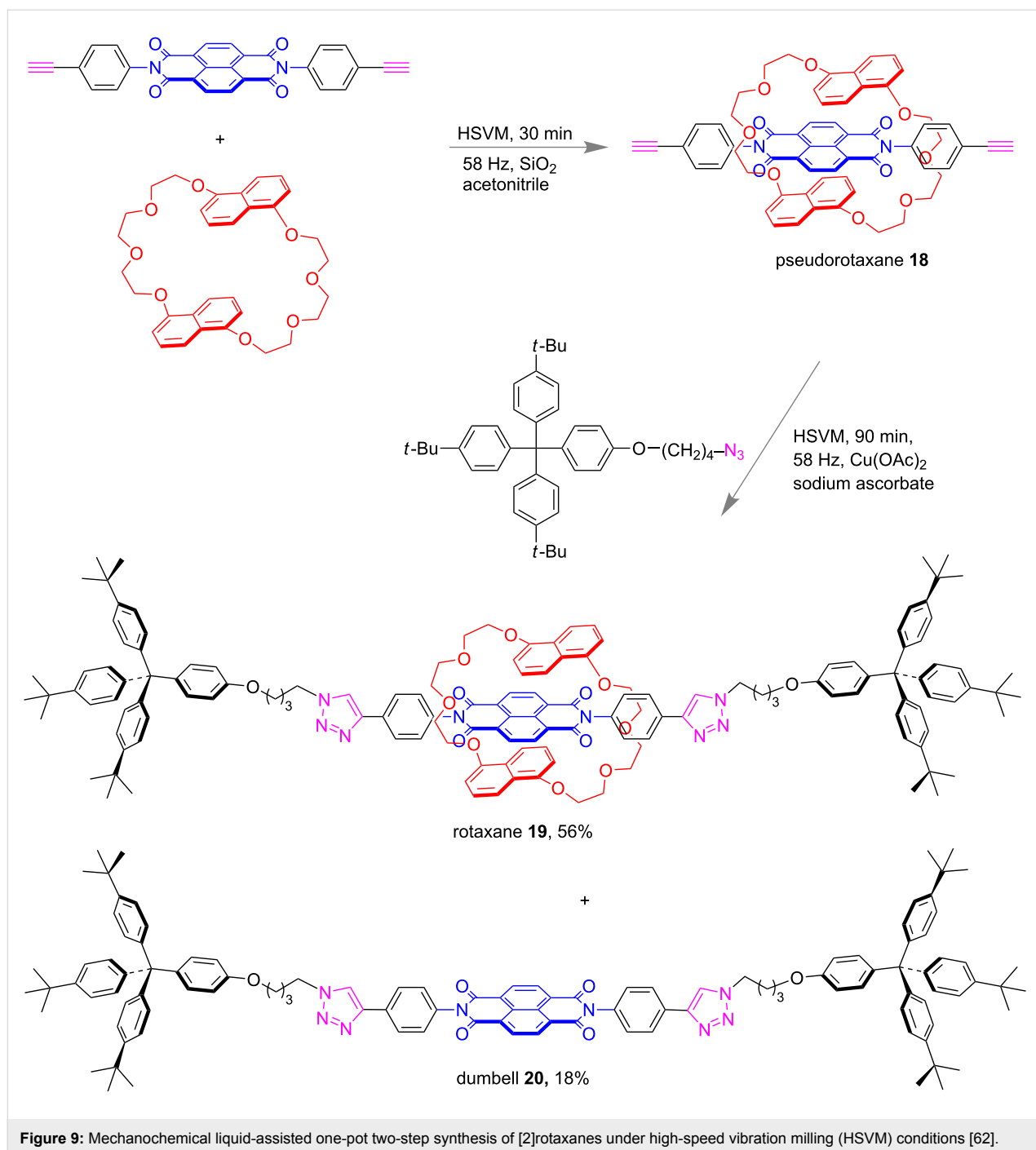
Figure 9: Mechanochemical liquid-assisted one-pot two-step synthesis of [2]rotaxanes under high-speed vibration milling (HSVM) conditions [62].

Subcomponent self-assembly and mechano-milling

Nature displays innumerable and beautiful creations [67,68] which include highly complex self-assembled structures made from smaller building blocks by using weak or non-covalent interactions [69,70]. Therefore, the supramolecular approach [71] and systems chemistry [1,72] are considered as the fastest growing areas of chemical research during the last couple of decades [73,74]. The concept of systems chemistry offers a thorough understanding of the building-up principles for creation of complex functional molecular systems from conventional materials [75,76]. The systems chemistry approach may give easy access to new structures or functional materials simply by controlling the inputs of a multicomponent system. The concept of self-sorting [77-79] and subcomponent self-assembly approach [80] are well-developed methods being practiced in supramolecular chemistry to produce complex molecules with topological diversity [81]. Therefore, organic trans-

Figure 10: Mechanochemical (ball-milling) synthesis of molecular sphere-like nanostructures [63].

Figure 11: High-speed vibration milling (HSVM) synthesis of boronic ester cages of type **22** [64].
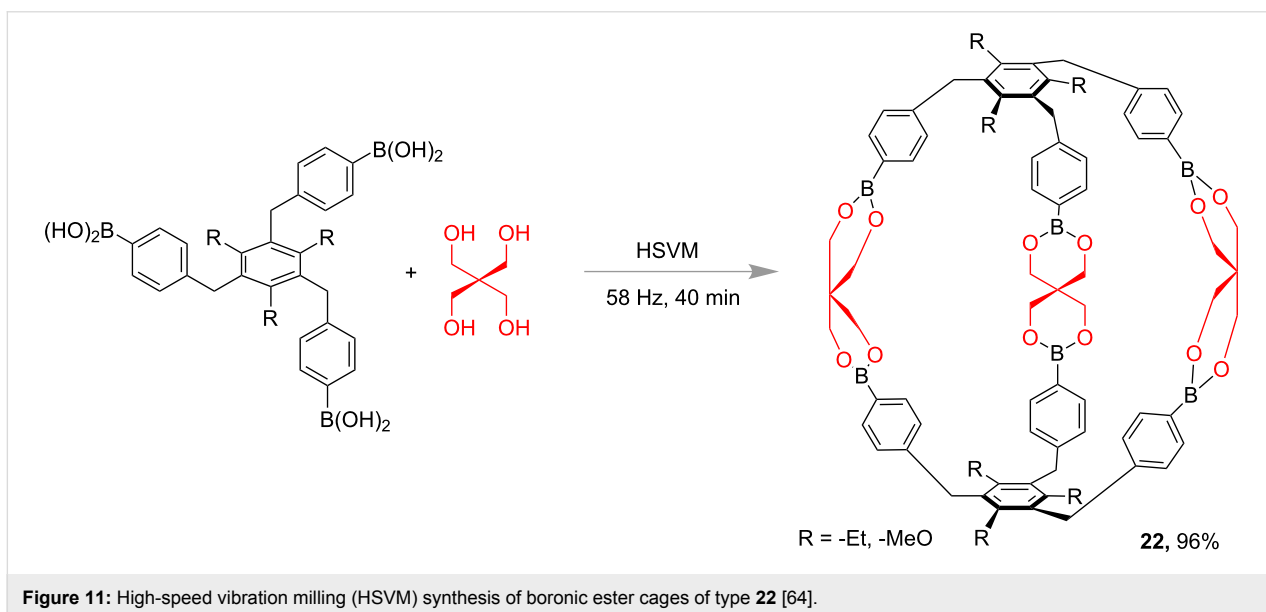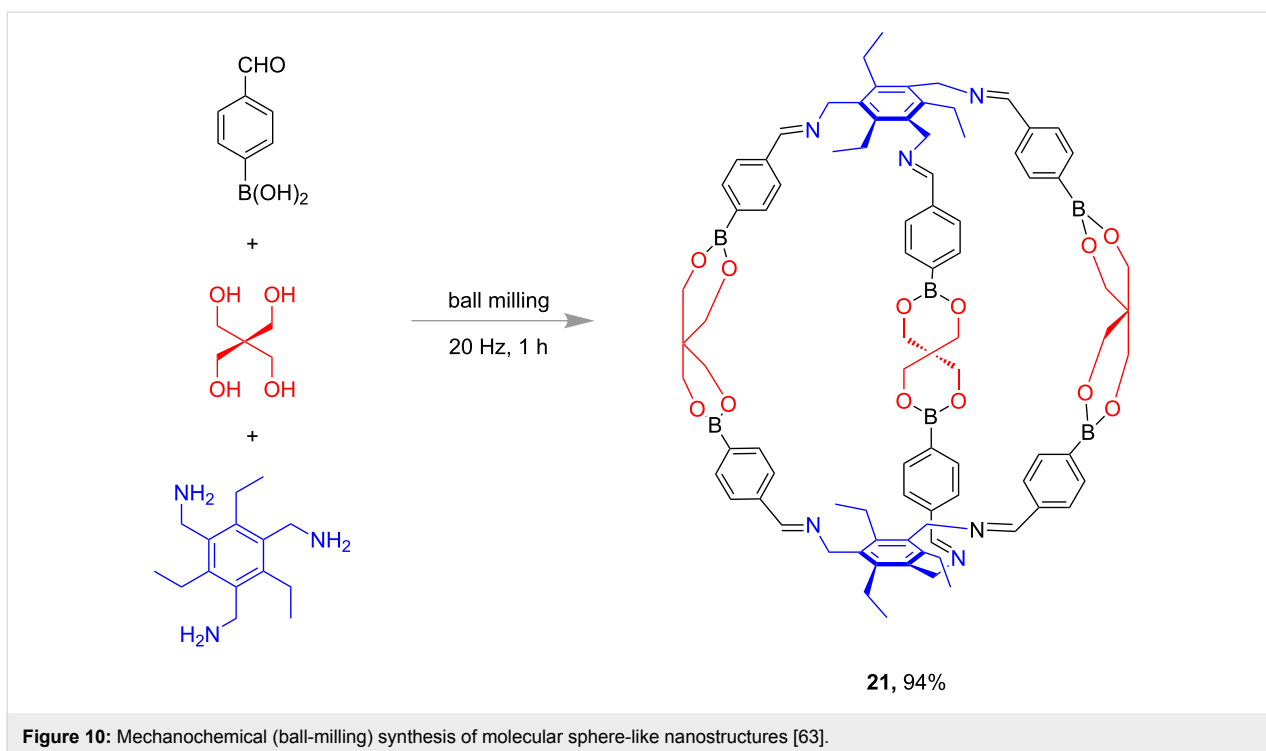
formations through subcomponent synthesis under mechano-milling conditions might be considered as a useful tool for performing a chemical reaction in a greener fashion.

The subcomponent self-assembly of a rigid aromatic linear bisamine, pyridine-2-carboxaldehyde and Fe(II) resulting in the tetrahedral $[M_4L_6]^{4-}$ cage **25** in water reported by Nitschke [82] was a milestone of supramolecular tetrahedral complex chemistry (Figure 14). The authors have thoroughly explored the

host–guest chemistry of that self-assembled Fe(II) cage [4,12,83].

In 2015, Mal's group successfully reproduced the synthesis of Nitschke's tetrahedral iron-cage molecule under solvent-free mechano-milling conditions [84]. Subcomponent self-assembly from components **A**, **B**, **C**, **D** and Fe(II) in a solvent-free environment through self-sorting led to three structurally different metallosupramolecular Fe(II) complexes. Under mechano-
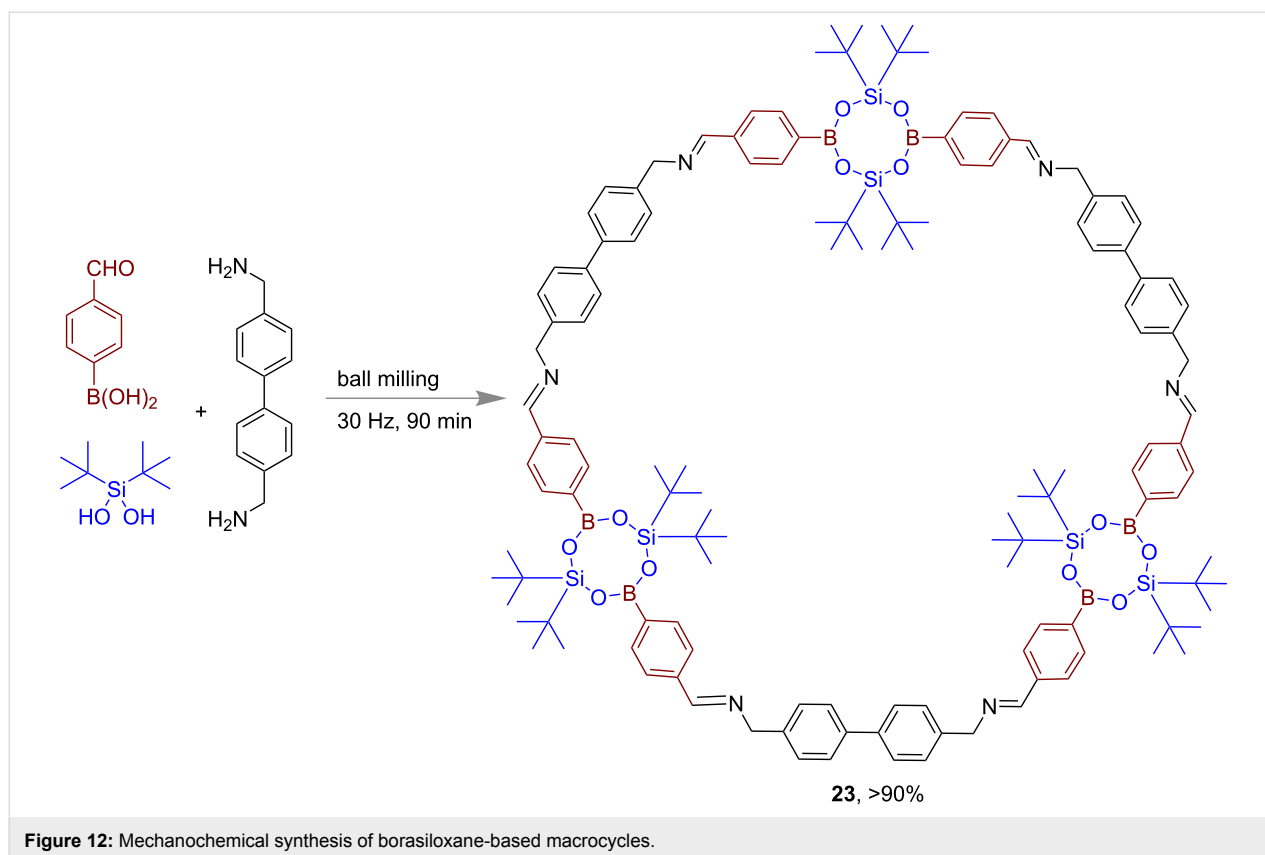
Figure 12: Mechanochemical synthesis of borasiloxane-based macrocycles.

milling conditions the tetranuclear $[Fe_4(\mathbf{AD}_2)_6]^{4-}$ 22-component cage **26**, dinuclear $[Fe_2(\mathbf{BD}_2)_3]^{2-}$ 11-component self-assembled helicate **27** and 5-component mononuclear $[Fe(\mathbf{CD}_3)]^{2+}$ complex **28** could be prepared simultaneously in a one-pot reaction starting from 38 components (Figure 15).

In 2015, Mal and co-workers described a multicomponent Biginelli [85] reaction following a subcomponent synthesis under mechanochemical conditions. They have developed a method in which dihydropyrimidone synthesis was achieved from benzyl alcohol using a Br^+ source as the catalyst (Figure 16). In the reaction pot subcomponents such as benzaldehydes and H^+ were formed which further participated in a cascade transformation to give dihydropyrimidones **29**.

Dynamic combinatorial chemistry and mechano-milling

Dynamic combinatorial chemistry (DCC) is one of the most important topics which make us understand the relationship between complex molecules and living systems. With this approach, a library of chemical species called dynamic combinatorial library (DCL) can be designed which are in thermodynamic equilibrium with each other. Nitschke and co-workers reported, that mixing of 2-formylpyridine (3.0 equiv), 6-methyl-2-formylpyridine (3.0 equiv), tris(2-aminoethyl)amine

(1.0 equiv) and ethanolamine (3.0 equiv) in aqueous solution afforded a dynamic library of imines which subsequently could be self-sorted into two distinct complexes **30** and **31** upon the addition of Cu(I) tetrafluoroborate (1.5 equiv) and Fe(II) sulfate (1.0 equiv) as shown in Figure 17 [86].

DCL formation was also shown to be possible in the solid-state by grinding or mechanochemical methods by Sanders and co-workers in 2011. They have demonstrated the reversibility and thermodynamic control in mechanochemical covalent synthesis, towards base-catalyzed metathesis of aromatic disulfides as a model reaction [87]. The outcome of solution-phase chemistry and mechanochemical synthesis were well distinguished and they have described the phenomenon based on differences in the crystal packing in the solid state. The products **32** were obtained via thermodynamic control (Figure 18) from a dynamic combinatorial library [53,88].

In 2010, Otto and co-workers observed unprecedented product selectivity for the formation of disulfide macromolecules based on mechanical shaking and stirring [89]. Peptide-chain containing distal thiol groups underwent an aerial oxidation process to give different disulfide-containing macromolecules. They observed that under mechanical shaking conditions preferentially the cyclic hexamer **33** is formed, whereas stirring resulted in
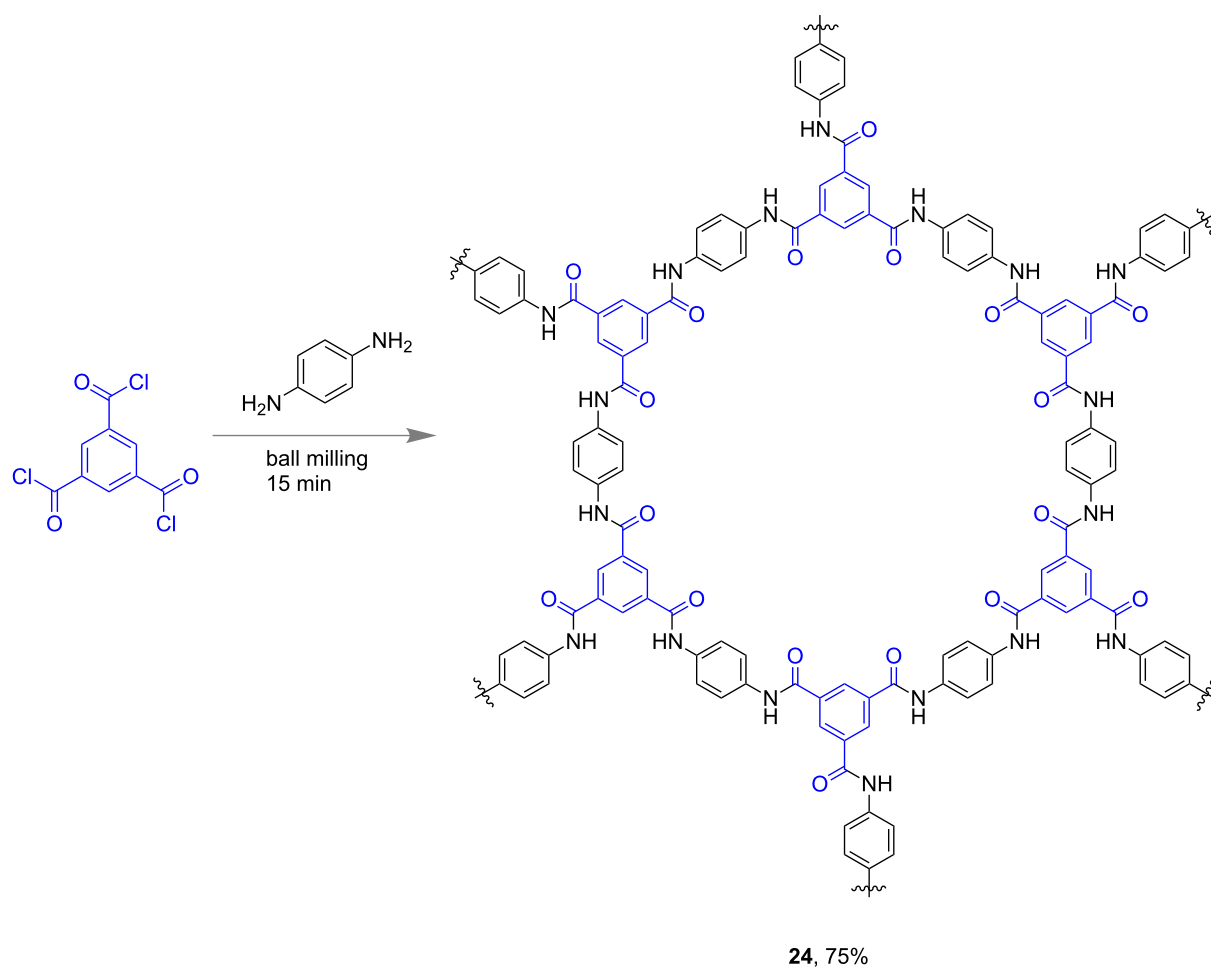
Figure 13: Mechanochemical synthesis of 2-dimensional aromatic polyamides.
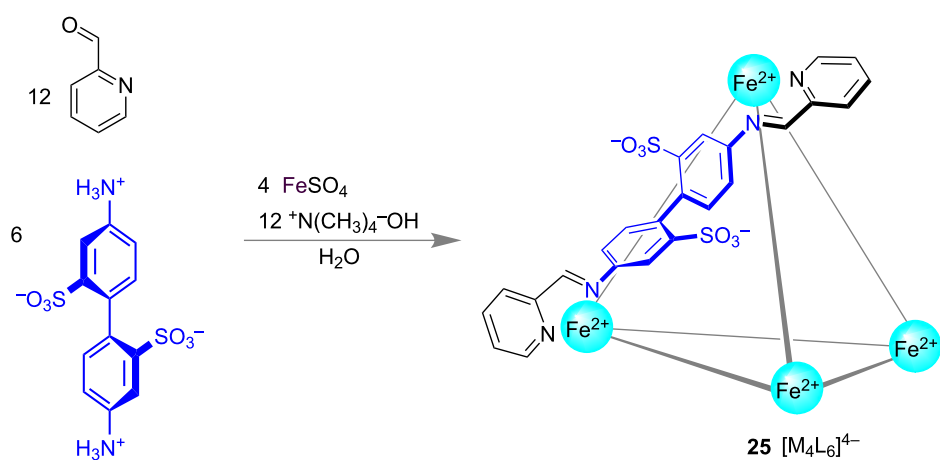
Figure 14: Nitschke's tetrahedral Fe(II) cage **25**.

Figure 15: Mechanochemical one-pot synthesis of the 22-component [Fe₄(**AD₂**)₆]⁴⁻ **26**, 11-component [Fe₂(**BD₂**)₃]²⁻ **27** and 5-component [Fe(**CD₃**)]²⁺ **28**.
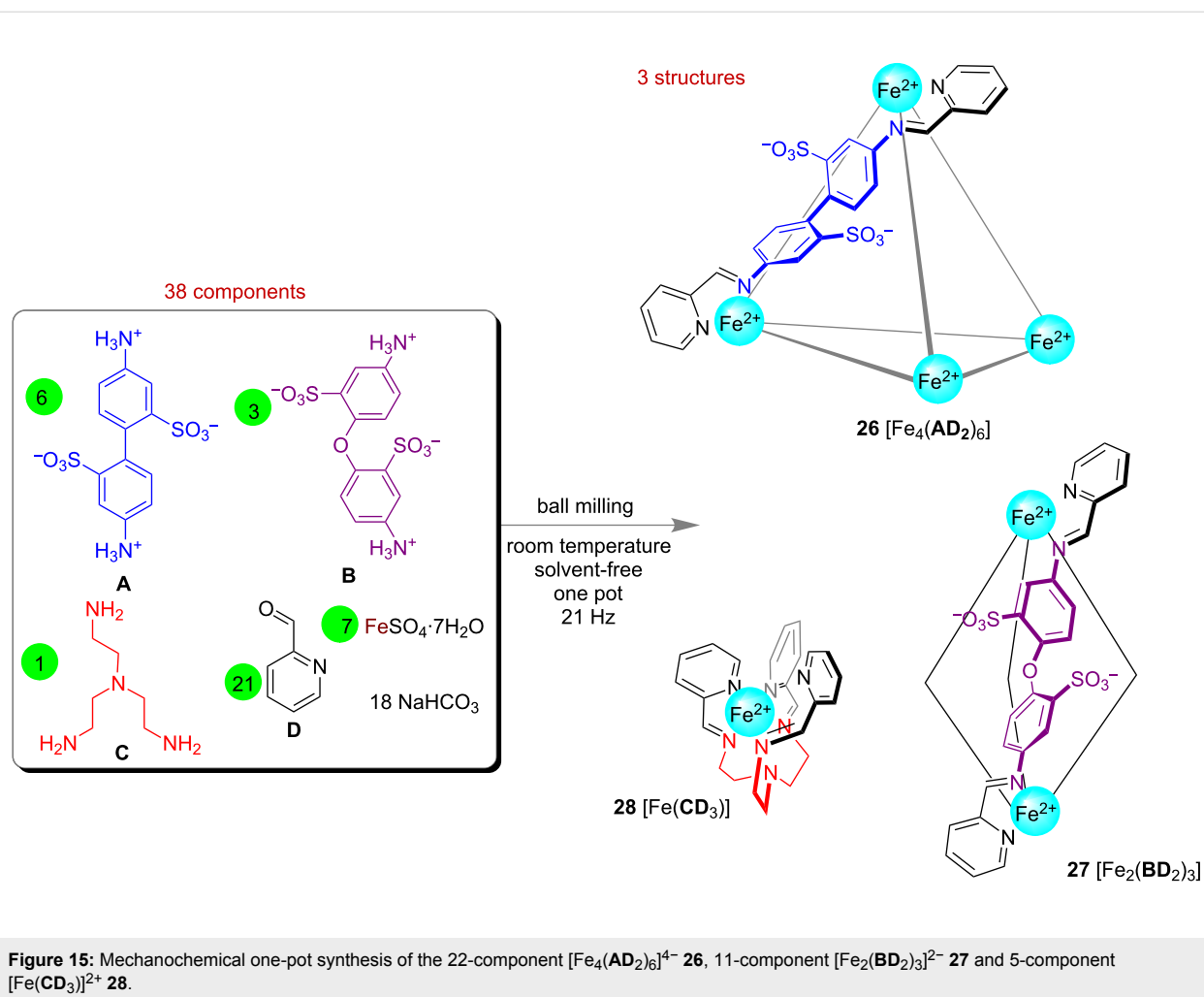
Figure 16: a) Subcomponent synthesis of catalyst and reagent and b) followed by multicomponent reaction for synthesis of dihydropyrimidones.
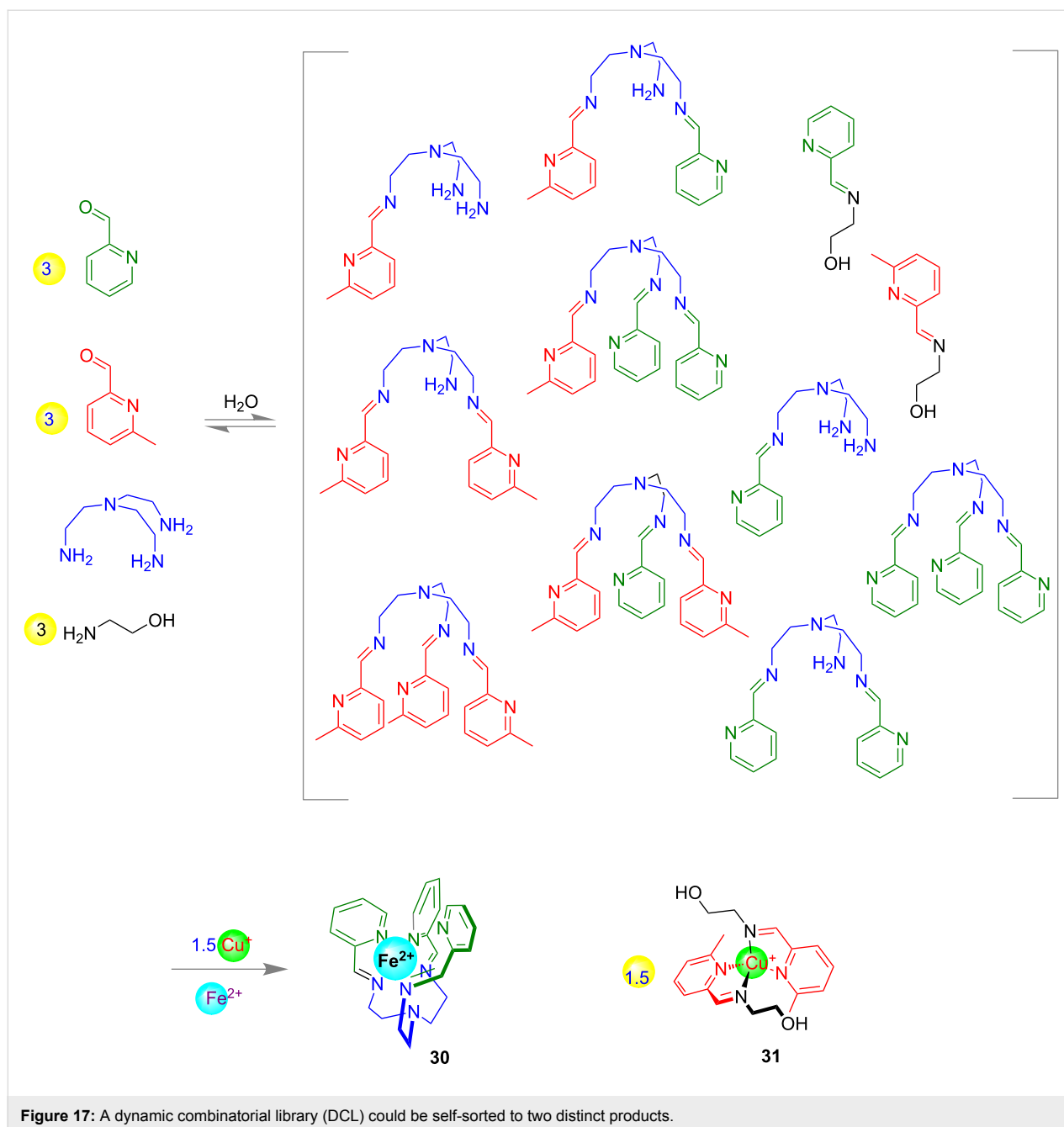
Figure 17: A dynamic combinatorial library (DCL) could be self-sorted to two distinct products.
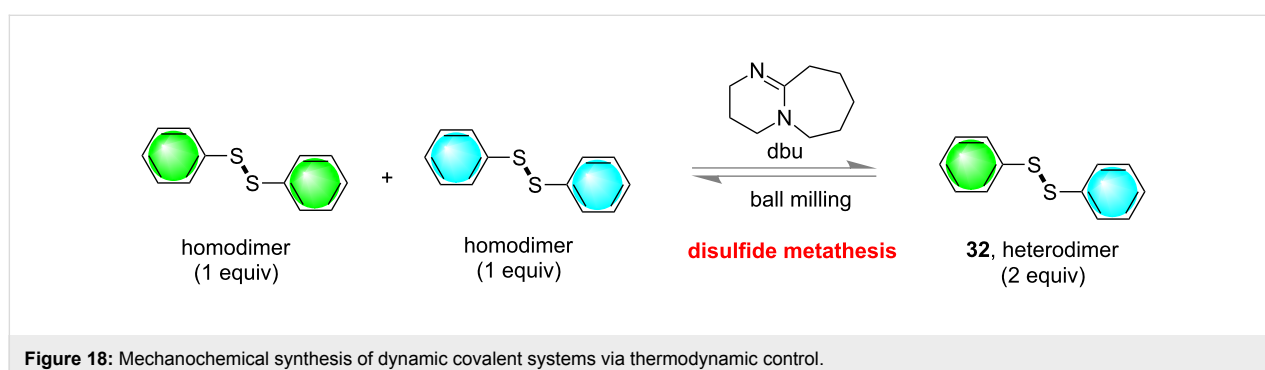
Figure 18: Mechanochemical synthesis of dynamic covalent systems via thermodynamic control.

Figure 19: Preferential formation of hexamer **33** under mechanochemical shaking via non-covalent interactions of peptide chains.
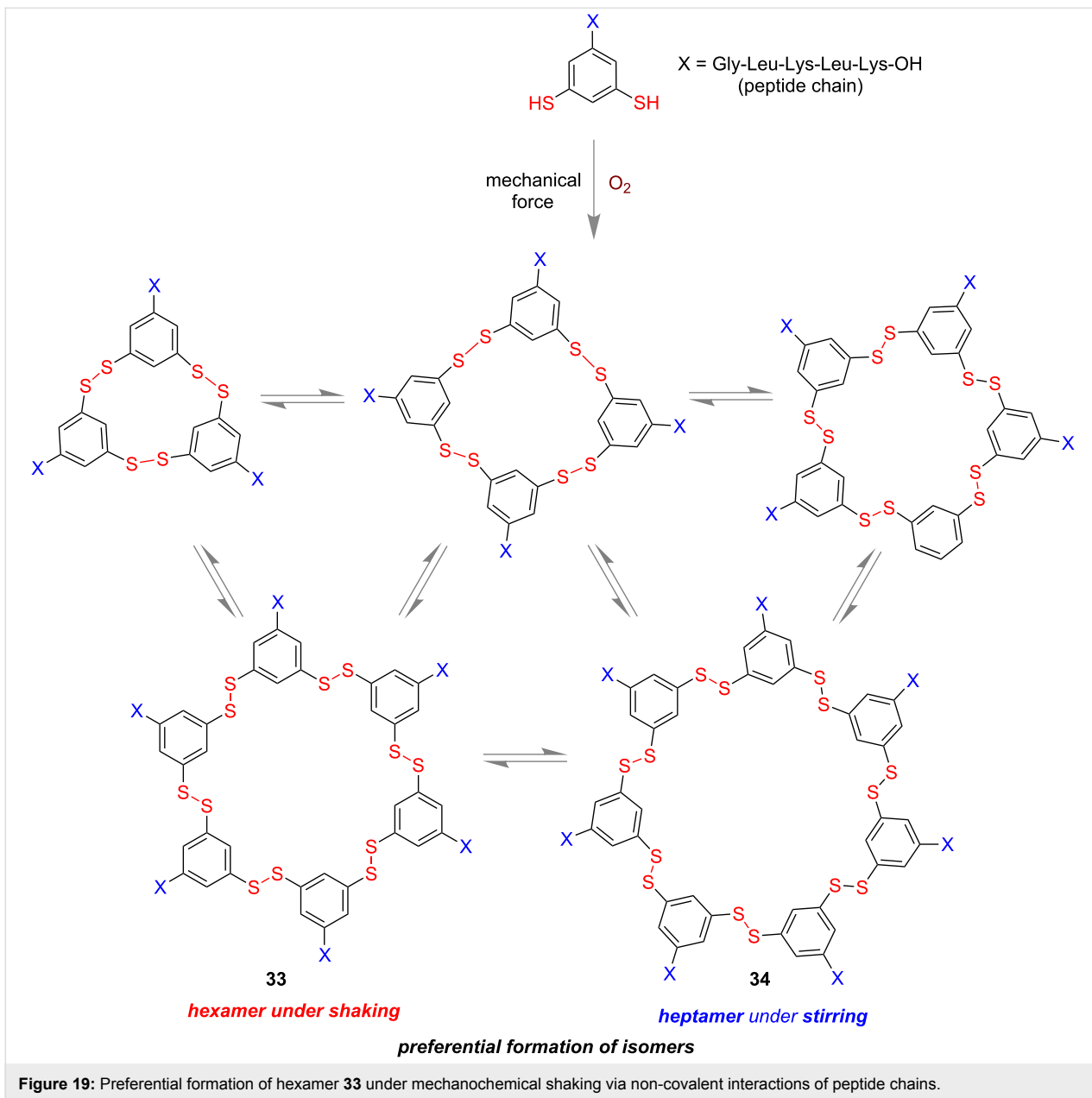
formation of heptamer **34** as the major isomer (Figure 19). From this observation the authors concluded that not only the thermodynamically controlled products but also the kinetically controlled products could be obtained in DCL depending on the non-covalent interactions present in the molecule. Non-covalent interactions of alternating hydrophilic and hydrophobic units in the peptide chains played the vital role in the system.

Friščić and Aav with co-workers reported the first solvent-free mechanochemical synthesis of hemicucurbiturils [90] through the anion template effect of dynamic covalent chemistry [47,91,92]. The mechanochemical milling of a 1:1 mixture of paraformaldehyde and (*R*,*R*)-hexahydro-2-benzimidazolinone along with a small amount of concentrated aqueous HCl for 30–60 min followed by aging at 45 °C for 6 days, resulted in the formation of six-membered macrocycle cycHC[6] **35** with 98% conversion by NMR (Figure 20). When ClO_4^- has been used as the anion template, the formation of the eight-membered macrocycle cycHC[8] **36** was observed in 98% conversion by NMR after 30 min of LAG, followed by aging for one day at 60 °C [90].

Template-assisted mechanochemistry

It was long believed that covalent-bond formation in supramolecular chemistry which occurs in solution-phase synthesis is

Figure 20: Anion templated mechanochemical synthesis of macrocycles cycHC[*n*] by validating the concept of dynamic covalent chemistry.
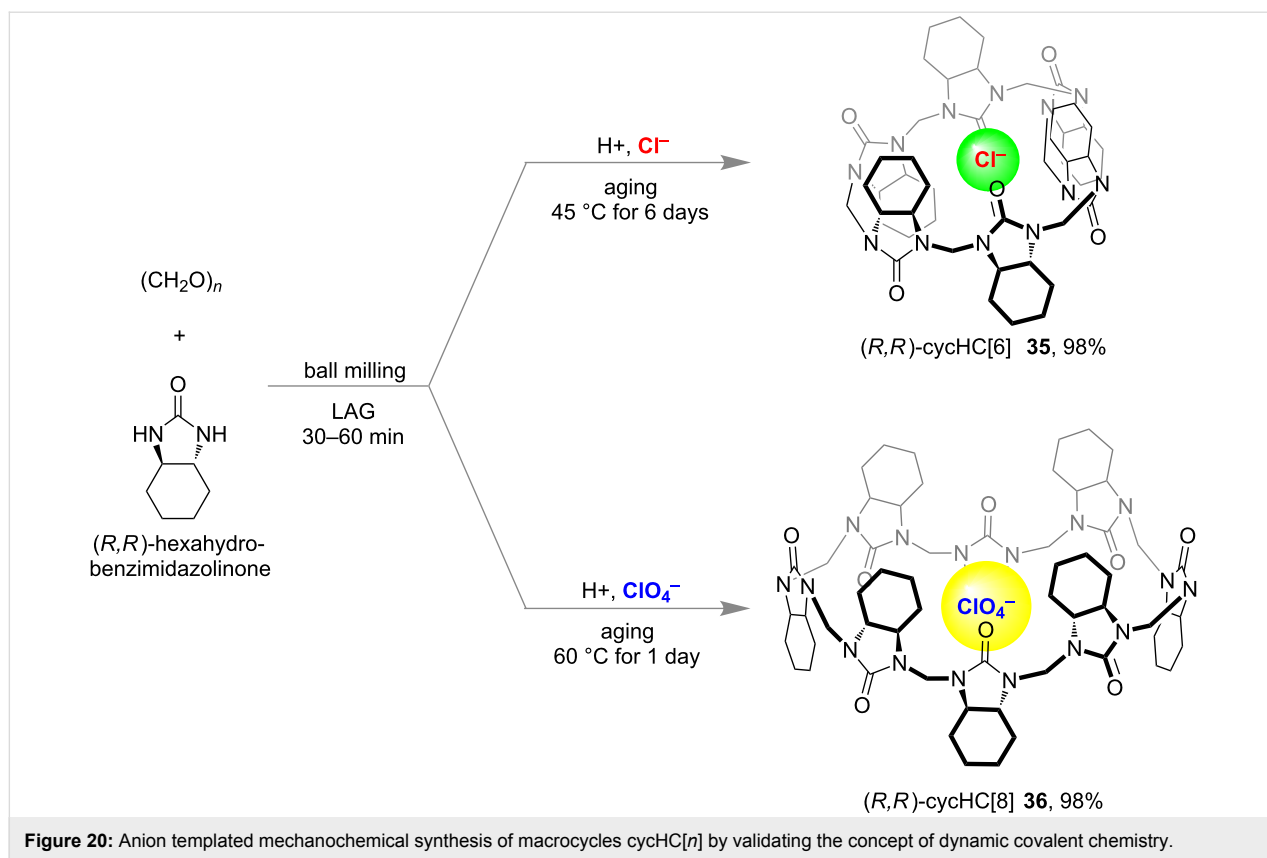
almost impossible in solid-state reactions. However, MacGillivray's group demonstrated several examples of co-crystal formation or supramolecular synthesis in the solid phase through mechano-milling or dry grinding. In 2008, they have established a [2 + 2] photodimerization through solid-state grinding either in neat or liquid-assisted conditions [93]. To achieve 100% stereospecific products they considered resorcinol derivatives as hydrogen-bond donors for the photodimerization of 1,2-di(pyridin-4-yl)ethylene (Figure 21a). However, 1,8-dipyridylnaphthalene was used as hydrogen-bond acceptor for the [2 + 2] cycloaddition of fumaric acid derivatives (Figure 21b).

In 2017 Purse and co-workers reported the host–guest chemistry of pyrogallo[4]arene (**39**) hexamers under mechanomilling conditions [94]. A hexameric capsule **40** formed through hydrogen-bonding and the cavity was found to be able to encapsulate different organic molecules such as alkanes, acids, amines, etc. The encapsulation of a [2.2]paracyclophane in the cage was achieved by ball milling at 30 Hz (Figure 22) and the host–guest product **40** was verified by NMR as well as other spectroscopic techniques.

Georghiou et al. demonstrated the mechanochemical formation of a 1:1 supramolecular complex C_{60}–*tert*-butylcalix[4]azulene

41 (Figure 23). The host–guest complexation was achieved by simple grinding the individual compounds in a mortar and pestle [95].

Supramolecular catalysis

The concept of supramolecular catalysis mainly is based on the use of supramolecular chemistry, molecular recognition, host–guest chemistry, etc. for catalysis [96]. The field originated with the understanding of enzymatic system which is conceptually different from traditional organic chemistry reactions, as it relies on soft force [97,98] or non-covalent interactions [2] such as hydrogen bonding [99], cation–π [100-102], anion–π [103], hydrophobic effect [104,105], halogen bonding [106-109], etc. As enzymes are structurally complex entities and are difficult to modify, supramolecular catalysis proposes a much simpler model to understand the catalytic activity of enzymes.

In 2010, MacGillivray and co-workers have demonstrated the concept of "supramolecular catalysis" in a hydrogen-bond-assisted self-assembled formation of a [2 + 2]-cycloaddition product. The reaction was found to be 100% stereospecific under dry mortar and pestle grinding [110]. The hydrogen-bond donor 4,6-dichlororesorcinol was used as the supramolecular catalyst for the transformation in the solid-state. From single

a) resorcinol as hydrogen-bond donor template
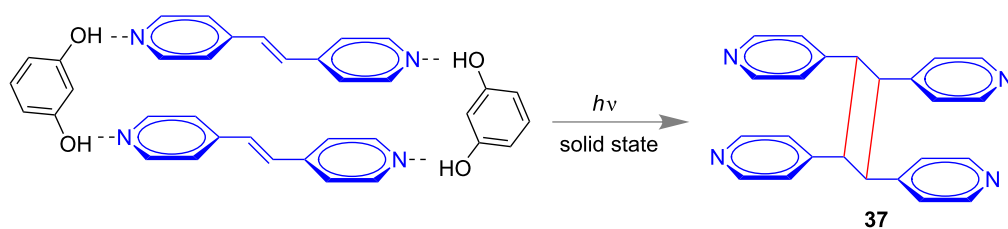
b) 1,8-dipyridylnaphthalene as hydrogen-bond acceptor template
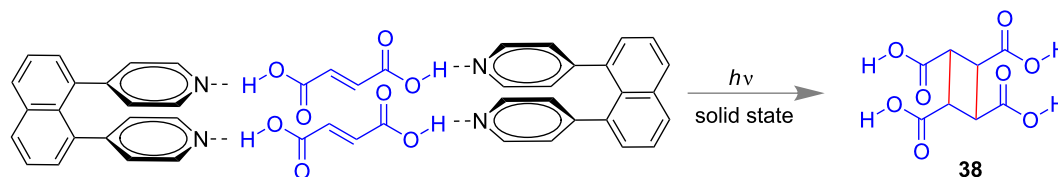
Figure 21: Hydrogen-bond-assisted [2 + 2]-cycloaddition reaction through solid-state grinding. Hydrogen-bond donors are a) resorcinol and b) 1,8-dipyridylnaphthalene, respectively.
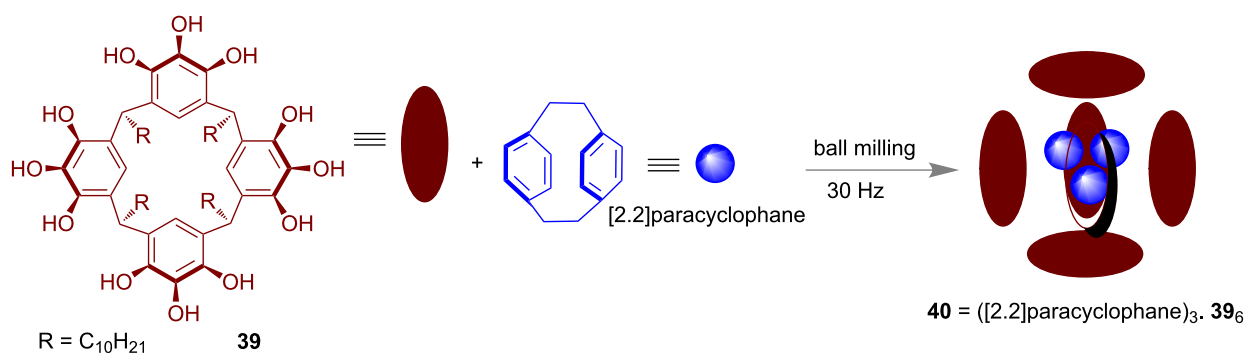
Figure 22: Formation of the cage and encapsulation of [2.2]paracyclophane guest molecule in the cage was done simultaneously under mechanochemical conditions.
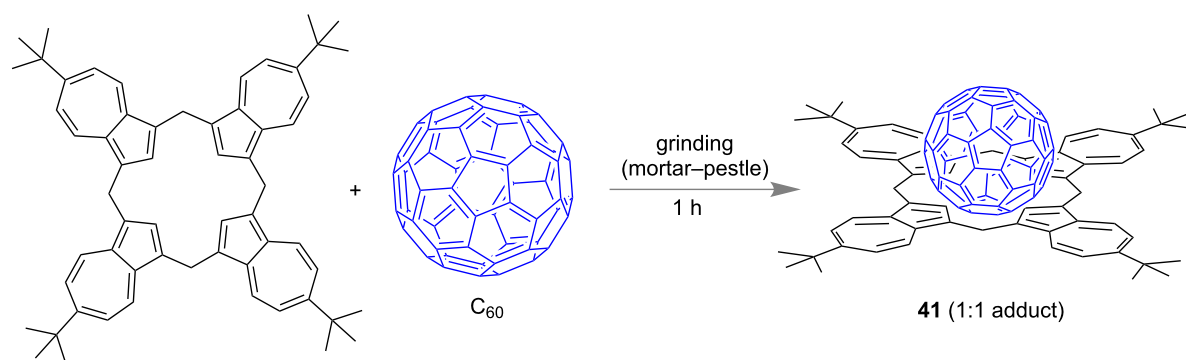
Figure 23: Formation of the 1:1 complex C_{60}–*tert*-butylcalix[4]azulene through mortar and pestle grinding of the host and the guest. The structure of the complex was obtained from DFT study.

crystal X-ray analysis the authors have proved the formation of the 2:2 complex **42** from 1,2-di(pyridin-4-yl)ethylene and 4,6-dichlororesorcinol in the transition state (Figure 24). Finally the cyclobutane derivative **43** was observed after the release of catalyst for the next cycle.

In 2012, again the MacGillivray group reported an improved version of the above mentioned [2 + 2]-cycloaddition methodology. They used the vertex grinding technique where solid-state grinding and UV irradiation was done simultaneously [111] and verified co-crystal formation of a resorcinol derivative with dipyridylethylene in the solid state. Also, the supramolecular

catalysis of [2 + 2] photodimerization has been shown to proceed with excellent turnover numbers.

Recently, Friščić and Cinčić with co-workers reported an elaborative study on the halogen bonding between 1,3,5-trifluoro-2,4,6-triiodobenzene and triphenylphosphine, -arsine, and -stibine under neat mechanochemical conditions or through solvent-assisted grinding using ethanol (Figure 25). The single crystal X-ray structures of the obtained co-crystals **44**–**46** were reported to match with the solution-phase co-crystals. They have also studied energy levels, thermal properties and the stability of these structures through DFT calculations [112]. In

Figure 24: Formation of a 2:2 complex between the supramolecular catalyst and the reagent in the transition state of the [2 + 2]-cycloaddition reaction of 1,2-di(pyridin-4-yl)ethylene and 4,6-dichlororesorcinol.

Figure 25: Halogen-bonded co-crystals via a) I⋯P, b) I⋯As, and c) I⋯Sb bonds [112].
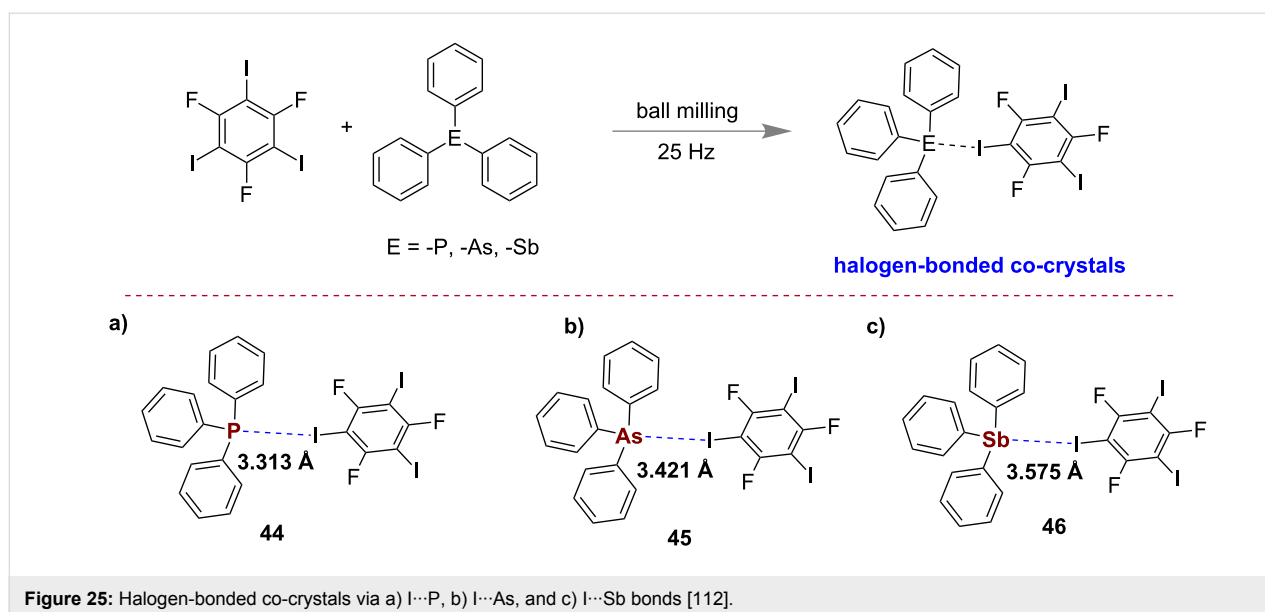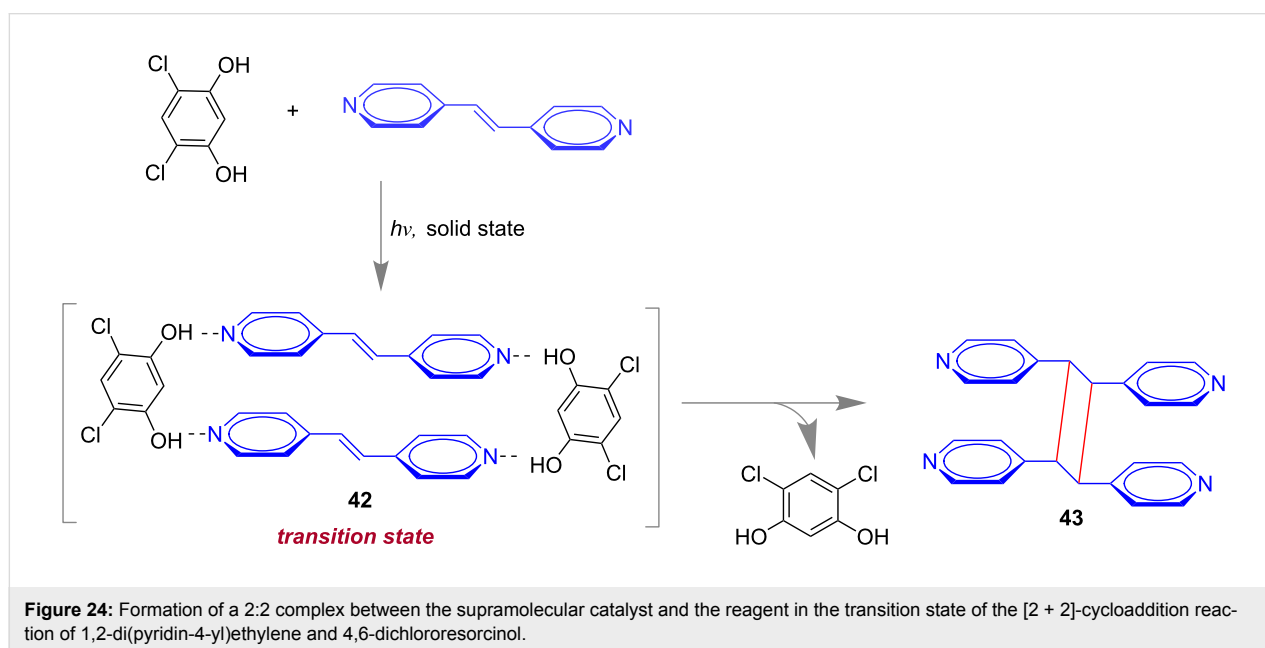
this work they have also demonstrated that metallic pnictogens do form sufficiently strong halogen bonds to enable co-crystal formation.

Mal and co-workers have shown that a contact explosive, i.e., the mixture of primary amines and phenyliodine diacetate led to a high-yielding reaction at maximum contact (solvent-free ball milling) of the reactants [113]. An acid salt, (sodium bisulfate) was used to control the reactivity of the highly basic primary amines to transform the exceedingly exothermic reactive substrates in a high-yielding cross-dehydrogenative coupling (CDC) reaction to obtain the amides **47** (Figure 26).

The development of sustainable methods for the activation of less-reactive undirected C(sp³)–H bonds is challenging however, highly desired in organic synthesis. Mal and co-workers also demonstrated that acidic C(sp³)–hydrogen bonds within a mole-

cule could be used to control exothermic reactions between amines and iodine(III) [114]. By this process undirected C(sp³)–H bonds were shown to be functionalized for dehydrogenative imination reactions. Overall, at 1,5-distances (remote) a dehydrogenative and intramolecular C(sp³)–H imination by 4H elimination was readily done via organocatalysis using PhI (10 mol %)–*m*CPBA at ambient conditions as well as under neat mixing [115]. The N^1,N^1-dibenzylbenzene-1,2-diamine (Figure 27) which is an integrated system by the combination of aniline and *N,N*-dibenzylaniline led to the successful formation of 1-benzyl-2-phenyl-benzo[*d*]imidazole **48** under the iodine(III) environment.

Conclusion
Over the last years, substantial progress has been made in the area of mechanochemistry as environmentally benign method in organic synthesis, materials science and supramolecular chem-
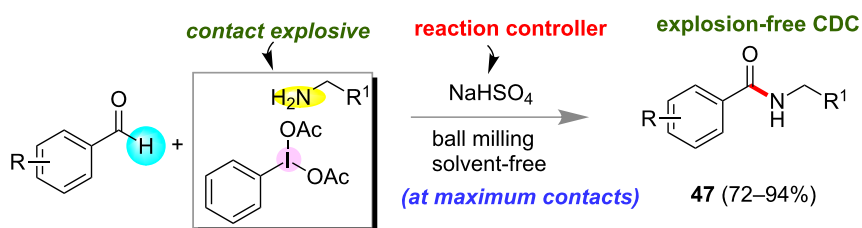
Figure 26: Transformation of contact-explosive primary amines and iodine(III) into a successful chemical reaction for amide synthesis.
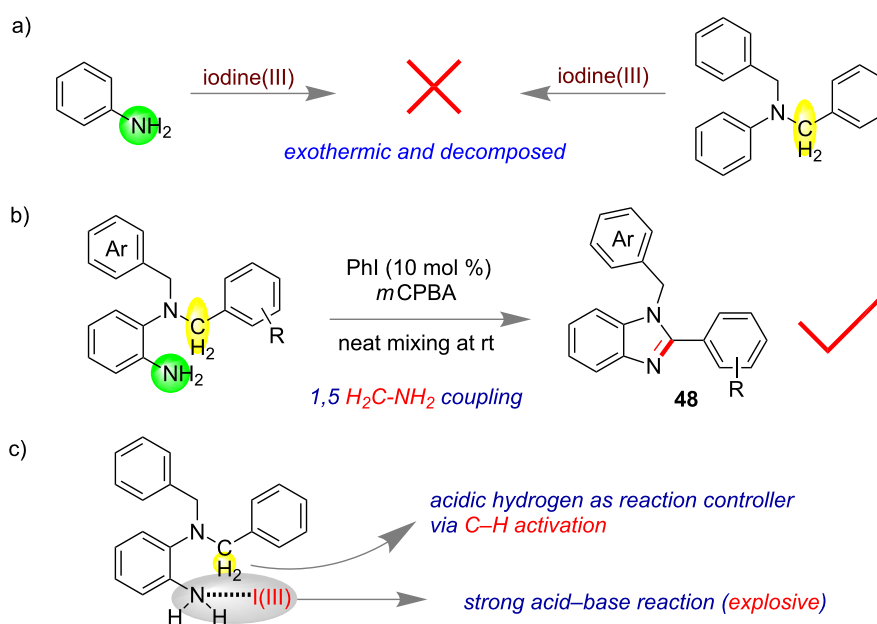
Figure 27: Undirected C–H functionalization by using the acidic hydrogen to control basicity of the amines [114]. a) Identified exothermic reactions. b) Successful reaction by quenching the heat intramolecularly. c) The plausible mechanism of acidic C–H functionalization intramolecularly.

istry. In this review the major focus has been to cover the concept and application of mechanochemistry in the formation of self-assembled supramolecules. In addition, we have included mechanochemical approaches to areas such as subcomponent self-assembly, dynamic combinatorial chemistry, systems chemistry, and supramolecular catalysis. We anticipate that the research area of supramolecular mechanochemistry is still in its infancy and needs significant improvement towards understanding and development of suitable methods [116-118].

Acknowledgements

ORCID® iDs

Prasenjit Mal - https://orcid.org/0000-0002-7830-9812

References

1. Ruiz-Mirazo, K.; Briones, C.; de la Escosura, A. *Chem. Rev.* **2014,** *114,* 285–366. doi:10.1021/cr2004844
2. Peyralans, J. J.; Otto, S. *Curr. Opin. Chem. Biol.* **2009,** *13,* 705–713. doi:10.1016/j.cbpa.2009.08.006
3. Li, J.; Nowak, P.; Otto, S. *J. Am. Chem. Soc.* **2013,** *135,* 9222–9239. doi:10.1021/ja402586c
4. Zarra, S.; Wood, D. M.; Roberts, D. A.; Nitschke, J. R. *Chem. Soc. Rev.* **2015,** *44,* 419–432. doi:10.1039/c4cs00165f
5. Zhang, G.; Mastalerz, M. *Chem. Soc. Rev.* **2014,** *43,* 1934–1947. doi:10.1039/c3cs60358j
6. Wilson, A.; Gasparini, G.; Matile, S. *Chem. Soc. Rev.* **2014,** *43,* 1948–1962. doi:10.1039/c3cs60342c
7. Bowman-James, K. *Acc. Chem. Res.* **2005,** *38,* 671–678. doi:10.1021/ar040071t
8. Cramer, F. Emil Fischer's Lock-and-Key Hypothesis after 100 years-Towards a Supracellular Chemistry. In *Perspectives in Supramolecular Chemistry;* Behr, J. P., Ed.; John Wiley & Sons, Ltd: Chichester, United Kingdom, 2007; pp 1–23. doi:10.1002/9780470511411.ch1
9. Lehn, J.-M. *Angew. Chem., Int. Ed. Engl.* **1988,** *27,* 89–112. doi:10.1002/anie.198800891
10. Mahadevi, A. S.; Sastry, G. N. *Chem. Rev.* **2016,** *116,* 2775–2825. doi:10.1021/cr500344e
11. Cougnon, F. B. L.; Sanders, J. K. M. *Acc. Chem. Res.* **2012,** *45,* 2211–2221. doi:10.1021/ar200240m
12. Zhang, D.; Ronson, T. K.; Nitschke, J. R. *Acc. Chem. Res.* **2018,** *51,* 2423–2436. doi:10.1021/acs.accounts.8b00303
13. Percástegui, E. G.; Mosquera, J.; Ronson, T. K.; Plajer, A. J.; Kieffer, M.; Nitschke, J. R. *Chem. Sci.* **2019,** *10,* 2006–2018. doi:10.1039/c8sc05085f
14. Haynes, C. J. E.; Zhu, J.; Chimerel, C.; Hernández-Ainsa, S.; Riddell, I. A.; Ronson, T. K.; Keyser, U. F.; Nitschke, J. R. *Angew. Chem., Int. Ed.* **2017,** *56,* 15388–15392. doi:10.1002/anie.201709544
15. Miljanić, O. Š. *Chem* **2017,** *2,* 502–524. doi:10.1016/j.chempr.2017.03.002
16. Islam, S.; Powner, M. W. *Chem* **2017,** *2,* 470–501. doi:10.1016/j.chempr.2017.03.001
17. Ashkenasy, G.; Hermans, T. M.; Otto, S.; Taylor, A. F. *Chem. Soc. Rev.* **2017,** *46,* 2543–2554. doi:10.1039/c7cs00117g
18. Mattia, E.; Otto, S. *Nat. Nanotechnol.* **2015,** *10,* 111–119. doi:10.1038/nnano.2014.337
19. Schultz, D. M.; Yoon, T. P. *Science* **2014,** *343,* 1239176. doi:10.1126/science.1239176
20. Prier, C. K.; Rankic, D. A.; MacMillan, D. W. C. *Chem. Rev.* **2013,** *113,* 5322–5363. doi:10.1021/cr300503r
21. de la Hoz, A.; Díaz-Ortiz, Á.; Moreno, A. *Chem. Soc. Rev.* **2005,** *34,* 164–178. doi:10.1039/b411438h
22. Toda, F. *Acc. Chem. Res.* **1995,** *28,* 480–486. doi:10.1021/ar00060a003
23. Toda, F.; Tanaka, K.; Iwata, S. *J. Org. Chem.* **1989,** *54,* 3007–3009. doi:10.1021/jo00274a007
24. Kimura, T. Application of Ultrasound to Organic Synthesis. In *Sonochemistry and the Acoustic Bubble;* Grieser, F.; Choi, P.-K.; Enomoto, N.; Harada, H.; Okitsu, K.; Yasui, K., Eds.; Elsevier: Amsterdam, Netherlands, 2015; pp 171–186.
25. Baig, R. B. N.; Varma, R. S. *Chem. Soc. Rev.* **2012,** *41,* 1559–1584. doi:10.1039/c1cs15204a
26. Varma, R. S. *Green Chem.* **2014,** *16,* 2027–2041. doi:10.1039/c3gc42640h
27. Cravotto, G.; Gaudino, E. C.; Cintas, P. *Chem. Soc. Rev.* **2013,** *42,* 7521–7534. doi:10.1039/c2cs35456j
28. Braga, D.; Maini, L.; Grepioni, F. *Chem. Soc. Rev.* **2013,** *42,* 7638–7648. doi:10.1039/c3cs60014a
29. James, S. L.; Adams, C. J.; Bolm, C.; Braga, D.; Collier, P.; Friščić, T.; Grepioni, F.; Harris, K. D. M.; Hyett, G.; Jones, W.; Krebs, A.; Mack, J.; Maini, L.; Orpen, A. G.; Parkin, I. P.; Shearouse, W. C.; Steed, J. W.; Waddell, D. C. *Chem. Soc. Rev.* **2012,** *41,* 413–447. doi:10.1039/c1cs15171a
30. Ley, S.; O'Brien, M.; Denton, R. *Synthesis* **2011,** 1157–1192. doi:10.1055/s-0030-1259979
31. Achar, T. K.; Maiti, S.; Mal, P. *RSC Adv.* **2014,** *4,* 12834–12839. doi:10.1039/c4ra00415a
32. Bose, A.; Mal, P. *Tetrahedron Lett.* **2014,** *55,* 2154–2156. doi:10.1016/j.tetlet.2014.02.064
33. Walsh, P. J.; Li, H.; de Parrodi, C. A. *Chem. Rev.* **2007,** *107,* 2503–2545. doi:10.1021/cr0509556
34. Beyer, M. K.; Clausen-Schaumann, H. *Chem. Rev.* **2005,** *105,* 2921–2948. doi:10.1021/cr030697h
35. Tanaka, K.; Toda, F. *Chem. Rev.* **2000,** *100,* 1025–1074. doi:10.1021/cr940089p
36. Wang, G.-W. *Chem. Soc. Rev.* **2013,** *42,* 7668–7700. doi:10.1039/c3cs35526h
37. Achar, T. K.; Bose, A.; Mal, P. *Beilstein J. Org. Chem.* **2017,** *13,* 1907–1931. doi:10.3762/bjoc.13.186
38. Stolle, A.; Szuppa, T.; Leonhardt, S. E. S.; Ondruschka, B. *Chem. Soc. Rev.* **2011,** *40,* 2317–2329. doi:10.1039/c0cs00195c
39. Zhu, S.-E.; Li, F.; Wang, G.-W. *Chem. Soc. Rev.* **2013,** *42,* 7535–7570. doi:10.1039/c3cs35494f
40. Tan, D.; Friščić, T. *Eur. J. Org. Chem.* **2018,** 18–33. doi:10.1002/ejoc.201700961
41. Cheng, B.; Cui, S. *Top. Curr. Chem.* **2015,** *369,* 97–134. doi:10.1007/128_2015_628
42. Delori, A.; Friščić, T.; Jones, W. *CrystEngComm* **2012,** *14,* 2350–2362. doi:10.1039/c2ce06582g
43. Thompson, M. C.; Busch, D. H. *J. Am. Chem. Soc.* **1964,** *86,* 3651–3656. doi:10.1021/ja01072a012
44. Thompson, M. C.; Busch, D. H. *J. Am. Chem. Soc.* **1962,** *84,* 1762–1763. doi:10.1021/ja00868a073

45. Leonardi, M.; Villacampa, M.; Menéndez, J. C. *Chem. Sci.* **2018,** *9,* 2042–2064. doi:10.1039/c7sc05370c

46. Saha, M. L.; Mittal, N.; Bats, J. W.; Schmittel, M. *Chem. Commun.* **2014,** *50,* 12189–12192. doi:10.1039/c4cc05465b

47. Nitschke, J. R. *Chem. Soc. Rev.* **2014,** *43,* 1798–1799. doi:10.1039/c4cs90006e

48. Han, M.; Engelhard, D. M.; Clever, G. H. *Chem. Soc. Rev.* **2014,** *43,* 1848–1860. doi:10.1039/c3cs60473j

49. Saha, M. L.; Schmittel, M. *Org. Biomol. Chem.* **2012,** *10,* 4651–4684. doi:10.1039/c2ob25098e

50. Schmittel, M.; Kalsani, V. *Top. Curr. Chem.* **2005,** *245,* 1–53. doi:10.1007/b98165

51. He, Z.; Jiang, W.; Schalley, C. A. *Chem. Soc. Rev.* **2015,** *44,* 779–789. doi:10.1039/c4cs00305e

52. Osowska, K.; Miljanić, O. Š. *Angew. Chem., Int. Ed.* **2011,** *50,* 8345–8349. doi:10.1002/anie.201102813

53. Ji, Q.; Lirag, R. C.; Miljanić, O. Š. *Chem. Soc. Rev.* **2014,** *43,* 1873–1884. doi:10.1039/c3cs60356c

54. Hubin, T. J.; Busch, D. H. *Coord. Chem. Rev.* **2000,** *200-202,* 5–52. doi:10.1016/s0010-8545(99)00242-8

55. Ferguson, M.; Giri, N.; Huang, X.; Apperley, D.; James, S. L. *Green Chem.* **2014,** *16,* 1374–1382. doi:10.1039/c3gc42141d

56. Orita, A.; Jiang, L.; Nakano, T.; Ma, N.; Otera, J. *Chem. Commun.* **2002,** 1362–1363. doi:10.1039/b203651g

57. Fujita, M.; Yazaki, J.; Ogura, K. *J. Am. Chem. Soc.* **1990,** *112,* 5645–5647. doi:10.1021/ja00170a042

58. Juribašić, M.; Užarević, K.; Gracin, D.; Ćurić, M. *Chem. Commun.* **2014,** *50,* 10287–10290. doi:10.1039/c4cc04423a

59. Hsueh, S.-Y.; Cheng, K.-W.; Lai, C.-C.; Chiu, S.-H. *Angew. Chem., Int. Ed.* **2008,** *47,* 4436–4439. doi:10.1002/anie.200800530

60. Hsu, C.-C.; Chen, N.-C.; Lai, C.-C.; Liu, Y.-H.; Peng, S.-M.; Chiu, S.-H. *Angew. Chem., Int. Ed.* **2008,** *47,* 7475–7478. doi:10.1002/anie.200803056

61. Holler, M.; Stoerkler, T.; Louis, A.; Fischer, F.; Nierengarten, J.-F. *Eur. J. Org. Chem.* **2019,** in press. doi:10.1002/ejoc.201900153

62. Li, H.-G.; Wang, G.-W. *J. Org. Chem.* **2017,** *82,* 6341–6348. doi:10.1021/acs.joc.7b00912

63. Icli, B.; Christinat, N.; Tönnemann, J.; Schüttler, C.; Scopelliti, R.; Severin, K. *J. Am. Chem. Soc.* **2009,** *131,* 3154–3155. doi:10.1021/ja809279s

64. Hai-Gen, L.; Liang, L.; Hui, X.; Guan-Wu, W. *Curr. Org. Chem.* **2018,** *22,* 923–929.

65. Pascu, M.; Ruggi, A.; Scopelliti, R.; Severin, K. *Chem. Commun.* **2013,** *49,* 45–47. doi:10.1039/c2cc37538a

66. Yang, Y.; Bu, F.; Liu, J.; Shakir, I.; Xu, Y. *Chem. Commun.* **2017,** *53,* 7481–7484. doi:10.1039/c7cc02648j

67. Bruns, C. J.; Stoddart, J. F. The Mechanical Bond: A Work of Art. In *Beauty in Chemistry;* Fabbrizzi, L., Ed.; Topics in Current Chemistry, Vol. 323; Springer Berlin: Berlin, Germany, 2011; pp 19–72. doi:10.1007/128_2011_296

68. Raymond, K. N.; Brown, C. J. Inner and Outer Beauty. In *Beauty in Chemistry;* Fabbrizzi, L., Ed.; Topics in Current Chemistry, Vol. 323; Springer: Berlin, Germany, 2012; pp 1–18. doi:10.1007/128_2011_295

69. Mitra, T.; Jelfs, K. E.; Schmidtmann, M.; Ahmed, A.; Chong, S. Y.; Adams, D. J.; Cooper, A. I. *Nat. Chem.* **2013,** *5,* 276–281. doi:10.1038/nchem.1550

70. Rotzler, J.; Mayor, M. *Chem. Soc. Rev.* **2013,** *42,* 44–62. doi:10.1039/c2cs35217f

71. Chakrabarty, R.; Mukherjee, P. S.; Stang, P. J. *Chem. Rev.* **2011,** *111,* 6810–6918. doi:10.1021/cr200077m

72. Giuseppone, N. *Acc. Chem. Res.* **2012,** *45,* 2178–2188. doi:10.1021/ar2002655

73. Sun, Q.-F.; Iwasa, J.; Ogawa, D.; Ishido, Y.; Sato, S.; Ozeki, T.; Sei, Y.; Yamaguchi, K.; Fujita, M. *Science* **2010,** *328,* 1144–1147. doi:10.1126/science.1188605

74. Ponnuswamy, N.; Cougnon, F. B. L.; Clough, J. M.; Pantos, G. D.; Sanders, J. K. M. *Science* **2012,** *338,* 783–785. doi:10.1126/science.1227032

75. Samanta, S. K.; Bats, J. W.; Schmittel, M. *Chem. Commun.* **2014,** *50,* 2364–2366. doi:10.1039/c3cc49476d

76. Su, X.; Aprahamian, I. *Chem. Soc. Rev.* **2014,** *43,* 1963–1981. doi:10.1039/c3cs60385g

77. Osowska, K.; Miljanić, O. Š. *Synlett* **2011,** 1643–1648. doi:10.1055/s-0030-1260815

78. Ji, Q.; Miljanić, O. Š. *J. Org. Chem.* **2013,** *78,* 12710–12716. doi:10.1021/jo402305p

79. Safont-Sempere, M. M.; Fernández, G.; Würthner, F. *Chem. Rev.* **2011,** *111,* 5784–5814. doi:10.1021/cr100357h

80. Nitschke, J. R. *Acc. Chem. Res.* **2007,** *40,* 103–112. doi:10.1021/ar068185n

81. Kassem, S.; van Leeuwen, T.; Lubbe, A. S.; Wilson, M. R.; Feringa, B. L.; Leigh, D. A. *Chem. Soc. Rev.* **2017,** *46,* 2592–2621. doi:10.1039/c7cs00245a

82. Mal, P.; Schultz, D.; Beyeh, K.; Rissanen, K.; Nitschke, J. R. *Angew. Chem., Int. Ed.* **2008,** *47,* 8297–8301. doi:10.1002/anie.200803066

83. Mal, P.; Breiner, B.; Rissanen, K.; Nitschke, J. R. *Science* **2009,** *324,* 1697–1699. doi:10.1126/science.1175313

84. Giri, C.; Sahoo, P. K.; Puttreddy, R.; Rissanen, K.; Mal, P. *Chem. – Eur. J.* **2015,** *21,* 6390–6393. doi:10.1002/chem.201500734

85. Sahoo, P. K.; Bose, A.; Mal, P. *Eur. J. Org. Chem.* **2015,** 6994–6998. doi:10.1002/ejoc.201501039

86. Schultz, D.; Nitschke, J. R. *Angew. Chem., Int. Ed.* **2006,** *45,* 2453–2456. doi:10.1002/anie.200504447

87. Belenguer, A. M.; Friščić, T.; Day, G. M.; Sanders, J. K. M. *Chem. Sci.* **2011,** *2,* 696–700. doi:10.1039/c0sc00533a

88. Herrmann, A. *Chem. Soc. Rev.* **2014,** *43,* 1899–1933. doi:10.1039/c3cs60336a

89. Carnall, J. M. A.; Waudby, C. A.; Belenguer, A. M.; Stuart, M. C. A.; Peyralans, J. J.-P.; Otto, S. *Science* **2010,** *327,* 1502–1506. doi:10.1126/science.1182767

90. Kaabel, S.; Stein, R. S.; Fomitšenko, M.; Järving, I.; Friščić, T.; Aav, R. *Angew. Chem., Int. Ed.* **2019,** in press. doi:10.1002/anie.201813431

91. Jin, Y.; Wang, Q.; Taynton, P.; Zhang, W. *Acc. Chem. Res.* **2014,** *47,* 1575–1586. doi:10.1021/ar500037v

92. Jin, Y.; Yu, C.; Denman, R. J.; Zhang, W. *Chem. Soc. Rev.* **2013,** *42,* 6634–6654. doi:10.1039/c3cs60044k

93. Atkinson, M. B. J.; Bučar, D.-K.; Sokolov, A. N.; Friščić, T.; Robinson, C. N.; Bilal, M. Y.; Sinada, N. G.; Chevannes, A.; MacGillivray, L. R. *Chem. Commun.* **2008,** 5713–5715. doi:10.1039/b812728j

94. Journey, S. N.; Teppang, K. L.; Garcia, C. A.; Brim, S. A.; Onofrei, D.; Addison, J. B.; Holland, G. P.; Purse, B. W. *Chem. Sci.* **2017,** *8,* 7737–7745. doi:10.1039/c7sc03821f

95. Georghiou, P. E.; Schneider, C.; Shamov, G.; Lash, T. D.; Rahman, S.; Sabrina Giddings, D. *Supramol. Chem.* **2016,** *28,* 396–402. doi:10.1080/10610278.2015.1108416

96. Vriezema, D. M.; Comellas Aragonès, M.; Elemans, J. A. A. W.; Cornelissen, J. J. L. M.; Rowan, A. E.; Nolte, R. J. M. *Chem. Rev.* **2005,** *105,* 1445–1490. doi:10.1021/cr0300688

97. Maharramov, A. M.; Mahmudov, K. T.; Kopylovich, M. N.; da Silva, M. F. C. G.; Pombeiro, A. J. L. Activation of Covalent Bonds Through Non-covalent Interactions. *Non-covalent Interactions in the Synthesis and Design of New Compounds;* John Wiley & Sons, Inc: Hoboken, NJ, 2016; pp 1–21. doi:10.1002/9781119113874.ch1

98. Bose, A.; Maiti, S.; Mal, P. Soft Forces in Organic Synthesis by C–N Coupling Reactions. In *Noncovalent Interactions in Catalysis;* Mahmudov, K. T.; Kopylovich, M. N.; Guedes da Silva, M. F. C.; Pombeiro, A. J. L., Eds.; Catalysis Series; Royal Society of Chemistry: Cambridge, United Kingdom, 2019; pp 188–208. doi:10.1039/9781788016490-00188

99. Amendola, V.; Fabbrizzi, L.; Mosca, L. *Chem. Soc. Rev.* **2010,** *39,* 3889–3915. doi:10.1039/b822552b

100. Dougherty, D. A. *Acc. Chem. Res.* **2013,** *46,* 885–893. doi:10.1021/ar300265y

101. Kennedy, C. R.; Lin, S.; Jacobsen, E. N. *Angew. Chem., Int. Ed.* **2016,** *55,* 12596–12624. doi:10.1002/anie.201600547

102. Achar, T. K.; Maiti, S.; Mal, P. *Org. Biomol. Chem.* **2016,** *14,* 4654–4663. doi:10.1039/c6ob00532b

103. Giese, M.; Albrecht, M.; Rissanen, K. *Chem. Rev.* **2015,** *115,* 8867–8895. doi:10.1021/acs.chemrev.5b00156

104. Li, C.-J. *Chem. Rev.* **2005,** *105,* 3095–3166. doi:10.1021/cr030009u

105. Percástegui, E. G.; Mosquera, J.; Nitschke, J. R. *Angew. Chem., Int. Ed.* **2017,** *56,* 9136–9140. doi:10.1002/anie.201705093

106. Breugst, M.; von der Heiden, D.; Schmauck, J. *Synthesis* **2017,** *49,* 3224–3236. doi:10.1055/s-0036-1588838

107. Bulfield, D.; Huber, S. M. *Chem. – Eur. J.* **2016,** *22,* 14434–14450. doi:10.1002/chem.201601844

108. Cavallo, G.; Metrangolo, P.; Pilati, T.; Resnati, G.; Sansotera, M.; Terraneo, G. *Chem. Soc. Rev.* **2010,** *39,* 3772–3783. doi:10.1039/b926232f

109. Turunen, L.; Warzok, U.; Schalley, C. A.; Rissanen, K. *Chem* **2017,** *3,* 861–869. doi:10.1016/j.chempr.2017.08.010

110. Sokolov, A. N.; Bučar, D.-K.; Baltrusaitis, J.; Gu, S. X.; MacGillivray, L. R. *Angew. Chem., Int. Ed.* **2010,** *49,* 4273–4277. doi:10.1002/anie.201000874

111. Stojaković, J.; Farris, B. S.; MacGillivray, L. R. *Chem. Commun.* **2012,** *48,* 7958–7960. doi:10.1039/c2cc33227b

112. Lisac, K.; Topić, F.; Arhangelskis, M.; Cepić, S.; Julien, P. A.; Nickels, C. W.; Morris, A. J.; Friščić, T.; Cinčić, D. *Nat. Commun.* **2019,** *10,* 61. doi:10.1038/s41467-018-07957-6

113. Kumar Achar, T.; Mal, P. *Adv. Synth. Catal.* **2015,** *357,* 3977–3985. doi:10.1002/adsc.201500914

114. Bose, A.; Maiti, S.; Sau, S.; Mal, P. *Chem. Commun.* **2019,** *55,* 2066–2069. doi:10.1039/c8cc09100e

115. Murarka, S.; Antonchick, A. P. Oxidative Heterocycle Formation Using Hypervalent Iodine(III) Reagents. In *Hypervalent Iodine Chemistry;* Wirth, T., Ed.; Topics in Current Chemistry; Springer International Publishing: Cham, Switzerland, 2015; pp 75–104. doi:10.1007/128_2015_647

116. Ribas-Arino, J.; Shiga, M.; Marx, D. *Angew. Chem., Int. Ed.* **2009,** *48,* 4190–4193. doi:10.1002/anie.200900673

117. Ribas-Arino, J.; Marx, D. *Chem. Rev.* **2012,** *112,* 5412–5487. doi:10.1021/cr200399q

118. Friščić, T.; Halasz, I.; Beldon, P. J.; Belenguer, A. M.; Adams, F.; Kimber, S. A. J.; Honkimäki, V.; Dinnebier, R. E. *Nat. Chem.* **2013,** *5,* 66–73. doi:10.1038/nchem.1505

Mechanochemical synthesis of poly(trimethylene carbonate)s: an example of rate acceleration

Sora Park and Jeung Gon Kim[*]

Abstract

Mechanochemical polymerization is a rapidly growing area and a number of polymeric materials can now be obtained through green mechanochemical synthesis. In addition to the general merits of mechanochemistry, such as being solvent-free and resulting in high conversions, we herein explore rate acceleration under ball-milling conditions while the conventional solution-state synthesis suffer from low reactivity. The solvent-free mechanochemical polymerization of trimethylene carbonate using the organocatalysts 1,8-diazabicyclo[5.4.0]undec-7-ene (DBU) and 1,5,7-triazabicyclo[4.4.0]dec-5-ene (TBD) are examined herein. The polymerizations under ball-milling conditions exhibited significant rate enhancements compared to polymerizations in solution. A number of milling parameters were evaluated for the ball-milling polymerization. Temperature increases due to ball collisions and exothermic energy output did not affect the polymerization rate significantly and the initial mixing speed was important for chain-length control. Liquid-assisted grinding was applied for the synthesis of high molecular weight polymers, but it failed to protect the polymer chain from mechanical degradation.

Introduction

Nowadays mechanochemical syntheses are widespread in many areas of chemistry [1-4]. The efficient mixing and energy input induced by mechanical motions have promoted many chemical reactions with superior efficiencies [5]. Sometimes, unexpected outcomes that cannot be achieved by solution synthesis occur, which makes mechanochemistry a topic of rigorous research [6].

In the area of polymer chemistry, the use of mechanical forces has a long history. Strong mechanical forces can break covalent bonds, including strong C–C bonds, thus their utilization has generally focused on destructive approaches [7-9]. Recently, along with rapid progress in mechanochemical small molecule syntheses, the constructive polymeric material synthesis also succeeded. In 2014, Swager and co-workers demonstrated that

poly(phenylene vinylene) could be obtained without any solvent after brief ball milling of monomer and base [10]. The remarkable reactivity exemplified that the general concepts of mechanochemical synthesis are applicable to polymerization reactions. Other examples of polymer syntheses have followed. The Borchardt research team reported the efficient mechanochemical synthesis of poly(azomethine) and poly(phenylene) [11,12]. Our group also contributed to this area by developing a ball-milling promoted high-molecular weight poly(lactic acid) synthesis [13,14] and a solvent-free post-polymerization modification of functional polystyrenes [15]. The Friščić team also showed that poly(ethylene oxide) end group modification is facile under ball-mill conditions [16]. Network polymeric material fabrications were also realized using ball milling [17-19].

As mentioned, many mechanochemical reactions realized exceptional efficiencies that solution synthesis cannot afford [5,20]. Chemical transformations at maximum concentrations benefit from no dilution, which results in fast conversions, as long as efficient mixing is provided. We envisioned that polymerization systems with low propagation efficiencies under solution conditions could be accelerated through mechanochemical ball milling. The organocatalytic polymerization of trimethylene carbonate to form aliphatic polycarbonates was found to be more efficient when using a mechanical ball-milling reaction than a solution polymerization (Scheme 1). The detailed findings are disclosed in this article.

Results and Discussion

Aliphatic polycarbonates are found in many biomedical applications since they have many desirable properties such as high biocompatibility, easy degradation, good mechanical properties, and low toxicity [21-23]. Many synthetic methods have been developed, and the chain-growth ring-opening polymerization of cyclic carbonates, such as trimethylene carbonate (TMC) and its derivatives have been used for the controlled synthesis of high-molecular weight polymers. Among many catalysts, organocatalysts have attracted considerable attention, since the use of nontoxic catalysts warrants a safe use in biomedical applications [24].

The amidine base 1,8-diazabicyclo[5.4.0]undec-7-ene (DBU) is one of the best studied and most popular organocatalysts for ring-opening polymerizations of cyclic carbonates and lactones [25-27]. In contrast to the high activity of lactone polymerization, cyclic carbonate polymerization usually requires long reaction times to achieve high conversions (Table 1) [27]. The DBU-catalyzed polymerization of trimethylene carbonate in chloroform, tetrahydrofuran, toluene, and methylene chloride converted less than 5% monomer into poly(trimethylene carbonate) (PTMC) within 1 h (Table 1, entries 1–8). It generally took 24 hours to produce PTMCs with over 2,000 g/mol number average molecular weights (M_n). Among the tested solvents, the reaction in CH_2Cl_2 was the fastest with 43% conversion after 24 h (Table 1, entry 8).

The same reaction was conducted using ball milling without any solvent added. All reagents were placed in a 10 mL stainless-steel milling jar with three 7 mm diameter stainless-steel balls. The solid-state reaction mixture was placed into a high-speed vibration ball mill. After 30 min of high-speed vibration (30 Hz), 43% conversion was recorded, and PTMC with an M_n of 3930 g/mol was obtained (Table 1, entry 9), which is comparable to that of PTMC obtained from a 24 h reaction with CH_2Cl_2 (Table 1, entry 8). Longer milling times pushed the reaction to higher degrees of polymerization. A one-hour vibration resulted in 75% conversion with an M_n of 7380 g/mol, and the polymerization reached over 90% conversion after 2 h

forward fast ball-milling

mechanochemical polymerization

- solvent-free   - fast reaction   -controlled molecular weight

Scheme 1: Fast trimethylene carbonate polymerization using a solvent-free ball-milling approach.
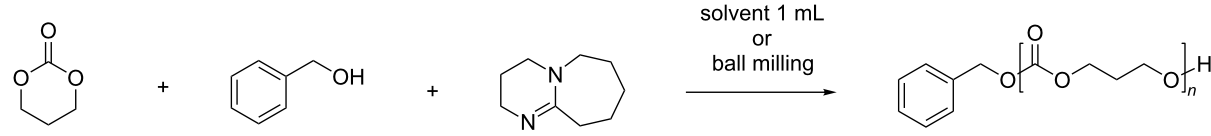
Table 1: DBU-catalyzed polymerization of trimethylene carbonate: solution vs ball milling.[a,b]

entry	solvent	time (h)	conv (%)[c]	M_n (g/mol)[d]	M_w (g/mol)[d]	M_w/M_n
1	chloroform	1	2	–	–	–
2		24	24	2120	2270	1.07
3	THF	1	<1	–	–	–
4		24	5	–	–	–
5	toluene	1	<1	–	–	–
6		24	23	2660	2950	1.10
7	CH_2Cl_2	1	3	–	–	–
8		24	43	3990	4200	1.05
9	ball mill no solvent	0.5	43	3930	4350	1.11
10		1	75	7380	8350	1.14
11		2	93	9230	10600	1.15

[a]Polymerization conditions: TMC (100 mg, 100 equiv), BnOH (1.02 µL, 1 equiv), and DBU (1.46 µL, 1 equiv) in 1 mL of the selected solvent at rt for the solution reactions, or in a 10 mL stainless-steel jar with three 7 mm diameter stainless-steel balls for the ball-milling reactions. [b]The average of two runs is reported for the ball-milling reactions. [c]Determined by ^{1}H NMR spectroscopy. [d]Determined by GPC calibrated with polystyrene standards in tetrahydrofuran (THF) at 40 °C.
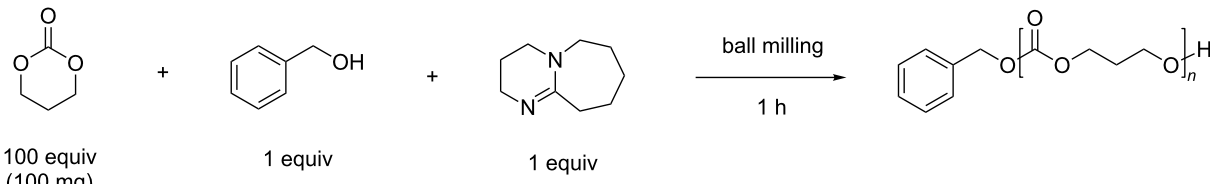
(Table 1, entries 10 and 11). While the reaction rate was higher than that of the solution reactions, polydispersity under ball-milling conditions remained low (M_w/M_n = 1.15). To maintain low polydispersity, fast initiation and slow propagation are required [28]. In the case of ball-milling polymerization, the time required for the physical mixing of monomer, catalyst, and initiator would result in a delayed initiation of the polymerization. However, the relatively slow propagation rate of DBU-mediated trimethyl carbonate polymerization allowed for well-controlled chain lengths. The previous examples on mechanochemical poly(lactic acid) synthesis resulted in broader molecular weight distributions due to the fast propagation rate [13,14].

Variations of the ball-milling parameters were then scrutinized (Table 2). Firstly, the vibration frequency was varied from 10 Hz to 30 Hz. Even with the low vibration experiment at 10 Hz for one hour, 60% of trimethylene carbonate were converted into the corresponding polymer (Table 2, entry 1), which is much faster than conversions observed in solution reactions collected in Table 1. An increase in the vibration frequencies exhibited only a marginal effect. At 20 Hz, only 3% increase in conversion was observed (63%, Table 2, entry 2) and at 30 Hz,

75% conversion was recorded (Table 2, entry 3). The effect of vibration frequency was found to be less pronounced as in the case of lactide polymerizations [13]. The changes in ball numbers and size were investigated as well, which will increase overall mass of a vibration system. The use of five balls instead of three improved the conversion to 84% and the vibration with a 12 mm ball gave 88% conversion. The mass increase in the vibration system resulted in the improvement of reaction efficiency.

The high impact collision energy [28,29] and exothermic nature of the given ring-opening polymerization [30] could increase the temperature of a ball-mill system, which would speed up the polymerization rate [31,32]. To gain insight into thermal effects, we monitored the temperature of the reactor and the reaction mixture (Figure 1). After two hours of high-speed ball milling, the temperature of the reactor and mixture increased to 36 °C. To allow a direct comparison, the solution reactions were also conducted at 40 °C. However, their efficiencies remained far behind those of the ball-milling polymerizations (Table 3). In chloroform (Table 3, entries 1 and 2) and toluene (Table 3, entries 5 and 6) rate enhancements by thermal energy were ob-

Table 2: Vibration frequency and ball size and number effects.[a,b]

| 100 equiv (100 mg) | + | 1 equiv | + | 1 equiv | ball milling 1 h | |

entry	frequency and ball diameter	conv (%)[c]	M_n (g/mol)[d]	M_w (g/mol)[d]	M_w/M_n
1	10 Hz, 7 mm × 3 ea	60	5690	6320	1.11
2	20 Hz, 7 mm × 3 ea	63	6000	6510	1.09
3	30 Hz, 7 mm × 3 ea	75	7380	8350	1.14
4	30 Hz, 7 mm × 5 ea	84	6660	7500	1.13
5	30 Hz, 12 mm × 1 ea	88	6880	7810	1.14

[a]Polymerization conditions: TMC (100 mg, 100 equiv), BnOH (1.02 µL, 1 equiv), and DBU (1.46 µL, 1 equiv) in a 10 mL stainless-steel jar. [b]The average of the two runs is reported. [c]Determined by ^{1}H NMR spectroscopy. [d]Determined by GPC calibrated with polystyrene standards in THF at 40 °C.

served, however, their efficiencies remained much lower than that of the ball-milling PTMC synthesis (Table 3, entries 9 and 10). The observed high efficiency of the mechanochemical transformation could originate from a large increase in concentration as well as a temperature difference [5]. In the synthesis of poly(trimethylene carbonate), the observations imply that concentration is a more influential factor than temperature increase for the rate enhancement under ball-milling conditions.
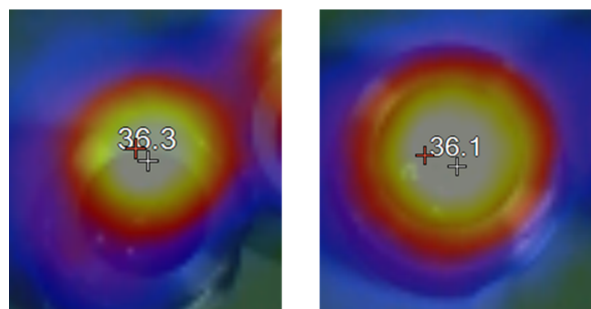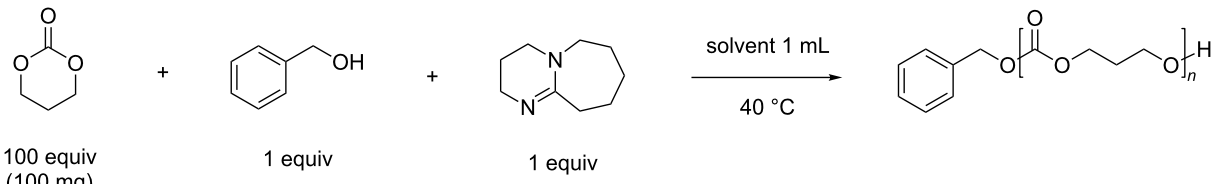
Figure 1: IR thermometer images showing reactor temperatures at the end of the two individual ball-milling reactions (averaged results collected in Table 1, entry 11; individual results, see Supporting Information File 1, left: Table S1, entry 11-1, right: Table S1, entry 11-2).

As another highly reactive organic catalyst, 1,5,7-triazabicyclo[4.4.0]dec-5-ene (TBD) was investigated next. The bicyclic guanidine base TBD has shown better efficiencies than DBU in many chemical transformations including the polymerization of lactides and cyclic carbonates [27,33]. As expected, TBD effectively promoted the polymerization of trimethylene carbonate both, in solution and under solvent-free ball-milling conditions. Nearly quantitative conversions into polymer were
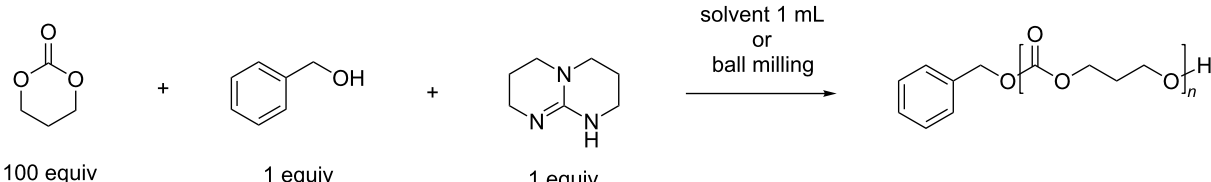
achieved within only 5 min (Table 4). Interestingly, TBD-based ball-milling polymerization did not allow for controlling the molecular weight distribution, resulting in a broad polydispersity (M_w/M_n) of 2.01 (Table 4, entry 5). As mentioned, fast initiation over chain propagation is one of the requirements in a controlled polymerization. While TBD could chemically enhance both the initiation and propagation steps, the mixing of catalyst, monomer, and initiator by heterogeneous ball milling may physically limit the initiation rate. Thus, a relatively slow initiation process resulted in poor molecular weight control. Most solution polymerizations had no issues with mixing and maintained good molecular weight control. The use of slower polymerization systems is advised for controlled polymerizations under ball-milling conditions.

Next, a high degree of polymerization was pursued. Polymerizations were conducted under the same conditions but with a higher monomer to initiator ratio ([TMC]:[I]:[DBU] = 200:1:2) (Table 5). The reaction reached over 90% conversion after 3 h. However, the molecular weight did not increase at all. The competitive degradation of poly(trimethyl carbonate) became significant after 100 degrees of polymerization. To validate mechanical degradation of PTMC under ball-milling conditions, high molecular weight PTMC (M_n = 22900 g/mol) was synthesized and grinded under the same mechanical conditions of Table 5, entry 1, which led to degradation to lower molecular weight (M_n = 8220 g/mol). In our previous study on poly(lactic acid) synthesis, liquid-assisted grinding (LAG), the addition of a very small amount of a liquid, prevented chain-degradation from high impact collisions, and afforded PLA with over 100,000 g/mol. Thus, LAG was also tested in the PTMC synthesis [13,14] with toluene and THF as liquids. A catalytic

Table 3: DBU-catalyzed polymerization of trimethylene carbonate at 40 °C.[a]

entry	solvent	time (h)	conv (%)[b]	M_n (g/mol)[c]	M_w (g/mol)[c]	M_w/M_n
1	chloroform	1	3	–	–	–
2		24	41	3500	3780	1.07
3	THF	1	<1	–	–	–
4		24	6	–	–	–
5	toluene	1	<1	–	–	–
6		24	70	7130	8380	1.13
7	CH_2Cl_2	1	4	–	–	–
8		41	41	3000	3210	1.07
9	ball milling	1	75	7380	8350	1.14
10	ball milling (36 °C)	2	93	9230	10600	1.15

[a]Polymerization conditions: TMC (100 mg, 100 equiv), BnOH (1.02 µL, 1 equiv), and DBU (1.46 µL, 1 equiv) in 1 mL of the selected solvent at 40 °C. [b]Determined by ^{1}H NMR spectroscopy. [c]Determined by GPC calibrated with polystyrene standards in tetrahydrofuran (THF) at 40 °C.

Table 4: TBD-catalyzed polymerization of trimethylene carbonate: solution vs ball milling.[a]

entry	solvent	time (min)	conv (%)[b]	M_n (g/mol)[c]	M_w (g/mol)[c]	M_w/M_n
1	toluene	5	99	12300	20000	1.71
2	$CHCl_3$	5	96	8650	9810	1.13
3	CH_2Cl_2	5	86	9330	10500	1.12
4	THF	5	76	7720	8750	1.09
5[d]	ball mill	5	99	12200	24400	2.01

[a]Polymerization conditions: (solution) TMC (100 mg, 100 equiv), BnOH (1.02 µL, 1 equiv), and TBD (1.4 mg, 1 equiv) in 1 mL selected solvent at rt; (ball milling) in a 10 mL stainless-steel jar with three stainless-steel balls with 7 mm diameter. [b]Determined by ^{1}H NMR spectroscopy. [c]Determined by GPC calibrated with polystyrene standards in tetrahydrofuran (THF) at 40 °C. [d]Average of two runs is reported.

amount of liquid (10 or 20 µL to 100 mg TMC), however, failed to protect the poly(trimethylene carbonate) chain from mechanical degradation and similar molecular weights were ob-tained, regardless of LAG. The LAG for mechanochemical po-lymerization reactions has been studied only in limited cases so far and the exact working mechanism is currently obscure. To

Table 5: PTMC synthesis with a high monomer to initiator ratio.[a]

| | 200 equiv (100 mg) | + | 1 equiv | + | 2 equiv | ball milling → | | | |

entry	liquid additives	time	conv (%)[b]	M_n (g/mol)[c]	M_w (g/mol)[c]	M_w/M_n
1	none	3 h	97	10900	13600	1.24
2	toluene (10 µL)	3 h	86	11900	13100	1.10
3	toluene (20 µL)	3 h	91	11500	13700	1.19
4	THF (20 µL)	3 h	96	11400	13900	1.22

[a]Polymerization conditions: TMC (100 mg, 200 equiv), BnOH (0.49 µL, 1 equiv), and DBU (1.46 µL, 2 equiv) in a 10 mL stainless-steel jar with three 7 mm diameter stainless-steel balls. [b]Determined by ^{1}H NMR spectroscopy. [c]Determined by GPC calibrated with polystyrene standards in tetrahydrofuran (THF) at 40 °C.

have a better understanding of LAG on chain protection, extensive studies are currently in progress.

Conclusion

A mechanochemical method, ball milling, was applied to the synthesis of poly(trimethylene carbonate). The representative organocatalyst, DBU, exhibited excellent polymerization efficiency and good chain-length control under solvent-free conditions. When compared to the very low rate obtained under solution conditions, this demonstrates that mechanochemical reactions can improve reaction efficiency and greenness. The use of TBD truly enhanced the efficiency, and all polymerizations reached completion within 5 min, despite physical mixing limitations. However, the mechanochemical polymerization was accompanied by degradation processes, which limited the molecular weight to 10,000 g/mol. Liquid-assisted grinding did not show any protective effect, and the search for other parameters to mitigate polymer-chain breaking is currently in progress.

Experimental

General considerations. Chemical reagents obtained from commercial sources were used without further purification. 1,8-Diazabicyclo[5.4.0]undec-7-ene (DBU) was distilled over CaH$_2$. All solvents (THF, CH$_2$Cl$_2$, CHCl$_3$, and toluene) were dried over a mixture of pre-activated neutral alumina and 3 Å molecular sieves. A Retsch Mixer Mill MM 400 was used for the ball-milling experiments with a 10 mL stainless-steel vessel and 7 mm stainless balls. ^{1}H NMR spectra were recorded with a 400 MHz Bruker Avance III HD Fourier transform NMR spectrometer and all signals were referenced to residual protonated solvent. Gel permeation chromatography (GPC) analyses with refractive index (RI) detection were used to determine the num-

ber-averaged molecular weights (M_n), weight-averaged molecular weights (M_w), and polydispersities (M_w/M_n). The RI measurements were carried out using an instrument set composed of a Waters 1515 isocratic pump, a 2414 differential refractive index detector, and a column-heating module with Shodex KF-804, KF-803, and KF-802.5 columns in series. The columns were eluted with tetrahydrofuran (preservative-free HPLC grade, Fisher) at 40 °C at 1.0 mL/min and calibrated using 14 monodisperse polystyrene standards (Alfa Aesar). The temperature was recorded using a Fluke VT04 Visual IR thermometer.

Synthesis of trimethylene carbonate. 1,3-Propanediol (4.72 mL, 0.657 mol) and ethyl chloroformate (12.5 mL, 0.131 mol) were dissolved in anhydrous THF (0.13 L). The mixture was stirred in an ice bath for 1 h and a solution of triethylamine (19.2 mL, 0.138 mol) in THF (9 mL) was slowly added. Then, the solution was transferred to ambient temperature and stirred for 2 h. The reaction mixture was filtered and the volume of the solution was reduced to 40–50 mL. The mixture was kept in a freezer for 12 h and the precipitate was recovered by filtration. The recovered solid was recrystallized in ethyl acetate and sublimed (2.9 g, 43%). ^{1}H NMR (400 MHz, CDCl$_3$) δ 4.47–4.44 (t, 4H), 2.18–2.12 (quintet, 2H).

Representative procedure for mechanochemical solvent-free poly(trimethylene carbonate) synthesis (Table 1, entry 11). Three 7 mm stainless-steel milling balls were placed in a 10 mL stainless-steel milling container and trimethylene carbonate (0.100 g), benzyl alcohol (1.02 µL), and DBU (1.46 µL) were added. The milling vessel was placed in a vibrational ball mill and vibrated at 30 Hz. After 2 hours, the vessel was opened and

benzoic acid (10 mg) was added followed by an additional 5 minutes of milling to quench the polymerization. To avoid data inconsistency due to inhomogeneity, all material was dissolved in methylene chloride and an aliquot was subjected to analysis by ^{1}H NMR spectroscopy and GPC measurements to determine the conversion and molecular weight.

Supporting Information

Supporting Information File 1
Raw data for tables, GPC and NMR spectra.
[https://www.beilstein-journals.org/bjoc/content/
supplementary/1860-5397-15-93-S1.pdf]

Acknowledgements

ORCID® iDs

Jeung Gon Kim - https://orcid.org/0000-0003-1685-2833

References

1. James, S. L.; Friščić, T. *Chem. Soc. Rev.* **2013,** *42,* 7494–7496. doi:10.1039/c3cs90058d
2. James, S. L.; Adams, C. J.; Bolm, C.; Braga, D.; Collier, P.; Friščić, T.; Grepioni, F.; Harris, K. D. M.; Hyett, G.; Jones, W.; Krebs, A.; Mack, J.; Maini, L.; Orpen, A. G.; Parkin, I. P.; Shearouse, W. C.; Steed, J. W.; Waddell, D. C. *Chem. Soc. Rev.* **2012,** *41,* 413–447. doi:10.1039/c1cs15171a
3. Hernández, J. G. *Beilstein J. Org. Chem.* **2017,** *13,* 2372–2373. doi:10.3762/bjoc.13.234
4. Do, J.-L.; Friščić, T. *ACS Cent. Sci.* **2017,** *3,* 13–19. doi:10.1021/acscentsci.6b00277
5. Howard, J. L.; Cao, Q.; Browne, D. L. *Chem. Sci.* **2018,** *9,* 3080–3094. doi:10.1039/c7sc05371a
6. Hernández, J. G.; Bolm, C. *J. Org. Chem.* **2017,** *82,* 4007–4019. doi:10.1021/acs.joc.6b02887
7. Li, J.; Nagamani, C.; Moore, J. S. *Acc. Chem. Res.* **2015,** *48,* 2181–2190. doi:10.1021/acs.accounts.5b00184
8. Kean, Z. S.; Craig, S. L. *Polymer* **2012,** *53,* 1035–1048. doi:10.1016/j.polymer.2012.01.018
9. Chen, Z.; Mercer, J. A. M.; Zhu, X.; Romaniuk, J. A. H.; Pfattner, R.; Cegelski, L.; Martinez, T. J.; Burns, N. Z.; Xia, Y. *Science* **2017,** *357,* 475–479. doi:10.1126/science.aan2797
10. Ravnsbæk, J. B.; Swager, T. M. *ACS Macro Lett.* **2014,** *3,* 305–309. doi:10.1021/mz500098r
11. Grätz, S.; Borchardt, L. *RSC Adv.* **2016,** *6,* 64799–64802. doi:10.1039/c6ra15677k
12. Grätz, S.; Wolfrum, B.; Borchardt, L. *Green Chem.* **2017,** *19,* 2973–2979. doi:10.1039/c7gc00693d
13. Ohn, N.; Shin, J.; Kim, S. S.; Kim, J. G. *ChemSusChem* **2017,** *10,* 3529–3533. doi:10.1002/cssc.201700873
14. Lee, G. S.; Moon, B. R.; Jeong, H.; Shin, J.; Kim, J. G. *Polym. Chem.* **2019,** *10,* 539–545. doi:10.1039/c8py01520a
15. Ohn, N.; Kim, J. G. *ACS Macro Lett.* **2018,** *7,* 561–565. doi:10.1021/acsmacrolett.8b00171
16. Malca, M. Y.; Ferko, P.-O.; Friščić, T.; Moores, A. *Beilstein J. Org. Chem.* **2017,** *13,* 1963–1968. doi:10.3762/bjoc.13.191
17. Zhu, X.; Tian, C.; Jin, T.; Browning, K. L.; Sacci, R. L.; Veith, G. M.; Dai, S. *ACS Macro Lett.* **2017,** *6,* 1056–1059. doi:10.1021/acsmacrolett.7b00480
18. Grätz, S.; Oltermann, M.; Troschke, E.; Paasch, S.; Krause, S.; Brunner, E.; Borchardt, L. *J. Mater. Chem. A* **2018,** *6,* 21901–21905. doi:10.1039/c8ta03684e
19. Grätz, S.; Beyer, D.; Tkachova, V.; Hellmann, S.; Berger, R.; Feng, X.; Borchardt, L. *Chem. Commun.* **2018,** *54,* 5307–5310. doi:10.1039/c8cc01993b
20. Immohr, S.; Felderhoff, M.; Weidenthaler, C.; Schüth, F. *Angew. Chem., Int. Ed.* **2013,** *52,* 12688–12691. doi:10.1002/anie.201305992
21. Dai, Y.; Zhang, X. *Polym. Chem.* **2017,** *8,* 7429–7437. doi:10.1039/c7py01815k
22. Xu, J.; Feng, E.; Song, J. *J. Appl. Polym. Sci.* **2014,** *131,* 39822. doi:10.1002/app.39822
23. Feng, J.; Zhuo, R.-X.; Zhang, X.-Z. *Prog. Polym. Sci.* **2012,** *37,* 211–236. doi:10.1016/j.progpolymsci.2011.07.008
24. Kamber, N. E.; Jeong, W.; Waymouth, R. M.; Pratt, R. C.; Lohmeijer, B. G. G.; Hedrick, J. L. *Chem. Rev.* **2007,** *107,* 5813–5840. doi:10.1021/cr068415b
25. Sherck, N. J.; Kim, H. C.; Won, Y.-Y. *Macromolecules* **2016,** *49,* 4699–4713. doi:10.1021/acs.macromol.6b00621
26. Nederberg, F.; Lohmeijer, B. G. G.; Leibfarth, F.; Pratt, R. C.; Choi, J.; Dove, A. P.; Waymouth, R. M.; Hedrick, J. L. *Biomacromolecules* **2007,** *8,* 153–160. doi:10.1021/bm060795n
27. Lohmeijer, B. G. G.; Pratt, R. C.; Leibfarth, F.; Logan, J. W.; Long, D. A.; Dove, A. P.; Nederberg, F.; Choi, J.; Wade, C.; Waymouth, R. M.; Hedrick, J. L. *Macromolecules* **2006,** *39,* 8574–8583. doi:10.1021/ma0619381
28. Andersen, J.; Mack, J. *Angew. Chem., Int. Ed.* **2018,** *57,* 13062–13065. doi:10.1002/anie.201805263
29. Kulla, H.; Wilke, M.; Fischer, F.; Röllig, M.; Maierhofer, C.; Emmerling, F. *Chem. Commun.* **2017,** *53,* 1664–1667. doi:10.1039/c6cc08950j
30. Matsuo, J.; Aoki, K.; Sanda, F.; Endo, T. *Macromolecules* **1998,** *31,* 4432–4438. doi:10.1021/ma971227q
31. Hutchings, B. P.; Crawford, D. E.; Gao, L.; Hu, P.; James, S. L. *Angew. Chem., Int. Ed.* **2017,** *56,* 15252–15256. doi:10.1002/anie.201706723
32. Užarević, K.; Ferdelji, N.; Mrla, T.; Julien, P. A.; Halasz, B.; Friščić, T.; Halasz, I. *Chem. Sci.* **2018,** *9,* 2525–2532. doi:10.1039/c7sc05312f
33. Baral, E. R.; Lee, J. H.; Kim, J. G. *J. Org. Chem.* **2018,** *83,* 11768–11776. doi:10.1021/acs.joc.8b01695

Unexpected polymorphism during a catalyzed mechanochemical Knoevenagel condensation

Sebastian Haferkamp[1,2], Andrea Paul[1], Adam A. L. Michalchuk[1]
and Franziska Emmerling[*1,2]

Abstract

The transformation of a base-catalyzed, mechano-assisted Knoevenagel condensation of mono-fluorinated benzaldehyde derivatives (*p*-, *m*-, *o*-benzaldehyde) with malonodinitrile was investigated in situ and in real time. Upon milling, the *para*-substituted product was found to crystallize initially into two different polymorphic forms, depending on the quantity of catalyst used. For low catalyst concentrations, a mechanically metastable phase (monoclinic) was initially formed, converting to the mechanically stable phase (triclinic) upon further grinding. Instead, higher catalyst concentrations crystallize directly as the triclinic product. Inclusion of catalyst in the final product, as evidenced by mass spectrometric analysis, suggests this complex polymorphic pathway may be due to seeding effects. Multivariate analysis for the in situ Raman spectra supports this complex formation pathway, and offers a new approach to monitoring multi-phase reactions during ball milling.

Introduction

Mechanochemistry offers a wide array of applications. It is used widely for synthesis of inorganic, metal-organic, and organic molecules and materials [1]. Interest in these methods stems largely from the fact that they are efficient and more environmentally friendly as compared to traditional approaches [2,3]. Mechanochemistry is a well-established method for the synthesis of coordination polymers, the formation of cocrystals, and in C–C coupling reactions [4-7].

Despite the increasing use of mechanochemistry, there is still a lack in understanding of the underlying processes involved during mechanically-facilitated reactions. This is particularly true of the potential role of transient polymorphic phases [8] and seeding effects [9] in understanding reaction kinetics of these processes. Early insight into formation pathways was provided ex situ, in which the mechanical treatment was stopped, and powder removed for analysis [10,11]. More recently,

further detail has been gained by monitoring mechanochemical transformations in real time, using in situ techniques [12,13]. The first in situ and real time study was performed by X-ray powder diffraction (XRPD) to monitor transformations during a milling process [12]. In situ studies allow novel insight into the mechanism of a mechanochemical process, without changing the reaction environment. It was subsequently demonstrated how a combination of different in situ methods can provide more thorough investigation of mechanochemical reaction mechanisms [14-16]. Of particular benefit to synthetic reactions, such as C–C bond formation [17,18], the use of Raman spectroscopy is of great interest. The characteristic bands are usually well separated, and the course of the reaction can be followed easily. The advantage of Raman spectroscopy was recently demonstrated [19], where its combination with XRPD allowed monitoring of the mechanochemically catalyzed Knoevenagel condensation in detail.

Results and Discussion

The catalyzed Knoevenagel condensations of mono-fluorinated benzaldehydes **1a**–**c** with malonodinitrile (**2**) are depicted in Scheme 1. In contrast to previous work, which reported the un-catalyzed reaction [19], piperidine was used as a basic catalyst. This was done as the inclusion of the base led to crystallization of the corresponding products **3a**–**c** during the milling process. In contrast, crystallization during the base-free reaction required an ex situ aging step. Figure 1 shows the XRPD pattern of the substrate **2** and the product **3a**. Due to the liquid state of the fluorinated benzaldehydes **1a**–**c** no XRPD pattern could be recorded.

For the reaction of **1a** with **2**, the amount of catalyst was varied and the reaction monitored in each case. XRPD analysis con-
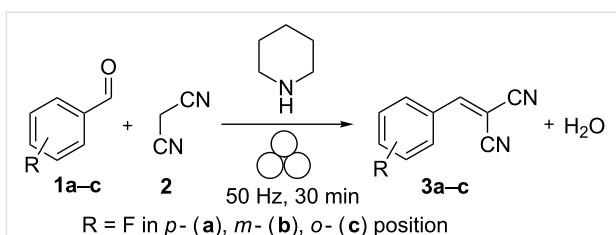
Scheme 1: Catalyzed mechanochemical Knoevenagel condensation of fluorobenzaldehydes and malonodinitrile. The milling process is symbolized by the three balls, proposed by Hanusa et al. [20].
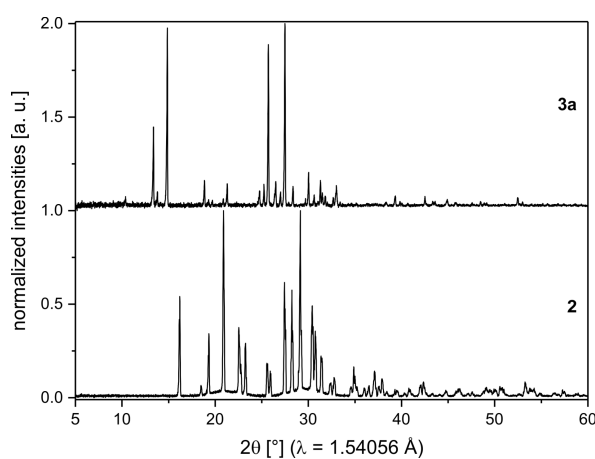
Figure 1: Comparison of XRPD pattern of malonodinitrile (**2**) and (*p*-fluorobenzylidene) malonodinitrile (**3a**). The patterns are baseline corrected.

firmed that, independent of the amount of catalyst, the same bulk product was formed. The intensity of the product powder color decreased from a deep orange to white, with decreasing quantity of catalyst (Figure 2b). Importantly, none of the
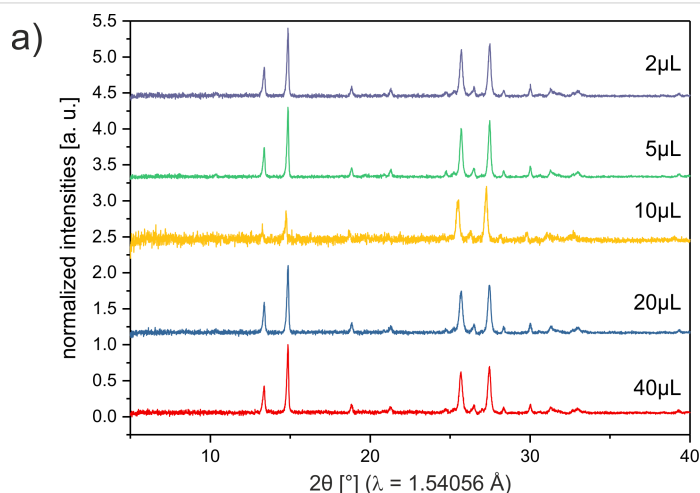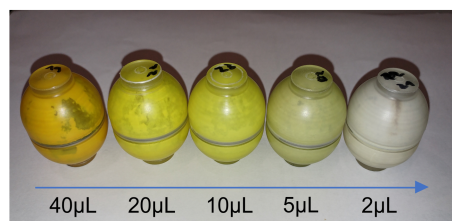
Figure 2: a) XRPD pattern of (*p*-fluorobenzylidene)malonodinitrile (**3a**) direct after the synthesis with different amounts of catalyst. b) Color change of the product **3a** after the synthesis with different amounts of catalyst. The amount is reduced in the direction of the arrow.

starting materials are colored, and the color of the product phase was found to vary systematically with increasing catalyst concentration. This coloring was observed throughout the bulk, which therefore suggested that the catalyst was incorporated into the structure of the solid product. Such effects have been previously reported, and have the potential to seed nucleation of polymorphic phases [21]. For that reason, mass spectrometric analyses of the powder phases were performed (Figure 3). The relative intensity of the peak corresponding to piperidine (Figure 3 red box) decreases systematically with respect to that of **3a** (Figure 3 blue box). Hence, this suggests that the catalyst is indeed present in the solid product. Further analysis is required to understand the nature of catalyst incorporation, and hence the origin of color.

The reactions containing between 40 µL and 5 µL catalyst show conversion of the substrates directly into the mechanically stable triclinic product phase, according to real-time in situ XRPD analysis (Supporting Information File 1, Figure S1). Consistent with previous reports [15], **2** melted at the beginning of the reaction and remained liquid or molten for the first few minutes of milling (Supporting Information File 1). This is due to increased temperatures within the jar during milling (T_{melt}(**2**) = 32 °C). Shortly after melting of **2**, Bragg reflections of a crystalline product phase were found to form (Figure 4). Comparison to literature crystallographic data suggests this to be the triclinic phase (**t3a**). This phase remained stable upon continued milling.

In contrast, reactions conducted with 2 µL were found to be more complex (Figure 4). Shortly after the melting of **2**, Bragg reflections were observed and remained visible for a period of approximately two minutes (Figure 4, gray box). These reflections, however, were found to correspond to the monoclinic phase of the product (**m3a**) [22,23]. Phase **m3a** remained stable under mechanical treatment for a few minutes, before transforming abruptly (over a period of 90 seconds) to the **t3a** phase. Having observed the inclusion of catalyst into the final product phase (see Figure 3), we suggest this change in polymorphic behavior to result from a templating phenomenon, which dominates at higher concentrations of catalyst.

To better observe this transformation pathway, the reaction (2 µL catalyst) was repeated at 30 Hz in order to extend the lifetime of **m3a**. The in situ XRPD pattern and Raman spectra are shown in Figure 4b and d, respectively. Decreasing the milling frequency has a number of notable effects. First, the lifetime of the initial molten/liquid phase was nearly doubled, suggesting that mechanical treatment has an important effect on this largely solution-phase reaction. This may be a result of heating, mechanical activation of the fluid-phase molecules or differences in energy for nucleation. While further work is required in this area, it is clear that mechanical treatment can have notable influence on 'solution-phase' chemistry. Second, the lifetime of the intermediate phase was extended. This allowed us to collect higher resolution XRPD data by extracting a sample from the milling vessel and confirming this intermediate to be the phase,

Figure 3: Mass spectra of the different products of **3a**. Red: peak off the molecular ion [M + H]+ of piperidine (*m/z* ≈ 86). Blue: peak of the molecular ion [M + H]+ of **3a** (*m/z* ≈ 173).
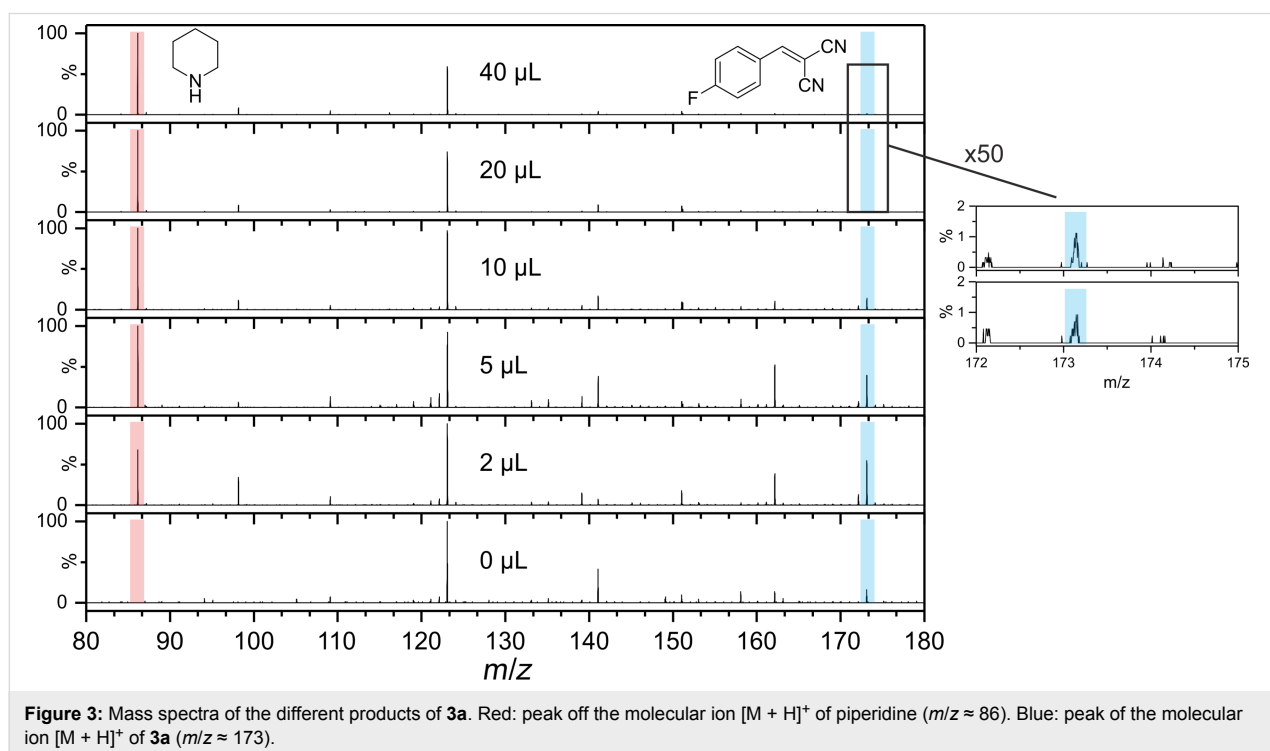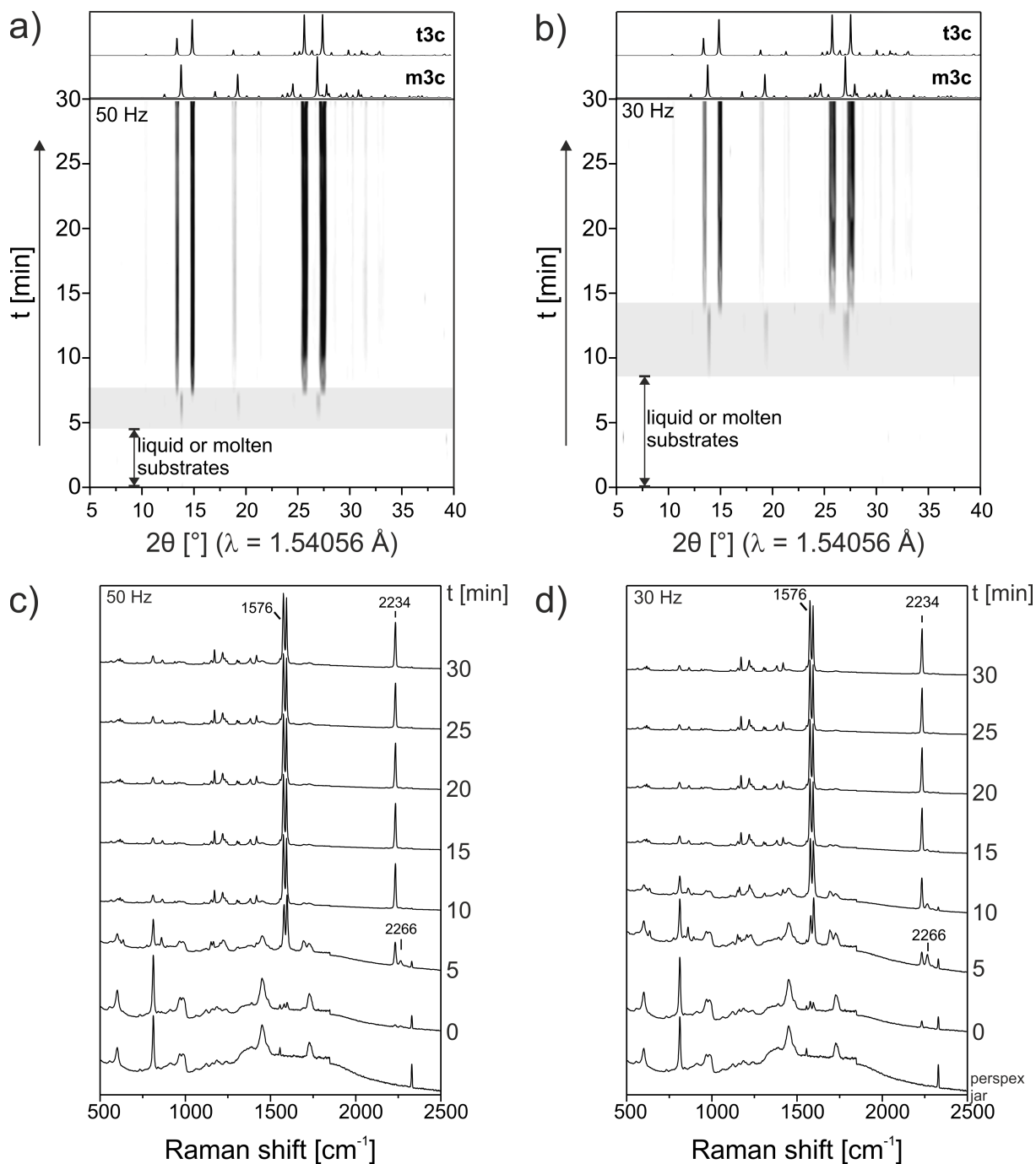
Figure 4: a) In situ XRPD pattern of the mechanochemical Knoevenagel condensation of **1a** and **2** with 2 µL catalyst at 50 Hz. Gray box: intermediate phase. b) In situ XRPD pattern of the reaction with a milling frequency of 30 Hz. c) In situ Raman spectra of the mechanochemical Knoevenagel condensation of **1a** and **2** with 2 µL catalyst at 50 Hz. d) In situ Raman spectra of the reaction with a milling frequency of 30 Hz. Raman bands: 1576 cm^{-1} – C-C stretching vibration; 2234 cm^{-1} – C≡N stretching vibration of the product; 2266 cm^{-1} – C≡N stretching vibration of malonodinitrile.

m3a (Figure 5). Despite this extension, however, the subsequent transformation **m3a** → **t3a** again occurs abruptly (ca. 120 seconds). This suggests that the transformation may result from the accumulation of defects within **m3a**, or upon comminution of the product phase [24].

While the XRPD patterns clearly show the occurrence of a transition phase within the first minutes of the reaction, the Raman spectra represent a superposition of all spectral components. These spectral features often remain unchanged for polymorphic series. For this reason, it is difficult to employ reliably
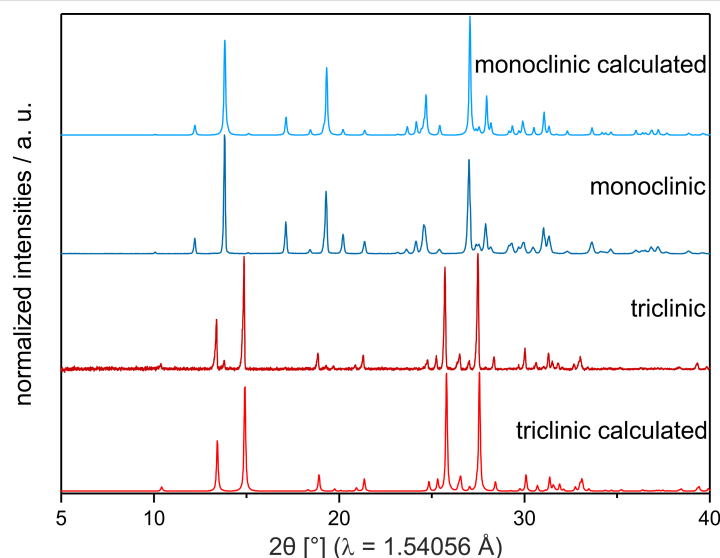
Figure 5: Comparison of XRPD patterns of both polymorphs of the product **3a**. Red: triclinic polymorph **t3a**. Blue: monoclinic polymorph **m3a**. The light XRPD pattern were calculated from single crystal diffraction data.

Raman spectroscopy for in situ mechanochemical data. Hence, despite its availability in many laboratories, in situ real-time monitoring of mechanochemistry by Raman scattering has remained underexplored. We therefore sought to identify a means to resolve this issue, using multivariate methods to analyze the reaction. Principal component analysis (PCA) is a bilinear modelling method [25,26] that helps to extract the main information from multi-dimensional data (here a time series of Raman spectra). The information contained within the original spectral variables is projected onto a small number of underlying ('latent') variables, called the principal components (PC). Typically, the first PC covers the highest variance, the second and following PCs cover less information. All PCs are orthogonal to one-another. Although the PCs themselves do not represent quantitative data, they represent the underlying chemical or physical processes. In order to understand the results of PCA, both scores and loadings must be scrutinized in parallel. Whereas the scores contain information regarding the samples, the loadings provide information on the variables. High loading values indicate spectral variables of high importance. The same applies for large negative values.

PCA of the in situ Raman spectra in this work reveals two principal components (PC) for both milling reactions (Supporting Information File 1, Figure S2a–d). The score and loading plots for the first (PC1) and second (PC2) principal component depicted in Figure 6a,b refer to the reaction performed at 30 Hz. PC1 and PC2 account for 96% and 3% of the spectral variance. The scores of PC1 exhibit high values at the beginning of the reaction. With increased milling time, the PC1 scores decline and eventually become negative, indicating the conversion of

1a to **3a**. Concerning PC1 in Figure 6b, the positive part corresponds to spectral features of **1a** and PMMA, and the negative part indicates features of **3a**. In contrast, the scores of PC2 are initially negative, rise to a peak value, and subsequently fall to zero (cf. Figure 6a). The spectral loadings of PC2 in Figure 6b show a dominant positive structure, which resembles the negative profile of PC1, albeit shifted slightly towards larger wavenumbers. We therefore conclude that PC2 represents an independent (orthogonality among principal components) transient species. A comparison with the Raman spectra summarized in Figure S2 indicates that PC2 correlates well with the formation of **m3a**. Identical results were found for the PCA of in situ Raman spectra at 50 Hz milling frequency (cf. Supporting Information File 1, Figure S2). However, the reduction of the milling frequency delays the onset of product formation. The kinetic profile obtained by PCA correlates well with XRPD data (cf. Figure 6a), in which the transformation is monitored by the normalized intensities of Bragg reflections at $2\theta = 13.87°$ and $14.78°$. While the XRPD patterns indicate formation of two clearly separated compounds, the Raman spectra suggest the parallel presence of **1a, m3a** and **t3a**.

Multivariate curve resolution (MCR) aims to extract information on the pure compounds [27]. In our case, the time series of Raman spectra may be considered as a superposition of all compounds present at a certain time of the reaction. In contrast to PCA, where only the variance of data is evaluated, in MCR chemical knowledge on the number of involved compounds, some constraints such as non-negativity are included. As a result, relative component concentrations as a function of time and the corresponding spectra can be evaluated. In this case,

Figure 6: Results of multivariate data analysis of Raman spectra for 30 Hz milling experiments. Principal component analysis (PCA) of Raman data, showing (a) scores, and (b) loadings for (black) PC1 and (blue) PC2. (a) PC1 scores show a decrease in spectral component of **1a** in the first minutes – cf. positive spectral signature of loadings of PC1 in (b). The negative scores of PC1 correspond to the negative part of PC1 loadings, i.e., **t3c**. Scores of PC2 indicate the presence of a compound with spectral features resembling **m3c**. For comparison, intensity of PXRD Bragg peaks at (green) 2θ = 13.87° and (red) 2θ = 14.78° are given in (a) for **m3c** and **t3c,** respectively. Multivariate curve resolution (MCR) of (c) composition profiles, and (d) component spectra. Coloring of (c) and (d) are used to indicate corresponding data. (c) Relative phase composition of (black) **1a** and the (grey) PMMA-background decrease within the first minutes of the reaction. Simultaneous formation of (green) **m3c**, shows pronounced increase followed immediately by a rapid decrease. The latter is accompanied by the formation of (red) **t3c**. In the final stage of the reaction, only contributions from **t3c** and the PMMA background can be observed.

four spectral compounds were used in form of an initial guess for MCR, namely fluorinated benzaldehyde, PMMA (background from the milling jar), monoclinic and triclinic fluorobenzylidene malonodinitrile.

MCR analysis without an initial guess resulted in models with three and four components, each containing mixed information from more than one chemical compound (not shown). However, MCR using spectra from the pure materials for an "initial guess" leads to component profiles for **m3a** and **t3a** (Figure 6c) that are in good agreement with XRPD results (Figure 6a and c). The component spectra obtained by MCR can be assigned to the **m3a, t3a, 1a,** and the milling jar, PMMA (Figure 6d, Figure S3, Supporting Information File 1). Negligible contributions of spectral features relating to (**2**) were observed. It should be noted that all component spectra, especially those of (**1a**) contain spectral properties belonging to PMMA (shaded areas in Figure S3, Supporting Information File 1).

The mechanochemical catalyzed reactions of **1b** and **1c** with **2** performed with 2 µL piperidine did not exhibit the same polymorphic transformations as with **1a.** Instead, reactions using **1b** and **1c** led directly to formation of **m3b** [23] and **m3c** [28], respectively, at both 30 Hz and 50 Hz milling frequency (Figures S4 and S5 in Supporting Information File 1).

Conclusion

The mechano-assisted catalyzed Knoevenagel condensation of mono-fluorinated benzaldehydes and malonodinitrile was explored in situ and in real-time by tandem synchrotron powder X-ray diffraction and Raman spectroscopy. For synthesis of *p*-fluorobenzylidene malonodinitrile (**3a**) the reaction product crystallizes according to two different pathways, depending on the concentration of base catalyst. At high concentrations of catalyst, the triclinic product phase is formed, and remains stable under continued mechanical treatment. In contrast, at lower concentrations of catalyst, the product crystallizes first as

the monoclinic phase. Subsequent milling causes this phase to transform abruptly to the triclinic phase. Due to the inclusion of base catalyst in the final product, we suggest this difference to be the result of a templating effect, which dominates at higher concentrations. For the reaction of *meta-* and *ortho*-substituted substrates, crystallization occurs directly into the monoclinic phase, regardless of milling conditions or catalyst concentration.

Multivariate analysis of in situ Raman spectra by both PCA and MCR suggests the formation of a transient product with almost identical spectral properties as the final product, the triclinic polymorph of **3a**. These results are consistent with those of XRPD analysis. Hence, we here identify a new approach to monitoring mechanically-induced polymorphic transitions in situ and in real-time.

Experimental

Materials: All chemicals used in this work were taken as supplied (>97% purity), without further purification.

Syntheses: The following procedure is similar as described in our previous work [29]. Milling experiments were performed using a commercially available vibratory ball mill (Pulverisette 23, Fritsch, Germany). For each experiment, stoichiometric quantities of reactants *p*-, *m*- and *o*- fluorobenzaldehyde (500 mg, ca. 4.03 mmol) and malonodinitrile (266.1 mg, ca. 4.03 mmol) were weighed into Perspex milling jars (10 mL). To each jar, a quantity (defined in the main text) of piperidine was added as catalyst. Two stainless steel milling balls (4 g, 10 mm diameter) were also included in each milling jar. The reactions were conducted at 30 Hz or 50 Hz, as indicated in the main text. The final products were characterized by XRPD.

X-ray powder diffraction (XRPD): All samples were characterized by XRPD analysis using a Bruker D8 diffractometer with Cu-Kα_1 radiation (λ = 1.54106 Å) in a range of 5.0° ≤ 2 θ ≤ 40°. The data were obtained in transmission mode with a step size of 0.009° and an acquisition time of 3 s per step.

In situ investigations: In situ and real-time monitoring of the milling reactions was conducted at the mySpot Beamline (BESSY II, Helmholtz Centre Berlin for Materials and Energy). The same mechanochemical reactor was used for these investigations, as was used for laboratory synthesis reactions; i.e., a Pulverisette 23, Fritsch, Germany. Perspex milling jars were used, which have been previously shown to permit collection of good quality XRPD data during milling reactions [14]. Diffraction was collected using an incident beam of 12.4 keV. 2D scattering images were recorded on a MarMosaic, CCD detector (resolution 3072 × 3072 pixel). All scattering data were

processed using FIT2D [30]. In situ real-time Raman data were collected using a non-contact probe (beam diameter 1 mm) and excitation wavelength of 785 nm. Raman scattering was collected on a RXN1^{TM} analyzer (Kaiser Optical systems, France), equipped with a CCD detector (1024 × 1024 pixel). Each Raman spectrum consists of 5 s accumulated scattering intensity, with successive Raman spectra collected every 30 s.

Chemometrics: The Raman spectra were evaluated using principle component analysis (PCA) and multivariate curve resolution (MCR) with the software The Unscrambler$^®$ X Vers. 10.5 (CAMO). Prior to multivariate analysis, Raman spectra were baseline corrected followed by unit vector normalization in the spectral range of 200–2500 cm^{-1}. PCA was conducted with mean centered data using cross validation with 20 randomly selected segments. MCR iterations were initialized with the constraints of "non-negative spectra" and "non-negative concentrations", and sensitivity to pure compounds was set to 100. The maximum number of iterations was set at 250.

Mass spectrometry: Mass spectra were recorded with electrospray ionization time of flight mass spectrometry. A Q-TOF Ultima ESI-TOF mass spectrometer (Micromass, Germany) running at 4 kV capillary voltage and a cone voltage of 35 V was used. The collision energy was set to 5 eV. The source temperature was 120 °C whereas the desolvation temperature was adjusted to 150 °C. The mass spectrometer was operating in positive ion mode. Around 0.1 mg of the samples were weigh-in and solved in methanol (HPLC grade).

Supporting Information

Supporting Information File 1
XRPD data and multivariate data analysis.
[https://www.beilstein-journals.org/bjoc/content/supplementary/1860-5397-15-110-S1.pdf]

ORCID$^®$ iDs
Sebastian Haferkamp - https://orcid.org/0000-0001-6049-1102
Andrea Paul - https://orcid.org/0000-0003-2849-4754
Adam A. L. Michalchuk - https://orcid.org/0000-0001-7405-3269
Franziska Emmerling - https://orcid.org/0000-0001-8528-0301

References
1. James, S. L.; Adams, C. J.; Bolm, C.; Braga, D.; Collier, P.; Friščić, T.; Grepioni, F.; Harris, K. D. M.; Hyett, G.; Jones, W.; Krebs, A.; Mack, J.; Maini, L.; Orpen, A. G.; Parkin, I. P.; Shearouse, W. C.; Steed, J. W.; Waddell, D. C. *Chem. Soc. Rev.* **2012**, *41*, 413–447. doi:10.1039/c1cs15171a
2. Stolle, A.; Szuppa, T.; Leonhardt, S. E. S.; Ondruschka, B. *Chem. Soc. Rev.* **2011**, *40*, 2317–2329. doi:10.1039/c0cs00195c

3. Andersen, J.; Mack, J. *Green Chem.* **2018,** *20,* 1435–1443. doi:10.1039/c7gc03797j

4. Hulvey, Z.; Furman, J. D.; Turner, S. A.; Tang, M.; Cheetham, A. K. *Cryst. Growth Des.* **2010,** *10,* 2041–2043. doi:10.1021/cg100121n

5. Chadwick, K.; Davey, R.; Cross, W. *CrystEngComm* **2007,** *9,* 732–734. doi:10.1039/b709411f

6. Nielsen, S. F.; Peters, D.; Axelsson, O. *Synth. Commun.* **2000,** *30,* 3501–3509. doi:10.1080/00397910008087262

7. Kaupp, G.; Reza Naimi-Jamal, M.; Schmeyers, J. *Tetrahedron* **2003,** *59,* 3753–3760. doi:10.1016/s0040-4020(03)00554-4

8. Kulla, H.; Greiser, S.; Benemann, S.; Rademann, K.; Emmerling, F. *Cryst. Growth Des.* **2017,** *17,* 1190–1196. doi:10.1021/acs.cgd.6b01572

9. Fischer, F.; Greiser, S.; Pfeifer, D.; Jäger, C.; Rademann, K.; Emmerling, F. *Angew. Chem., Int. Ed.* **2016,** *55,* 14281–14285. doi:10.1002/anie.201607358

10. Caira, M. R.; Nassimbeni, L. R.; Wildervanck, A. F. *J. Chem. Soc., Perkin Trans. 2* **1995,** 2213–2216. doi:10.1039/p29950002213

11. Štrukil, V.; Fábián, L.; Reid, D. G.; Duer, M. J.; Jackson, G. J.; Eckert-Maksić, M.; Friščić, T. *Chem. Commun.* **2010,** *46,* 9191–9193. doi:10.1039/c0cc03822a

12. Friščić, T.; Halasz, I.; Beldon, P. J.; Belenguer, A. M.; Adams, F.; Kimber, S. A. J.; Honkimäki, V.; Dinnebier, R. E. *Nat. Chem.* **2013,** *5,* 66–73. doi:10.1038/nchem.1505

13. Gracin, D.; Štrukil, V.; Friščić, T.; Halasz, I.; Užarević, K. *Angew. Chem., Int. Ed.* **2014,** *53,* 6193–6197. doi:10.1002/anie.201402334

14. Batzdorf, L.; Fischer, F.; Wilke, M.; Wenzel, K.-J.; Emmerling, F. *Angew. Chem., Int. Ed.* **2015,** *54,* 1799–1802. doi:10.1002/anie.201409834

15. Kulla, H.; Haferkamp, S.; Akhmetova, I.; Röllig, M.; Maierhofer, C.; Rademann, K.; Emmerling, F. *Angew. Chem., Int. Ed.* **2018,** *57,* 5930–5933. doi:10.1002/anie.201800147

16. Lukin, S.; Tireli, M.; Lončarić, I.; Barišić, D.; Šket, P.; Vrsaljko, D.; di Michiel, M.; Plavec, J.; Užarević, K.; Halasz, I. *Chem. Commun.* **2018,** *54,* 13216–13219. doi:10.1039/c8cc07853j

17. Trotzki, R.; Hoffmann, M. M.; Ondruschka, B. *Green Chem.* **2008,** *10,* 873. doi:10.1039/b808265k

18. Trotzki, R.; Hoffmann, M. M.; Ondruschka, B. *Green Chem.* **2008,** *10,* 767–772. doi:10.1039/b801661e

19. Haferkamp, S.; Kraus, W.; Emmerling, F. *J. Mater. Sci.* **2018,** *53,* 13713–13718. doi:10.1007/s10853-018-2492-0

20. Rightmire, N. R.; Hanusa, T. P. *Dalton Trans.* **2016,** *45,* 2352–2362. doi:10.1039/c5dt03866a

21. Simone, E.; Steele, G.; Nagy, Z. K. *CrystEngComm* **2015,** *17,* 9370–9379. doi:10.1039/c5ce01878a

22. El-Agrody, A. M.; Al-Omar, M. A.; Amr, A. E.-G. E.; Ng, S. W.; Tiekink, E. R. T. *Acta Crystallogr., Sect. E: Struct. Rep. Online* **2013,** *69,* o515. doi:10.1107/s1600536813006235

23. Antipin, M. Y.; Nesterov, V. N.; Jiang, S.; Borbulevych, O. Y.; Sammeth, D. M.; Sevostianova, E. V.; Timofeeva, T. V. *J. Mol. Struct.* **2003,** *650,* 1–20. doi:10.1016/s0022-2860(02)00468-4

24. Belenguer, A. M.; Lampronti, G. I.; Cruz-Cabeza, A. J.; Hunter, C. A.; Sanders, J. K. M. *Chem. Sci.* **2016,** *7,* 6617–6627. doi:10.1039/c6sc03457h

25. Pearson, K. *London, Edinburgh Dublin Philos. Mag. J. Sci.* **1901,** *2,* 559–572. doi:10.1080/14786440109462720

26. Hotelling, H. *J. Educ. Psychol.* **1933,** *24,* 417–441. doi:10.1037/h0071325

27. Casassas, E.; Marqués, I.; Tauler, R. *Anal. Chim. Acta* **1995,** *310,* 473–484. doi:10.1016/0003-2670(95)00140-u

28. Timofeeva, T. V.; Nesterov, V. N.; Antipin, M. Y.; Clark, R. D.; Sanghadasa, M.; Cardelino, B. H.; Moore, C. E.; Frazier, D. O. *J. Mol. Struct.* **2000,** *519,* 225–241. doi:10.1016/s0022-2860(99)00305-1

29. Haferkamp, S.; Fischer, F.; Kraus, W.; Emmerling, F. *Beilstein J. Org. Chem.* **2017,** *13,* 2010–2014. doi:10.3762/bjoc.13.197

30. Hammersley, A. P.; Brown, K.; Burmeister, W.; Claustre, L.; Gonzalez, A.; McSweeney, S.; Mitchell, E.; Moy, J. P.; Svensson, S. O.; Thompson, A. W. *J. Synchrotron Radiat.* **1997,** *4,* 67–77. doi:10.1107/s0909049596015087

Extending mechanochemical porphyrin synthesis to bulkier aromatics: tetramesitylporphyrin

Qiwen Su[1,2] and Tamara D. Hamilton[*1]

Abstract

Aldehydes with bulky substituents in the *ortho*-positions have been historically difficult in porphyrin synthesis, presumably owing to steric hindrance around the reactive site. We have used mechanochemistry for the simple, room-temperature synthesis of tetra-*meso*-substituted porphyrins. In the present study, mesitaldehyde undergoes acid-catalyzed mechanochemical condensation with pyrrole to give *meso*-tetrakis[2,4,6-(trimethyl)phenyl]porphyrin (TMP) after oxidation in solution. Yields are similar to those obtained using high-temperature porphyrin synthesis, although they remain significantly lower than some optimized room-temperature, solution-based methods. Yields of the mechanochemical synthesis were found to increase slightly upon longer exposure to an organic oxidizing agent in solution. This indicates that the mechanochemical condensation step may be more successful than initially realized. This work shows that mechanochemistry is a successful, simple, room-temperature method for producing tetra-*meso*-substituted porphyrins with bulky substituents.

Introduction

Porphyrins and related macrocycles such as chlorins, corroles, and bacteriochlorins carry out important functions in nature including light harvesting (i.e., chlorophyll), oxygen transport (i.e., heme), biocatalysis, and electron transfer. The ability to synthesize porphyrins bearing a variety of chemical and steric functionalities on the periphery is important in fields as diverse as catalysis [1], photovoltaics [2], photodynamic therapy [3,4], environmental remediation [5,6], biomimetic modelling [7] and metal-organic self-assembly [8]. Porphyrins may be substituted in the *meso* or β-positions (Figure 1A). Tetra-*meso*-substituted porphyrins are usually synthesized from simple starting materials, namely: pyrrole and an aldehyde (Scheme 1). Porphyrin synthesis is interesting to study as a mechanochemical reaction because it involves the combination of reactive molecules under appropriate conditions to give a very stable, aromatic product. Furthermore, depending on the nature of the substituents, the porphyrin product can be labor-intensive to produce and purify in good yield and large quantities using other methods. The

process involves multiple condensations, together with oxidation that may happen in one pot or as separate steps. Other no-solvent-added methods of porphyrin synthesis have been reported [9,10], while optimization of solvent, dilution and catalysis conditions using solvent-based approaches have been investigated for the synthesis of many porphyrins [11-14].

Figure 1: A) Porphyrin structure and labelling system. B) Substituents in the *ortho*-position of the group attached to the methane bridge create steric hindrance around the *meso*-position, above and below the plane of the porphyrin ring.
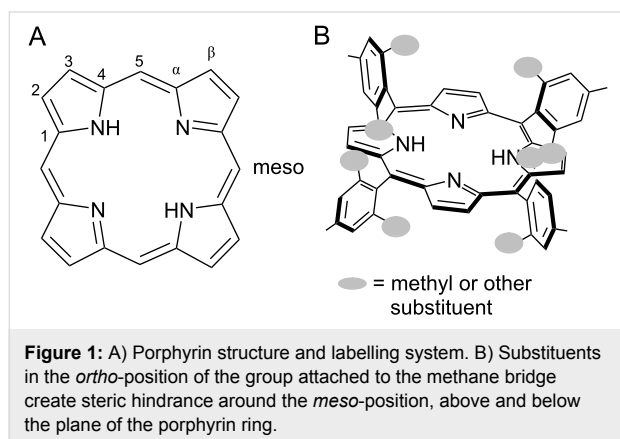
Tetraphenylporphyrin (TPP) synthesis, as first reported in 1935 by Rothemund [15-17], involved placing reactants in a sealed tube at high temperatures (150 °C or higher) for 24 to 48 hours in the absence of air or any oxidant. Not every substituted benzaldehyde could survive this process and yield the porphyrin. Adler and Longo later introduced refluxing propionic acid (141 °C) open to air as a reaction medium [18]. This widened the variety of substituted aldehydes successfully converted to porphyrins, but employment of a caustic solvent at high temperature is a drawback. These conditions also proved inappropriate for several substituted benzaldehydes, and the best yields have been in the order of 20% with many porphyrins needing extensive work-up to isolate from tar-like byproducts. Working from

the premise that the cyclized condensation product (called a porphyrinogen) should be thermodynamically favored over linear alternatives (Scheme 1), Lindsey et al. sought to maximize yields under milder conditions by promoting the establishment of an equilibrium for the cyclization step, then adding a gentle oxidizer (*p*-chloranil or 2,3-dichloro-5,6-dicyano-1,4-benzoquinone (DDQ)) in a second step to obtain irreversibly the aromatized porphyrin [11]. The symmetrical tetra-*meso*-substituted porphyrins are synthesized through a four-fold acid-catalyzed condensation to form a porphyrinogen which is then oxidized (− 6H) to form the conjugated porphyrin product. Lindsey's reaction takes place at room temperature and utilizes chlorinated solvents under optimized dilution conditions (10^{-2} M reactant concentration). The cyclization step necessitates an oxygen-free environment, in order to allow the equilibrium to be fully established before any oxidation takes place. Tar-like byproducts are avoided under these conditions, and purification is achieved using only a short chromatography column.

Our previous work on mechanochemical porphyrin synthesis has demonstrated that it is possible to synthesize tetraphenylporphyrin (TPP) by grinding benzaldehyde and pyrrole (two liquids) in the presence of an acid catalyst, followed by oxidation with DDQ in minimal amounts of solvent [19]. TPP was produced in a yield similar to that obtained from the Lindsey synthesis. Additionally, several monosubstituted benzaldehydes, as well as two isomers of naphthaldehyde, were shown to undergo successful mechanochemical reaction in reasonable yields.

Mesitaldehyde has been considered a representative "sterically-hindered" reagent, serving as a touchstone for the wider applicability of porphyrin reaction conditions [12]. Porphyrins with

Scheme 1: Steps leading to the formation of a porphyrin.
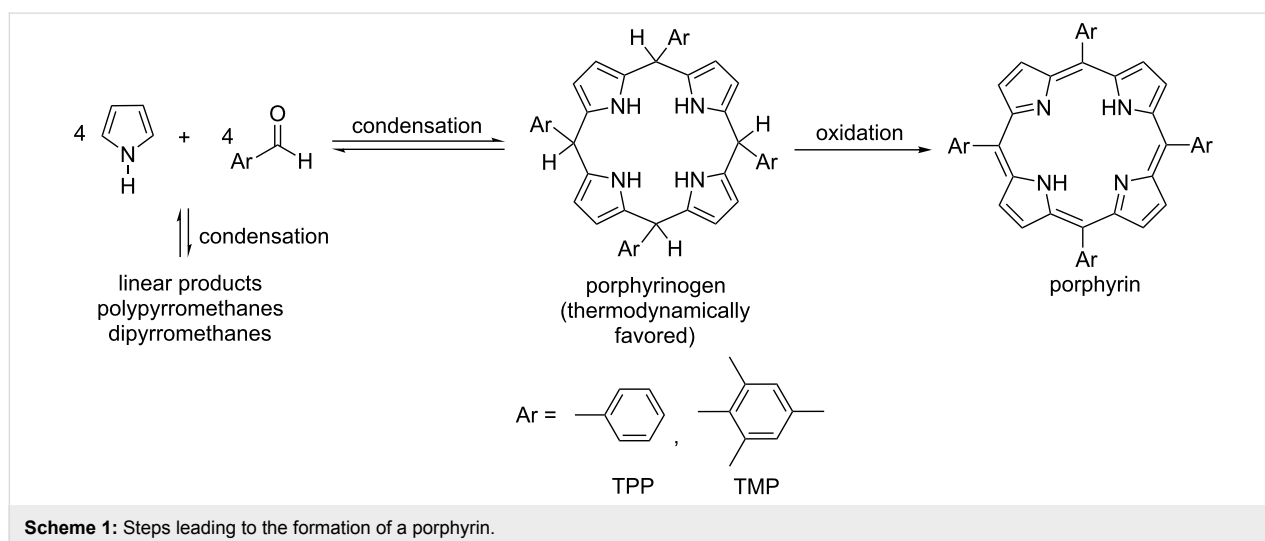
bulky groups in the *meso*-positions, especially aromatics with bulky substituents in the position *ortho* to the methine bridge, have been used for biological modelling. The large groups become oriented above and below the plane of the porphyrin ring, forming a protective shroud around the reactive center, much like some protein systems (Figure 1B) [12,20-22]. The corresponding substituted benzaldehydes, however, have not easily yielded results upon reaction with pyrrole under any traditional synthetic method. High-temperature (>170 °C) sealed-bomb reactions in the presence of metal salts will, after 2–3 days, yield 1–6% of *meso*-tetrakis[2,4,6-(trimethyl)phenyl]porphyrin (TMP) [20,21,23,24], and a gas-phase synthesis in the presence of TFA yielded 7% TMP [9]. Under the first-reported conditions of the Lindsey synthesis, mesitaldehyde "failed to give good yields" of TMP [11]. Later studies of modified reaction conditions employing boron trifluoride as the acid catalyst, and small amounts of ethanol as a co-catalyst, were successful in producing TMP with yields around 30% at room temperature [13,25,26]. Optimized conditions still required reactant concentrations of 10^{-2} M. Increasing or decreasing the concentration lowered the yield, as did increasing the temperature. In the present study we set out to test whether our mechanochemical porphyrin synthesis could accommodate a sterically-hindered aldehyde, and produce TMP at room temperature and in the absence of added solvent for the condensation step, using relatively simple reaction conditions. The use of mechanochemistry to bring about a no-solvent-added acid-catalyzed condensation between aldehydes and pyrrole enables the reduction of solvent and elimination of high temperatures from the synthesis of these important compounds, representing a significant reduction in environmental impact.

Results and Discussion

When mesitaldehyde and pyrrole, both colorless liquids, are combined in the presence of an acid catalyst and ground using a mixer mill for 10 minutes (Scheme 2), a pink powder is formed. As in the case of benzaldehyde, the powder is found to contain no porphyrin, evidenced by the lack of a Soret band at 410–420 nm in the electronic spectrum. Our work with benzaldehyde showed that even when grinding is carried out manually and open to air using a mortar and pestle, no Soret band is observed in the spectrum of the freshly-ground powder [19]. Also in the case of benzaldehyde, it was found that allowing the mechanochemically-generated powder to sit on a benchtop open to air for several weeks brought about the appearance of TPP in small amounts. More immediate oxidation of this power, by dissolving in chloroform and stirring with DDQ for 2 hours, allowed isolation of TPP in 28% yield [19]. Appearance of TPP upon oxidation confirms that mechanochemistry successfully brought about the condensation step. The freshly-ground "pink powder" must contain cyclized products, perhaps including porphyrinogen (colorless) and various other reduced-porphyrin intermediates having one to five more hydrogens than TPP. Many of these intermediates have absorbance in the visible region.

Other no-solvent-added routes to porphyrins, including high-temperature sealed-bomb methods [15-17], gas-phase synthesis [9], and microwave irradiation [10] do not employ a second oxidation step. Presumably for the latter two methods open to air, dioxygen serves as a rapid oxidizer under high-temperature conditions, while the sealed-bomb reaction products are heavily contaminated with chlorins [27-29], byproducts that contain two more hydrogens than the porphyrin, and which easily undergo chemical oxidation to yield porphyrin.

In contrast, since the no-solvent-added mechanochemical synthesis takes place at room temperature, like the Lindsey synthesis, it may be that the equilibrium is reached between starting materials and cyclocondensation products before conditions are
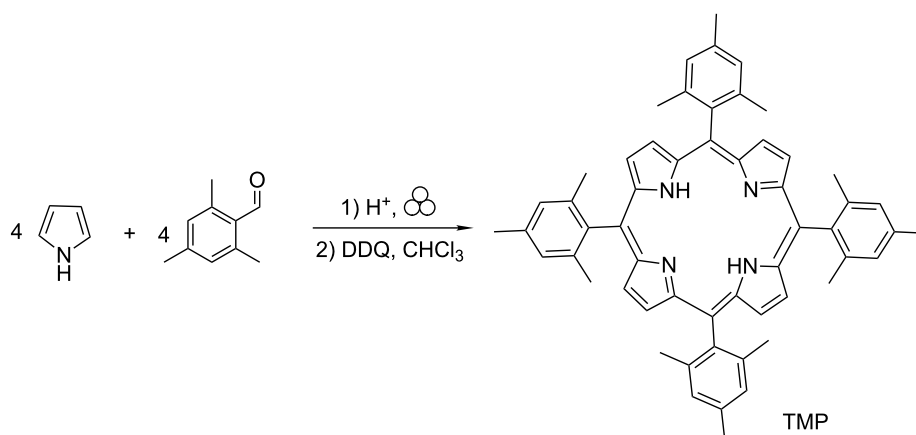
Scheme 2: Mechanochemical synthesis of tetramesitylporphyrin.

introduced to trigger the irreversible oxidation of porphyrinogen to porphyrin. Optimization of conditions could maximize the porphyrinogen yield by adjusting the equilibrium, even though the absence of added solvent means the concentration of reagents is at a maximum, and high concentrations are usually thought to favour linear over cyclic products.

In the present work for the mesitaldehyde reaction, the pink powder obtained upon grinding was immediately combined with DDQ, dissolved in a small amount (ca. 50 mL) of chloroform, and left to stir for one week. This is the same oxidation method as used by Lindsey et al. and is presumed in their case to convert any porphyrinogen or partially-oxidized intermediate present into porphyrin instantaneously [11]. In the case of the mechanochemical synthesis, the results show that a longer oxidation time results reproducibly in a somewhat higher yield (Table 1), although the isolated yield remains around 5%. Identity and purity of TMP was confirmed by UV–vis and ^{1}H NMR spectroscopy (see Supporting Information File 1). Although we are not certain of the identity of intermediates or side products from the mechanochemical reaction, it may be possible that via milling they are activated enough so that mechanical stirring during the oxidation with DDQ in solution continues to promote the formation of porphyrinogen. Throughout the oxidation process, the porphyrinogen immediately gets irreversibly oxidized to porphyrin. It is clear that further work is needed to elucidate differences between the mechanochemical and the solvent-based porphyrin syntheses.

Table 1: Tetramesitylporphyrin yields.

Milling time (minutes)	Oxidation time[a]	Average isolated yield (%)[b]
10	1 week	1.82
10	1 month	5.10

[a]Stirring in chloroform with DDQ; [b]Average based on isolated, purified mass from three replicates.

Conclusion

Mechanochemical milling has successfully led to cyclocondensation of pyrrole with a sterically-hindered aldehyde. After oxidation to give a porphyrin with bulky substituents, isolated yields are comparable to those obtained from high-temperature syntheses (though still lower than the 30% obtainable with added solvent at room temperature). The mechanochemical synthesis is carried out at room temperature with no added solvent during the condensation step, simplifying and reducing the environmental impact for the synthesis of this important class of molecules. Notably, James et al. have reported the simple and clean mechanochemical metalation of porphyrins, extending

these advantages even further [30]. Further studies aimed at understanding the mechanism of the mechanochemical porphyrin synthesis and its differences and similarities compared to the solvent-based methods will be important advances for the field of mechanochemistry.

Experimental
Materials and methods

All chemicals used were purchased from Sigma-Aldrich and used without further purification. Mesitaldehyde (98%), *p*-toluenesulfonic acid monohydrate (*p*-TSA, 98.5%), chloroform (99.8%), alumina (99.9%), triethylamine (99.5%), silica gel (technical grade, pore size 60 Å, 200–425 mesh particle size), ethyl acetate (anhydrous, 99.8%), hexane (mixture of isomers, 98.5%), deuterated chloroform (99.8 atom % D) were used. 2,3-Dichloro-5,6-dicyano-1,4-benzoquinone (DDQ, 97.0%) was purchased from TCI America and used without further purification. Pyrrole (98%) was purchased from Sigma-Aldrich and purified by distillation once per week after discoloration appeared. The electronic spectra were recorded on a Perkin Elmer Lambda 850 UV–vis spectrophotometer, measured from 200–800 nm at 1 nm intervals. The samples were placed in quartz cuvettes with a 1 cm path length. ^{1}H NMR spectra were recorded on a Varian 300 MHz nuclear magnetic resonance spectrometer.

Mechanochemical synthesis

meso-**Tetrakis[2,4,6-(trimethyl)phenyl]porphyrin.** Equimolar amounts of pyrrole (0.259 g, 3.75 mmol) and 2,4,6-trimethylbenzaldehyde (0.556 g, 3.75 mmol) were placed in a 10 mL stainless steel grinding jar along with acid catalyst *p*-toluenesulfonic acid (0.026 g, 0.151 mmol, 4%) and two stainless steel balls of 5 mm diameter (0.52 g/ball; 0.81 mass-to-balls ratio). The mixture was ground using the Retsch Mixer Mill MM200 for 10 minutes at a frequency of 25 Hz, resulting in formation of a dark pink-colored powder. The powder was then dissolved in 50 mL chloroform and 3 molar equivalents of DDQ (2.554 g, 11.20 mmol) were added. The mixture was stirred to undergo oxidation for a period of one week. The mixture was then passed through a 1 cm alumina plug and 3–5 drops of triethylamine were added to the filtrate. The filtrate was passed through a silica gel column using 1:3 ethyl acetate/hexanes as the mobile phase. Fractions containing porphyrin, as determined by thin-layer chromatography and UV–vis spectroscopy were combined and the solvent was removed using a rotary evaporator. *meso*-Tetrakis[2,4,6-(trimethyl)phenyl]porphyrin was isolated as a purple-red crystalline powder in 1.8% average yield, which could be increased to 5.1% if oxidation time was lengthened to one month. ^{1}H NMR (300 MHz, CDCl$_3$) δ 8.62 (s, 8H), 6.91 (s, 8H), 2.62 (s, 12H), 1.85 (s, 24H), −2.52 (s, 2H); ^{13}C NMR (300 MHz, CDCl$_3$) δ 138.4, 137.2, 136.6, 126.7,

116.5, 37.1, 30.9; UV–vis (CHCl$_3$) λ = 414 (Soret band), 513, 543, 590, 648 (Q-bands).

Supporting Information

Supporting Information File 1

Spectroscopic characterization of
meso-tetrakis[2,4,6-(trimethyl)phenyl]porphyrin (TMP).
[https://www.beilstein-journals.org/bjoc/content/
supplementary/1860-5397-15-111-S1.pdf]

ORCID® iDs

Qiwen Su - https://orcid.org/0000-0003-0965-9947
Tamara D. Hamilton - https://orcid.org/0000-0001-8936-4342

References

1. Barona-Castaño, J.; Carmona-Vargas, C.; Brocksom, T.;
   de Oliveira, K. *Molecules* **2016,** *21,* 310.
   doi:10.3390/molecules21030310
2. Hadmojo, W. T.; Yim, D.; Aqoma, H.; Ryu, D. Y.; Shin, T. J.;
   Kim, H. W.; Hwang, E.; Jang, W.-D.; Jung, I. H.; Jang, S.-Y. *Chem. Sci.*
   2017, *8,* 5095–5100. doi:10.1039/c7sc01275f
3. Ethirajan, M.; Chen, Y.; Joshi, P.; Pandey, R. K. *Chem. Soc. Rev.*
   2011, *40,* 340–362. doi:10.1039/b915149b
4. Josefsen, L. B.; Boyle, R. W. *Theranostics* **2012,** *2,* 916–966.
   doi:10.7150/thno.4571
5. Wang, X.-S.; Liu, J.; Bonefont, J. M.; Yuan, D.-Q.; Thallapally, P. K.;
   Ma, S. *Chem. Commun.* **2013,** *49,* 1533–1535.
   doi:10.1039/c2cc38067f
6. Lesage, S.; Xu, H.; Durham, L. *Hydrol. Sci. J.* **1993,** *38,* 343–354.
   doi:10.1080/02626669309492679
7. Rodriguez, K. J.; Hanlon, A. M.; Lyon, C. K.; Cole, J. P.; Tuten, B. T.;
   Tooley, C. A.; Berda, E. B.; Pazicni, S. *Inorg. Chem.* **2016,** *55,*
   9493–9496. doi:10.1021/acs.inorgchem.6b01113
8. Huh, S.; Kim, S.-J.; Kim, Y. *CrystEngComm* **2016,** *18,* 345–368.
   doi:10.1039/c5ce02106e
9. Drain, C. M.; Gong, X. *Chem. Commun.* **1997,** 2117–2118.
   doi:10.1039/a704600f
10. Petit, A.; Loupy, A.; Maiuard, P.; Momenteau, M. *Synth. Commun.*
    1992, *22,* 1137–1142. doi:10.1080/00397919208021097
11. Lindsey, J. S.; Schreiman, I. C.; Hsu, H. C.; Kearney, P. C.;
    Marguerettaz, A. M. *J. Org. Chem.* **1987,** *52,* 827–836.
    doi:10.1021/jo00381a022
12. Lindsey, J. S.; Wagner, R. W. *J. Org. Chem.* **1989,** *54,* 828–836.
    doi:10.1021/jo00265a021
13. Wagner, R. W.; Li, F.; Du, H.; Lindsey, J. S. *Org. Process Res. Dev.*
    1999, *3,* 28–37. doi:10.1021/op9800459
14. Geier, G. R., III; Riggs, J. A.; Lindsey, J. S.
    J. Porphyrins Phthalocyanines **2001,** *5,* 681–690. doi:10.1002/jpp.380
15. Rothemund, P. *J. Am. Chem. Soc.* **1935,** *57,* 2010–2011.
    doi:10.1021/ja01313a510
16. Rothemund, P. *J. Am. Chem. Soc.* **1939,** *61,* 2912–2915.
    doi:10.1021/ja01265a096
17. Rothemund, P.; Menotti, A. R. *J. Am. Chem. Soc.* **1941,** *63,* 267–270.
    doi:10.1021/ja01846a065

18. Adler, A. D.; Longo, F. R.; Finarelli, J. D.; Goldmacher, J.; Assour, J.;
    Korsakoff, L. *J. Org. Chem.* **1967,** *32,* 476. doi:10.1021/jo01288a053
19. Shy, H.; Mackin, P.; Orvieto, A. S.; Gharbharan, D.; Peterson, G. R.;
    Bampos, N.; Hamilton, T. D. *Faraday Discuss.* **2014,** *170,* 59–69.
    doi:10.1039/c3fd00140g
20. Eaton, S. S.; Eaton, G. R. *J. Am. Chem. Soc.* **1975,** *97,* 3660–3666.
    doi:10.1021/ja00846a016
21. Bortolini, O.; Meunier, B. *J. Chem. Soc., Perkin Trans. 2* **1984,**
    1967–1970. doi:10.1039/p29840001967
22. Suslick, K. S.; Fox, M. M. *J. Am. Chem. Soc.* **1983,** *105,* 3507–3510.
    doi:10.1021/ja00349a023
23. Badger, G. M.; Jones, R. A.; Laslett, R. L. *Aust. J. Chem.* **1964,** *17,*
    1157–1163. doi:10.1071/ch9641157
24. Groves, J. T.; Nemo, T. E. *J. Am. Chem. Soc.* **1983,** *105,* 6243–6248.
    doi:10.1021/ja00358a009
25. Wagner, R. W.; Lawrence, D. S.; Lindsey, J. S. *Tetrahedron Lett.* **1987,**
    28, 3069–3070. doi:10.1016/s0040-4039(00)96287-7
26. van der Made, A. W.; Hoppenbrouwer, E. J. H.; Nolte, R. J. M.;
    Drenth, W. *Recl. Trav. Chim. Pays-Bas* **1988,** *107,* 15–16.
    doi:10.1002/recl.19881070104
27. Aronoff, S.; Calvin, M. *J. Org. Chem.* **1943,** *8,* 205–223.
    doi:10.1021/jo01191a002
28. Calvin, M.; Ball, R. H.; Aronoff, S. *J. Am. Chem. Soc.* **1943,** *65,* 2259.
    doi:10.1021/ja01251a508
29. Ball, R. H.; Dorough, G. D.; Calvin, M. *J. Am. Chem. Soc.* **1946,** *68,*
    2278–2281. doi:10.1021/ja01215a046
30. Ralphs, K.; Zhang, C.; James, S. L. *Green Chem.* **2017,** *19,* 102–105.
    doi:10.1039/c6gc02420c

License and Terms

Mechanochemical synthesis of hyper-crosslinked polymers: influences on their pore structure and adsorption behaviour for organic vapors

Sven Grätz[*1], Sebastian Zink[2], Hanna Kraffczyk[3], Marcus Rose[3] and Lars Borchardt[*1]

Abstract

This study elucidates a mechanochemical polymerization reaction towards a hyper-crosslinked polymer as an alternative to conventional solvent-based procedures. The swift and solvent-free Friedel–Crafts alkylation reaction yields a porous polymer with surface areas of up to 1720 m^2g^{-1} and pore volumes of up to 1.55 cm^3g^{-1}. The application of LAG (liquid-assisted grinding) revealed a profound impact of the liquid´s boiling point on the textural properties of the obtained polymer materials. Finally, the materials are characterized by vapour sorption experiments with benzene and cyclohexane.

Introduction

The widespread use of microporous materials in areas like gas storage, gas separation, and catalysis has led to the development of a wide variety of these materials [1]. While inorganic materials such as activated carbons, porous metal oxides, and zeolites have been investigated for decades, hybrid materials such as metal-organic frameworks [2], purely organic frameworks such as crystalline covalent-organic frameworks [3], and amorphous POPs (porous organic polymers) [4] are currently in the focus of research. The modular bottom-up building concept of these organic materials allows for tailoring of materials properties towards desired applications. POPs synthesis can be achieved by a huge variety of reactions ranging from Friedel-Crafts alkylations [5], cross-coupling reactions [6] and cyclotrimerizations [7], to amine-based chemistry with Schiff base reactions [8], imidisation, and amidisation reactions [9]. In the recent past, a strong focus was also set on the development of HCPs (hyper-crosslinked polymers) [10]. Typically, they are formed by a non-directed aromatic substitution (Friedel–Crafts alkylation) either by intramolecular functional groups or using external crosslinkers. These reactions yield very high crosslinking degrees in amorphous framework structures and hence, enable highest specific BET (Brunauer–Emmett–Teller) sur-

face areas of up to 2000 m^{2}g^{-1} for fully amorphous materials [10]. Typically, chloromethyl or methoxy groups are used to crosslink aromatic building blocks by using stoichiometric or even excess amounts of FeCl$_3$ as catalyst. Recently, also a metal-free Brønsted acid-catalyzed reaction using trifluoromethanesulfonic acid or sulfuric acid was developed yielding basically the same polymer but avoiding residual traces of the metal [11]. These synthetic pathways often afford a gel from the dissolved monomers upon the crosslinking that is subsequently washed and dried with a significant volume loss. Still, a high amount of permanent micro- and mesoporosity is retained. This gel formation is kinetically fast and thus, hard to control. Hence, an initial intensive mixing is crucial to achieve a homogeneous material. Also, due to the shrinkage upon the drying step, a high flexibility of the framework remains as an intrinsic property. Thus, the pore volume and specific surface area that is permanently accessible can be increased by a severe swelling behaviour especially during the adsorption and combined with absorption of organic vapors or liquids. The swelling is fully reversible, thus, rendering these materials interesting adsorbents with a dynamic adsorption behaviour.

However, the low solubility of POPs is a main challenge in their synthesis protocols. Solution-based procedures, for example, suffer from almost instant precipitation and thus only produce materials with a low degree of polymerization [10]. In the recent past it has been shown that for reactions, where the solu-

bility of the reactants or products is an issue, mechanochemistry – a field which is currently gaining momentum – can be a promising workaround [12-20]. It has already been established as a versatile tool for the synthesis of several porous materials [21-29] and polymers [30-42].

In this contribution, we employed mechanochemistry for a protocol for the solvent-free crosslinking of HCP (Figure 1). This is supported by an investigation of chemical and milling parameters on the yield and surface area of the resulting polymer.

Results and Discussion
Polymer synthesis and characterization
In our standard procedure HCP was synthesised via a mechanochemical reaction. This was accomplished by transferring BCMCP (4,4'-bis(chloromethyl)-1,1'-biphenyl) and six equiv of anhydrous iron(III) chloride as mediator into a 45 mL zirconium oxide milling vessel filled with 22 balls (10 mm, 3.19 ± 0.05 g) of the same material (Figure 1). Consequently, the vessel was transferred into a (Pulverisette 7) premium line (Fritsch GmbH) and milled at 500 rpm for 35 minutes. After the synthesis, the resulting polymers were washed with 200 mL of water and 100 mL of ethanol and dried at 80 °C for 12 hours to yield a beige powder (denoted NG-HCP (neat grinding-HCP)). For more details on the experimental procedure see Supporting Information File 1.

Figure 1: A: Mechanochemical polymerization of BCMBP (4,4'-bis(chloromethyl)-1,1'-biphenyl) towards the porous polymer HCP. B: Picture of a vial of BCMBP (left) and LAG-HCP (right).
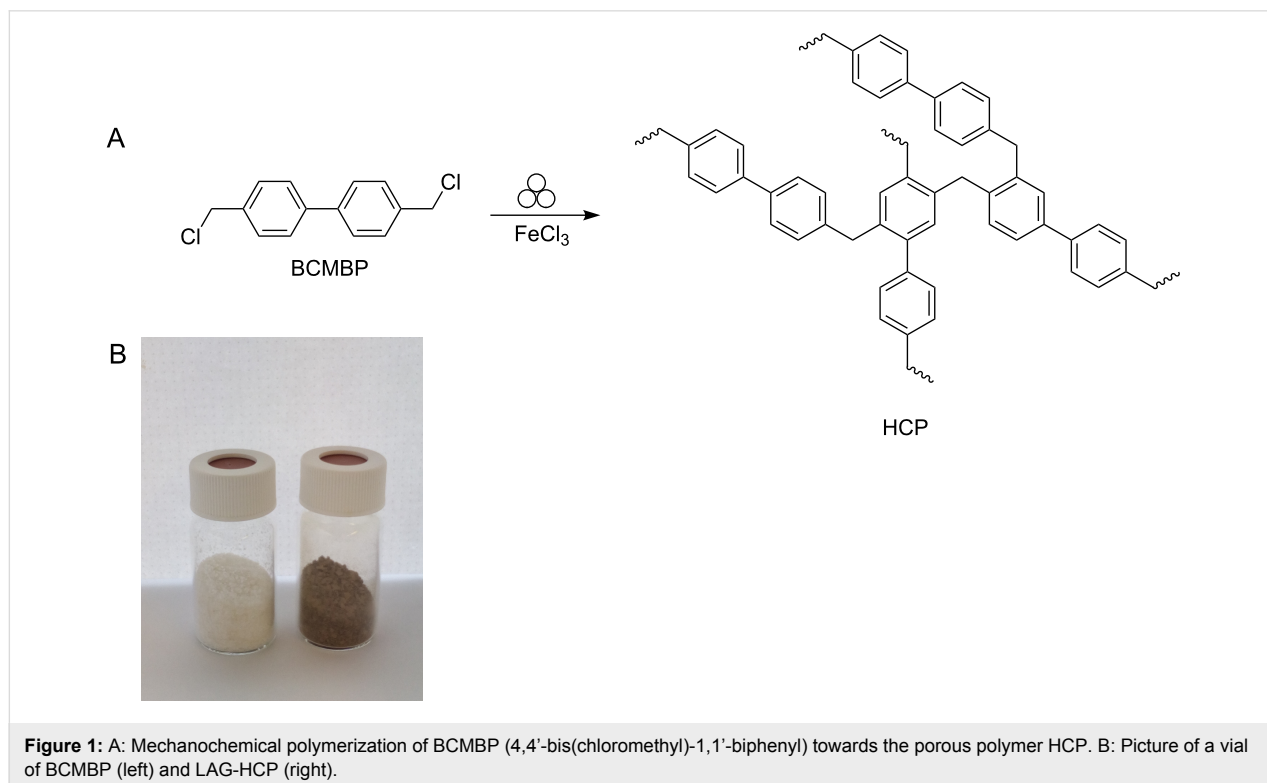
After validating the complete insolubility in common organic solvents (like DCM, ethanol, DMF, chlorofrom, *n*-hexane), the nature of the polymer was investigated via IR spectroscopy. In the past the C–Cl vibration at 680 cm^{-1} has commonly been used to establish whether the desired crosslinking via the chloromethylene groups has occurred [43]. While this vibration is dominant in the monomer, it has completely vanished in the IR (infrared) spectrum of the polymer (Figure 2A). Moreover, several other changes in the spectrum are observed for the polymer as well. Especially in the region of the C–H$_{oop}$ the vibration is shifted to 885 cm^{-1} hinting towards one isolated hydrogen atom which further confirms the cross-linking between the monomers. The creation of these aliphatic connections is also evident based on the appearance of vibrations around 1400 cm^{-1} [43]. As reported in the literature for the solvent-based protocol the polymer obtained through this mechanochemical route is also amorphous as visualized by the XRD (X-ray diffraction) patters recorded (Supporting Information File 1, Figure S1) [43].

Furthermore, NG-HCP similarly shows a high thermal stability with a decomposition onset in air (Supporting Information File 1, Figure S2) at around 310 °C. The residual mass of only 1.9% confirms the absence of both, excessive abrasion and oxidant inside the polymer. This is further supported by the SEM-EDX (scattering electron microscope, energy-dispersive X-ray spectroscopy) measurements showing both Cl and Fe contents below the limit of detection (Supporting Information File 1, Figure S3). Scattering electron microscopy also revealed an agglomerated morphology of the samples (Supporting Information File 1, Figure S4).

After successfully establishing the occurrence of the cross-linking reaction and investigating the physical and thermal properties of the polymer, the textural properties of the NG-HCP were evaluated utilizing nitrogen physisorption. While the first tries directly yielded a microporous polymer (SSA$_{BET}$ = 850 m^{2}g^{-1}, V_p = 0.60 cm^{-3}g^{-1}, Figure 2B in Supporting Information File 1), the SSA (specific surface area) achieved with the classical solvent-based approach (Sol-HCP, SSA$_{BET}$ = 1450 m^{2}g^{-1}, V_p = 1.55 cm^{-3}g^{-1}) [11] could not be reached. In order to improve this property, we varied the mechanochemical reaction parameters such as milling time and amount of oxidant in a systematic (DOE) design of experiments approach (see Supporting Information File 1 for details). While changes in these parameters translated to variations in the specific surface, it was not possible to achieve surface areas as high as the solution-based method solely by adapting the aforementioned parameters. The most influential parameter was determined to be the rotational speed of the ball mill. At 200 rpm this led to a low SSA (7–66 m^{2}g^{-1}) due to an incomplete polymerization, while 800 rpm resulted in a medium SSA (600–820 m^{2}g^{-1}). This observation is hinting towards a partial degradation of the porosity by the high energy input and the resulting thermal and frictional stress of the material and reinforces our prior findings regarding the synthesis of porous polymers inside a ball mill [30,35].

Development of vessel pressure during the reaction

In an attempt to track and understand the kinetics of the mechanochemical polymerisation further, we employed the so-called GTM-system (gas pressure and temperature measurement system), which allows us to measure the temperature and pressure inside the milling vessel during the milling process. While a release of gas was observed when opening the vessel, the GTM measurement revealed that even small amounts of the monomer (3.2 mmol) lead to a swift and rise in vessel pressure
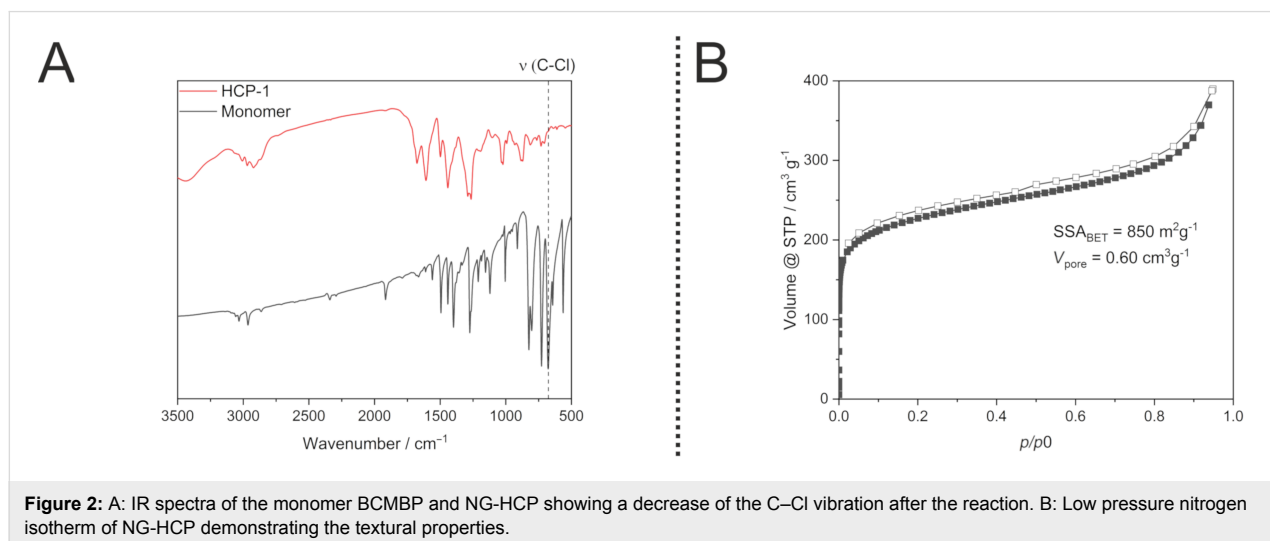
Figure 2: A: IR spectra of the monomer BCMBP and NG-HCP showing a decrease of the C–Cl vibration after the reaction. B: Low pressure nitrogen isotherm of NG-HCP demonstrating the textural properties.

exceeding 12 bar (Figure 3A) caused by the released HCl in the course of the reaction. This behaviour can be handled under laboratory conditions but is hampering the potential scale up of the process. In the recent past we have already observed this behaviour for other reactions including iron(III) chloride [42,44], and thus we have proposed several countermeasures which greatly reduce the vessel pressure during such reactions. For this polymerization reaction we decided to add small quantities of liquid to dissolve the gas, as the method of choice. At first 1 mL of ethanol was added to the reaction mixture prior to the milling. This measure resulted in a decrease of vessel pressure of the whole course of the reaction. With diethyl ether instead of ethanol the pressure could be reduced even more limiting the maximum pressure to 0.42 bar (Figure 3B).

Influence of the LAG additive

Interestingly, besides decreasing the vessel pressure, this 1 mL of solvent also affected the textural properties of the polymer positively. Consequently, we went on to investigate the influence of the LAG reagent by changing the nature of the latter. The surface area of the polymer was increased up to 1720 m^{2}g^{-1} when utilizing diethyl ether (Table 1, entry 7), therefore almost doubled, while the pore volume is also growing. In the pore size distribution one can observe a shift from 0.75 nm micropores for NG-HCP to a mixture of 0.67 and 0.97 nm micropores for LAG-HCP (Figures S5 and S6 in Supporting Information File 1). In addition, the amount of mesopores in the sample is also slightly higher for the LAG sample. The solubility of the released gas inside the liquid seems to play a minor role since good results can be obtained with either dichloromethane (poor HCl solvent) as well as diethyl ether (good HCl solvent). On the other hand, the boiling point of the added liquid seems to be an important parameter for the surface area of the synthesised polymer, with lower boiling point solvents resulting in higher surface areas than their high boiling

point counterparts (Figure 4). This might indicate that the additive acts as a porogene in the synthesis of the polymer, with the vapour being a more effective than the liquid. However, to test this hypothesis a profound control over the vessel temperature is necessary which cannot be achieved with our current experimental setup but is generally possible [45]. Nevertheless, the GTM systems showed that macroscopic temperatures exceeding the boiling points of dichloromethane and diethyl ether have been reached in the course of the experiments. Since the best results were obtained for diethyl ether (Table 1, entry 7) this sample has been denoted LAG-HCP and was investigated further.
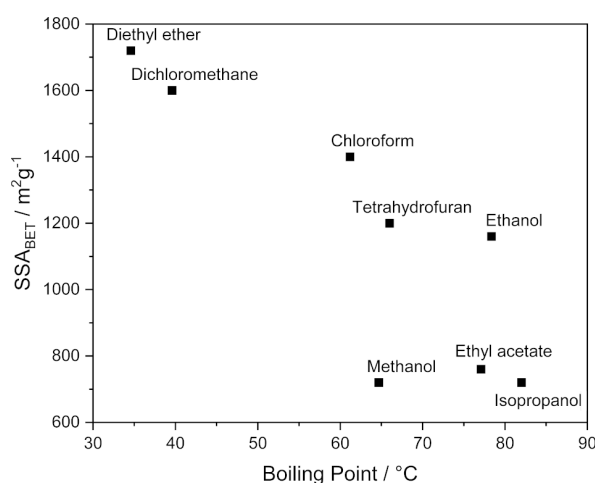
Figure 4: The correlation between the liquids' boiling point and the SSA of the polymer. In general, a lower boiling point of the LAG additive leads to a higher SSA.

Vapor physisorption

Since HCP is highly hydrophobic (proven before by water vapor physisorption [11]), the adsorption of non-polar adsorp-
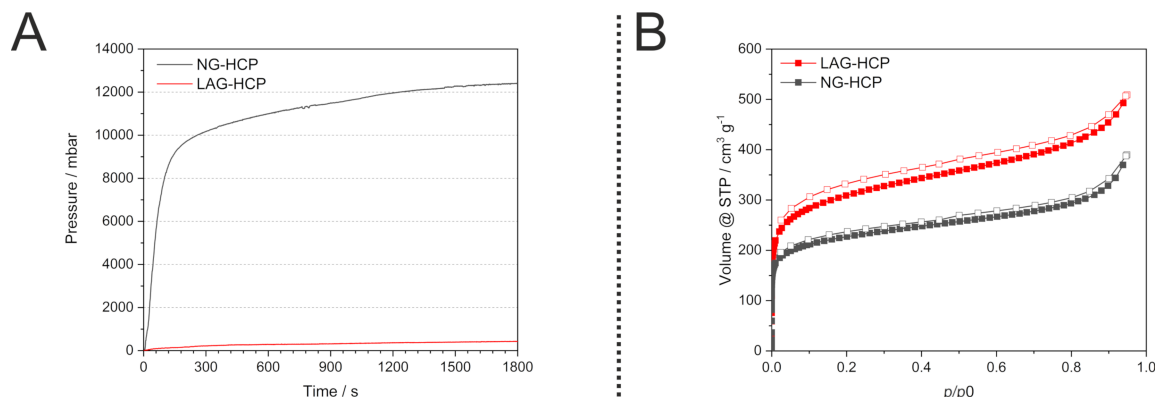
Figure 3: A: Evolution of pressure in the course of the reaction measured by the GTM system. The addition of 1 mL of Et$_2$O is sufficient to drastically reduce the released pressure. B: Comparison of the low pressure nitrogen isotherm of NG-HCP and LAG-HCP.

Table 1: Influence of the LAG additive on the textural properties of HCP[a].

Entry	Liquid additive	SSA$_{BET}$[b] [m^{2}g^{-1}]	V_{Pore}[c] [cm^{3}g^{-1}]
1	–	850	0.60
2	ethanol	1160	0.98
3	methanol	720	0.61
4	chloroform	1400	0.91
5	dichloromethane	1550	1.12
6	isopropanol	720	0.52
7[d]	diethyl ether	1720	1.06
8	ethyl acetate	760	0.51
9	tetrahydrofuran	1200	1.00
10[e]	–	1450	1.55

[a]All samples were synthesised under the following conditions: 35 min, 500 rpm, 6 equiv FeCl$_3$, 22 balls á 10 mm, 1 mL of liquid additive; [b]according to the Brunauer–Emmett–Teller theory, utilizing the Rouquerol method; [c]determined at p/p_0 = 0.99; [d]in the following denoted as LAG-HCP; [e]solution-based references, Sol-HCP.

tives in the gas and liquid phase is strongly favored. Recently, the advantage of HCP over various commonly available adsorbents in the selective liquid phase adsorption of least polar component in aqueous solution has been demonstrated [46,47]. Herein, the adsorption properties for the organic vapors benzene and cyclohexane are reported and the differences between LAG- HCP and the solvent-based reference material Sol-HCP are demonstrated.

First of all, is has to be noted that Sol-HCP (reference according to Schute et al. [11]) showed a specific BET surface area of 1450 m^{2}g^{-1}, hence, slightly below the LAG-HCP with a SSA of 1720 m^{2}g^{-1}. Still, it showed a higher total pore volume of 1.55 cm^{3}g^{-1} due to the higher ratio of mesopores and hence, a lower share of micropore volume (0.24 cm^{3}g^{-1}). Also, the pore size distribution proved to be rather broad (as reported before) compared to the mechanochemically synthesised material. For

both materials the overall uptake of benzene is higher than for previously reported HCP materials [48], resulting from the large BET surface areas (Figure 5A).

Compared to nitrogen physisorption, the benzene vaporsorption isotherms show a much more pronounced hysteresis over the whole relative pressure range. This effect can be explained by the strong interactions of the benzene molecules with the aromatic surface of the polymer via π–π interactions. The rather strong adsorption at the inner surface is overlapped by pore filling due to a condensation-like effect. Thereby, swelling results in a reversible structural change. Interestingly, this swelling effect occurs only moderately up to a temperature of 298 K. With further increasing temperature the swelling is much more pronounced with a significantly higher uptake at high relative pressure by condensation and a very pronounced hysteresis upon pressure-driven desorption (Figure 5B). A very
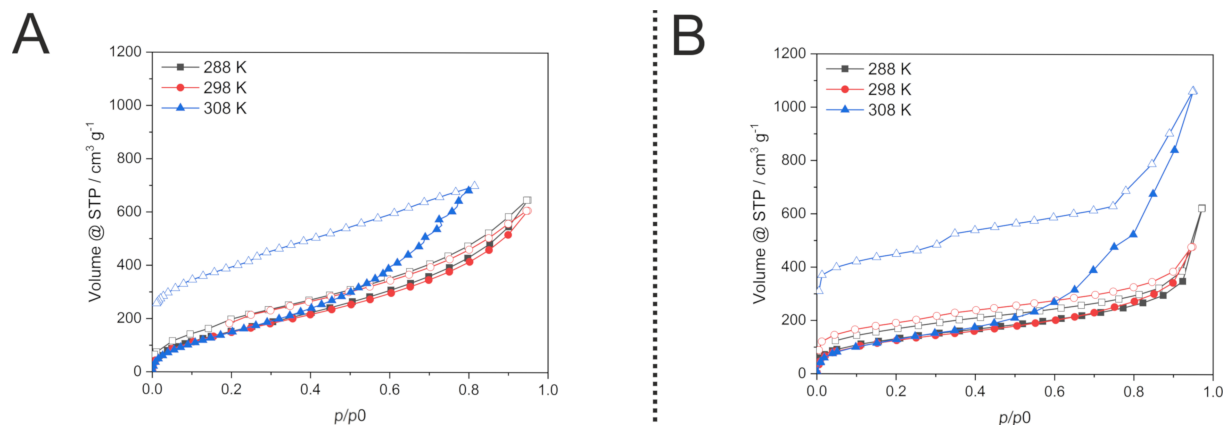
Figure 5: Physisorption isotherms of benzene vapour at different temperatures on HCP synthesised classically from solution (left, A) and mechanochemically (right, B). Filled symbols denote adsorption and open symbols desorption, respectively.

similar behaviour is observed for both HCP samples LAG-HCP and Sol-HCP. However, the Sol-HCP shows a steeper slope of the adsorption isotherm due to the broader pore size distribution. In contrast, the LAG-HCP with the narrow PSD shows a more pronounced uptake at low relative pressures.

In addition, cyclohexane vapour was measured in the same temperature range (Figure 6A). Over the whole relative pressure region a lower uptake is observed compared to the benzene vapour. In a similar fashion, but slightly weaker pronounced, an adsorption-desorption-hysteresis is found at higher temperature >298 K due to severe swelling. The difference in the uptake towards a favoured adsorption of benzene already points towards the potential for an adsorptive separation process of aromatic and aliphatic molecules with very similar physical properties.

To quantify the strength of adsorptive interactions from isotherms at various temperatures the isostatic heat of adsorption is calculated. Although in case of flexible materials with varying textural properties during adsorption and hence, a varying surface potential, this method should only be applied with great care and only used for a relative comparison of similar materials [49]. Absolute values calculated by this method are prone to great errors and should not be over-interpreted. Still, in our case the mechanochemically synthesised HCP shows an adsorption enthalpy at low loading of benzene of 70–80 kJ mol^{-1} that steadily decreases until it approximates the condensation enthalpy of pure benzene (Figure 6B). Interestingly, the heat of adsorption of cyclohexane is much lower with a maximum at low loading of approximately 50 kJ mol^{-1} and also decreasing until the condensation enthalpy is reached. Also, the condensation enthalpy of cyclohexane is reached at ca. 40% lower loading compared to benzene. This data points out the signifi-

cantly favoured adsorption of benzene due to aromatic π–π interaction in comparison to the significantly weaker bonding of aliphatic cyclohexane.

Conclusion

Summing up, we have demonstrated that mechanochemistry can be a suitable alternative in the synthesis of hyper-crosslinked polymers. By avoiding chlorinated solvents (typically 1,2-dichloroethane), the synthesis of this promising material can be undertaken in a greener, faster, and cheaper fashion. The obtained materials show surface areas as high as 1720 m^{2}g^{-1} with a narrower pore size distribution compared to solvent-based analogues. It has been found that the addition of small amounts of liquid (LAG) is not only reducing the vessel pressure during the synthesis, but is also beneficial towards the textural properties of the material. In organic vaporsorption experiments the adsorption of benzene was favoured over cyclohexane by strong π–π interaction with the aromatic framework. This has been proven by differences in uptake as well as by comparison of isosteric heat of adsorptions as direct indicator of the adsorption interactions.

Experimental

In our standard procedure HCP was synthesised through a mechanochemical reaction. This was accomplished by transferring 0.821 g 4,4'-bis(chloromethyl)-1,1'-biphenyl (Sigma-Aldrich) and 3.179 g (six equiv) of anhydrous iron(III) chloride (Sigma-Aldrich) as mediator into a 45 mL zirconium oxide milling vessel filled with 22 balls (10 mm, 3.19 ± 0.05 g) of the same material. Consequently, the vessel was transferred into a P7 premium line (Fritsch GmbH) and milled at 500 rpm for 35 minutes. After the synthesis the resulting polymers were washed with 200 mL of water and 100 mL of ethanol and dried at 80 °C for 12 hours.
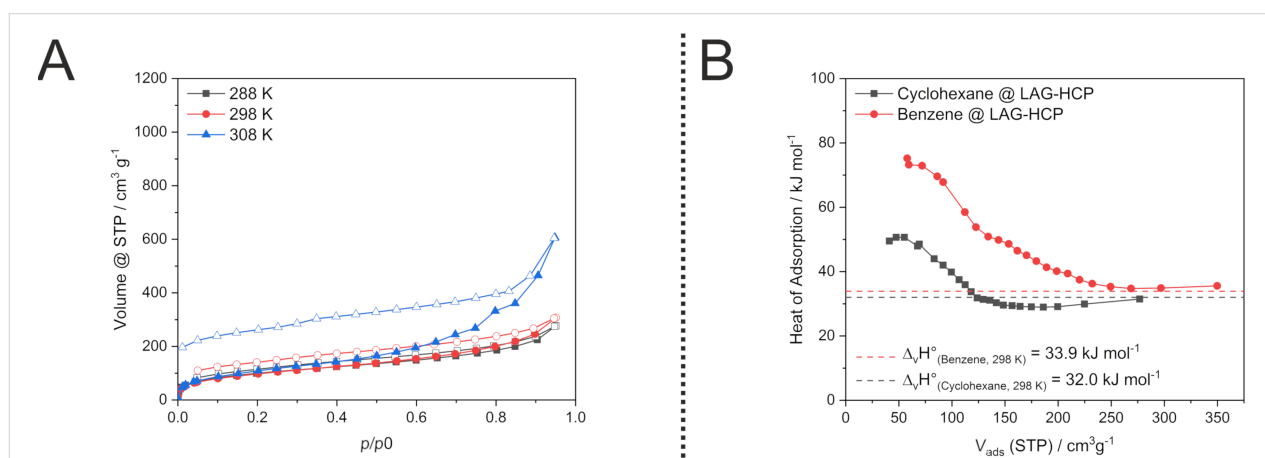

Figure 6: Physisorption isotherms of cyclohexane on mechanochemically synthesised HCP at temperatures 288, 298 and 303 K (left) and isosteric heat of adsorption of benzene and cyclohexane on HCP synthesised mechanochemically (LAG-HCP) (right).

For the LAG experiments the same quantities were used and 1 mL of the given liquid was added prior to the milling. The synthesis of the reference HCP from solution was carried out according to the procedure of Schute et al. [11]. Nitrogen physisorption measurements were performed at 77 K on an Autosorb-IQ-C-XR and Quadrasorb (Quantachrome Instruments). High purity gases were used for physisorption measurements (N_2: 99.999%). Specific surface areas (SSA_{BET}) were calculated using the equation from Brunauer, Emmet and Teller (BET) in a relative pressure range that fits to the consistency criteria proposed by Rouquerol and Llewellyn. Pore size distributions were calculated using the quenched solid density functional theory (QSDFT) method for carbon (slit pores, equilibrium kernel) on the adsorption branch. Total pore volumes were determined from the adsorption branch at $p/p_0 = 0.95$. Prior to physisorption experiments, all samples were activated at 353 K for 24 h under vacuum. Ball mill syntheses were carried out in a Fritsch Pulverisette 7 premium line planetary ball mill. Infrared spectroscopy (IR) was carried out on a Bruker Vertex 70 with a Specac Golden Gate ATR unit. A resolution of 2 cm^{-1} was utilized and the resulting spectra were treated with ATR-correction by the OPUS 6.5 software. Powder X-ray diffraction (PXRD) patterns were collected in transmission geometry (MYTHEN 1K detector) with a STOE STADI P diffractometer operated at 40 kV and 30 mA with a Ge monochromator using Cu Kα_1 radiation. Scanning electron microscopy (SEM/EDX) images were obtained using a Hitachi SU8020 SEM equipped with a secondary electron (SE) detector. Prior to the measurement the samples were prepared on an adhesive carbon pad and sputtered with gold to obtain the necessary electron conductivity. Thermogravimetric analysis (TGA) was performed on a Netzsch STA 409 PC/PG system using alumina crucibles under argon stream with the heating rate of 10 K min^{-1}. The vapor sorption experiments were carried out using a Autosorb iQ from Quantachrome equipped with a vapor source and a heated manifold. Before evaporation the adsorptive solvent was dried using molecular sieves 4 Å and degassed under vacuum.

Supporting Information

Supporting Information File 1
Additional information and figures.
[https://www.beilstein-journals.org/bjoc/content/supplementary/1860-5397-15-112-S1.pdf]

Acknowledgements

ORCID® iDs

Sven Grätz - https://orcid.org/0000-0001-6026-097X
Marcus Rose - https://orcid.org/0000-0001-8196-1353
Lars Borchardt - https://orcid.org/0000-0002-8778-7816

References

1. Schüth, F.; Sing, K. S. W.; Weitkamp, J., Eds. *Handbook of Porous Solids;* Wiley-VCH Verlag GmbH: Weinheim, Germany, 2002. doi:10.1002/9783527618286
2. Schneemann, A.; Bon, V.; Schwedler, I.; Senkovska, I.; Kaskel, S.; Fischer, R. A. *Chem. Soc. Rev.* **2014,** *43,* 6062–6096. doi:10.1039/c4cs00101j
3. Ding, S.-Y.; Wang, W. *Chem. Soc. Rev.* **2013,** *42,* 548–568. doi:10.1039/c2cs35072f
4. Chaoui, N.; Trunk, M.; Dawson, R.; Schmidt, J.; Thomas, A. *Chem. Soc. Rev.* **2017,** *46,* 3302–3321. doi:10.1039/c7cs00071e
5. Martín, C. F.; Stöckel, E.; Clowes, R.; Adams, D. J.; Cooper, A. I.; Pis, J. J.; Rubiera, F.; Pevida, C. *J. Mater. Chem.* **2011,** *21,* 5475–5483. doi:10.1039/c0jm03534c
6. Li, C.; Liu, M.; Pschirer, N. G.; Baumgarten, M.; Müllen, K. *Chem. Rev.* **2010,** *110,* 6817–6855. doi:10.1021/cr100052z
7. Kuhn, P.; Antonietti, M.; Thomas, A. *Angew. Chem., Int. Ed.* **2008,** *47,* 3450–3453. doi:10.1002/anie.200705710
8. Pandey, P.; Katsoulidis, A. P.; Eryazici, I.; Wu, Y.; Kanatzidis, M. G.; Nguyen, S. T. *Chem. Mater.* **2010,** *22,* 4974–4979. doi:10.1021/cm101157w
9. Ritter, N.; Senkovska, I.; Kaskel, S.; Weber, J. *Macromol. Rapid Commun.* **2011,** *32,* 438–443. doi:10.1002/marc.201000714
10. Tan, L.; Tan, B. *Chem. Soc. Rev.* **2017,** *46,* 3322–3356. doi:10.1039/c6cs00851h
11. Schute, K.; Rose, M. *ChemSusChem* **2015,** *8,* 3419–3423. doi:10.1002/cssc.201500829
12. Rightmire, N. R.; Hanusa, T. P. *Dalton Trans.* **2016,** *45,* 2352–2362. doi:10.1039/c5dt03866a
13. Tan, D.; Loots, L.; Friščić, T. *Chem. Commun.* **2016,** *52,* 7760–7781. doi:10.1039/c6cc02015a
14. Xu, C.; De, S.; Balu, A. M.; Ojeda, M.; Luque, R. *Chem. Commun.* **2015,** *51,* 6698–6713. doi:10.1039/c4cc09876e
15. Bolm, C.; Hernández, J. G. *Angew. Chem., Int. Ed.* **2019,** *58,* 3285–3299. doi:10.1002/anie.201810902
16. Michalchuk, A. A. L.; Tumanov, I. A.; Boldyreva, E. V. *CrystEngComm* **2019,** *21,* 2174–2179. doi:10.1039/c8ce02109k
17. Tan, D.; García, F. *Chem. Soc. Rev.* **2019,** *48,* 2274–2292. doi:10.1039/c7cs00813a
18. Howard, J. L.; Cao, Q.; Browne, D. L. *Chem. Sci.* **2018,** *9,* 3080–3094. doi:10.1039/c7sc05371a
19. Andersen, J.; Mack, J. *Green Chem.* **2018,** *20,* 1435–1443. doi:10.1039/c7gc03797j
20. Do, J.-L.; Friščić, T. *Synlett* **2017,** *28,* 2066–2092. doi:10.1055/s-0036-1590854
21. Užarević, K.; Wang, T. C.; Moon, S.-Y.; Fidelli, A. M.; Hupp, J. T.; Farha, O. K.; Friščić, T. *Chem. Commun.* **2016,** *52,* 2133–2136. doi:10.1039/c5cc08972g

22. Leistenschneider, D.; Jäckel, N.; Hippauf, F.; Presser, V.; Borchardt, L. *Beilstein J. Org. Chem.* **2017,** *13,* 1332–1341. doi:10.3762/bjoc.13.130

23. Schneidermann, C.; Jäckel, N.; Oswald, S.; Giebeler, L.; Presser, V.; Borchardt, L. *ChemSusChem* **2017,** *10,* 2416–2424. doi:10.1002/cssc.201700459

24. Zhang, E.; Hao, G.-P.; Casco, M. E.; Bon, V.; Grätz, S.; Borchardt, L. *J. Mater. Chem. A* **2018,** *6,* 859–865. doi:10.1039/c7ta10783h

25. Karak, S.; Kandambeth, S.; Biswal, B. P.; Sasmal, H. S.; Kumar, S.; Pachfule, P.; Banerjee, R. *J. Am. Chem. Soc.* **2017,** *139,* 1856–1862. doi:10.1021/jacs.6b08815

26. Karadeniz, B.; Howarth, A. J.; Stolar, T.; Islamoglu, T.; Dejanović, I.; Tireli, M.; Wasson, M. C.; Moon, S.-Y.; Farha, O. K.; Friščić, T.; Užarević, K. *ACS Sustainable Chem. Eng.* **2018,** *6,* 15841–15849. doi:10.1021/acssuschemeng.8b04458

27. Fidelli, A. M.; Karadeniz, B.; Howarth, A. J.; Huskić, I.; Germann, L. S.; Halasz, I.; Etter, M.; Moon, S.-Y.; Dinnebier, R. E.; Stilinović, V.; Farha, O. K.; Friščić, T.; Užarević, K. *Chem. Commun.* **2018,** *54,* 6999–7002. doi:10.1039/c8cc03189d

28. Chen, Y.; Wu, H.; Liu, Z.; Sun, X.; Xia, Q.; Li, Z. *Ind. Eng. Chem. Res.* **2018,** *57,* 703–709. doi:10.1021/acs.iecr.7b03712

29. Casco, M. E.; Badaczewski, F.; Grätz, S.; Tolosa, A.; Presser, V.; Smarsly, B. M.; Borchardt, L. *Carbon* **2018,** *139,* 325–333. doi:10.1016/j.carbon.2018.06.068

30. Ohn, N.; Shin, J.; Kim, S. S.; Kim, J. G. *ChemSusChem* **2017,** *10,* 3529–3533. doi:10.1002/cssc.201700873

31. Grätz, S.; Borchardt, L. *RSC Adv.* **2016,** *6,* 64799–64802. doi:10.1039/c6ra15677k

32. Ravnsbæk, J. B.; Swager, T. M. *ACS Macro Lett.* **2014,** *3,* 305–309. doi:10.1021/mz500098r

33. Malca, M. Y.; Ferko, P.-O.; Friščić, T.; Moores, A. *Beilstein J. Org. Chem.* **2017,** *13,* 1963–1968. doi:10.3762/bjoc.13.191

34. Ohn, N.; Kim, J. G. *ACS Macro Lett.* **2018,** *7,* 561–565. doi:10.1021/acsmacrolett.8b00171

35. Grätz, S.; Wolfrum, B.; Borchardt, L. *Green Chem.* **2017,** *19,* 2973–2979. doi:10.1039/c7gc00693d

36. Zhu, X.; Tian, C.; Jin, T.; Browning, K. L.; Sacci, R. L.; Veith, G. M.; Dai, S. *ACS Macro Lett.* **2017,** *6,* 1056–1059. doi:10.1021/acsmacrolett.7b00480

37. Troschke, E.; Grätz, S.; Lübken, T.; Borchardt, L. *Angew. Chem.* **2017,** *129,* 6963–6967. doi:10.1002/ange.201702303

38. Jamal, R.; Shao, W.; Xu, F.; Abdiryim, T. *J. Mater. Res.* **2013,** *28,* 832–839. doi:10.1557/jmr.2013.23

39. Biswal, B. P.; Chaudhari, H. D.; Banerjee, R.; Kharul, U. K. *Chem. – Eur. J.* **2016,** *22,* 4695–4699. doi:10.1002/chem.201504836

40. Zhu, X.; Hua, Y.; Tian, C.; Abney, C. W.; Zhang, P.; Jin, T.; Liu, G.; Browning, K. L.; Sacci, R. L.; Veith, G. M.; Zhou, H.-C.; Jin, W.; Dai, S. *Angew. Chem., Int. Ed.* **2018,** *57,* 2816–2821. doi:10.1002/anie.201710420

41. Posudievsky, O. Y.; Kozarenko, O. A. *Polym. Chem.* **2011,** *2,* 216–220. doi:10.1039/c0py00212g

42. Grätz, S.; Oltermann, M.; Troschke, E.; Paasch, S.; Krause, S.; Brunner, E.; Borchardt, L. *J. Mater. Chem. A* **2018,** *6,* 21901–21905. doi:10.1039/c8ta03684e

43. Rose, M.; Klein, N.; Senkovska, I.; Schrage, C.; Wollmann, P.; Böhlmann, W.; Böhringer, B.; Fichtner, S.; Kaskel, S. *J. Mater. Chem.* **2011,** *21,* 711–716. doi:10.1039/c0jm02998j

44. Grätz, S.; Beyer, D.; Tkachova, V.; Hellmann, S.; Berger, R.; Feng, X.; Borchardt, L. *Chem. Commun.* **2018,** *54,* 5307–5310. doi:10.1039/c8cc01993b

45. Andersen, J.; Mack, J. *Angew. Chem., Int. Ed.* **2018,** *57,* 13062–13065. doi:10.1002/anie.201805263

46. Detoni, C.; Gierlich, C. H.; Rose, M.; Palkovits, R. *ACS Sustainable Chem. Eng.* **2014,** *2,* 2407–2415. doi:10.1021/sc5004264

47. Schute, K.; Detoni, C.; Kann, A.; Jung, O.; Palkovits, R.; Rose, M. *ACS Sustainable Chem. Eng.* **2016,** *4,* 5921–5928. doi:10.1021/acssuschemeng.6b00096

48. Wang, G.; Dou, B.; Wang, J.; Wang, W.; Hao, Z. *RSC Adv.* **2013,** *3,* 20523–20531. doi:10.1039/c3ra41450g

49. de Lange, M. F.; Verouden, K. J. F. M.; Vlugt, T. J. H.; Gascon, J.; Kapteijn, F. *Chem. Rev.* **2015,** *115,* 12205–12250. doi:10.1021/acs.chemrev.5b00059

Mechanochemical amorphization of chitin: impact of apparatus material on performance and contamination

Thomas Di Nardo and Audrey Moores[*]

Abstract

Herein, we present a study of the impact of the jar and ball medium on the performance in the mechanochemical amorphization of chitin. We measured the crystallinity index of chitin after milling it in a vibration mill in an apparatus made of copper, aluminum, brass, tungsten carbide, zirconia, stainless steel, polytetrafluoroethylene (PTFE), or poly(methyl methacrylate) (PMMA). These materials offer a range of Vickers hardness values and the impact of these parameters is discussed. The role of the size and mass of the balls is also studied in the case of stainless steel. This study also highlights one of the major challenges during milling, which is contamination of the studied samples.

Introduction

The last decade has seen a tremendous development in the field of mechanochemistry, which was notably covered in the *New York Times* in 2016 [1]. Yet, mechanochemistry is hardly a novel concept, since it is likely among the most ancient methods for human beings to practice chemistry. Indeed the ability to produce fire is considered a crucial landmark for human development, and archeological evidences indicate that anthropogenic fire production relied on wood-on-wood friction or on percussion or friction of a siliceous rock against pyrite [2,3]. Mechanochemistry comes with intrinsic advantages associated with the lack of solvent use during reaction, thus largely reducing the generation of waste [4] even in active pharmaceu-

tical ingredient synthesis [5]. Yet mechanochemistry also allows the production of novel materials, which are distinct from what is enabled via solvothermal methods [6-8]. Finally, it also opens novel opportunities to react and functionalize solvent recalcitrant materials [9-13], including biomass-based materials [14-25]. Although the technique has been demonstrated to be useful, there are still many questions yet to be answered on the effects of reaction conditions on performance in mechanochemical systems. A number of groups have looked into better understanding the role of temperature, mixing frequency, pressure, reactor medium and atmosphere to relative degrees depending on equipment [5,26-34]. In particular, the

Mack group has used an elegant strategy to evaluate the energy delivery for a Diels−Alder reaction performed under mechanochemical conditions and was able to correlate reactivity, or lack thereof, with the specific reaction kinetic parameters [33]. There is, however, an interest in investigating these aspects further. In particular, it would be interesting to track the role of parameters such as ball size and mass on the progress of the reaction. In mechanochemistry, it is accepted that chemical reactions are induced by the delivery of energy, by collision. The impact force is thus of importance and depends on the weight of the balls and [26] the surface of impact [28]. Also, in the context of the milling of crystalline and/or fairly hard materials, the nature of the milling media composing the balls and jars, and their hardness parameter, should have an impact [33], an effect that needs better documentation.

Additionally, mechanochemical treatment may cause materials to be contaminated by the apparatus material through wear from friction and impact. This wear would incidentally leave residual amounts of material from the jars and balls in the reagents and products as a contamination. Milling media can have a catalytic effect due to leaching or surface adsorption [7,35-37]. Contamination has been noted in alloying [26,38] as well as amorphization of hard materials [39], and could cause doping effects in coordination polymers [40,41]. Yet a systematic study of quantitative contamination as a function of the medium has not been reported.

Mechanochemistry is a promising strategy towards the activation, functionalization and deconstruction of biomass. Mechanochemical activation can expedite polysaccharide hydrolytic cleavage [20-23]. Milling can also facilitate chitin depolymerization [24] and when used with base simultaneously deacetylate and depolymerize chitin [42]. One of the key processes in the context of biomass upgrading is amorphization. Indeed, both chitin and cellulose are extracted as highly crystalline material and their mechanochemical amorphization has been explored as a means to favor subsequent depolymerization [16], or functionalization [18]. For functionalization of these materials, it has been shown that amorphization as a pretreatment can be utilized to expose more functional groups to the surface, increasing the rate of reaction. Amorphization can also be used for better materials packing increasing hardness after sintering [17].

This study is important as the choice of milling media may be conditioned by the need to select, for instance, transparent jars to perform in situ measurements [6,43-47]. In these cases, better understanding of milling ball choice would allow one to control energy input in the system as well as minimize jar damage and contamination. Creative setups have also been developed where

the measurement window lies outside of the milling chamber where sample can pass in and out for continuous monitoring [48]. This allows for varying milling media with the benefit of in situ measurements.

For some processes like reactive aging with enzymes [22], polytetrafluoroethylene (PTFE) jars were preferred over stainless steel ones, since the latter caused the reactive mixture to adhere to the jars, which was not the case of the former. In another example, for the metal-free transfer hydrogenation of carbonyl compounds, PTFE was used instead of steel to eliminate the possibility of catalysis from the milling media [9]. In these cases, milling is used as a mixing method, whereby the reactions did not require large activation energies to be driven forward [33]. Soft and hard milling can be considered from a multitude of parameters where ball to powder ratio (BPR) is used as a way to "concentrate" or "dilute" kinetic energy from the milling media by reducing or increasing the milled powder ratio [26]. Furthermore, the size of the jar, the size, mass [28] and number of balls [29,49,50], as well as jar filling [26,30] will affect kinetic energy transfer. Although some comparisons on milling media hardness have been considered and showed an effect on the yield [29-31], to the best of our knowledge, there are no larger studies comparing several materials, especially with consideration to biomass amorphization and contamination.

Amorphization is a common process whereby the crystallinity of a material is reduced by mechanical forces [17,24,50,51] or otherwise [52] by deforming particles and breaking lattice imperfections [50]. For biomass processing, amorphization has been used in several studies [24,53,54], either as a pretreatment [21] prior to deacetylation [18,55], enzymatic [22,56,57] or acidic depolymerization [23,24] and simultaneously during processing [42], yielding oligomers and monomers. Differentiating these regions of impact would be of great value for biomass processing. It is therefore important to understand precisely how to master media selection: finding the right combination of balls, size and apparatus materials can help to optimize the energy input while allowing the desired loss of crystallinity for hard milling or maintaining crystallinity for soft milling techniques.

In order to better understand the role of the milling medium on polymer reactivity, we launched a systematic study of the effects of a number of medium parameters onto a model reaction, namely the amorphization of chitin where interchain stabilization is greater than 250 kJ/mol based on density functional theory (DFT) calculation [58]. We explored the role of the material of the jar and the ball, ball size and mass, while concentration on amorphization performance, measured by powder X-ray

diffraction (PXRD). We selected for this study reaction jars made of copper, aluminum, brass, tungsten carbide, zirconia, stainless steel, PTFE, or poly(methyl methacrylate) (PMMA) paired with one ball of the same composition with either a diameter of 9.5 mm or mass of approximately 2 g. We could determine that Vickers hardness is a key parameter determining the ability to perform amorphization of biomass materials especially when considering efficient kinetic energy transfer [59]. Finally, the effect of materials contamination on mills samples was tested by inductively coupled plasma optical emission spectrometry (ICP–OES) and X-ray photoelectron spectroscopy.

Results and Discussion
Study of chitin amorphization as a function of medium hardness

In this study, we probed the effect of milling parameters on the performance of chitin amorphization. As a first experiment, we wanted to screen the effect of the milling media. In a typical experiment, a jar was filled with 200 mg of shrimp PG chitin, fitted with one ball of the same material as the jar and milled in a vibrational mill for 30 min. Eight milling media were tested: stainless steel (SS), zirconia (ZrO_2), copper (Cu), aluminum (Al), brass, tungsten carbide (WC), poly(methyl methacrylate) (PMMA), and polytetrafluoroethylene (PTFE). These media have distinct density; we needed to normalize the resulting experiments. We expected two ball parameters to play a role in the process: the contact surface area of the ball with the jar (impact density), which depends on the ball size, and the mass of the ball, which impacts the kinetic energy delivered during milling.

We thus ran two series of tests with balls of different materials (mentioned above), one where ball mass was chosen to be as close as possible to 2 g (2.16 +/− 0.22 g, see Table S1, Supporting Information File 1 for exact values), while its diameter varied based on density, and one with balls of 9.5 mm in diameter which vary in mass also based on density. Both fixed parameters were chosen based on the availability of such milling balls in our inventories or from suppliers, and based on physical constraints. The lowest density material in our study, PMMA, has a 2 g ball diameter of 16 mm, which just fits the inner diameter of the jar, i.e. 19 mm. Amorphization progress was followed by PXRD. Characterization of the crystallinity index (CrI) of chitin can be determined by comparing the area of the crystalline region to the global area in the PXRD spectrum (Figure S2, Supporting Information File 1) [60]. Untreated chitin powder CrI was measured to be 65.8%. CrI of samples after the milling reaction were plotted as a function of the medium for each of the two series (Figure 1). A clear trend was observed with the effect of material hardness on amorphization. PTFE afforded poor amorphization, whether we look at 2 g balls or 9.5 mm ones. Al, Cu, brass, SS, WC and ZrO_2 were all performing well to reduce crystallinity by at least a half and give a range of values between 10 and 30%. PMMA gave an intermediate result, whereby 9.5 mm (0.5349 g) gave poor amorphization (61%) while the 2 g equivalent (2.4588 g) afforded a good one (33.5%).

The different materials tested in this experiment feature very distinct hardness values. We retrieved Vickers hardness values from material specification sheets to correlate amorphization
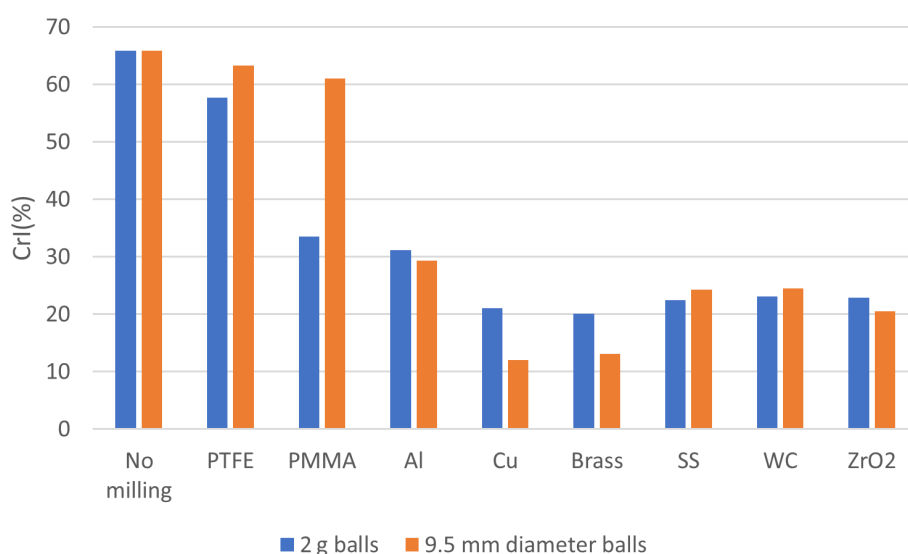

Figure 1: CrI% for chitin samples, before and after milling in a jar with one ball made of SS, ZrO_2, Cu, Al, brass, WC, PMMA, PTFE. One series has ball mass = 2 g (blue) and one ball diameter = 9.5 mm (in orange). Experimental conditions: 200 mg of chitin, milling time: 30 min, milling frequency 29.5 Hz.

performance with them (Figure 1). With the 2 g ball series, a clear trend can be seen. A crossover point exists where all materials of Vickers hardness larger than the one of chitin itself, which was estimated to be 25–80 kgf/mm^2 (245–784 MPa) from chitin insect cuticle [61], performed very well for the amorphization, while materials of lower hardness hardly affected the crystallinity of the substrate. Interestingly, when comparing the balls by size, Cu and brass gave really low values of crystallinity, despite a middle range hardness. This indicates that the comparison by mass is more relevant. Cu and brass are fairly dense materials, which explain their good performance, particularly for the 9.5 mm series where their mass would comparatively be more significant (Figure 2).

It was interesting to note that while the Vickers hardness of SS, WC and ZrO$_2$ are vastly different, these three materials seem to behave similarly as jar and ball mechanochemical media for the studied reaction. We were curious to investigate if varying the frequency of milling could reveal an effect of these materials density. We thus selected SS and ZrO$_2$ media and varied the frequency from 10, to 20 and finally 29.5 Hz (Figure 3). When milling at 29.5 Hz, with a ≈2 g ball in ZrO$_2$ and SS (Table S1, Supporting Information File 1 for exact mass values), little difference was observed in the CrI of chitin after milling, achieving values of 22.9 and 22.4, respectively. Decreasing the frequency decreases the kinetic energy delivered from the ball providing greater differentiation between ball mass and density in terms of amorphization efficiency. Decreasing the frequency

to 20 Hz maintained overall higher CrI of 30.4 and 30.2 for ZrO$_2$ and SS, respectively. At 10 Hz, however, we clearly observed a difference in the resulting CrI, reaching 62.3 and 51.4, for ZrO$_2$ and SS, respectively. At this frequency, the lower density material, ZrO$_2$ (6.0 g/cm^3) afforded less amorphization than the denser one, SS (7.7 g/cm^3). At this frequency the impact force seems to play a more important role in amorphization efficacy.

In order to deepen hardness analysis, we decided to vary the ball and jar composition to test materials with hardness below and over the one of chitin cuticle (245 MPa). PTFE has a lower hardness of 30 MPa, while SS and ZrO$_2$ have hardness values of 2000 and 10,000 MPa, respectively. Figure 4 displays the crystallinity index of chitin after being milled for 30 min in jars of PTFE, SS or ZrO$_2$, fitted with balls of PTFE, SS or ZrO$_2$. This study revealed clearly that materials featuring a Vickers hardness higher than the one of the reactive mediums are needed, for both the jar and the ball. If either the jar or the ball is composed of PTFE, the crystallinity of chitin is hardly affected. We thus demonstrated that the milling medium choice is very important in the case of chitin amorphization, and concluded that we have an on/off effect whereby as long as we have a jar and ball of sufficiently hard material, the performance towards amorphization will be essentially the same. Based on this, we wanted to explore the effect of the kinetic energy on the progress of amorphization and thus looked at the effect of ball mass and size.
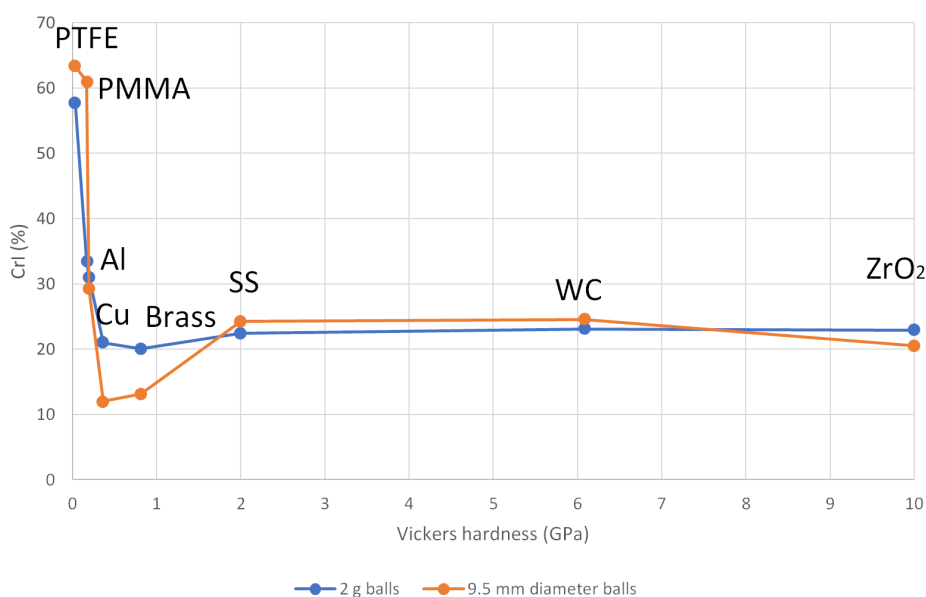
Figure 2: Value of CrI after milling as a function of the Vickers hardness values of the media (Jar and ball) used in this study. Two series are compared: One where the balls are 2 g, and one where they are 9.5 mm in diameter. Experimental conditions: 200 mg of chitin, milling time: 30 min, milling frequency 29.5 Hz.
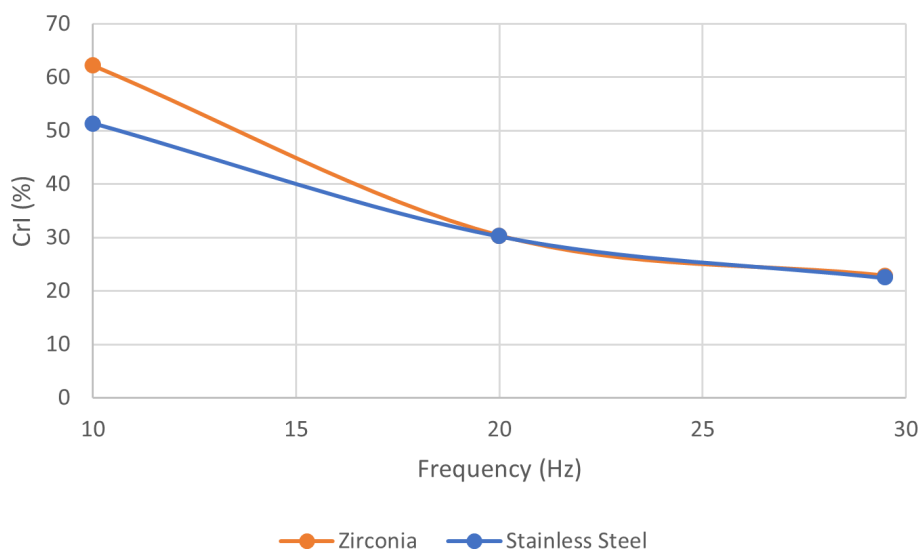
Figure 3: Crystallinity index (%) after milling as a function of frequency. ZrO_2 and SS jars are compared, both with 1 2 g ball of the same material. Experimental conditions: 200 mg of chitin, milling time: 30 min, milling frequencies varied from 10, to 20 and 29.5 Hz.
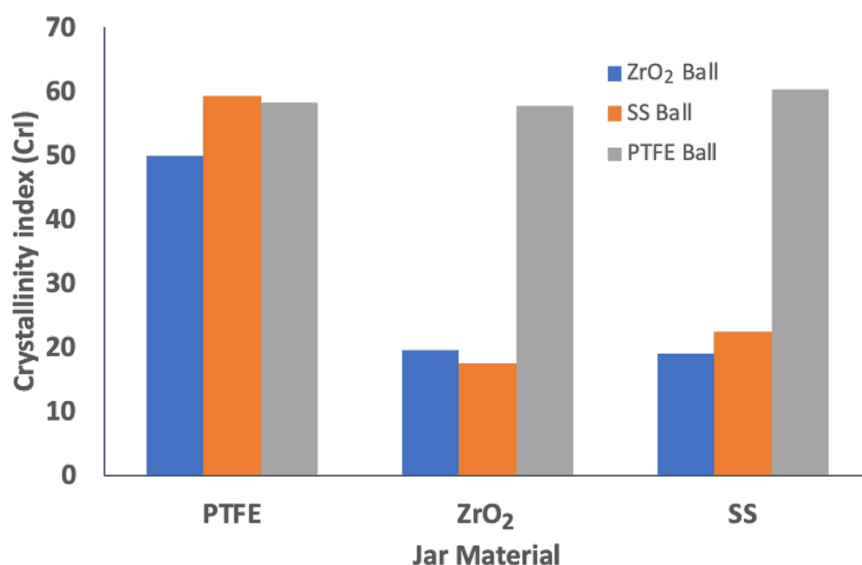
Figure 4: Crystallinity index (%) of chitin milled with 9.5 mm balls of PTFE, ZrO_2 and SS each used in jars of PTFE, ZrO_2 or SS. Experimental conditions: 200 mg of chitin, milling time: 30 min, milling frequency 29.5 Hz.

Study of chitin amorphization as a function of SS ball size and mass

To explore the effect of the ball size and mass, we selected one single medium, stainless steel (SS), based on the fact it has sufficient hardness to afford good chitin amorphization. SS is also a common medium used in mechanochemistry, meaning we could easily purchase SS balls of various sizes and masses. Specifically, chitin amorphization was performed with one SS ball in a SS jar, with ball sizes of 7.8, 9.5, 10 and 15 mm.

The mass of these balls also differed accordingly. The resulting crystal index (CrI) for chitin after 30 min of milling is provided in Figure 5. This demonstrates that the ball mass has a direct impact on amorphization. In the initial phase, where ball mass is small (1–5 g), crystallinity was drastically reduced from values of 65% to between 23 and 35%. Beyond this point (ball masses of 5 to 12 g), further reduction takes place but was more modest with final values of CrI between 17 and 22%.

Figure 5: Correlation between the ball mass (orange line) or kinetic energy (blue line) with the crystallinity of chitin after milling in SS jar fitted with 1 SS ball. Experimental conditions: 200 mg of chitin, milling time: 30 min, frequency 29.5 Hz.
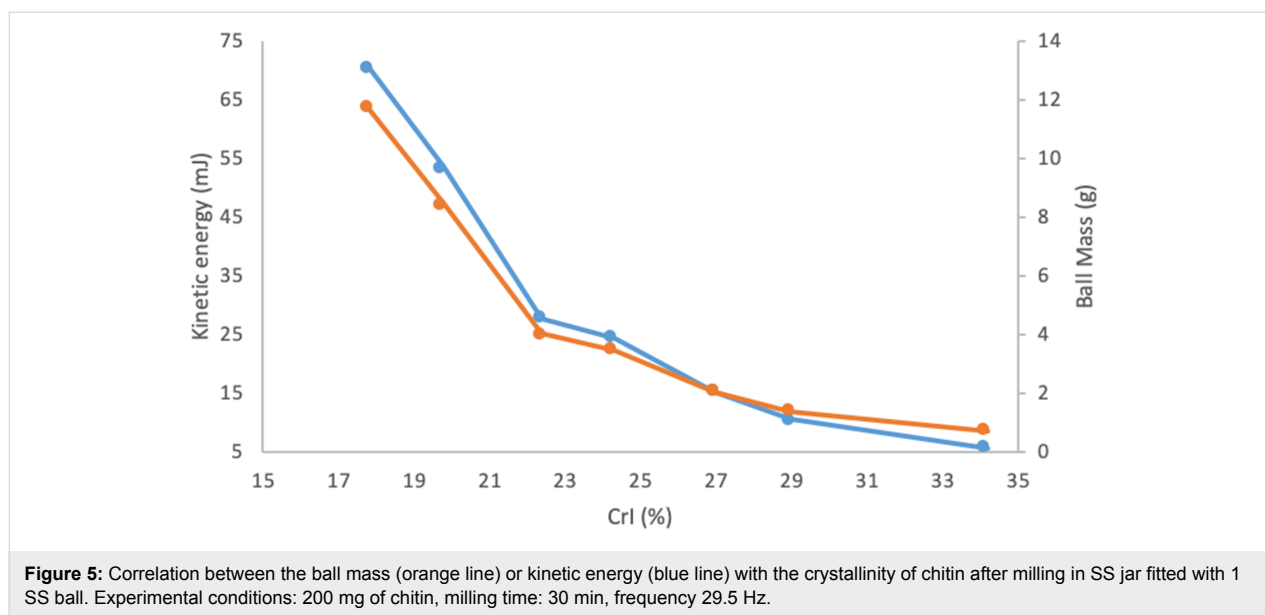
This suggested we should further correlate amorphization with kinetic energy formally. To calculate the kinetic energy, we assume a simplified linear motion of the ball in the jar, the time to travel the linear path length based on the frequency of milling, the diameter and mass of the ball. Although not all kinetic energy is transferred from the ball to the powder, the difference is considered negligible [59].

$$E_k = \frac{1}{2}mv^2, \tag{1}$$

where *m* is the mass of the ball, *v* is the average speed of the ball in the jar and *v* is determined by

$$v = \frac{d}{t}, \tag{2}$$

where *d* is the overall path length composed of the internal jar path length (varied by jar) less the ball diameter plus the additional distance from movement of the arm swing in the mill (26.4 mm) and *t* is the time it takes to for the mill arm to swing from left to right, considering the frequency used (29.5 Hz) is equal to 1/59 seconds.

We varied the SS ball mass and recorded the performance in terms of chitin amorphization. In Figure 5, we present these results, overlaid with the plotting of the kinetic energy as a function of chitin amorphization. Both the kinetic energy and the mass of the ball are strongly positively correlated with the obtained chitin amorphization. There is a deviation in kinetic

energy at higher masses since the ball size decrease the internal milling path length.

Study of chitin contamination by ball milling medium

Chitin is an off-white yellow powder. Milling in ZrO_2 with a ZrO_2 ball did not affect its aspect, while milling in SS milling media yielded a gray powder (Figure S4 and Figure S5, Supporting Information File 1). This raises the question of contamination in the milling process, which we explored further. ICP–OES is the technique of choice to establish the metal content in organic matrices. 50 mg of sample was digested in 5 mL aqua regia for 2 h at 90 °C, dissolving the organic biomass and metal contaminants. Milling was conducted in the same manner as amorphization above. The contamination Zr, Fe, W, Al, Cu and Cu was then measured by ICP–OES after milling in ZrO_2, SS, WC, Al, Cu and brass media (jar and ball), respectively (Figure 6). ZrO_2 afforded almost no biomass contamination. All other metal containing systems did afford more contamination. SS was actually the least polluting with a contamination value of 1.6 ppm and the others were between 37 and 212 ppm. While Vickers hardness can give a good indication of impact energy transfer from ball to material, it did not correlate as well with the contamination trend. It suggests also that metal release during milling took place from scratching between the ball, the powder and the jar. Contamination by fluorine containing species is harder to establish by ICP–OES, so in order to measure potential release when milling in PTFE, we turned to XPS (Figure S1, Supporting Information File 1). When milling in a PTFE jar with ZrO_2, fluorine was found in the high concentration of 6.9%. This very high contamination level results from the fact PTFE is very soft and easily
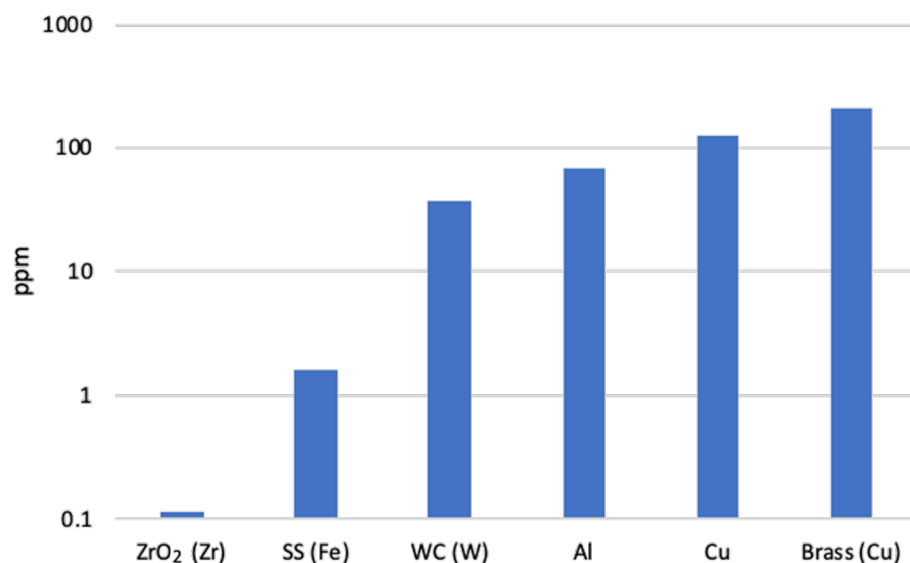
Figure 6: Metal contamination of milled chitin determined by ICP–OES, as a function of the milling medium. The contaminating element is provided in parenthesis.

scratched by chitin. Clear signs of wear were observed in PTFE jars after several runs, confirming the mechanism.

Conclusion

Milling is an effective way to amorphize polysaccharides. Amorphization is dependent on factors such as mass, impact area, and material hardness. There is a crossover point for jar and ball hardness, if the jar and ball hardness are below the hardness of the milling mass there is little effect on amorphization, and above this hardness there is a significant degree of amorphization. There is a plateau as well where increased hardness does not increase amorphization as max impact energy transfer to the sample has been achieved. This can give control over mixing or physical modification of the polysaccharides for mechanochemistry experiments and allow for better selection of milling media. Contamination has been demonstrated as potential issue for milling. Milling is considered a neat method, yielding clean products but careful considerations must be taken when selecting milling media for this reason as well.

Experimental
Chemicals

Practical grade chitin was purchased from Sigma-Aldrich Co. LLC (St-Louis, MO). Milling media was purchased from McMaster-Carr Supply Co. (Elmhurst, IL) with the exception of ZrO_2 balls, which were purchased from Glen Mills Inc. (Clifton, NJ). The aluminum and copper balls were carved out of aluminum and copper rods purchased from Home Depot and McMaster-Carr, respectively. The brass jar was carved out of a brass hex rod from McMaster-Carr. The copper jar was made out of copper pipe and copper end caps purchased from Canadian tire. The end caps were domed to provide the standard milling jar internal rounded ends. All other jars were purchased from Retsch.

Mechanochemical amorphization of polysaccharides

In a typical experiment, 200 mg of polysaccharide, chitin was placed in a jar equipped with one ball and milled in a MM 400 mixer mill for 30 min at 29.5 Hz. The resulting powder was used as is for analysis.

Powder X-ray diffraction (PXRD)

Sample diffractogram was recorded from 5° to 40° on a zero-background plate using a Bruker D8 ADVANCE X-ray diffractometer equipped using Cu Kα (λ = 1.54 Å) source. Chitin crystallinity was determined by comparing the entire area of the diffractogram (global area) and the area of the crystalline peaks (reduced area). Where CrI (%) = 100%amorphous and %amorphous = [(global area – reduced area)/global area] × 100 [60].

X-ray photoelectron spectroscopy (XPS)

Samples were analyzed on a Fischer Scientific Kα spectrometer using a spot size of 200 μm, running 5 survey scans at 200 mV for 50 ms residence times, and 10 scans for specific elements, also at residence times of 50 ms. Deconvolution and peak position were determined using Avantage processing software.

IR

ATR-IR spectra were recorded using a Perkin-Elmer Spectrum 400 for 16 scans from 4000 cm^{-1} to 450 cm^{-1} using approximately 2 mg of sample.

ICP

ICP analysis was conducted on a Thermo iCap 6500 Duo Series spectrometer. The samples were digested in aqua regia (5 mL) for 2 hours at 90 °C. The samples were then diluted to total volume of 50 mL with DI water and run against standards of the elements of interest.

Kinetic energy calculation

Kinetic energy of the ball determined by using the mass of the ball and the maximum estimated velocity based on frequency and internal jar milling length plus swing arm movement distance of mixer mill.

Supporting Information

Supporting Information File 1

Additional experimental data and spectra.
[https://www.beilstein-journals.org/bjoc/content/
supplementary/1860-5397-15-119-S1.pdf]

Acknowledgements

ORCID® iDs

Thomas Di Nardo - https://orcid.org/0000-0003-3696-8470
Audrey Moores - https://orcid.org/0000-0003-1259-913X

References

1. Lim, X. Grinding Chemicals Together in an Effort to Be Greener. *New York Times.* New York July 18, 2016, pp 1–6.
2. Stapert, D.; Johansen, L. *Geol. Mijnbouw* **1999,** *78,* 147–164. doi:10.1023/a:1003802432463
3. Sorensen, A.; Roebroeks, W.; van Gijn, A. *J. Archaeol. Sci.* **2014,** *42,* 476–486. doi:10.1016/j.jas.2013.11.032
4. Baláž, P. Applied Mechanochemistry. *Mechanochemistry in Nanoscience and Minerals Engineering;* Springer-Verlag: Berlin, 2008; pp 297–405. doi:10.1007/978-3-540-74855-7_6
5. Colacino, E.; Porcheddu, A.; Halasz, I.; Charnay, C.; Delogu, F.; Guerra, R.; Fullenwarth, J. *Green Chem.* **2018,** *20,* 2973–2977. doi:10.1039/c8gc01345d
6. Katsenis, A. D.; Puškarić, A.; Štrukil, V.; Mottillo, C.; Julien, P. A.; Užarević, K.; Pham, M.-H.; Do, T.-O.; Kimber, S. A. J.; Lazić, P.; Magdysyuk, O.; Dinnebier, R. E.; Halasz, I.; Friščić, T. *Nat. Commun.* **2015,** *6,* No. 6662. doi:10.1038/ncomms7662
7. Rak, M. J.; Saadé, N. K.; Friščić, T.; Moores, A. *Green Chem.* **2014,** *16,* 86–89. doi:10.1039/c3gc41827h
8. Howard, J. L.; Cao, Q.; Browne, D. L. *Chem. Sci.* **2018,** *9,* 3080–3094. doi:10.1039/c7sc05371a
9. Li, A. Y.; Segalla, A.; Li, C.-J.; Moores, A. *ACS Sustainable Chem. Eng.* **2017,** *5,* 11752–11760. doi:10.1021/acssuschemeng.7b03298
10. Grätz, S.; Beyer, D.; Tkachova, V.; Hellmann, S.; Berger, R.; Feng, X.; Borchardt, L. *Chem. Commun.* **2018,** *54,* 5307–5310. doi:10.1039/c8cc01993b
11. Wang, L.; Solin, N. *J. Mater. Sci.* **2018,** *53,* 13719–13732. doi:10.1007/s10853-018-2461-7
12. Sharma, L.; Kiani, D.; Honer, K.; Baltrusaitis, J. *ACS Sustainable Chem. Eng.* **2019,** *7,* 6802–6812. doi:10.1021/acssuschemeng.8b06129
13. Leonardi, M.; Villacampa, M.; Menéndez, J. C. *Chem. Sci.* **2018,** *9,* 2042–2064. doi:10.1039/c7sc05370c
14. Dabral, S.; Wotruba, H.; Hernández, J. G.; Bolm, C. *ACS Sustainable Chem. Eng.* **2018,** *6,* 3242–3254. doi:10.1021/acssuschemeng.7b03418
15. Weißbach, U.; Dabral, S.; Konnert, L.; Bolm, C.; Hernández, J. G. *Beilstein J. Org. Chem.* **2017,** *13,* 1788–1795. doi:10.3762/bjoc.13.173
16. Yu, Y.; Long, Y.; Wu, H. *Energy Fuels* **2016,** *30,* 1571–1578. doi:10.1021/acs.energyfuels.5b02196
17. Sopicka-Lizer, M.; Pawlik, T. *J. Korean Ceram. Soc.* **2012,** *49,* 337–341. doi:10.4191/kcers.2012.49.4.337
18. Di Nardo, T.; Hadad, C.; Nguyen Van Nhien, A.; Moores, A. *Green Chem.* **2019**. doi:10.1039/c9gc00304e
19. Fiss, B. G.; Hatherly, L.; Stein, R. S.; Friščić, T.; Moores, A. *ACS Sustainable Chem. Eng.* **2019,** *7,* 7951–7959. doi:10.1021/acssuschemeng.9b00764
20. Nakagawa, Y. S.; Oyama, Y.; Kon, N.; Nikaido, M.; Tanno, K.; Kogawa, J.; Inomata, S.; Masui, A.; Yamamura, A.; Kawaguchi, M.; Matahira, Y.; Totani, K. *Carbohydr. Polym.* **2011,** *83,* 1843–1849. doi:10.1016/j.carbpol.2010.10.050
21. Razumovskii, S. D.; Podmaster'ev, V. V.; Zelenetskii, A. N. *Catal. Ind.* **2011,** *3,* 23–27. doi:10.1134/s2070050411010107
22. Hammerer, F.; Loots, L.; Do, J.-L.; Therien, J. P. D.; Nickels, C. W.; Friščić, T.; Auclair, K. *Angew. Chem., Int. Ed.* **2018,** *57,* 2621–2624. doi:10.1002/anie.201711643
23. Hick, S. M.; Griebel, C.; Restrepo, D. T.; Truitt, J. H.; Buker, E. J.; Bylda, C.; Blair, R. G. *Green Chem.* **2010,** *12,* 468–474. doi:10.1039/b923079c
24. Margoutidis, G.; Parsons, V. H.; Bottaro, C. S.; Yan, N.; Kerton, F. M. *ACS Sustainable Chem. Eng.* **2018,** *6,* 1662–1669. doi:10.1021/acssuschemeng.7b02870

25. Chen, X.; Yang, H.; Zhong, Z.; Yan, N. *Green Chem.* **2017,** *19,* 2783–2792. doi:10.1039/c7gc00089h
26. Suryanarayana, C. *Prog. Mater. Sci.* **2001,** *46,* 1–184. doi:10.1016/s0079-6425(99)00010-9
27. Renita, A. A.; Sivasubramanian, V.; Kumar, P. S. Characterization and Optimization Studies on Hydroxyapatite Bioceramic Powder from Waste Eggshells. In *Bioprocess Engineering for a Green Environment;* Sivasubramanian, V., Ed.; CRC Press: Boca Raton, 2018; pp 310 ff.
28. Michalchuk, A. A. L.; Tumanov, I. A.; Boldyreva, E. V. *CrystEngComm* **2019,** *21,* 2174–2179. doi:10.1039/c8ce02109k
29. McKissic, K. S.; Caruso, J. T.; Blair, R. G.; Mack, J. *Green Chem.* **2014,** *16,* 1628–1632. doi:10.1039/c3gc41496e
30. Rojac, T.; Kosec, M.; Malič, B.; Holc, J. *J. Eur. Ceram. Soc.* **2006,** *26,* 3711–3716. doi:10.1016/j.jeurceramsoc.2005.11.013
31. Concas, A.; Lai, N.; Pisu, M.; Cao, G. *Chem. Eng. Sci.* **2006,** *61,* 3746–3760. doi:10.1016/j.ces.2006.01.007
32. Blair, R. G.; Chagoya, K.; Biltek, S.; Jackson, S.; Sinclair, A.; Taraboletti, A.; Restrepo, D. T. *Faraday Discuss.* **2014,** *170,* 223–233. doi:10.1039/c4fd00007b
33. Andersen, J. M.; Mack, J. *Chem. Sci.* **2017,** *8,* 5447–5453. doi:10.1039/c7sc00538e
34. Adzila, S.; Sopyan, I.; Chou, T.; Singh, R.; Yew, W.; Purbolaksono, J.; Hamdi, M. *Indian J. Chem.* **2013,** *52,* 1570–1575.
35. Tireli, M.; Maračić, S.; Lukin, S.; Juribašić Kulcsár, M.; Žilić, D.; Cetina, M.; Halasz, I.; Raić-Malić, S.; Užarević, K. *Beilstein J. Org. Chem.* **2017,** *13,* 2352–2363. doi:10.3762/bjoc.13.232
36. Cook, T. L.; Walker, J. A.; Mack, J. *Green Chem.* **2013,** *15,* 617–619. doi:10.1039/c3gc36720g
37. Haley, R. A.; Zellner, A. R.; Krause, J. A.; Guan, H.; Mack, J. *ACS Sustainable Chem. Eng.* **2016,** *4,* 2464–2469. doi:10.1021/acssuschemeng.6b00363
38. Nakajima, K.; Takeda, O.; Miki, T.; Matsubae, K.; Nakamura, S.; Nagasaka, T. *Environ. Sci. Technol.* **2010,** *44,* 5594–5600. doi:10.1021/es9038769
39. Mitrovic, A.; Zdujic, M. *J. Serb. Chem. Soc.* **2013,** *78,* 579–590. doi:10.2298/jsc120829107m
40. Caruso, M. M.; Davis, D. A.; Shen, Q.; Odom, S. A.; Sottos, N. R.; White, S. R.; Moore, J. S. *Chem. Rev.* **2009,** *109,* 5755–5798. doi:10.1021/cr9001353
41. Thanh, M. T.; Thien, T. V.; Du, P. D.; Hung, N. P.; Khieu, D. Q. *J. Porous Mater.* **2018,** *25,* 857–869. doi:10.1007/s10934-017-0498-7
42. Chen, X.; Yang, H.; Zhong, Z.; Yan, N. *Green Chem.* **2017,** *19,* 2783–2792. doi:10.1039/c7gc00089h
43. Julien, P. A.; Malvestiti, I.; Friščić, T. *Beilstein J. Org. Chem.* **2017,** *13,* 2160–2168. doi:10.3762/bjoc.13.216
44. Kulla, H.; Fischer, F.; Benemann, S.; Rademann, K.; Emmerling, F. *CrystEngComm* **2017,** *19,* 3902–3907. doi:10.1039/c7ce00502d
45. Friščić, T.; Reid, D. G.; Halasz, I.; Stein, R. S.; Dinnebier, R. E.; Duer, M. J. *Angew. Chem., Int. Ed.* **2010,** *49,* 712–715. doi:10.1002/anie.200906583
46. Friščić, T.; Halasz, I.; Beldon, P. J.; Belenguer, A. M.; Adams, F.; Kimber, S. A. J.; Honkimäki, V.; Dinnebier, R. E. *Nat. Chem.* **2013,** *5,* 66–73. doi:10.1038/nchem.1505
47. Gracin, D.; Štrukil, V.; Friščić, T.; Halasz, I.; Užarević, K. *Angew. Chem., Int. Ed.* **2014,** *53,* 6193–6197. doi:10.1002/anie.201402334
48. Ban, V.; Sadikin, Y.; Lange, M.; Tumanov, N.; Filinchuk, Y.; Černý, R.; Casati, N. *Anal. Chem. (Washington, DC, U. S.)* **2017,** *89,* 13176–13181. doi:10.1021/acs.analchem.7b02871
49. Shin, H.; Lee, S.; Suk Jung, H.; Kim, J.-B. *Ceram. Int.* **2013,** *39,* 8963–8968. doi:10.1016/j.ceramint.2013.04.093
50. Shinozaki, M.; Senna, M. *Ind. Eng. Chem. Fundam.* **1981,** *20,* 59–62. doi:10.1021/i100001a011
51. Baláž, P. High-Energy Milling. *Mechanochemistry in Nanoscience and Minerals Engineering;* Springer Berlin: Berlin, Germany, 2008; pp 103–132. doi:10.1007/978-3-540-74855-7_2
52. Nemtsev, S. V.; Gamzazade, A. I.; Rogozhin, S. V.; Bykova, V. M.; Bykov, V. P. *Appl. Biochem. Microbiol.* **2002,** *38,* 521–526. doi:10.1023/a:1020766325395
53. Yuan, L.; Chen, Z.; Zhu, Y.; Liu, X.; Liao, H.; Chen, D. *J. Appl. Polym. Sci.* **2013,** *128,* 3338–3345. doi:10.1002/app.38551
54. Zhang, Q.; Honda, I.; Watanabe, A.; Tongamp, W.; Kang, I.; Saito, F. *High Temp. Mater. Processes (Berlin, Ger.)* **2010,** *29,* 435–446.
55. Di Nardo, T.; Hadad, C.; Nguyen Van Nhien, A.; Moores, A. *ChemRxiv* **2019**. doi:10.26434/chemrxiv.7312070.v3
56. Ishiguro, M.; Endo, T. *Bioresour. Technol.* **2014,** *153,* 322–326. doi:10.1016/j.biortech.2013.12.015
57. Osada, M.; Miura, C.; Nakagawa, Y. S.; Kaihara, M.; Nikaido, M.; Totani, K. *Carbohydr. Polym.* **2013,** *92,* 1573–1578. doi:10.1016/j.carbpol.2012.10.068
58. Deringer, V. L.; Englert, U.; Dronskowski, R. *Biomacromolecules* **2016,** *17,* 996–1003. doi:10.1021/acs.biomac.5b01653
59. Boschetto, A.; Bellusci, M.; La Barbera, A.; Padella, F.; Veniali, F. *Int. J. Adv. Manuf. Technol.* **2013,** *69,* 2423–2435. doi:10.1007/s00170-013-5201-9
60. Park, S.; Baker, J. O.; Himmel, M. E.; Parilla, P. A.; Johnson, D. K. *Biotechnol. Biofuels* **2010,** *3,* No. 10. doi:10.1186/1754-6834-3-10
61. Vincent, J. F. V.; Wegst, U. G. K. *Arthropod Struct. Dev.* **2004,** *33,* 187–199. doi:10.1016/j.asd.2004.05.006

Understanding the unexpected effect of frequency on the kinetics of a covalent reaction under ball-milling conditions

Ana M. Belenguer[*1], Adam A. L. Michalchuk[*2], Giulio I. Lampronti[*1,3] and Jeremy K. M. Sanders[*1]

Full Research Paper

Address:
[1]Department of Chemistry, University of Cambridge, Lensfield Road, Cambridge CB2 1EW, UK, [2]BAM Federal Institute for Materials Research and Testing, Richard-Willstätter Str. 11, 12489 Berlin, Germany and [3]Department of Earth Sciences, University of Cambridge, Downing Street, Cambridge CB2 3EQ, UK

Email:
Ana M. Belenguer[*] - amb84@cam.ac.uk; Adam A. L. Michalchuk[*] - adam.michalchuk@bam.de; Giulio I. Lampronti[*] - gil21@cam.ac.uk; Jeremy K. M. Sanders[*] - jkms@cam.ac.uk

* Corresponding author

Abstract

We here explore how ball-mill-grinding frequency affects the kinetics of a disulfide exchange reaction. Our kinetic data show that the reaction progress is similar at all the frequencies studied (15–30 Hz), including a significant induction time before the nucleation and growth process starts. This indicates that to start the reaction an initial energy accumulation is necessary. Other than mixing, the energy supplied by the mechanical treatment has two effects: (i) reducing the crystal size and (ii) creating defects in the structure. The crystal-breaking process is likely to be dominant at first becoming less important later in the process when the energy supplied is stored at the molecular level as local crystal defects. This accumulation is taken here to be the rate-determining step. We suggest that the local defects accumulate preferentially at or near the crystal surface. Since the total area increases exponentially when the crystal size is reduced by the crystal-breaking process, this can further explain the exponential dependence of the onset time on the milling frequency.

Introduction

We describe here an unusual frequency-dependence in the induction period of a covalent reaction carried out using ball-mill grinding. We present a kinetic analysis indicating that this is due to the successive fracture of crystals into smaller particles followed by the accumulation of energy in crystal defects. In recent years, manual and ball-mill grinding have become increasingly routine solid-state synthesis tools [1]. Generally referred to as mechanochemistry, these methods are more envi-

ronmentally friendly and usually less expensive than traditional solution-based methods, because they require little or no solvent. Moreover, mechanochemical syntheses often give quantitative yields of products [2-4]. Manual or mechanical grinding can be performed "neat", i.e., in the absence of solvent (neat grinding, NG). Alternatively, very small quantities of liquid can be added to the grinding mixture [5], a procedure known as "kneading" or "liquid-assisted grinding" (LAG) [4]. The liquid often accelerates reactions between solids or even enables new reactions [5-7]. Mechanochemical methods have been successfully applied for a wide range of different syntheses and chemical reactions of inorganic [8,9] and organic [10,11] compounds. Even supramolecular architectures such as co-crystals and metal-organic frameworks [4,12-14], cages [15] and rotaxanes [16] could be formed mechanochemically. Crucially, the mechanisms and driving forces which underpin mechanochemical transformations and supramolecular reactions remain poorly understood and are subject to considerable debate [2,4,7,8,14,17-25]. The future successful academic and industrial application of these methods depends on developing a fundamental understanding of these solid-state processes.

The validation of reaction kinetic models has been a powerful approach for investigating fundamental processes in chemistry and physics. This has led to significant advancement in the understanding of molecular and submolecular phenomena. A number of researchers have attempted to rationalize organic mechanochemical transformation profiles in a similar way [26-28], with far more developed with respect to inorganic reactions [29-36]. However, despite many advances in developing

mathematical models based on various kinetic treatments, an understanding of mechanochemical reaction dynamics remains largely elusive. While mechanochemical kinetics must obey the general principles of reactivity (collision, energy gain and relaxation), there remains a poorly understood, complex interplay between physical and chemical phenomena [37], which are not captured in traditional fluid-phase kinetics treatments. Furthermore, many physical parameters are intimately coupled (e.g., milling-ball size and mass), and carefully designed studies are required to understand their independent effects on the reaction rate [29,38-43]. Hence, before one can develop elementary kinetic equations for these processes, it is crucial to understand the types of processes that must be independently considered.

Recently, we have been investigating the final reaction equilibrium achieved under ball-mill LAG conditions [17,18,44]. It is generally accepted that when the milling reaction reaches completion in a sealed system, a steady state is eventually achieved. The final phase composition does not change as long as the milling conditions are maintained [1,17,18,45,46]. Such equilibria depend on numerous factors, including ball-mill jar size, shape and material, ball-bearing size, weight and material, milling frequency, temperature, and the nature and concentration of the added liquid [17,18]. In this paper we investigate how the ball-mill grinding frequency affects the kinetics of the covalent reaction of bis(2-nitrophenyl) disulfide and bis(4-chlorophenyl) disulfide in the presence of a small amount of the base catalyst 1,8-diazabicyclo[5.4.0]undec-7-ene (DBU) to produce 4-chlorophenyl 2-nitrophenyl disulfide (see Scheme 1). Reliable experimental procedures have already been estab-

Scheme 1: Solid-state exchange reaction through ball-mill grinding under neat ball-mill-grinding conditions (left) and under ball-mill LAG conditions (right). From the solid-state reaction of the homodimers (CCDC [48] codes ODNPDS02 and DCPHDS for **1-1** and **2-2**, respectively) only the relevant stable polymorph of the heterodimer, form A and form B respectively, crystallizes. The details of form A (CCDC code FUQLIM01) and form B (CCDC code FUQLIM) have been previously reported.

lished for this system [47]. While the experimental operations for the system are given below and in Supporting Information File 1, we refer to our methodology paper for further and more general details and considerations [47].

The results presented here show a significant induction time before the reaction starts. We interpret this as a consequence of a two-stage process: a first stage that is dominated by crystal breaking, and a second stage in which the energy supplied by the ball-bearing impact is stored as structural defects (within crystalline or cohesive states [37] at the molecular level). Indeed, it has been suggested that a number of mechanochemical transformations depend greatly on the accumulation of energy [29,49-51]. We therefore propose that this energy accumulation is the rate-determining step: when a certain threshold is overcome the reaction starts very suddenly and occurs rapidly. The idealized model presented here serves as proof-of-

concept for an often-overlooked aspect of the coupling between physical and chemical phenomena, required to rationalize the unconventional kinetics associated with mechanochemical transformations.

Results and Discussion

Figure 1 show the experimental results for the progress of product formation as a function of grinding time.

Purposely designed stability experiments of the ball mill NG and LAG reactions were conducted by interrupting the milling experiments of **1-1** + **2-2** + DBU at different times and storing the grinding jars sealed. After several months and up to years, these sample jars were opened and the materials reanalyzed by HPLC in order to obtain their chemical composition. We observed that the nanocrystals of **1-1** and **2-2** homodimers had reacted during storage in the absence of further mechanochem-
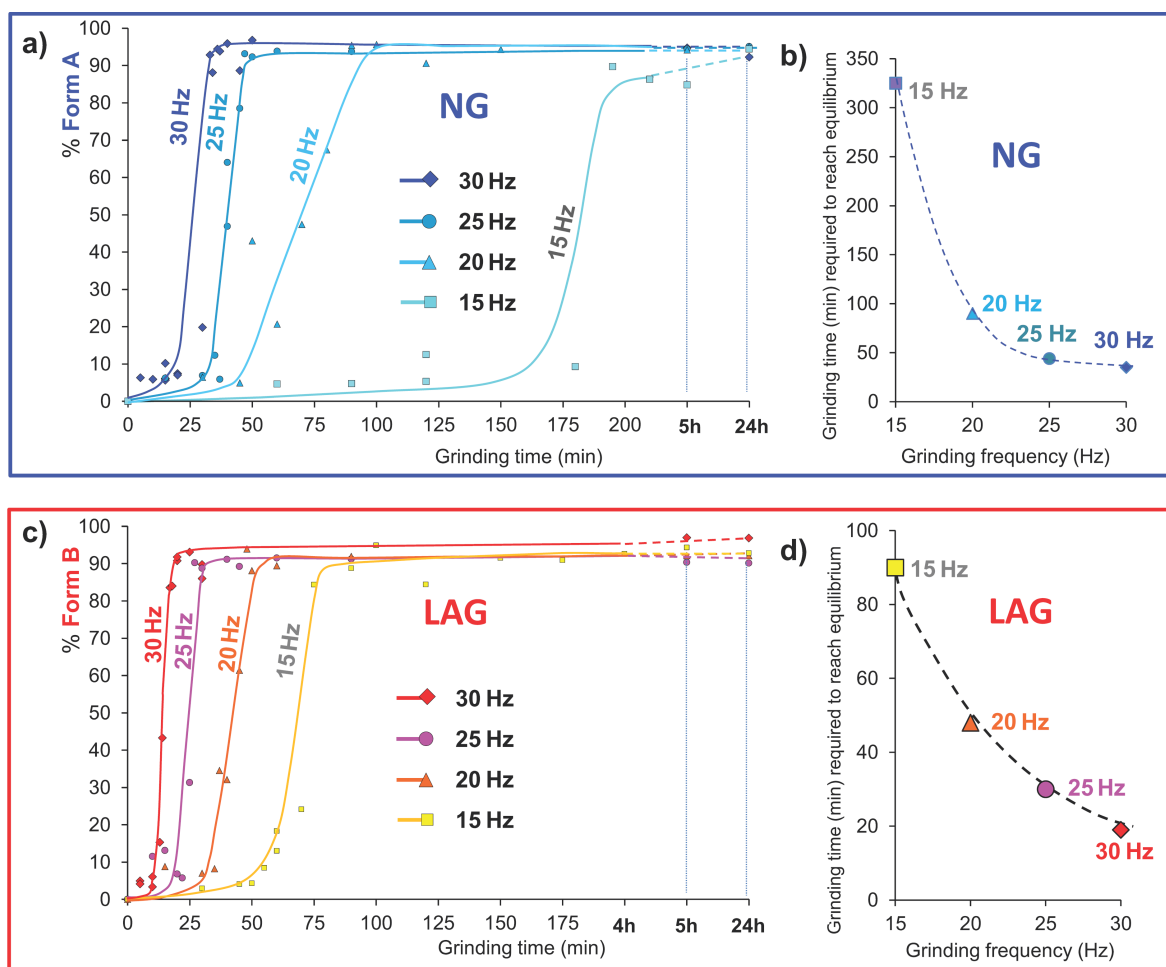
Figure 1: Solid-state studies reacting **1-1** and **2-2** in an equimolar ratio in the presence of DBU as catalyst to give the heterodimer **1-2**. (a) And (c) show the dependence of reaction progress (obtained by the Rietveld quantitative phase analysis) on milling frequency under ball-mill NG and LAG conditions (with 50 µL of MeCN), respectively. No fitting was performed, and the kinetic curves are only a guide to the eye. Each time point in these kinetic plots corresponds to a separate grinding experiment.

ical activation, thereby resulting in an increased concentration of **1-2**. This increase in **1-2** was only observed with aged NG and LAG samples that contained more than 2 mol % of **1-2** seeds. Higher concentrations of **1-2** seeds in the initial sample led to a higher overall conversion with aging. Importantly, we stress that the detectable increase in **1-2** with time required a period of months, or even years. Hence, the kinetics that we observe in the experiments reported in this work pertain only to the mechanochemical phenomena themselves.

The rate (*r*) associated with any physical or chemical transformation can be described by generic Equation 1

$$r \propto f(\alpha) \times A \times \exp(-E/RT) \qquad (1)$$

where $A \times \exp(-E/RT)$ is the Arrhenius-type rate constant, and $f(\alpha)$ is the functional form of rate, dependent on the specific mechanism of the transformation. Many of the traditional kinetic equations for solid-state transformations (e.g., the Avrami–Erofeyev and Prout–Tompkins models) are derived for single phase solid-state transformations [52]. Their general application to multiphase mechanochemical reactions is thus limited.

A general mechanochemical reaction can (macroscopically) be taken to consist of two stages: (1) mass transport (i.e., mixing) and formation of heterogeneous, reactive contacts and (2) activation of these contacts by mechanical impact. This is analogous to traditional chemical kinetics, limited by collision and activation. Macroscopically, a general irreversible mechanochemical reaction reaching equilibrium can be thus considered according to Scheme 2. A notable assumption is that all combinations of the physical complex [AB] yield the same product phase. While the latter is not strictly true in all cases [28], it does hold for the general case. The equilibria between complex [AB] and the pure components represent de-mixing, as well as surface regeneration by expulsion of C.
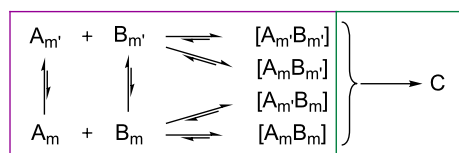
Scheme 2: Schematic representation of a solid + solid mechanochemical reaction. Subscript denote macroscopic (m) and comminuted (m') particles.

In such a scheme, it is irrelevant which intermediate state forms, and thus the kinetic constant for reactive contact formation

represents an average of all such states. Hence, Scheme 2 can be drastically simplified to Scheme 3.
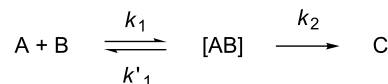
Scheme 3: Simplified reaction equation for the mechanochemical transformation. Note that [AB] is a physical complex.

The kinetic profiles presented in Figure 1 (b and d) exhibit striking non-linearity in their dependence on the milling frequency. Furthermore, they each exhibit sizeable induction periods, far greater than most reported kinetic profiles of multiphase mechanochemical non-covalent supramolecular chemical reactions [28,45]. The notable exceptions are similar synthetic reactions, which induce covalent bond formation, conducted by mechanochemistry [46]. A large induction period can be explained by two mechanisms: (1) time required for mass transport (mixing), or (2) time required for the accumulation of energy. While mass transport surely plays some role in the observed induction period, it requires that no reaction occurs for several tens of minutes, followed by a sudden onset of covalent chemistry. This does not appear likely. Furthermore, this induction period, with sudden and rapid onset of reaction, is not typical of most solid-state kinetic models, but is instead typical of temperature (energy)-dependent kinetics in which a reaction does not occur until sufficient energy is present in the system [53].

Instead, it has been suggested that the kinetics in covalent mechanochemical transformations depend greatly on the accumulation of energy, which can be stored as local defects, or trapped within the energetic framework of the submolecular system [29,54,55]. However, the latter is not expected to contribute substantially to macroscopic mechanochemical phenomena, assuming typical relaxation times in the order of microseconds or less [29,56]. Macroscopically, energy can also accumulate as heat, which itself is known to have an effect on the rate of the mechanochemical transformation [23]. This accumulation is taken here to be the rate-limiting step. For the purpose of this proof-of-concept study, we do not consider any particular energy accumulation (or relaxation) pathway. Instead, only the total of all phenomena is considered. In reality, this accumulation and subsequent relaxation is highly complex, involving submolecular (electronic and vibrational) effects, as well as defect generation and temperature development [54,57].

A rate constant, k_2, is hence developed as a modification from that originally proposed by Butyagin [29], in which the rate is proportional to the frequency of collision (A), and the initial ac-

tivation energy (E_0) for the chemical reaction. For systems in which the reaction is limited by the distribution of mechanical energy, it has been suggested that the temperature term of the traditional Arrhenius equation can be (to a first approximation) replaced by the rate of supply of mechanical energy, W [29], (Equation 2)

$$k_2 = A \times \exp\left(-\frac{E_0 - E_{acc}}{W}\right) \qquad (2)$$

Hence, k_2 represents the 'per impact' probability of reaction. We note that the individual terms of Equation 2 are indeed expected to be dependent on the equilibrium temperature of the system, although this dependence is outside the scope of the present manuscript. With the rate of energy relaxation, τ, normalized to 1 Hz, the energy accumulation can be approximated (see Supporting Information File 2 and Equation 3),

$$E_{acc} = \begin{cases} W(\nu - \tau); \nu/\tau \geq 1 \\ 0; \nu/\tau < 1 \end{cases} \qquad (3)$$

thus denoting the accumulation of energy at a rate proportional to the difference in milling frequency ν (Hz) and the relaxation of energy τ (Hz). We note that this is a somewhat simplified form, not considering the differences between the mechanism for energy accumulation. Furthermore, this simplification assumes a linear increase in stored energy throughout the bulk material. Note that all attempts at scaling energy accumulation resulted only in shifting of the relative onset times (Supporting Information File 2).

If it is assumed that k_1, $k_1' \gg k_2$, the rate equation for the transformation can be expressed as in Equation 4:

$$f(\alpha_C(t)) = \alpha_{AB}(t)\exp(-k_2 t) \qquad (4)$$

The energy of an ideal impact can be worked out from the classical equations of motion, assuming an ideal linear trajectory of the milling ball along the entire length of the milling jar at the acceleration of the mill. Note that we have made the assumption that 'double-impacts' do not occur and that the two milling balls simultaneously impact the powder directly. This has a similar effect as simply modelling a milling ball with a larger surface area [38]. Double impacts, and ball–ball collisions are certainly important considerations for future development of this simple model. The resulting impact energies, W, are given in Table 1, and it is assumed that the milling ball is subsequently ejected at the same velocity after impact. Unfortunately, Equation 2 cannot be solved without knowledge of E_0 and τ.

However, the relative rate is proportional only to E_0:τ (Supporting Information File 2), which we selected here to fit the experimental curve for 15 Hz ball-mill neat grinding.

Table 1: Approximate kinetic energy of an ideal impact of a 1.43 g milling ball at different milling frequencies. The relative frequency is shown in each case. Note that the milling jar oscillation distance was measured at 4 cm.

Frequency, ν	W /mJ
15 Hz	0.489
20 Hz	0.870
25 Hz	1.359
30 Hz	1.958

If a model is built on Scheme 2, with k_1, $k_1' \gg k_2$, Figure 2A is generated. Remarkably, despite the simplifying assumptions used in this model, the general features of the experimental curve are well reproduced. Based solely on the consideration of the physical parameters W and ν, the significant non-linearity observed in experiment is obtained, with the onset time t_{on} decreasing as t_{on} (15 Hz) >>> t_{on} (20 Hz) >> t_{on} (25 Hz) > t_{on} (30 Hz). The on-set time is taken as the point where the tangent to the pre-accumulation plateau meets that of the accumulation curve. Although the model explains the general features, it cannot capture the resolution in onset frequencies for the three fastest milling reactions. We believe this to be due to the crude assumption of ideal impact trajectory; non-ideal trajectory should decrease the energy accumulation and hence elongate the induction period.

If the raw values are used, it is found that the relative rate of conversion for the 15 Hz milling reaction is substantially overestimated with respect to the experiment. However, we note that the present model assumes energy accumulation beginning immediately, and does not allow for initial comminution or mixing, as is required [58]. The discrepancy in the 15 Hz milling onset time may represent an effect of the approximate mixing and comminution rate. Indeed, specimens taken from different areas of the milling jar showed significant compositional differences even after 75 minutes (see Supporting Information File 1). The re-normalized onset times predicted by the model match very well the ones observed experimentally (Figure 2b).

The generation of the observed kinetic profiles requires a consideration of the energy accumulation. If energy is not permitted to accumulate, each individual impact is too small to induce a chemical transformation. If each impact is taken to be sufficient for chemical reaction, then the entire induction period must be taken to be the result of mass transport, in which case

Figure 2: Reaction profiles for mechanochemical milling according to Equation 4. (a) Kinetic profiles for 30 Hz, 25 Hz, 20 Hz and 15 Hz NG milling. Raw (fine line curves) and corrected (base onset time + 10 min; thick line curves) are given and labelled. Onset time (normalized relative to 30 Hz model data) correction approximated from experimental curves. (b) Comparison of relative conversion onset times from raw kinetic curves (black rectangles), onset time corrected (brown triangles), and from experimental ball mill NG curves (blue circles) in Figure 1. $E_0{:}\tau$ = 17.48.

slow, gradual kinetics would be expected. Unfortunately, the need to account for energy accumulation does not permit the assessment of E_0 for the present system.

In our attempts to model Scheme 2 using $k_1, k_1{'} \propto k_2$, no noticeable effect could be observed on the onset time. Instead, it was found that the relative mixing rate affects the slope of accumulation (Figure 3). By comparison to the experimental curves in Figure 1, this effect appears to dominate in the 20 Hz and 15 Hz profiles. This suggests that on the macroscopic scale, lower frequency milling is limited not only in the rate of energy input, but also by its ability to facilitate mass transport.

Having ascertained that the model of Equation 4 well describes the non-linear kinetics observed for neat grinding, it is worth considering this model with respect to LAG kinetics. While the non-linearity is not so evident under LAG conditions, the consideration of the relative onset rate does suggest its presence, albeit shifted towards lower grinding times. This is captured by reducing the $E_0{:}\tau$ ratio in the kinetic model (Figure 4). The general structure of the experimental curves is reproduced well, with the 15 Hz profile considerably higher in onset time than the others. Unfortunately, it seems that again the three fastest milling frequencies are clustered somewhat too closely. One important aspect that our model does not take into

Figure 3: Modelled kinetic profiles for 15 Hz neat milling, with variation in the magnitude of the mixing term. Experimental data points for NG at 15 Hz are provided as yellow squares. Note that no parameters in the model are fit from experiment.

Figure 4: Reaction profiles for LAG mechanochemical milling according to Equation 4. The modelled curves are given for each milling frequency, and experimental data points are provided for 25 Hz (pink circles) and 15 Hz (yellow squares). No fitting was performed for the experimental data and the kinetic curves drawn are only a guide to the eye. $E_0{:}\tau = 19.23$

account is the crystal size and the relative surface-to-volume ratio. The latter could explain an exponential dependence of the onset time on the frequency, as the specific area increases exponentially with the reduction of crystal size. For the specific area to affect the onset time, the local submolecular defects responsible for the energy accumulation should cluster preferentially at or near the crystal surface [59]. Our relatively simple model

does not consider the non-ideal ball trajectory and this may play a role. Further work is therefore required to account for these important aspects.

While we are cautious about deriving mechanistic information from this result, it suggests that LAG primarily lowers the relative activation energy of mechanochemical reactions or facili-

tates the energy accumulation when compared to experiments run under ball mill NG conditions. These two explanations are not mutually exclusive. While the activation may be facilitated by partial dissolution of components, it is possible that crystallite aggregation plays a significant role under NG conditions: the energy supplied by the impact would therefore be used to break down aggregates as well as crystallites, the aggregation itself being limited by the MeCN solvent under LAG conditions. Indeed, aggregation seems to be a rather important phenomenon in the reaction kinetics under mechanochemical conditions [59].

Conclusion

The kinetic profiles observed for neat and LAG processes described in this work are anomalous when compared to traditional solid-state processes. They are characterized by lengthy induction periods and a sudden, rapid conversion to the product phase. Traditional equilibrium kinetics demonstrates such behavior when insufficient energy is initially present in the system. Unique to mechanochemical transformations, however, is the periodic nature of the input energy. A simple model was therefore employed to account for this periodicity. Remarkably, the abnormal kinetic behavior of the system was captured within such a model, requiring only two physical parameters from the milling system: milling frequency and ideal impact energy. While induction periods in mechanochemistry can be the result also of mixing, these effects are considerably smaller. For such an effect to dominate in the present case, one must assume that no reaction takes place until ideal mixing is achieved, which is unrealistic. Indeed, the inclusion of a mixing term does not affect the onset time for reaction. However, it was found that the inclusion of a mixing term does lead to 'shaping' of the accumulation profile. Such effects appear necessary to capture the kinetic profile of the lower frequency kinetic curves. This suggests that, while onset time is dependent on frequency and input energy, the mixing (mass transport) can dominate subsequent stages of the transformation, as the probability of contact formation decreases. While further work is required to capture detailed mechanistic insight, we can suggest that kinetic modelling of covalent mechanochemical reactions likely requires a model that accounts for both the accumulation of energy and mixing effects. The induction time is significantly shorter under LAG conditions. This can be explained by either a lower activation energy under LAG conditions, or aggregation playing a more important role under NG conditions. The crystal breaking process is likely to be dominant at first, and it involves breaking crystallites as well as crystallite aggregates. When the particles are reduced in size, the energy supplied is stored at the molecular level as local crystal defects. This accumulation is taken here to be the rate-determining step. We suggest that the local defects accumulate preferentially at or near the crystal sur-

face. Since the total area increases exponentially when the crystal size is reduced by the crystal breaking process, this can further explain the exponential nature of the onset-time dependence on the milling frequency.

Milling reaction kinetics is a relatively unexplored field, and we have explored only one reaction, but it seems likely that similar effects will operate for other reactions.

Experimental

The kinetic studies presented here were performed under ball-mill neat grinding (NG) and under ball mill liquid-assisted grinding (LAG) conditions with 50 μL of acetonitrile added to 200 mg of powder. The kinetic points prepared for this study are all single point experiments. The reaction under study is a base-catalyzed disulfide exchange reaction starting from equimolar amounts of homodimers using DBU as the base catalyst to result in the formation of the heterodimer. The homodimers (0.34 mmol) bis(2-nitrophenyl) disulfide (**1-1**, 104.83 mg) and bis(4-chlorophenyl) disulfide (**2-2**, 97.66 mg) were accurately weighed, resulting in a load of 200 mg. The material was quantitatively transferred to a 14.5 mL snap closure stainless steel grinding jar and two 7.0 mm in diameter stainless steel balls were placed on top of the powder. Then, 2 μL (2 mol %) of the base catalyst 1,8-diazabicyclo[5.4.0]undec-7-ene (DBU) were carefully added on top of the milling balls. For NG experiments nothing else was added while for LAG experiments, 50 μL of acetonitrile were added on top of the powder. The grinding jars were snap-closed, the closure secured with insulating tape milling was conducted at 15–30 Hz using a MM400 Retsch automated grinder for the specified period of time (see Figure 1 and Supporting Information File 1). The grinding jars were opened immediately after completion of the grinding period; the PXRD sample prepared on a slide and then scanned ex situ by PXRD as soon as possible so as to get the most reliable data. HPLC analysis to obtain the chemical composition of the sample was performed as soon as possible and always within the same day, reported as mol % and documented in Supporting Information File 1. The solid product was dissolved in MeCN + 0.2% trifluoroacetic acid (TFA) at a concentration of 1 mg/mL and injected in the HPLC system. TFA was added to the sample for HPLC analysis to neutralize the base DBU and to quench the disulfide exchange reaction. The results of the milling experiments were plotted as mol % concentration of phase composition versus grinding time (see Figure 1, Figure 4 and Supporting Information File 1). The phase composition is calculated from the Rietveld refinement of the PXRD scans. The estimated accuracy of the phase composition by Rietveld refinement is ±3 mol % of the absolute and estimated sensitivity while the limit of detection (LOD) is 3 mol %. The estimated sensitivity of the HPLC analysis result-

ing in the chemical composition of the samples is 0.1 mol % relative to the main component. Therefore, while the PXRD analysis is not as sensitive or accurate as the HPLC analysis, it supplies the phase composition. There is an excellent agreement between the phase composition obtained by PXRD and the chemical composition obtained by HPLC (see Supporting Information File 1). Additional details about the analytical PXRD and HPLC methods can be found in Supporting Information File 1.

A sufficient number of independent kinetic milling points were performed so as to obtain a good resolution of the sigmoidal segment of the kinetic curves and to demonstrate that the milling reaction had finally reached a plateau. To achieve this level of accurate and reproducible kinetic profiles, rigorous experimental procedures detailed in Supporting Information File 1 and in reference [47] were found necessary.

Supporting Information

Supporting Information File 1

Experimental methodology for ball mill grinding experiments, analysis by HPLC and PXRD; quantitation by Rietveld refinement and particle size analysis by Scherrer equation.

[https://www.beilstein-journals.org/bjoc/content/supplementary/1860-5397-15-120-S1.pdf]

Supporting Information File 2

Kinetic model parameterization and additional model features.

[https://www.beilstein-journals.org/bjoc/content/supplementary/1860-5397-15-120-S2.pdf]

Acknowledgements

ORCID® iDs

Ana M. Belenguer - https://orcid.org/0000-0002-0443-4856
Adam A. L. Michalchuk - https://orcid.org/0000-0001-7405-3269
Giulio I. Lampronti - https://orcid.org/0000-0002-1430-3446
Jeremy K. M. Sanders - https://orcid.org/0000-0002-5143-5210

References

1. Baláž, P.; Achimovičová, M.; Baláž, M.; Billik, P.; Cherkezova-Zheleva, Z.; Criado, J. M.; Delogu, F.; Dutková, E.; Gaffet, E.; Gotor, F. J.; Kumar, R.; Mitov, I.; Rojac, T.; Senna, M.; Streletskii, A.; Wieczorek-Ciurowa, K. *Chem. Soc. Rev.* **2013,** *42,* 7571–7637. doi:10.1039/c3cs35468g
2. Do, J.-L.; Friščić, T. *Synlett* **2017,** *28,* 2066–2092. doi:10.1055/s-0036-1590854
3. Hernández, J. G.; Bolm, C. *J. Org. Chem.* **2017,** *82,* 4007–4019. doi:10.1021/acs.joc.6b02887
4. James, S. L.; Adams, C. J.; Bolm, C.; Braga, D.; Collier, P.; Friščić, T.; Grepioni, F.; Harris, K. D. M.; Hyett, G.; Jones, W.; Krebs, A.; Mack, J.; Maini, L.; Orpen, A. G.; Parkin, I. P.; Shearouse, W. C.; Steed, J. W.; Waddell, D. C. *Chem. Soc. Rev.* **2012,** *41,* 413–447. doi:10.1039/c1cs15171a
5. Braga, D.; Giaffreda, S. L.; Grepioni, F.; Chierotti, M. R.; Gobetto, R.; Palladino, G.; Polito, M. *CrystEngComm* **2007,** *9,* 879–881. doi:10.1039/b711983f
6. Belenguer, A. M.; Friščić, T.; Day, G. M.; Sanders, J. K. M. *Chem. Sci.* **2011,** *2,* 696–700. doi:10.1039/c0sc00533a
7. Bowmaker, G. A. *Chem. Commun.* **2013,** *49,* 334–348. doi:10.1039/c2cc35694e
8. Boldyreva, E. *Chem. Soc. Rev.* **2013,** *42,* 7719–7738. doi:10.1039/c3cs60052a
9. Šepelák, V.; Düvel, A.; Wilkening, M.; Becker, K.-D.; Heitjans, P. *Chem. Soc. Rev.* **2013,** *42,* 7507–7520. doi:10.1039/c2cs35462d
10. Stolle, A.; Szuppa, T.; Leonhardt, S. E. S.; Ondruschka, B. *Chem. Soc. Rev.* **2011,** *40,* 2317–2329. doi:10.1039/c0cs00195c
11. Wang, G.-W. *Chem. Soc. Rev.* **2013,** *42,* 7668–7700. doi:10.1039/c3cs35526h
12. Braga, D.; Giaffreda, S. L.; Grepioni, F.; Pettersen, A.; Maini, L.; Curzi, M.; Polito, M. *Dalton Trans.* **2006,** 1249–1263. doi:10.1039/b516165g
13. Friščić, T. *J. Mater. Chem.* **2010,** *20,* 7599–7605. doi:10.1039/c0jm00872a
14. Friščić, T.; Halasz, I.; Beldon, P. J.; Belenguer, A. M.; Adams, F.; Kimber, S. A. J.; Honkimäki, V.; Dinnebier, R. E. *Nat. Chem.* **2013,** *5,* 66–73. doi:10.1038/nchem.1505
15. Orita, A.; Jiang, L.; Nakano, T.; Ma, N.; Otera, J. *Chem. Commun.* **2002,** 1362–1363. doi:10.1039/b203651g
16. Hsu, C.-C.; Chen, N.-C.; Lai, C.-C.; Liu, Y.-H.; Peng, S.-M.; Chiu, S.-H. *Angew. Chem., Int. Ed.* **2008,** *47,* 7475–7478. doi:10.1002/anie.200803056
17. Belenguer, A. M.; Lampronti, G. I.; Cruz-Cabeza, A. J.; Hunter, C. A.; Sanders, J. K. M. *Chem. Sci.* **2016,** *7,* 6617–6627. doi:10.1039/c6sc03457h
18. Belenguer, A. M.; Lampronti, G. I.; De Mitri, N.; Driver, M.; Hunter, C. A.; Sanders, J. K. M. *J. Am. Chem. Soc.* **2018,** *140,* 17051–17059. doi:10.1021/jacs.8b08549
19. Fischer, F.; Fendel, N.; Greiser, S.; Rademann, K.; Emmerling, F. *Org. Process Res. Dev.* **2017,** *21,* 655–659. doi:10.1021/acs.oprd.6b00435
20. Fischer, F.; Wenzel, K.-J.; Rademann, K.; Emmerling, F. *Phys. Chem. Chem. Phys.* **2016,** *18,* 23320–23325. doi:10.1039/c6cp04280e
21. Friščić, T.; Jones, W. *Cryst. Growth Des.* **2009,** *9,* 1621–1637. doi:10.1021/cg800764n
22. Hasa, D.; Miniussi, E.; Jones, W. *Cryst. Growth Des.* **2016,** *16,* 4582–4588. doi:10.1021/acs.cgd.6b00682

23. Kulla, H.; Wilke, M.; Fischer, F.; Röllig, M.; Maierhofer, C.; Emmerling, F. *Chem. Commun.* **2017,** *53,* 1664–1667. doi:10.1039/c6cc08950j

24. Lien Nguyen, K.; Friščić, T.; Day, G. M.; Gladden, L. F.; Jones, W. *Nat. Mater.* **2007,** *6,* 206–209. doi:10.1038/nmat1848

25. Trask, A. V.; Shan, N.; Motherwell, W. D. S.; Jones, W.; Feng, S.; Tan, R. B. H.; Carpenter, K. J. *Chem. Commun.* **2005,** 880–882. doi:10.1039/b416980h

26. Colacino, E.; Carta, M.; Pia, G.; Porcheddu, A.; Ricci, P. C.; Delogu, F. *ACS Omega* **2018,** *3,* 9196–9209. doi:10.1021/acsomega.8b01431

27. Ma, X.; Yuan, W.; Bell, S. E. J.; James, S. L. *Chem. Commun.* **2014,** *50,* 1585–1587. doi:10.1039/c3cc47898j

28. Michalchuk, A. A. L.; Tumanov, I. A.; Konar, S.; Kimber, S. A. J.; Pulham, C. R.; Boldyreva, E. V. *Adv. Sci.* **2017,** *4,* 1700132. doi:10.1002/advs.201700132

29. Butyagin, P. Y. *Russ. Chem. Rev.* **1971,** *40,* 901–915. doi:10.1070/rc1971v040n11abeh001982

30. Butyagin, P. Yu. *Russ. Chem. Rev.* **1984,** *53,* 1025–1038. doi:10.1070/rc1984v053n11abeh003138

31. Urakaev, F. K.; Boldyrev, V. V. *Powder Technol.* **2000,** *107,* 93–107. doi:10.1016/s0032-5910(99)00175-8

32. Urakaev, F. K.; Boldyrev, V. V. *Powder Technol.* **2000,** *107,* 197–206. doi:10.1016/s0032-5910(99)00200-4

33. Delogu, F.; Orrù, R.; Cao, G. *Chem. Eng. Sci.* **2003,** *58,* 815–821. doi:10.1016/s0009-2509(02)00612-7

34. Delogu, F.; Takacs, L. *J. Mater. Sci.* **2018,** *53,* 13331–13342. doi:10.1007/s10853-018-2090-1

35. Vasconcelos, I. F.; de Figueiredo, R. S. *J. Phys. Chem. B* **2003,** *107,* 3761–3767. doi:10.1021/jp027698i

36. Boldyrev, V. V.; Avvakumov, E. G. *Russ. Chem. Rev.* **1971,** *40,* 847–859. doi:10.1070/rc1971v040n10abeh001977

37. Hutchings, B. P.; Crawford, D. E.; Gao, L.; Hu, P.; James, S. L. *Angew. Chem.* **2017,** *129,* 15454–15458. doi:10.1002/ange.201706723

38. Michalchuk, A. A. L.; Tumanov, I. A.; Boldyreva, E. V. *CrystEngComm* **2019,** *21,* 2174–2179. doi:10.1039/c8ce02109k

39. Butyagin, P. Y.; Pavlichev, I. K. *React. Solids* **1986,** *1,* 361–372. doi:10.1016/0168-7336(86)80027-4

40. Butyagin, P. *J. Mater. Synth. Process.* **2000,** *8,* 205–211. doi:10.1023/a:1011316227193

41. Cherdyntsev, V. V.; Kaloshkin, S. D.; Tomillin, I. A. *Phys. Met. Metallogr.* **2003,** *95,* 39–47.

42. Padella, F.; Paradiso, E.; Burgio, N.; Magini, M.; Martelli, S.; Guo, W.; Iasonna, A. *J. Less-Common Met.* **1991,** *175,* 79–90. doi:10.1016/0022-5088(91)90351-4

43. Boytsov, O.; Ustinov, A. I.; Gaffet, E.; Bernard, F. *J. Alloys Compd.* **2007,** *432,* 103–110. doi:10.1016/j.jallcom.2006.05.101

44. Belenguer, A. M.; Lampronti, G. I.; Wales, D. J.; Sanders, J. K. M. *J. Am. Chem. Soc.* **2014,** *136,* 16156–16166. doi:10.1021/ja500707z

45. Halasz, I.; Kimber, S. A. J.; Beldon, P. J.; Belenguer, A. M.; Adams, F.; Honkimäki, V.; Nightingale, R. C.; Dinnebier, R. E.; Friščić, T. *Nat. Protoc.* **2013,** *8,* 1718–1729. doi:10.1038/nprot.2013.100

46. Kulla, H.; Haferkamp, S.; Akhmetova, I.; Röllig, M.; Maierhofer, C.; Rademann, K.; Emmerling, F. *Angew. Chem., Int. Ed.* **2018,** *57,* 5930–5933. doi:10.1002/anie.201800147

47. Belenguer, A. M.; Lampronti, G. I.; Sanders, J. K. M. *J. Visualized Exp.* **2018,** No. 131. doi:10.3791/56824

48. Allen, F. H. *Acta Crystallogr., Sect. B: Struct. Sci.* **2002,** *58,* 380–388. doi:10.1107/s0108768102003890

49. Boldyrev, V. V.; Tkáčová, K. *J. Mater. Synth. Process.* **2000,** *8,* 121–132. doi:10.1023/a:1011347706721

50. Xu, C.; De, S.; Balu, A. M.; Ojeda, M.; Luque, R. *Chem. Commun.* **2015,** *51,* 6698–6713. doi:10.1039/c4cc09876e

51. Mulas, G.; Schiffini, L.; Cocco, G. *Mater. Sci. Forum* **1996,** *235–238,* 15–22. doi:10.4028/www.scientific.net/msf.235-238.15

52. Khawam, A.; Flanagan, D. R. *J. Phys. Chem. B* **2006,** *110,* 17315–17328. doi:10.1021/jp062746a

53. Drebushchak, V. A.; Drebushchak, T. N.; Boldyreva, E. V. *J. Therm. Anal. Calorim.* **2013,** *113,* 419–424. doi:10.1007/s10973-013-3120-5

54. Boldyrev, V. V. *Russ. Chem. Rev.* **2006,** *75,* 177–189. doi:10.1070/rc2006v075n03abeh001205

55. Takacs, L. *Chem. Soc. Rev.* **2013,** *42,* 7649–7659. doi:10.1039/c2cs35442j

56. Dlott, D. D. *J. Opt. Soc. Am. B* **1990,** *7,* 1638–1652. doi:10.1364/josab.7.001638

57. Boldyrev, V. V. *Solid State Ionics* **1993,** *63–65,* 537–543. doi:10.1016/0167-2738(93)90157-x

58. Boldyrev, V. V.; Pavlov, S. V.; Goldberg, E. L. *Int. J. Miner. Process.* **1996,** *44–45,* 181–185. doi:10.1016/0301-7516(95)00028-3

59. Tkáčová, K.; Heegn, H.; Števulová, N. *Int. J. Miner. Process.* **1993,** *40,* 17–31. doi:10.1016/0301-7516(93)90037-b

Mechanochemical Friedel–Crafts acylations

Mateja Đud, Anamarija Briš, Iva Jušinski, Davor Gracin and Davor Margetić[*][§]

Abstract

Friedel–Crafts (FC) acylation reactions were exploited in the preparation of ketone-functionalized aromatics. Environmentally more friendly, solvent-free mechanochemical reaction conditions of this industrially important reaction were developed. Reaction parameters such as FC catalyst, time, ratio of reagents and milling support were studied to establish the optimal reaction conditions. The scope of the reaction was explored by employment of different aromatic hydrocarbons in conjunction with anhydrides and acylation reagents. It was shown that certain FC-reactive aromatics could be effectively functionalized by FC acylations carried out under ball-milling conditions without the presence of a solvent. The reaction mechanism was studied by in situ Raman and ex situ IR spectroscopy.

Introduction

The Friedel–Crafts reaction (FCR) is a very powerful tool in organic chemistry for the synthesis of aromatic ketones. It is of great industrial importance and widely used in fine chemicals production [1,2]. In recent years, public awareness of the negative impact of chemical processes on the environment instigates chemists to improve processes by the reduction of waste material, energy consumption and reagents (materials). In this respect, carrying out FCR at room temperature without the use of solvents, which are usually highly toxic (halogenated hydrocarbons) will improve the eco-friendliness of the process. Until now, FCRs have been rarely applied to organic functionaliza-

tions which are carried out in solid state by mortar and pestle [3-5]. We are aware of only a few examples of FCRs employing manual grinding: reserpine acylation with $AlCl_3$ [6] and acylation reaction of aromatics [7]. One of the reasons for this scarcity is the hygroscopic nature of the aluminum trichloride catalyst [8-12] when exposed to air humidity. This problem could be easily avoided by conducting the reaction in a closed vessel, by the aid of automated ball milling, which became a very effective synthetic method in recent time [13-18]. The first account on mechanochemical FC alkylation by Borchardt [19] demonstrates the utility of the mechanochemical method in the

synthesis of covalent triazine frameworks. Herein, we report related results on solvent-free FC acylation reactions conducted in a ball mill, which is the continuation of our program in organic mechanosynthesis [20-24].

Results and Discussion

Mechanochemical FCR of pyrene (**1**) and phthalic anhydride (**2**) producing 1-(*o*-carboxybenzoyl)pyrene (**3**) was selected for the optimization of reaction conditions since all reagents and catalyst are solids (Scheme 1, Table 1) [25]. In solution, this reaction is facile and the product could be obtained in quantitative yield (Table 1, entry 15). The results on optimization of reaction conditions in the ball mill indicate that FC acylation could be effectively carried out mechanochemically. The best mechanochemical reaction conditions (Table 1, entry 4): 2 h, equimolar amount of phthalic anhydride and 2.5 equivalents of AlCl$_3$, afforded product **3** in high yield (79%). Identical yields were obtained by the change of reaction time to 1 h and alternative work-up procedures (Table 1, entries 1 and 4). When the catalyst amount was decreased to one equivalent, a significant decrease of yield was attained (Table 1, entry 2). Addition of various grinding additives to improve mass transfer and prevent pasting of the reaction mixture [26-28] (Table 1, entries 5–8) was detrimental to reaction yields. The addition of a small amount of solvents which was reported to facilitate several ball milling reactions (liquid assisted grinding, LAG) [29-32], also decreased yields (Table 1, entries 9 and 10). The reaction carried out in a planetary mill (Table 1, entry 11) afforded yields comparable to the MM400 vibrational mill. We have also performed screening of efficacy of various Lewis acid catalysts [33-38] (Table 1, entries 18–23), which did not lead to formation of products.

Table 1: Reaction of pyrene with phthalic anhydride[a].

Entry	Conditions	Work-up[b]	Yield (%)[c]
1	1 h	B	78
2	1 h, ratio 1:1:1	A	44
3	1 h	A	76
4	**2 h**	**A**	**79**
5	1 h, silicagel 1 g	A	n.r.
6	1 h, dry silicagel 0.5 g	A	42
7	1 h, dry NaCl 0.5 g	A	37
8	1 h, dry Na$_2$SO$_4$ 0.5 g	A	43
9	1 h, LAG dry DCM	A	51
10	1 h, LAG dry THF	A	16
11	1 h, planetary mill[d]	A	79
12	1 h, teflon jar	A	71
13	3 h, reflux, dry DCM	B	94 [39]
14	1 h, reflux, dry DCM	B	98
15	1 h, reflux, dry DCM	A	83
16	1 h, rt, dry DCM	A	99
17	10 min, melt, 180 °C, dry NaCl	C [40]	n.r.[e]
18	1 h, FeCl$_3$	A	n.r.
19	1 h, ZnCl$_2$	A	n.r.
20	1 h, ZnI$_2$	A	n.r.
21	1 h, ZnBr$_2$	A	n.r.
22	1 h, CuBr$_2$	A	n.r.
23	1 h, CuCl$_2$	A	n.r.
24	3 h, scale-up	A	73[f]

[a]Retsch MM400 ball mill, 16 mL stainless steel vial, 1 × 12 mm stainless steel ball, 30 Hz, substrate/anhydride/AlCl$_3$ ratio 1:1:2.5; [b]Work-up A: mixture suspended in H$_2$O, pH adjusted with conc. HCl, chromatography; work-up B: identical to work-up A, but recrystallisation from AcOH instead of chromatography; work-up C: suspended in aq oxalic acid, extracted with DCM, chromatography; [c]isolated yields; [d]Retsch planetary ball mill PM-200, 500 rpm, 25 mL stainless steel vial, 30 × 3 mm steel balls; [e]melted in open flask; [f]scaled up to 500 mg of pyrene.

Scheme 1: FCR of pyrene and phthalic anhydride.

Experiments collected in Table 1 demonstrate that a FC acylation reaction could be effectively carried out under ball-milling conditions at room temperature without the use of solvent. This reaction could be easily scaled up from 94 to 500 mg of pyrene without the decrease in yield (Table 1, entry 24) [41,42]. To investigate the scope of the reaction, several acylation reagents were employed in conjunction with pyrene (Scheme 2) and a variety of aromatic substrates was subjected to FC acylation (Scheme 3).

Acylation reagents shown in Scheme 2 were less reactive in comparison to phthalic anhydride. Benzoic anhydride was used as a substitute for benzoyl chloride and the reaction proceeded in better yield. The observed disparity in reactivity might be associated with the difference in the physical state of the reagents. Furthermore, succinic anhydride poorly reacted with pyrene, but the reaction proceeds well with the more reactive biphenyl (69%, see Supporting Information File 1). Di-*tert*-butyl dicarbonate and 4-nitrobenzoyl chloride were unreactive under ball-milling conditions. Similary unreactive was 4-nitrophthalic anhydride, which only in forced conditions (by melting at 200 °C) reacted sluggishly with pyrene affording mixture of regioisomeric products **6** and **7**. The advantage of the employment of
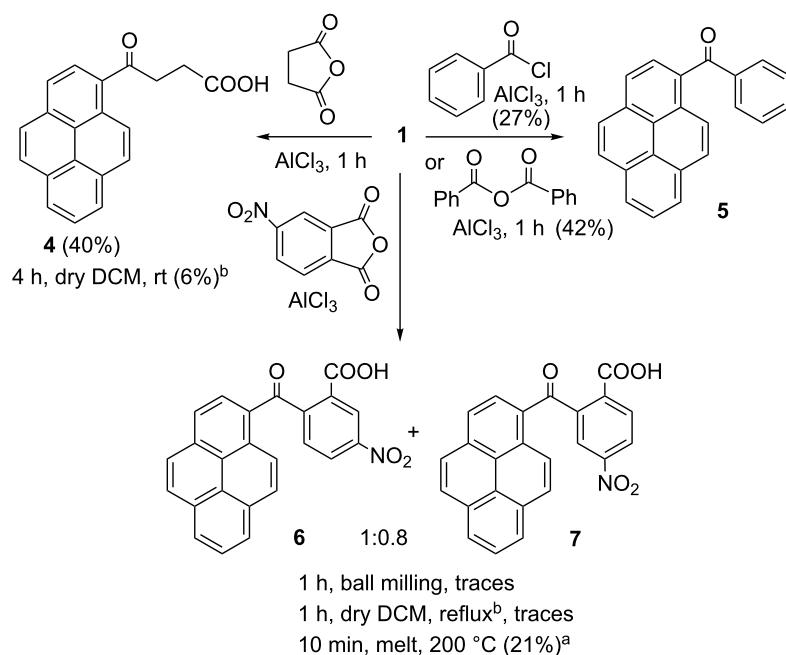
Scheme 2: Scope of acylation reagents in FCR under mechanochemical activation conditions and comparison with other reaction conditions (isolated yields); [a]conversion from NMR analysis; [b]solution reaction in flask, substrate/acylation reagent/AlCl₃ ratio is 1:1:2.5; ball-milling details are given in Table 1.
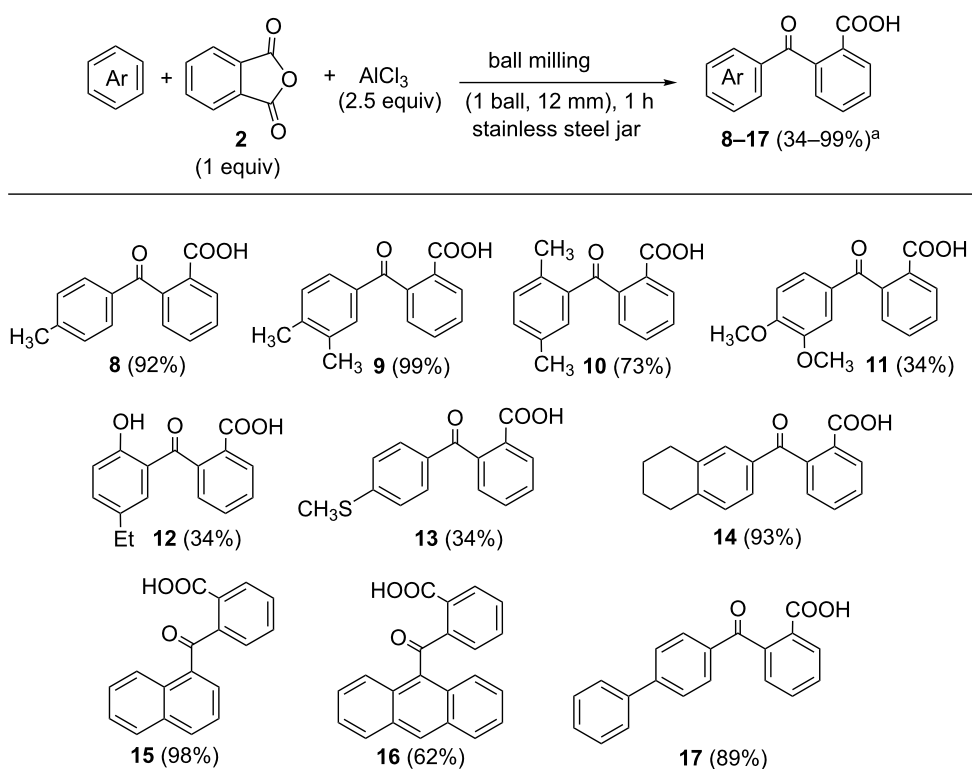
Scheme 3: Scope of aromatic substrates in FCR under mechanochemical activation conditions. [a]Isolated yields.

mechanochemical conditions is evidenced by solid state milling of pyrene with succinic anhydride which showed remarkably better performance than the reaction carried out in solution (40% vs 6% yield).

The screening of substrates showed disparate reactivities, ranging from quantitative to low (Scheme 3). Most rewarding are reactions of toluene, *o*-xylene, naphthalene and tetralin. Interestingly, ball milling of 4-ethylanisole provided phenol **12**, in which acylation was accompanied with the cleavage of the methoxy group [43-45]. A striking advantage of the automated ball milling over manual grinding [46] is evident in the reaction of anthracene with phthalic anhydride which gave no product by manual grinding and the yield of the toluene reaction is increased from 68% to 92%.

When anthracene was subjected to a milling reaction with succinic anhydride, 9-substituted product **22** was obtained in low yield, and accompanied with a small amount of 2-acylated product **23** (Scheme 4), with same regioselectivity to that reported in the literature [47,48]. FC acylation at the 2-position of anthracene was achieved by Levy by the employment of 9,10-dihydroanthracene and subsequent oxidation to anthracene. To direct the acylation towards the 2-position, we devised the use of anthracene photodimer **19** [49] for the protection of 9,10-positions. The photodimer would act as 9,10-dihydroanthracene, and 2-acylated product should be regioselectively formed, which could be converted by thermal retrocyclization via flash vacuum pyrolysis (FVP) [50,51] to **23**. However, ball milling of **19** with **20** provided 95% conversion of **19** to anthracene, with a small amount (<5%) of **22**. This result indicates that rapid [4π − 4π] cycloreversion of **19** takes place, even in solid state ball-milling conditions at room temperature. Produced anthracene then subsequently participates in FCR. In control

reaction of milling of photodimer **19** itself for 1 h was converted to anthracene in 95% yield. This [4π + 4π] cycloreversion in mechanochemical conditions is analogous to previously described dissociation of labile anthracene/C$_{60}$ cycloadduct [52]. When the reaction of **19** with **20** was carried out in solution (DCM, overnight), 60% of dimer was converted to anthracene, and traces of FC product **22** were observed. Further attempts were made to lower the reaction temperature by cryomilling [53] (reaction vessel was cooled down by dipping into liquid nitrogen every 3–5 min, and ball milled for 30 min in total). This procedure partially suppressed cycloreversion and led to the mixture of **19** and **18** (3:2 ratio), accompanied with a small amount of **22**.

As a substitute for dianthracene **19**, thermally more stable substrate, anthracene-*N*-methyl maleimide adduct **25** [54] was prepared by Diels–Alder reaction under high pressure conditions as well as by microwave-assisted reaction and mechanochemically (Scheme 5). In this molecule, *N*-methylmaleimide could be used as protection of the 9,10-positions of anthracene and then removed by FVP. We thought that the maleimide moiety will not be affected in the FC acylation, since the precedencies exist in the literature on imide moiety withstanding the FC reaction [55,56]. However, mechanochemical reaction of **25** with succinic anhydride and 2.5 equiv of AlCl$_3$ showed no reaction and the increase of the excess of catalyst to 5 equiv gave a very complex mixture.

Phthaloyl chloride was applied in mechanochemical FCR with the goal of obtaining a double reaction leading to the anthraquinone core in a single reaction pot in solid state [57,58]. Indeed, milling of *p*-xylene, AlCl$_3$ and phthaloyl chloride led to the formation of a mixture of **10** and intramolecular FC product **29** [59] in a 1:3 ratio (Scheme 6). The ratio of 1,4-dimethylan-
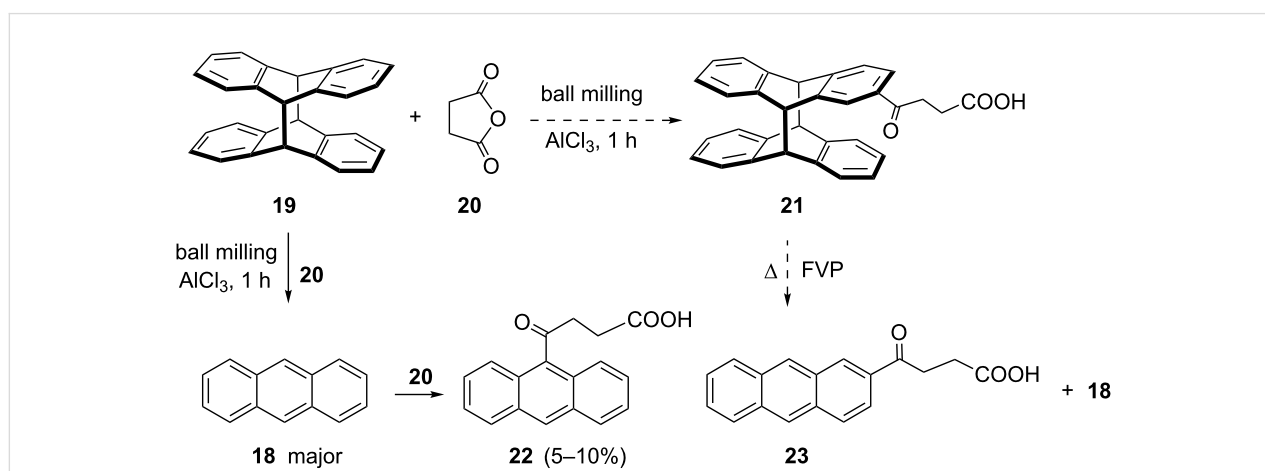
Scheme 4: Mechanochemical regiodirected FCR of anthracene dimer and succinic anhydride.
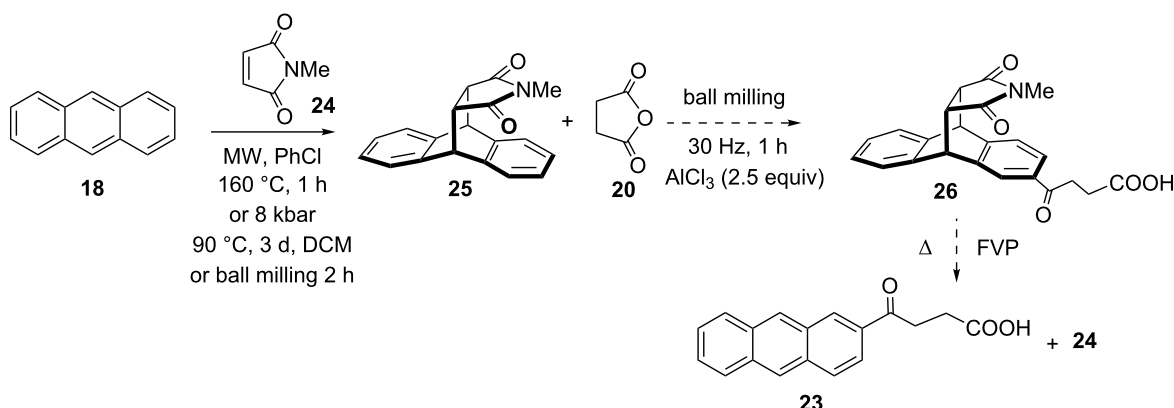
Scheme 5: Regioselectivity direction by protection of 9,10-anthracene ring positions.
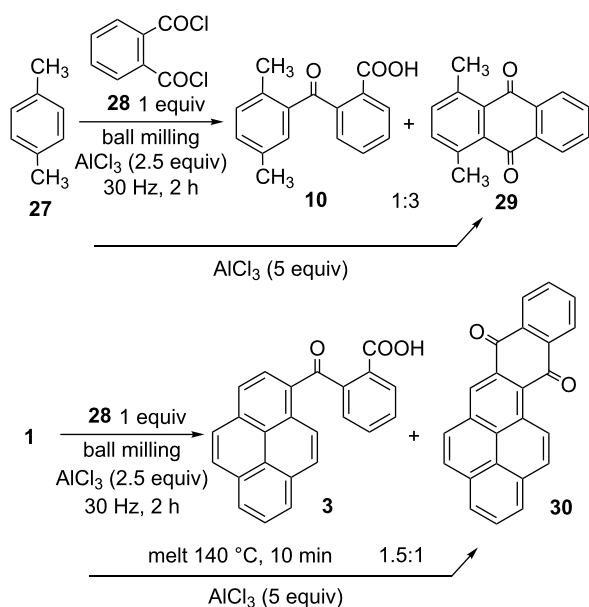
Scheme 6: Double FCR of phthaloyl chloride and aromatics.

thraquinone (**29**) did not increase in the presence of 5 equivalents of AlCl$_3$. Formation and ratio of these two products could be conveniently established by ^{1}H NMR analysis, due to a difference in the symmetry of products: there are two methyl signals for **10** and a single methyl line at δ 2.81 ppm in the case of **29**. Pyrene and naphthalene were less reactive under the same ball milling conditions and reactions stopped at the stage of formation of product **3** and **15**. One-step preparation of quinone **30** [39], was achieved by melting reactants at 140 °C for 10 min. Under these conditions, a mixture of adducts **3** and **30** (1.5:1 ratio) was obtained. The product ratio was established by ^{1}H NMR analysis of the characteristic H-10 proton signal of product **3** (peak resonance doublet at δ 9.2 ppm), which is shifted towards lower magnetic field in quinone **30** (δ 10.0

ppm), and concurrent appearance of singlet for H-3 at δ 9.1 ppm. These experiments demonstrate that quinones could be prepared by simple one-pot FC protocols in the case of reactive aromatics.

In situ Raman spectroscopy [60] was applied to study mechanistic aspects of the solid state reaction of phthalic anhydride with *p*-xylene. Raman spectra were simulated and positions of signals for transient reactive intermediates were predicted by density functional theory method B3LYP/6-31G* (Supporting Information File 1) [61]. The stretching of the $^+$C≡O bond of the acylium ion was predicted to be at about 2300 cm^{-1}. Raman spectroscopy revealed that the complexation of phthalic anhydride with AlCl$_3$ is rapid, and within 3 minutes of milling all anhydride is consumed (Figure 1). After 3 minutes of milling, high fluorescence prevents further following of the reaction progress. These spectra indicate that rapid complexation of anhydride with AlCl$_3$ takes place, whereas the formation of the acylium ion intermediate could not be unequivocally verified.

Similar conclusions could be drawn from ex situ IR spectroscopy [62] which indicates rapid complexation and disappearance of phthalic anhydride (Supporting Information File 1, Figures S43 and S44). A further study was carried on complexation of phthalic anhydride with AlCl$_3$ (Supporting Information File 1, Figure S45). Although there are weak signals at 2300 and 3050 cm^{-1} which could be associated with the acylium ion and the intermediate cation, the raise of intensities of these signals over the time is quite unlikely to come from reactive species (time needed to transfer sample from ball mill to IR spectrophotometer and acquire spectra are within several minutes, which could be detrimental to reactive species to survive in the open air). These signals are not visible after the standard acidic workup and further study would require the use of in situ IR spectroscopy in solution [63].
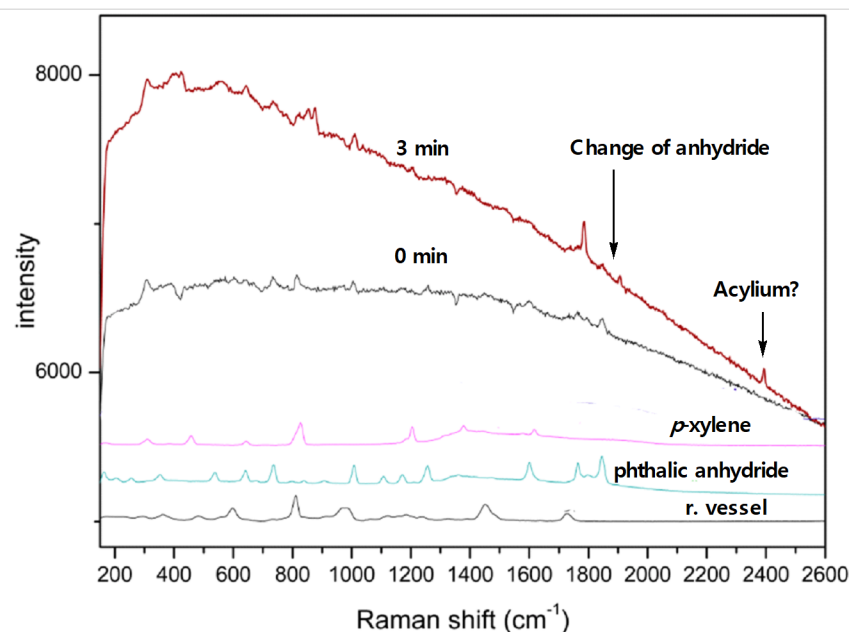
Figure 1: In situ Raman monitoring of reaction of phthalic anhydride with *p*-xylene.

Conclusion

In conclusion, the experimental results demonstrate that Friedel–Crafts acylations could be effectively carried out under solid state ball-milling conditions. The reaction takes place by the initial complexation of the carbonyl group of the acylation reagent with aluminium trichloride.

Supporting Information

Supporting Information File 1

Details of experimental procedures, spectroscopic characterization data of compounds and computational procedures.

[https://www.beilstein-journals.org/bjoc/content/supplementary/1860-5397-15-130-S1.pdf]

Acknowledgements

ORCID® iDs

Anamarija Briš - https://orcid.org/0000-0002-2718-3711
Davor Margetić - https://orcid.org/0000-0002-1039-6569

References

1. Olah, G. A.; Reddy, V. P.; Prakash, G. K. S. Friedel-Crafts Reactions. *Kirk-Othmer Encyclopedia of Chemical Technology;* Wiley: New York, 2000. doi:10.1002/0471238961.0618090515120108.a01

2. Sartori, G.; Maggi, R. *Advances in Friedel-Crafts Acylation Reactions: Catalytic and Green Processes;* CRC Press: Boca Raton, FL, U.S.A., 2009. doi:10.1201/9781420067934

3. Toda, F., Ed. *Organic Solid-State Reactions;* Topics in Current Chemistry, Vol. 254; Springer: Heidelberg, Germany, 2005. doi:10.1007/b98357

4. Tanaka, K.; Toda, F. *Chem. Rev.* **2000**, *100*, 1025–1074. doi:10.1021/cr940089p

5. Tanaka, K. *Solvent-free Organic Synthesis;* Wiley-VCH: Weinheim, Germany, 2003. doi:10.1002/3527601821

6. Begum, S.; Zehra, S. Q.; Siddiqui, B. S. *Synth. Commun.* **2006**, *36*, 3203–3224. doi:10.1080/00397910600908900

7. Matlack, A. *Introduction to Green Chemistry;* CRC Press: Boca Raton, 2010; pp 219 ff.

8. Pivsa-Art, S.; Okuro, K.; Miura, M.; Murata, S.; Nomura, M. *J. Chem. Soc., Perkin Trans. 1* **1994,** 1703–1707. doi:10.1039/p19940001703
   $AlCl_3$ is the most common Lewis acid employed in FCR. Other LA catalysts were applied in solution reactions. See this reference for: $InCl_3$, $SbCl_5$, $TiCl_4$, $FeCl_3$, $SnCl_4$, $ZnCl_2$.

9. Garkhedkar, A. M.; Senadi, G. C.; Wang, J.-J. *Org. Lett.* **2017**, *19*, 488–491. doi:10.1021/acs.orglett.6b03642
   See for $ZnBr_2$.

10. Makarov, A. S.; Kekhvaeva, A. E.; Hall, C. J. J.; Price, D. R.; Trushkov, I. V.; Uchuskin, M. G. *Tetrahedron* **2017**, *73*, 7042–7053. doi:10.1016/j.tet.2017.10.054
   See for $CuBr_2$.

11. Ichikawa, K.; Chano, K.; Inoue, M.; Sugita, T. *Bull. Chem. Soc. Jpn.* **1982,** *55*, 3039–3040. doi:10.1246/bcsj.55.3039
   See for $CuCl_2$.

12. Peng, C.; Zhang, J.; Xue, J.; Li, S.; Wang, X.-N.; Chang, J. *J. Org. Chem.* **2018,** *83*, 9256–9266. doi:10.1021/acs.joc.8b01255
   See for ZnI_2.

13. *Ball Milling Towards Green Synthesis: Applications, Projects, Challenges;* Stolle, A.; Ranu, B., Eds.; RSC Green Chemistry, Vol. 31; Royal Society of Chemistry: Cambridge, UK, 2015. doi:10.1039/9781782621980

14. Wang, G.-W. *Chem. Soc. Rev.* **2013,** *42,* 7668–7700. doi:10.1039/c3cs35526h

15. Stolle, A.; Szuppa, T.; Leonhardt, S. E. S.; Ondruschka, B. *Chem. Soc. Rev.* **2011,** *40,* 2317–2329. doi:10.1039/c0cs00195c

16. James, S. L.; Adams, C. J.; Bolm, C.; Braga, D.; Collier, P.; Friščić, T.; Grepioni, F.; Harris, K. D. M.; Hyett, G.; Jones, W.; Krebs, A.; Mack, J.; Maini, L.; Orpen, A. G.; Parkin, I. P.; Shearouse, W. C.; Steed, J. W.; Waddell, D. C. *Chem. Soc. Rev.* **2012,** *41,* 413–447. doi:10.1039/c1cs15171a

17. Kaupp, G. *CrystEngComm* **2009,** *11,* 388–403. doi:10.1039/b810822f

18. Margetić, D.; Štrukil, V. *Practical Considerations in Mechanochemical Organic Synthesis;* Mechanochemical Organic Synthesis; Elsevier: Amsterdam, Netherlands, 2016; pp 1–54. doi:10.1016/b978-0-12-802184-2.00001-7

19. Troschke, E.; Grätz, S.; Lübken, T.; Borchardt, L. *Angew. Chem., Int. Ed.* **2017,** *56,* 6859–6863. doi:10.1002/anie.201702303

20. Briš, A.; Đud, M.; Margetić, D. *Beilstein J. Org. Chem.* **2017,** *13,* 1745–1752. doi:10.3762/bjoc.13.169

21. Glasovac, Z.; Trošelj, P.; Jušinski, I.; Margetić, D.; Eckert-Maksić, M. *Synlett* **2013,** *24,* 2540–2544. doi:10.1055/s-0033-1339876

22. Štrukil, V.; Sajko, I. *Chem. Commun.* **2017,** *53,* 9101–9104. doi:10.1039/c7cc03510a

23. Portada, T.; Margetić, D.; Štrukil, V. *Molecules* **2018,** *23,* No. 3163. doi:10.3390/molecules23123163

24. Đud, M.; Margetić, D. *Int. J. Org. Chem.* **2017,** *7,* 140–144. doi:10.4236/ijoc.2017.72011

25. Caution: Aluminium trichloride dust is very irritant and corrosive and reacts violently with water. For its handling appropriate protection measures should be implemented (Supporting Information File 1).

26. Howard, J. L.; Sagatov, Y.; Browne, D. L. *Tetrahedron* **2018,** *74,* 3118–3123. doi:10.1016/j.tet.2017.11.066

27. Yu, J.; Hong, Z.; Yang, X.; Jiang, Y.; Jiang, Z.; Su, W. *Beilstein J. Org. Chem.* **2018,** *14,* 786–795. doi:10.3762/bjoc.14.66

28. Su, W.; Yu, J.; Li, Z.; Jiang, Z. *J. Org. Chem.* **2011,** *76,* 9144–9150. doi:10.1021/jo2015533

29. Friščić, T.; Trask, A. V.; Jones, W.; Motherwell, W. D. S. *Angew. Chem., Int. Ed.* **2006,** *45,* 7546–7550. doi:10.1002/anie.200603235

30. Denlinger, K. L.; Ortiz-Trankina, L.; Carr, P.; Benson, K.; Waddell, D. C.; Mack, J. *Beilstein J. Org. Chem.* **2018,** *14,* 688–696. doi:10.3762/bjoc.14.57

31. Gonnet, L.; Tintillier, T.; Venturini, N.; Konnert, L.; Hernandez, J.-F.; Lamaty, F.; Laconde, G.; Martinez, J.; Colacino, E. *ACS Sustainable Chem. Eng.* **2017,** *5,* 2936–2941. doi:10.1021/acssuschemeng.6b02439

32. Howard, J. L.; Brand, M. C.; Browne, D. L. *Angew. Chem., Int. Ed.* **2018,** *57,* 16104–16108. doi:10.1002/anie.201810141

33. Liu, M.; Wu, L. *Faming Zhuanli Shenqing* 106905136, Jun 30, 2017. See for FeCl$_3$ employed in FCR acylations with phthalic anhydride in solution.

34. Clar, E. *Chem. Ber.* **1948,** *81,* 169–175. doi:10.1002/cber.19480810215 See for ZnCl$_2$ employed in FCR acylations with phthalic anhydride in solution.

35. Kehoe, T. D.; Sabnis, R. W.; Balchunis, R. J. Oral care compositions with color changing indicator. PCT Int. Appl. WO2006105260, Oct 5, 2006. *Chem. Abstr.* **2006,** *145,* 397365. See for ZnCl$_2$ employed in FCR acylations with phthalic anhydride in solution.

36. Nakamura, H.; Tanaka, N.; Matsuhashi, H. *J. Jpn. Pet. Inst.* **2010,** *53,* 276–282. doi:10.1627/jpi.53.276 See for sulfated ZrO$_2$ employed in FC acylations with phthalic anhydride in solution.

37. Madje, B. R.; Shelke, K. F.; Sapkal, S. B.; Kakade, G. K.; Shingare, M. S. *Green Chem. Lett. Rev.* **2010,** *3,* 269–273. doi:10.1080/17518251003776877 See for sulfated ZrO$_2$ employed in FCR acylations with phthalic anhydride in solution.

38. Maeimi, H.; Brojerdi, S. S. *Polycyclic Aromat. Compd.* **2014,** *34,* 504–517. doi:10.1080/10406638.2014.910238 See for SiO$_2$/sulfuric acid employed in FCR acylations with phthalic anhydride in solution.

39. Casas-Solvas, J. M.; Mooibroek, T. J.; Sandramurthy, S.; Howgego, J. D.; Davis, A. P. *Synlett* **2014,** *25,* 2591–2594. doi:10.1055/s-0034-1379026

40. Arcamone, F.; Bernardi, L.; Patelli, B.; Giardino, P.; Di Marco, A.; Casazza, A. M.; Soranzo, C.; Pratesi, G. *Experientia* **1978,** *34,* 1255–1257. doi:10.1007/bf01981401

41. Andersen, J.; Mack, J. *Green Chem.* **2018,** *20,* 1435–1443. doi:10.1039/c7gc03797j

42. Kaupp, G.; Funk, B.; Benz, H. U.; Heupel, A.; Zoz, H. Conference paper APMA-2017. The 4th International Conference on Powder Metallurgy in Asia, Hsinchu, Taiwan, April 9–11, 2017.

43. Sato, H.; Dan, T.; Onuma, E.; Tanaka, H.; Aoki, B.; Koga, H. *Chem. Pharm. Bull.* **1991,** *39,* 1760–1772. doi:10.1248/cpb.39.1760 Methyl ether cleavage is a common process in Friedel–Crafts reactions with AlCl$_3$, when acylation occurs at the *ortho*-position. See also references [40,44,45].

44. Sato, H.; Kuromaru, K.; Ishizawa, T.; Aoki, B.; Koga, H. *Chem. Pharm. Bull.* **1992,** *40,* 2597–2601. doi:10.1248/cpb.40.2597

45. Saha, K.; Lajis, N. H.; Abas, F.; Naji, N. A.; Hamzah, A. S.; Shaari, K. *Aust. J. Chem.* **2008,** *61,* 821–825. doi:10.1071/ch08084

46. Ghiaci, M.; Asghari, J. *Synth. Commun.* **1998,** *28,* 2213–2220. doi:10.1080/00397919808007036

47. Wiznycia, A. V.; Desper, J.; Levy, C. J. *Dalton Trans.* **2007,** 1520–1527. doi:10.1039/b700001d

48. Schoental, R. *J. Chem. Soc.* **1952,** 4403–4406. doi:10.1039/jr9520004403

49. Breton, G. W.; Vang, X. *J. Chem. Educ.* **1998,** *75,* 81–82. doi:10.1021/ed075p81

50. Margetić, D.; Butler, D. N.; Warrener, R. N.; Murata, Y. *Tetrahedron* **2011,** *67,* 1580–1588. doi:10.1016/j.tet.2010.12.032

51. Margetić, D.; Butler, D. N.; Warrener, R. N. *Synlett* **2013,** *24,* 2609–2613. doi:10.1055/s-0033-1339879

52. Murata, Y.; Kato, N.; Fujiwara, K.; Komatsu, K. *J. Org. Chem.* **1999,** *64,* 3483–3488. doi:10.1021/jo990013z

53. Waddell, D. C.; Mack, J. *Green Chem.* **2009,** *11,* 79–82. doi:10.1039/b810714a

54. Alibert, S.; Santelli-Rouvier, C.; Castaing, M.; Berthelot, M.; Spengler, G.; Molnar, J.; Barbe, J. *Eur. J. Med. Chem.* **2003,** *38,* 253–263. doi:10.1016/s0223-5234(03)00018-7

55. Reifenrath, W. G.; Bertelli, D. J.; Micklus, M. J.; Fries, D. S. *Tetrahedron Lett.* **1976,** *17,* 1959–1962. doi:10.1016/s0040-4039(00)78089-0

56. Xu, Q.; Wang, G.; Wang, X.; Wu, T.; Pan, X.; Chan, A. S. C.;
    Yang, T.-K. *Tetrahedron: Asymmetry* **2000,** *11,* 2309–2314.
    doi:10.1016/s0957-4166(00)00193-2

57. Reference [2], p. 43: Product **29** was also prepared by double acylation
    reaction of *p*-xylene with phthalic anhydride or with phthaloyl chloride
    using TfOH.

58. Sartori, G.; Casnati, G.; Bigi, F.; Foglio, F. *Gazz. Chim. Ital.* **1990,** *120,*
    13–19.

59. Rosenfeld, S.; VanDyke, S. *J. Chem. Educ.* **1991,** *68,* 691–692.
    doi:10.1021/ed068p691

60. Gracin, D.; Štrukil, V.; Friščić, T.; Halasz, I.; Užarević, K.
    Angew. Chem., Int. Ed. **2014,** *53,* 6193–6197.
    doi:10.1002/anie.201402334

61. Comparison of signals obtained experimentally was performed with
    Raman spectra calculated at the B3LYP/6-31G* level and corrected by
    scaling factor of 0.9614.

62. Đud, M.; Glasovac, Z.; Margetić, D. *Tetrahedron* **2019,** *75,* 109–115.
    doi:10.1016/j.tet.2018.11.038

63. Huang, Z.; Jin, L.; Han, H.; Lei, A. *Org. Biomol. Chem.* **2013,** *11,*
    1810–1814. doi:10.1039/c3ob27094g
    Further study would require in situ IR spectroscopy in solution. See for
    details.

Reaction of oxiranes with cyclodextrins under high-energy ball-milling conditions

László Jicsinszky[*], Federica Calsolaro, Katia Martina, Fabio Bucciol, Maela Manzoli and Giancarlo Cravotto[*]

Abstract

This work presents a proof of concept for a green cyclodextrin derivatisation method that uses low-boiling epoxide reagents in a high-energy ball mill (HEBM). The simplified preparation and purification of low substitution-degree common (2-hydroxy)propylated β- and γ-cyclodextrins (β/γ-CDs) has been realised. The intelligent use of propylene oxide has also facilitated the more effective synthesis of highly substituted γ-CD. Epichlorohydrin-crosslinked CD-polymers (CDPs) have also been effectively prepared in the ball mill. The unoptimised preparations of soluble and insoluble CDPs displayed very small particle size distributions, while the prepared polymers currently have different complexation properties to those of their classically prepared analogues.

Introduction

The derivatisation of natural cyclodextrins (CDs, cyclic α(1->4)-linked glucopyranosides) is always a difficult task, particularly when the attached moiety is prone to further derivatisation. In many cases, statistical (random) substitution results in essential changes in the hydrogen bonding systems of the cyclodextrin hydroxy rims, and is especially useful when the crystalline complex formation with the guest is undesirable. The aggregation properties, by the ready-to-associate secondary rim, are considerably affected by these substituents. One of the most important reactions of CDs occurs with oxiranes (epoxides) under basic conditions to provide (2-hydroxy)propyl-CDs

(HPCDs) that are commonly used in pharmaceutical formulations and household products. Furthermore, a class of non-hydrolysable, soluble and insoluble CD polymers (CDP) can be prepared by crosslinking CDs with epichlorohydrin or 1,2:3,4-diepoxybutane. These are the oldest and most commonly used CDPs [1], more so than the so-called "nanosponges" [2], as well as being more chemically stable in both aqueous and alcoholic media.

Their industrial-scale preparation has been designed and uses sodium hydroxide as the base in a very concentrated aqueous

CD solution [3]. The low solubility of β-CD can be dramatically increased using a base, which occurs via the ionisation of the secondary hydroxy groups, near pH ≈12 (secondary hydroxy dissociation starts around ≈11.5–11.8 in water) [4,5]. In basic aqueous medium, the high reactivity and low water-miscibility of 1,2-propylene oxide make the formation of (oligo)propylene glycol (oligo-PGs) unavoidable. Moreover, at higher degree of substitution (DS, number of substituent/macrocycle) the HP moiety can be further substituted, giving oligo-PG sidechains on the CDs [6]. At low DS values, occasional residual unsubstituted CDs can be removed (by aluminium oxide) and "recrystallisation" (from acetone) eliminates (oligo)-PG to a pharmaceutically acceptable level [6,7]. However, the low boiling point of the 1,2-propylene oxide generates some safety concerns. The low reaction temperature favours the secondary hydroxy group in CD substitution, which results in products having some DS-dependent solubilisation properties [8-11]. In solvent-free conditions, although the nature of the reaction means that they are not absolutely water free, not only the PG formation can be optimised but also the reagent use. As previously demonstrated, mechanochemical reactions usually give a more balanced substitution pattern for the randomly substituted derivatives [12].

In CDP preparations almost the same reaction conditions are used, but 1,2-propylene oxide is replaced with epichlorohydrin [13-16]. The disadvantage of this reaction is that the first step produces CD-propyl chlorohydrin, which is immediately transformed into an epoxide that can either react with other CDs, to form CDP, or with a hydroxy ion, to produce a (2,3-dihydroxy)propyl side chain. The hydrolytic reaction is unavoidable because of the aqueous solution and the higher reaction temperature. As the epichlorohydrin is in a large molar excess at the beginning of the reaction, its partial hydrolysis can result in the presence of glycerol moieties. Although it is true that the hydrolysis can be impeded somewhat by adding the reagents to the reaction mixture in a controlled manner, this side reaction cannot be completely eliminated.

The solubilisation/complexation potential of the polymers can be increased by the application of a chemically inert guest, using the so-called molecular imprinting strategy [17-19].

Despite the early patents and a promising beginning, CDPs are poorly applied CD derivatives and a standardised quality product is still missing. Detailed studies of the complexation properties of bead polymers have demonstrated their slow and structure-dependent complexation properties [13]. The preparation of an insoluble CDP is always challenging. Achieving a uniform insoluble CDP particle size is difficult and usually requires special, poorly transferable techniques [13,14,16,20].

The drawbacks of classical derivatisation methods include their problematic scale-up, which explains the limited number of sources of insoluble CDPs and also their high prices. Insoluble CDPs have excellent separation power in both regio- and enantiomer separations, as initially described by Zsadon et al., many decades ago [21-24]. More widespread use of CDPs in analytical and preparative applications is not only restricted by the aforementioned factors, but also by the lack of uniformity and the site-by-site variability of prepared CDPs, which have hampered the extensive CDP use.

Mechanochemistry has proven to be a useful green tool in the hands of synthetic chemists [25-28]. The reaction of epoxides with cyclodextrins under green and solventless conditions is discussed in this report. The HEBM technique was performed in a planetary ball mill for this purpose [12,29]. Proof of concept and reagent use were investigated for the most common HPCDs. Substitution patterns were not the target of our study as the modification of current industrial methods cannot be expected to occur in the near future. In the case of CDPs, our main aims were to find an effective, reproducible and green method for the preparation of a uniform insoluble CDP and to study its complexation properties in order to discover the right direction for synthesis optimisation.

Results and Discussion
Reaction of epoxides with CDs

The reactions of oxiranes, particularly propylene oxide, with CDs in solution have been extensively studied and the products are synthesised on the ton-scale by various companies [6,30-32]. The reaction is based on the activation of hydroxy groups with a base, which also increases CD solubility in water. Although the reaction proceeds in a completely random manner at a moderate molar ratio of base and low reaction temperatures, secondary hydroxy substitution is preferred. Primary OH and HP moiety substitution is suppressed at low DS values [9,33-36]. The aqueous solubility of propylene oxide is limited, meaning that only the dissolved reagent can react with the CD OH groups, which results in a permanent high excess of OH⁻. While the formation of a complex between propylene oxide and the CDs increases the solubility, OH⁻ can react with the reagent and the PG that is formed contaminates the product. Further reaction between propylene oxide, PG and the substituent(s) on the CDs leads to (oligo)PGs in the product and 2-(2-hydroxypropoxy)propyl moieties on the CDs. Although PG/oligo-PG is a pharmaceutically accepted solvent, its amount is limited, especially in parenteral applications [37]. Generally, 60–70% propylene oxide is utilized in the CD substitution reaction, which can result in 5–10% oligo-PG content in the crude product [6]. The hazardous nature of the reagent makes full conversion a necessity.

The substitution of propylene oxide with other reagents that are commonly used in CD derivatisation, such as 1,2:3,4-diepoxybutane and epichlorohydrin, further complicates the problems of reactions in solution. The hydrolysis of these reagents, whether in the free form or bound to CDs, results in a very complex structure that renders analyses and in-process control even more difficult. Furthermore, complications in reproducibility limit CDP use. Epichlorohydrin, which is used for the preparation of soluble CDPs, can also be used in the synthesis of insoluble CDPs. Although many kinds of insoluble CDPs [38], not only those based on epichlorohydrin, have been reported, their accessibility even on a kg-scale is very limited. The spread of insoluble polymer use can be easily improved by the existence of a readily transferable and engineered method, which would eliminate the main limiting factors of solution chemistry.

The restricted mobility of solid-state components further reduces the aforementioned side-reactions and enhances the utilization in the CD substitution. Although many side reactions are suppressed in ball milling, they cannot be completely eliminated when alkaline hydroxides are used to activate the CD OH groups. The formation of CD alkali salts always results in residual water when no metals or metal hydrides are used. The safer use of the hydroxides, in comparison with alkali metals or their hydrides, considerably outweighs the purification costs. Scheme 1 shows a general reaction scheme for CD substitution. This scheme is also valid for solution reactions.
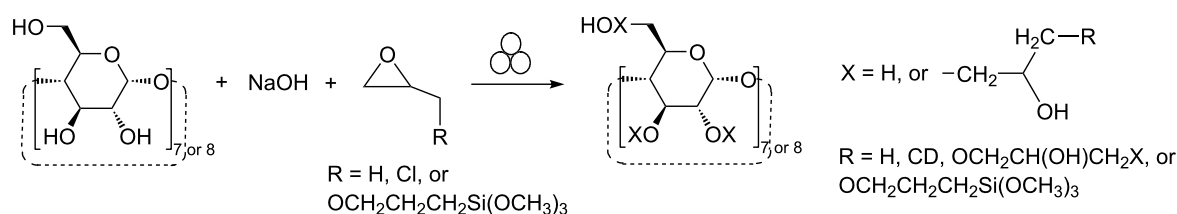
(*R/S*)-1,2-Epoxypropane ((±)-propylene oxide)

The solution method proceeded as a typical reaction run of hydroxypropylation; after a short period of intense stirring, a precipitate started to form (monoHP CDs), which slowly re-dissolved as the reaction mixture warmed and the reaction became faster. In order to allow the complete conversion of propylene oxide to occur, the reaction mixture was stirred for 4 days, after the ice in the bath had completely melted. The relatively large bath volume kept the reaction temperature practically constant at around room temperature (rt) during stirring.

Freshly dried CDs were generally used in ball-milling reactions to minimise the hydrolysis of propylene oxide, but we also tested CD-hydrates. Unlike in the solution method, HEBM experiments provide for relatively poor opportunities to visually inspect reaction progress. The low boiling point of propylene oxide means that the reaction-mixture temperature inside the jar cannot be monitored, but as our previous experiments have shown that monitoring the jar temperature, between certain limits, can give information about the energetics of the reaction [39]. The well-sealed jar is able to keep all the epoxides inside over the total milling time and, despite the necessity to have a considerable amount of propylene oxide in the vapour phase, the reagent also remains in the reaction vessel. In order to minimise the destruction of the reagent, which can occur either via hydrolysis by the residual water or escape via evaporation, the jar was cooled with liquid N_2 below −30 °C after the sodium salt formation of the CDs and before the epoxide was added to the light, electrostatic powder. Liquid N_2 not only worked as a cooling medium, but its evaporation completely excluded the humidity of air. Salt formation was exothermic, although the milling of CDs and NaOH also increased the internal temperature of the powder. Milling also increases the solid's temperature, as was previously found to occur without a reagent. Whereas the internal temperature increased to around 40–45 °C when CDs were milled alone, the temperature of the powder could reach 60–65 °C during salt formation when the NaOH was added, while the external jar temperature stabilised at around 40–45 °C until the end of the milling periods.

As the propylene oxide was added, milling rapidly increased the jar temperature from less than −30 °C to between 40–45 °C. It then remained almost constant over 2 h of milling, as seen in Figure 1. The jar temperature reached rt in the first 5 minutes and the jar temperature started to decrease slowly after around 2 hours. The jar fixer needed to be adjusted often over the first minutes of milling due to its loosing as the system warmed.

As the jar temperature started to decrease after 2 hours, it was assumed that the reaction was finished. However, some hissing and powder blow-off upon jar opening indicated propylene-

Scheme 1: The reaction of CDs with oxiranes.

Figure 1: Jar-temperature changes during the reaction of 1,2-propylene oxide and cyclodextrins in the presence of NaOH.
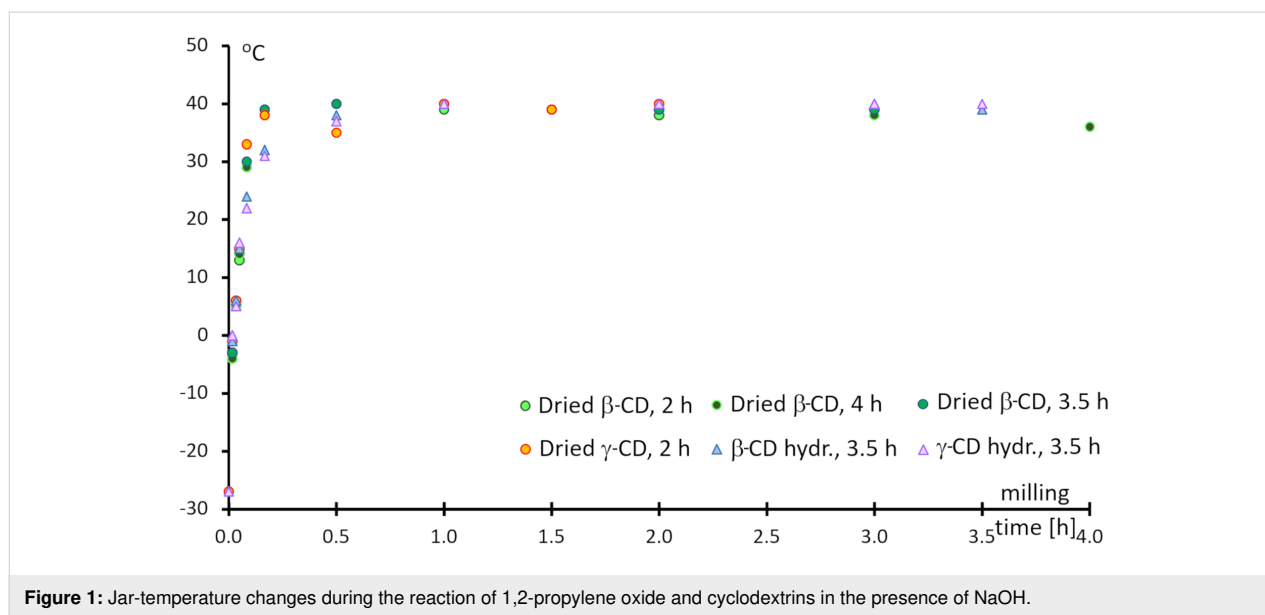
oxide overpressure, which signified its incomplete conversion. This effect was found in both β- and γ-CD reactions after 2 hours. The complete conversion of the reagent was found upon increasing the milling time to 4 hours. Finally, 3.5 h milling was found to completely convert the propylene oxide in cases with low DS values. The reaction mixtures were always in a fine powder state over the entire course of the reactions, including salt formation.

When using CD-hydrates, their natural state and as they are available from the suppliers, a hard CD-salt solid stuck to the jar wall in both β- and γ-CD, unlike with dried CDs. This solid should be removed from the wall to maximise reagent contact before cooling and the addition of propylene oxide. As the reaction proceeded, the solids became light and very electrostatic powders, just like in the dried CD tests. Product isolation was considerably easier than in the solution reactions because water elimination was not necessary. Any residual unsubstituted CDs were also removed and yields were quite acceptable, as seen in

Table 1. Because the use of propylene oxide was found to be better here than in the solution reaction, higher DSs were obtained than would have been expected based on the solution reactions. Although the TLC of the powders after the reaction showed very little unsubstituted CD content, the removal of the very poorly soluble monoHPs also increased the average DS of the products.

The easiest and cheapest product removal was dissolution in MeOH as nearly all of the components, except unsubstituted CDs and some monoHPs (these are somehow solubilized by the higher-DS HPCDs), are soluble in MeOH. At the end of the reaction, the MeOH contained some solids, but the filtration failed because of the very small particles. While centrifugation resulted in a clear solution, the clean removal of the supernatant was practically impossible because of re-suspension. Finally, due to the negligible amount of the fine powder, the suspension was treated immediately with a cation-exchanger to remove the sodium ion from the system. Some anion-exchanger

Table 1: Summary of HPCD syntheses in HEBM.

No.	CD	Milling time [h]	B2M ratio[a]	Product[b] [g]	DS[c]	Yield[d] [%]
1	β	2	14.6	2.3	4.4	84
2	β	4	14.6	2.3	5.6	78
3	β	3.5	14.6	2.5	5.3	87
4	β-hydrate	3.5	13.0	2.4	3.7	89
5	γ	2	13.2	2.7	5.1	84
6	γ-hydrate	3.5	12.2	2.4	5.5	73

[a]Ball-to-mass (mass of balls/mass of reagents); [b]isolated, purified; [c]calculated from the integration of the anomeric-proton and CH$_3$ signals of ^{1}H NMR spectra and corrected using the residual solvent content; [d]on the base of DS.

was added before further treatment in order to remove the occasionally present fragments of the strong cation-exchanger. According to the supplier's specifications, a few tenths of a per cent of linear dextrins (having reducing ends) cause strong colouration in the reaction mixture, in both the solid and solution methods. In order to reduce the colour intensity and remove the few insolubles, such as unsubstituted CDs, etc., from the solution, 5% charcoal was used.

The addition of acetone to the concentrated MeOH solution, to around 50% product content, completely removed the formed PGs. It was found that sometimes a small percentage of residual solvent was observed, despite the long drying times at temperatures above the solvent boiling points, as seen in the ^{1}H NMR spectra. The DS of the product was calculated from the ^{1}H NMR spectra, according to the pharmacopoeia method, using the integrals of the anomeric protons of the CDs and the integration of the methyl signal of the HP moiety (DS = Int_{Me}/3, the anomeric proton signal integral is set to 7.0 or 8.0, according to the CD used). Similar calculations using the CD core-proton integral, which overlaps with the methine and methylene protons of the HP, resulted in similar DS values within the calculation limits. The lack of sharp signals in both the core- and methyl signal regions allowed us to assume that PGs were present in amounts that were below the detection limits. The mother liquors of the MeOH–acetone crystallisation of the products were hygroscopic and slightly waxy, which demonstrates their PG content.

A comparison of DS, by ^{1}H NMR, and the product distribution of the ESIMS data showed a Gaussian-like distribution of masses in the range of 1–11, which was independent of the target DS. The ESIMS of the neutral HPCDs resulted in a complex spectral composition and showed mass distributions that were centred differently to the average DS that were calculated using ^{1}H NMR.

The recovery of CD derivatives from the adsorbents showed minimal unsubstituted CDs and monoHP contents dominated, which explains the shift of DS toward the higher substitution range of the worked-up products. It is in agreement with previous findings [7].

The synthesis of high DS HP-γ-CD in solution is a multistep process used to minimise reagent loss and the formation of oligo-PGs during synthesis. The high DS and the oligo-PG side chain do not permit acetone crystallisation to remove oligo-PGs. Dialysis can completely remove PG contaminants but, particularly when DS < 10, leads to considerable product losses. High reagent utilisation in the reaction allowed the preparation of highly substituted CDs to be simplified and reduced the number of reaction steps, which could also cut down on purification as well as minimising residual PG impurities. In all cases, ball-to-mass ratios were reasonable and the yield acceptable, as seen in Table 2.

Although hydroxypropylation was found to be very effective, unlike in the solution reactions, the HEBM method prefers water-free components, otherwise CD-hydrates form a hard solid, which sticks to the jar wall, during the salt preparation. While this is currently a considerable drawback for the mechanochemical method, the optimisation of the reagent ratios and milling parameters can offer a truly fine-tunable HPCD preparation method.

1-Chloro-2,3-epoxypropane ((±)-epichlorohydrin)

The potential of insoluble CDPs in various fields was recognised at a very early stage of CD derivatisation, and earlier than (2-hydroxy)propylation [15,16,22]. The use of epichlorohydrin can result in variously crosslinked polymers, depending on the molar ratio of the CD and epichlorohydrin [40-43]. As in the HPCD preparations, the aqueous basic solution can crosslink the macrocycles, while the relatively large OH⁻ excess can hydrolyse both the reagent and the simultaneously formed oxirane. In order to prepare bead CDPs, limited water miscibility solvents are added. Controlled addition to a homogeneous reaction mixture gives an alternative reaction product; soluble CD polymers. Unfortunately, the originally unfavourable CD/guest mass ratio worsens further, despite the good aqueous solubility of the CD polymers.

The molar ratio of CDs/epichlorohydrin was set to 1:10, which was based on the preparation of a soluble polymer [44]. Surprisingly, insoluble CDPs were almost exclusively formed at this

Table 2: (2-Hydroxy)propylation of γ-CD of high DS.

No.	Molar fold of reagent	Milling time [h]	B2M ratio[a]	Product[b] [g]	DS[c]	Yield[d] [%]
7	10	8	8.5	2.0	8.8	56
8	20	8	10.9	2.9	17.6	63

[a]Ball-to-mass (mass of balls/mass of reagents); [b]isolated, purified; [c]calculated from the integration of anomeric-proton and CH_3 signals of ^{1}H NMR spectra and corrected with the residual-solvent content; [d]on the base of DS.

molar ratio, unlike in the solution method. This result suggests that, in accordance with the practice, the soluble polymer contains a considerable amount of the glycidyl (2,3-dihydroxypropyl) sidechain in the solution reaction instead of the cross-linking ether units. It is known that the reaction can be directed to the glycidyl CD derivatives instead of polymerisation by varying the conditions [45-47].

Centrifugation of the neutralised suspension completely removed not only the inorganic salts but also all the soluble contaminants. No unsubstituted CDs were found in the solution phase and only a few charrable spots could be seen on the TLC plate. The slightly TLC running CD-dimers were also found to be soluble and were removed from the product with the washing, and the almost complete conversion of both CDs and epichlorohydrin could be deduced from the mass of dried products in all cases, as seen in Table 3. The supernatants were always hazy suggesting the presence of submicron particles, but their amounts were considered negligible.

Salt formation in the 10-fold scaled-up synthesis of the β-CD polymer resulted in some materials that became stuck on the jar wall. However, these were considerably easier to remove than the salts of hydrated CDs. The scale-up experiment (20 mmol scale) did not give a significantly lower yield. This lower yield may be due to the larger particles of the larger-scale experiments at the experiment start.

Attempts to prepare soluble CDPs provide a complex picture. While the ≈3 molar-fold crosslinker resulted in a clear solution, the 5 molar-fold reactions gave a colloid solution and actually it is not clear that it is a very fine, inseparable by centrifugation suspension, or a highly associated soluble polymer. When 10 molar-fold epichlorohydrin was added portionwise, both

insoluble and soluble/solubilised polymers seemed to be formed. The soluble part was similar to the 5 molar-fold experiments; a very hazy solution was obtained, which was inseparable by centrifugation, after dialysis. Filtration through a 0.22 μm hydrophilic membrane showed poor resistance, meaning that particle sizes were low and dominantly <0.2 μm. Experiments to clarify the situation and determine the composition of the formed polymers are in progress.

Under an electron microscope, the bead polymer showed a smooth surface and a non-Gaussian particle-size distribution that was centred around 65–70 μm, while the ball-milled CDPs were completely bumpy and considerably smaller than the bead polymer, as seen in Figure 2 and Figure 3. Higher aggregation of particles of β-CDP was found when it had been prepared on a 2 mmol scale as compared to either the γ-CDP or β-CDP on a 20 mmol scale.

The particle-size distribution, which was determined using the quasi elastic light scattering (QELS) method, was relatively tight and the 20 mmol scale reaction resulted in considerably larger particles, as seen in the normalised size distributions in Figure 4. However, it is necessary to mention that the cracking of the dried polymers of different scales were conducted under different conditions and that the larger particles can be assigned to the larger balls of the scaled-up product. The β-CDPs have a Gaussian distribution, while the γ-CDP does not. While it is interesting to note that γ-CDP gave smaller particles, although not significantly, it may also be true that the small β-CDP particles are more aggregated, as seen in Figure 2 and Figure 3.

Although scaled-up β-CDP has somehow larger particles, complexation studies with methyl orange (MO) only showed small differences. Although complex formation with MO showed

Table 3: Synthesis of CDPs.

No.	Used CD	Total milling time [h]	B2M ratio[a]	Product[b] [g]	Soluble part[c] [g]	Yield[d] [%]
9	β	6	8.8	3.3	<0.1	96
10[e]	β	9	4.5	32.4	1.4	88
11	β-hydrate	6	8.2	3.19	<0.1	91
12	γ	6	8.3	3.4	0.1	92
13	γ-hydrate	6	7.9	3.4	0.1	92
14[f]	β	9	11.7->8.8	0.9	1.3	–
15[g]	β	5	12.8	<0.1	2.2	75
16[h]	β	5	11.2	0.1	2.4[i]	76
17[h]	γ	5	10.3	0.2	2.5[i]	73

[a]Ball-to-mass (mass of balls/mass of reagents); [b]isolated, purified; [c]calculated from the freeze-dried washing-solution theoretical NaCl content; [d]assuming that all epichlorohydrin was used for crosslinking; [e]scale-up, used 125 mL jar; [f]epichlorohydrin was added in 3 portions: at the beginning, after 3 h milling and after 6 h milling; [g]3.3 molar-fold epichlorohydrin; [h]5 molar-fold epichlorohydrin; [i]not necessarily soluble but not sedimented and cannot be centrifuged.
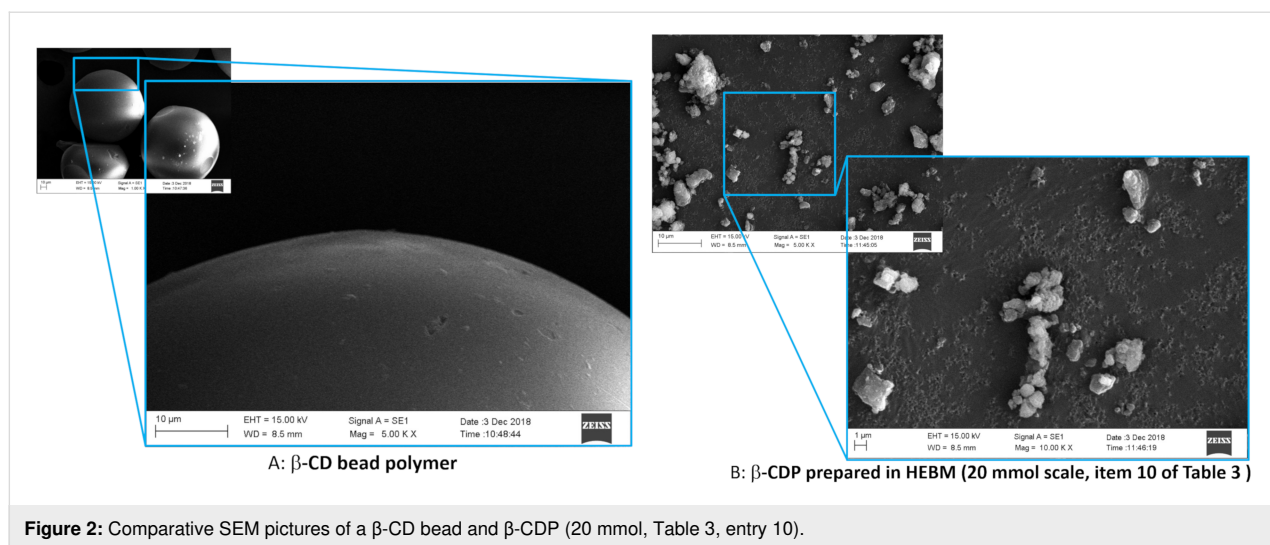
Figure 2: Comparative SEM pictures of a β-CD bead and β-CDP (20 mmol, Table 3, entry 10).
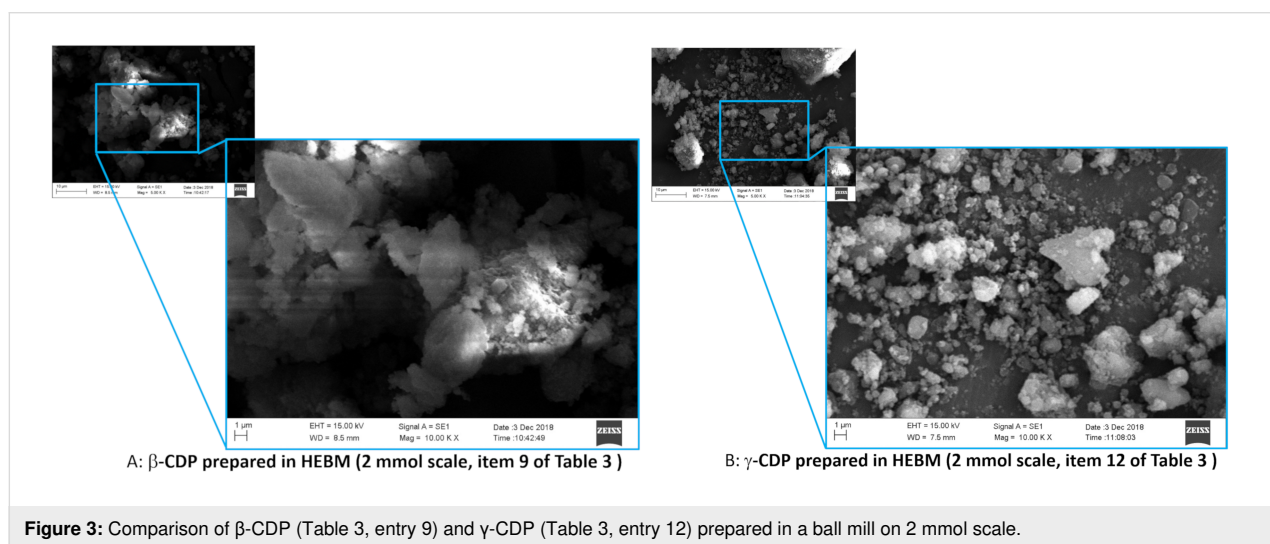
Figure 3: Comparison of β-CDP (Table 3, entry 9) and γ-CDP (Table 3, entry 12) prepared in a ball mill on 2 mmol scale.
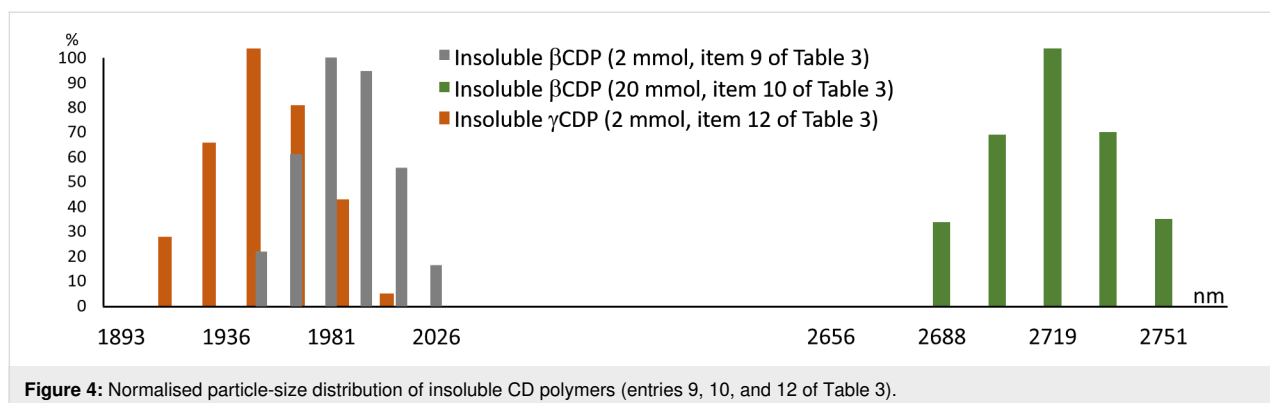
Figure 4: Normalised particle-size distribution of insoluble CD polymers (entries 9, 10, and 12 of Table 3).

similar behaviour to previous reports [13], adsorption capacity seems to be considerably lower than that of bead polymers in all cases. The adsorption of MO shows apparent first order kinetics, and the largest adsorption rates were accordingly found at the beginning of adsorption. The adsorption isotherm of insoluble β-CDP was recorded after 1 day and 2 weeks of equilibration. The adsorption isotherm of β-CDP showed linear concentration dependency, as seen in Figure 5.

Figure 5: UV–vis spectra and adsorption isotherm of the insoluble β-CDP polymer in 10 ml 0.050 mM MO solution (entry 10 of Table 3) after 1 day of stirring.
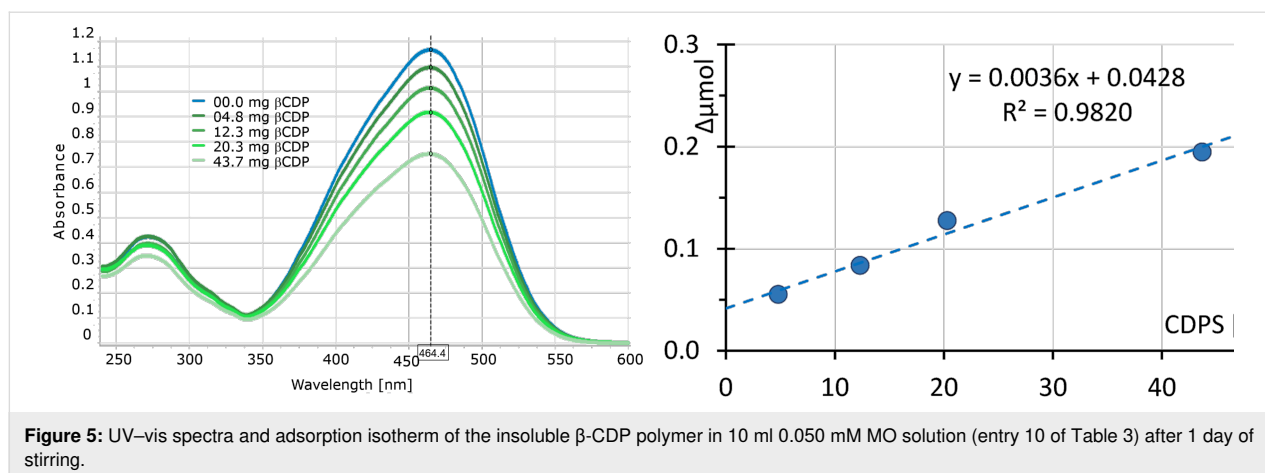
It is known that, although γ-CD is able to form complexes with MO (they are less stable than those of β-CD), the prepared insoluble γ-CDP has few affinity towards MO. It can be also assumed that it is only the association rate that is lower than in the monomer. Particularly interesting results were observed when the same property of γ-CDP was compared to the corresponding (3-glycidyloxy)propylsilane γ-CD composite (next section). The complexation efficacy of the prepared CDPs is summarised in Table 4. No significant differences were found between the products that were prepared from the dried and hydrated CDs.

(3-Glycidyloxypropyl)trimethoxysilane (GPTS)

The hydrolysis of GPTS occurs at two sites; on the oxirane ring and on the silyl ether moiety. The cleavage of trimethoxysilyl ether is unavoidable in the aqueous phase under basic conditions, while the oxirane ring seems to be more stable than in propylene oxide or epichlorohydrin. This is partially the consequence of its considerably lower aqueous solubility. It was found that the substitution reaction does not proceed, or at least does so very slow at temperatures below 60 °C. The GPTS

reagent in water was found to be present at around 60–70%, like in case of propylene oxide. Although the neutralised reaction mixture was homogeneous, the isolation and NMR analysis of the isolated product showed poor methoxy content, demonstrating the almost complete hydrolysis of the silyl ethers. Unlike in the solution reaction, the HEBM isolated reaction products of β-CD were almost completely insoluble in water, while the γ-CD derivative was somehow soluble or solubilised, as seen in the UV–vis spectra. Both the β- and γ-CD derivatives showed high complexation affinity toward MO, as seen in the UV spectra in Figure 6 and Figure 7. However, unlike the epichlorohydrin polymers, their "concentration-dependency" was not linear. The solution and solid state reactions showed similar yields, as can be concluded from Table 5.

A significant difference was found between GPTS-β-CD and -γ-CD that were prepared under HEBM conditions; a considerable part of the GPTS-γ-CD composite was solubilised. Not only were there no residual unsubstituted CDs seen on TLC of the prepared GPTS-CDs, but no running charrable spots were found either. GPTS, or its hydrolytic product(s), were run with

Table 4: Complexation efficacy of ≈20 mg insoluble CDPs in 0.050 mM MO solution after 1 day and 2 weeks (entry numbers are identical as those in Table 3.)

No.	CD used in CDP synthesis	Milling time [h]	Particle size[a] [μm]	MO binding capacity [μmol/mg]		Relative MO binding capacity[b]
				1 day	14 days	
9	β	6	≈1.9	0.004	0.006	0.33
10[e]	β	9	≈2.9	0.005	0.009	0.51
11	β*H_2O	6	≈1.7	0.007	0.010	0.61
12	γ	6	≈1.8	0.003	0.004	0.25
13	γ*H_2O	6	≈2.2	<0.001	0.002	0.10
14	bead polymer[c]	N/A	≈77[d]	0.011	0.017	1.00

[a]By QELS; [b]bead polymer = 1, calculated with not rounded values; [c]Cyclolab's CYL-2011; [d]by electron microscope.
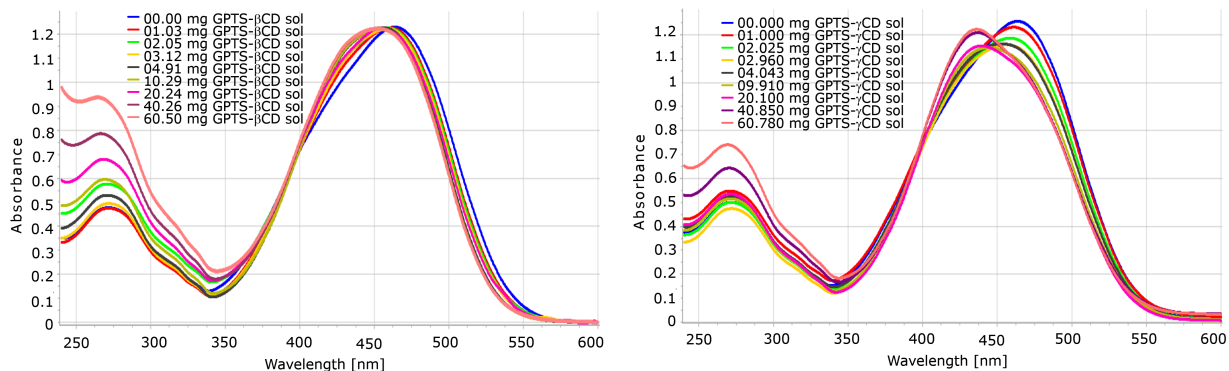
Figure 6: UV–vis spectral changes of 0.050 mM MO solution by GPTS-β-CD (left) and GPTS-γ-CD (right), as prepared in solution (entries 15 and 17 of Table 5).
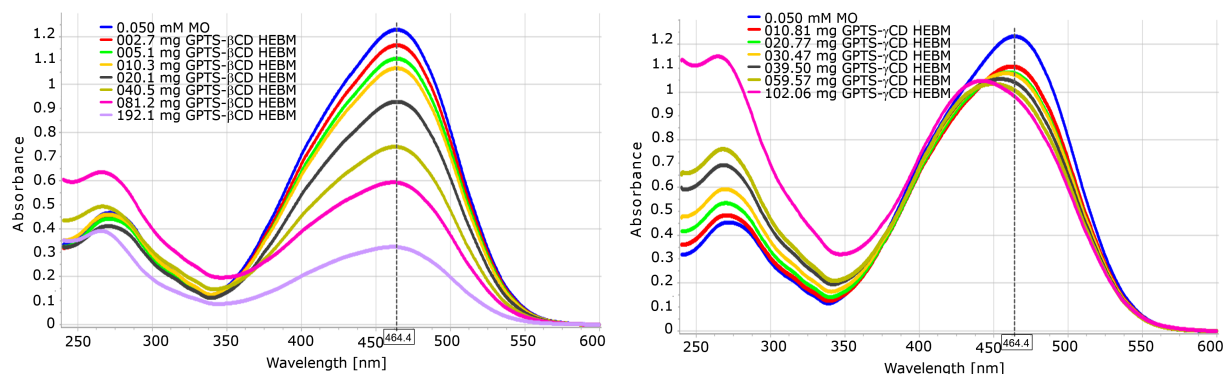
Figure 7: UV–vis spectral changes of 0.050 mM MO solution by GPTS-β-CD (left) and GPTS-γ-CD (right), as prepared in ball mill (entries 16 and 18 of Table 5).

Table 5: Summary of GPTS-derivatisation of β- and γ-CD.

No.	Used CD	Reaction time [h]	B2M ratio	Product[c] [g]	Yield[d] [%]
15	β	48[a]	N/A	1.3	57
16	β	3[b]	10	4.2	76
17	γ	48[a]	N/A	2.2	88
18	γ	3[b]	10	5.3	88

[a]Solution reaction, at 70–75 °C; [b]milling time; [c]isolated purified compounds; [d]on the base of DS, as determined by ^{1}H NMR, in cases of solution reactions and in HEBM reactions, assuming that all GPTS is attached to the CDs.

the front, and they were found to be very poorly charrable. While it is not clear whether the product itself was dissolved or whether the particle size was smaller than <0.22 µm, the UV–vis spectra clearly show the hypsochromic shift that was caused by complexation with increasing amounts of added GPTS-γ-CD. The adsorption isotherm can also be divided in two parts; the simple adsorptive removal of MO can be seen at the beginning, while the MO peak showed a noticeable blue-shift as the amount of solubilised/dissolved γ-CD-derivative increased.

Conclusion

The use of the HEBM method to force the reaction between epoxides and CDs was successful. It was also found that reagent

utilization was higher than in solution reactions and that oxirane hydrolysis in the presence of a strong base, NaOH, could be hampered under ball-milling conditions.

Although the work-up and purification of the HEBM-reaction-synthesised CD derivatives was simpler in the (2-hydroxy)propylated cases, it does not seem possible to alter the current industrial method to make it more green.

Preparations of water-insoluble CD derivatives were more effective than the solution reactions, but the particle size of the solid state reaction products were very small, which also affected the complexation properties. Further studies to compare the physicochemical and complexation properties of the insoluble CD polymers are necessary and may be able to develop a feasible and reproducible alternative synthetic process. This would lead to the wider dissemination of insoluble epichlorohydrin-crosslinked CD polymers. The postmanipulation of fine CDP powder, such as granulation on a hard support, can improve the physicochemical and complexation properties of the polymers. Although the complexation properties of the prepared insoluble CD polymers are far from those of solution-method β-CD bead polymers, the fine-tuning and optimisation of the reaction conditions can be improved to offer a truly green synthesis that can exploit the combination of CD complexation and the elimination of aqueous solubility. Further optimisation of the synthesis conditions and structure elucidation are both in progress and will aid the development of an, at least, kilolab-scale procedure for standardised quality products.

Experimental

The details of the reactions are described in Supporting Information File 1.

All reagents and organic solvents were used without further purification, except the ion-exchangers. The ion-exchangers were freshly washed with water and methanol until the washing solutions became colourless and UV inactive.

Reactions were carried out in a planetary ball mill (Retsch PM100 High Speed Planetary Ball Mill), using a 50 mL stainless steel jar and mix of stainless-steel balls ($m = 44.1$ g, in which ø = 5 mm, $m = 28.1$ g and 550 ø = 1–1.2 mm, $m = 16.0$ g) at 650 rpm for various time periods. The rotation direction was changed every 15 min (3 min during CD-Na salt preparation) with 3 seconds of silent periods between the alternating rotations. The scale-up of the insoluble CDP was done in a 125 mL stainless steel jar with a mixture of larger balls ($m = 236.2$ g, in which 7 ø = 12–13 mm, $m = 97.1$ g and 70 ø = 7 mm, $m = 145.1$ g) at 650 rpm. The same balls were

used for 2 min at 450 rpm to crack the CDP solids after purification.

In the HEBM experiments the CD-sodium salts were cooled below −30 °C with liquid nitrogen before the addition of the reagents.

Supporting Information

Supporting Information File 1
Experimental details, and the NMR and MS spectra of the soluble products.
[https://www.beilstein-journals.org/bjoc/content/supplementary/1860-5397-15-145-S1.pdf]

ORCID® iDs
László Jicsinszky - https://orcid.org/0000-0002-1422-2857
Federica Calsolaro - https://orcid.org/0000-0001-8059-1071
Katia Martina - https://orcid.org/0000-0003-2256-5021
Fabio Bucciol - https://orcid.org/0000-0003-0548-9127
Maela Manzoli - https://orcid.org/0000-0002-4427-7939
Giancarlo Cravotto - https://orcid.org/0000-0001-7574-7350

References
1. Cyclodextrins. In *Comprehensive Supramolecular Chemistry;* Szejtli, J.; Osa, T., Eds.; Pergamon Press: New York, NY, USA, 1996; Vol. 3, pp 57–188.
2. Trotta, F. Cyclodextrin Nanosponges and Their Applications. In *Cyclodextrins in Pharmaceutics, Cosmetics, and Biomedicine;* Bilensoy, E., Ed.; John Wiley & Sons, Inc.: New York, U.S.A., 2011; pp 323–342. doi:10.1002/9780470926819.ch17
3. Řezanka, M. Synthesis of Cyclodextrin Derivatives. Cyclodextrin Fundamentals. In *Reactivity and Analysis;* Fourmentin, S.; Crini, G.; Lichtfouse, E., Eds.; Springer International Publishing AG: Cham, Switzerland, 2018; pp 57–103.
4. Gelb, R. I.; Schwartz, L. M.; Laufer, D. A. *Bioorg. Chem.* **1982,** *11,* 274–280. doi:10.1016/0045-2068(82)90003-7
5. Gelb, R. I.; Schwartz, L. M.; Bradshaw, J. J.; Laufer, D. A. *Bioorg. Chem.* **1980,** *9,* 299–304. doi:10.1016/0045-2068(80)90039-5
6. Szabo, T.; Szejtli, J.; Szente, L.; Horvath, G.; Peterdi, V.; Szeman, J.; Toth, A.; Komar, P. Process for producing 2-hydroxy-propyl-alpha-, beta- and gamma-cyclodextrin. Hungarian Patent HU202889, Sept 30, 1991.
7. Jicsinszky, L.; Szejtli, J.; Szente, L.; Ujhazy, A.; Weiszfeiler, V. Process for Purifying Alkylated and Hydroxyalkylated Cyclodextrins and for Reducing Their Unsubstituted Cyclodextrin Content. Hungarian Patent HUT56584, Sept 30, 1991.

8. Vikmon, M.; Gerloczy, A.; Fenyvesi, E.; Jicsinszky, L. Comparative Characterization of Complex-forming Ability of HP-beta-CDs with Phenolphthalein. In *Minutes of the 6th International Symposium on Cyclodextrins,* Chicago, Il, April 21–24, 1992; Hedges, A. R., Ed.; Éditions de Santé: Paris, France, 1992; pp 144–148.

9. Pitha, J.; Trinadha Rao, C.; Lindberg, B.; Seffers, P. *Carbohydr. Res.* **1990,** *200,* 429–435. doi:10.1016/0008-6215(90)84208-c

10. Müller, B. W.; Brauns, U. *J. Pharm. Sci.* **1986,** *75,* 571–572. doi:10.1002/jps.2600750609

11. Buvári-Barcza, Á.; Bodnár-Gyarmathy, D.; Barcza, L. *J. Inclusion Phenom. Mol. Recognit. Chem.* **1994,** *18,* 301–306. doi:10.1007/bf00708736

12. Jicsinszky, L.; Caporaso, M.; Calcio Gaudino, E.; Giovannoli, C.; Cravotto, G. *Molecules* **2017,** *22,* 485. doi:10.3390/molecules22030485

13. Fenyvesi, E.; Decsei, L.; Ujhazy, A.; Zsadon, B.; Szejtli, J. Complexes of Insoluble Cyclodextrin Polymers. In *Proceedings of the Fourth International Symposium on Cyclodextrins,* Munich, West Germany, April 20–22, 1988; Huber, O.; Szejtli, J., Eds.; Springer Netherlands, 1988; pp 227–235. doi:10.1007/978-94-009-2637-0_35

14. Malanga, M.; Bálint, M.; Puskás, I.; Tuza, K.; Sohajda, T.; Jicsinszky, L.; Szente, L.; Fenyvesi, É. *Beilstein J. Org. Chem.* **2014,** *10,* 3007–3018. doi:10.3762/bjoc.10.319

15. Solms, J.; Egli, R. H. *Helv. Chim. Acta* **1965,** *48,* 1225–1228. doi:10.1002/hlca.19650480603

16. Solms, J. Process for the Preparation of Inclusion Complexes of High Molecular Weight. Swiss Patent CH445129, April 29, 1964.

17. Yuan, D.-Q.; Tahara, T.; Chen, W.-H.; Okabe, Y.; Yang, C.; Yagi, Y.; Nogami, Y.; Fukudome, M.; Fujita, K. *J. Org. Chem.* **2003,** *68,* 9456–9466. doi:10.1021/jo035229m

18. Hishiya, T.; Shibata, M.; Kakazu, M.; Asanuma, H.; Komiyama, M. *Macromolecules* **1999,** *32,* 2265–2269. doi:10.1021/ma9816012

19. Mallard, I.; Baudelet, D.; Castiglione, F.; Ferro, M.; Panzeri, W.; Ragg, E.; Mele, A. *Beilstein J. Org. Chem.* **2015,** *11,* 2785–2794. doi:10.3762/bjoc.11.299

20. Pitha, J. Selective Alkylations of Cyclodextrins Leading to Derivatives Which Have a Rigidly Extended Cavity. U.S. Patent US5681828, Oct 28, 1997.

21. Zsadon, B.; Décsei, L.; Szilasi, M.; Tüdős, F.; Szejtli, J. *J. Chromatogr.* **1983,** *270,* 127–134. doi:10.1016/s0021-9673(01)96357-5

22. Szejtli, J.; Fenyvesi, É.; Zsadon, B. *Starch/Staerke* **1978,** *30,* 127–131. doi:10.1002/star.19780300407

23. Zsadon, B.; Szilasi, M.; Décsei, L.; Ujházy, A.; Szejtli, J. *J. Chromatogr.* **1986,** *356,* 428–432. doi:10.1016/s0021-9673(00)91511-5

24. Zsadon, B.; Ács, M.; Fogassy, E.; Faigl, F.; Novak, C.; Pokol, G.; Ujházy, A. *React. Polym., Ion Exch., Sorbents* **1987,** *6,* 197–202. doi:10.1016/0167-6989(87)90089-4

25. Cravotto, G.; Caporaso, M.; Jicsinszky, L.; Martina, K. *Beilstein J. Org. Chem.* **2016,** *12,* 278–294. doi:10.3762/bjoc.12.30

26. Stolle, A.; Szuppa, T.; Leonhardt, S. E. S.; Ondruschka, B. *Chem. Soc. Rev.* **2011,** *40,* 2317–2329. doi:10.1039/c0cs00195c

27. Hernández, J. G.; Avila-Ortiz, C. G.; Juaristi, E. Useful Chemical Activation Alternatives in Solvent-Free Organic Reactions. In *Comprehensive Organic Synthesis,* 2nd ed.; Knochel, P.; Molander, G. A., Eds.; Elsevier BV, 2014; Vol. 9, pp 287–314. doi:10.1016/b978-0-08-097742-3.00935-6

28. Do, J.-L.; Friščić, T. *ACS Cent. Sci.* **2017,** *3,* 13–19. doi:10.1021/acscentsci.6b00277

29. Jicsinszky, L.; Caporaso, M.; Martina, K.; Calcio Gaudino, E.; Cravotto, G. *Beilstein J. Org. Chem.* **2016,** *12,* 2364–2371. doi:10.3762/bjoc.12.230

30. Tokuda, K.; Morii, S.; Kazuhiko, Y. Novel Cyclodextrin Derivative and Production Thereof. Japanese Patent JPH085923, Nov 12, 1986.

31. Gramera, R. E.; Caimi, R. J. Cyclodextrin Polyethers and their Production. U.S. Patent US3459731, Dec 16, 1996.

32. Zheng, L.; Liang, M.; Wang, S.; Liu, X.; Qi, Y.; He, Y.; He, L. Preparation Method of Hydroxypropyl-beta-cyclodextrin. Chinese Patent CN102558394, Dec 7, 2012.

33. Jicsinszky, L.; Fenyvesi, E.; Hashimoto, H.; Ueno, A. Cyclodextrin derivatives. In *Cyclodextrins;* Szejtli, J.; Osa, T., Eds.; Comprehensive Supramolecular Chemistry, Vol. 3; Pergamon Press: New York, NY, USA, 1996; pp 57–188.

34. Pitha, J. (Hydroxypropyl)cyclodextrins, mixtures are beautiful if properly characterized. In *Minutes of 6th Int. Symp. Cyclodextrins,* Chicago, Il, April 21–24, 1992; Hedges, A. R., Ed.; Éditions de Santé: Paris, France, 1992; pp 424–430.

35. Trinadha Rao, C.; Pitha, J.; Lindberg, B.; Lindberg, J. *Carbohydr. Res.* **1992,** *223,* 99–107. doi:10.1016/0008-6215(92)80009-p

36. Mischnick, P. *Carbohydr. Res.* **1989,** *192,* 233–241. doi:10.1016/0008-6215(89)85182-1

37. EMA/CHMP/704195/2013. https://www.ema.europa.eu/documents/scientific-guideline/questions-answers-propylene-glycol-used-excipient-medicinal-products-human-use_en.pdf (accessed Jan 8, 2019).

38. Krause, R.; Mamba, B. B.; Bambo, M.; Malefetse, T. J. Cyclodextrin polymers: Synthesis and Application in Water Treatment. In *Cyclodextrins: Chemistry and Physics;* Hu, J., Ed.; Transworld Research Network: Trivandrum, Kerala, India, 2011; pp 185–210.

39. Jicsinszky, L.; Caporaso, M.; Tuza, K.; Martina, K.; Calcio Gaudino, E.; Cravotto, G. *ACS Sustainable Chem. Eng.* **2016,** *4,* 919–929. doi:10.1021/acssuschemeng.5b01006

40. Crini, G.; Bertini, S.; Torri, G.; Naggi, A.; Sforzini, D.; Vecchi, C.; Janus, L.; Lekchiri, Y.; Morcellet, M. *J. Appl. Polym. Sci.* **1998,** *68,* 1973–1978. doi:10.1002/(sici)1097-4628(19980620)68:12<1973::aid-app11>3.0.co;2-t

41. Crini, G.; Cosentino, C.; Bertini, S.; Naggi, A.; Torri, G.; Vecchi, C.; Janus, L.; Morcellet, M. *Carbohydr. Res.* **1998,** *308,* 37–45. doi:10.1016/s0008-6215(98)00077-9

42. Komiyama, M.; Hirai, H. *Polym. J.* **1987,** *19,* 773–775. doi:10.1295/polymj.19.773

43. Harada, K.; Morimoto, S. Production of Bead-foam Insoluble Cyclodextrin Polymer. Japanese Patent JPS6020924 , Jan 28, 1983.

44. Szejtli, J.; Fenyvesi, E.; Sarkoezi, P.; Felmeray, I.; Zsoldos, A. Pharmaceuticals Containing Cyclodextrin-iodine Inclusion Compounds for Controlled Release of Iodine. German Patent DE19883819498, June 8, 1988.

45. Másson, M.; Pitha, J.; Loftsson, T. *J. Inclusion Phenom. Macrocyclic Chem.* **1999,** *33,* 459–467. doi:10.1023/a:1008050825635

46. Pitha, J. Preparation of Dioxane-substituted Cyclodextrin Macromolecules and Inclusion Complexes with Cholesterol and Hydrocortisone. U.S. Patent US6001821, Dec 14, 1999.

47. Pitha, J. Alkylations of Cyclodextrins with Epichlorohydrin Leading to Derivatives Which Have a Rigidly Extended Cavity. U.S. Patent US5935941, Aug 10, 1999.

Metal-free mechanochemical oxidations in Ertalyte® jars

Andrea Porcheddu[*1], Francesco Delogu[2], Lidia De Luca[3], Claudia Fattuoni[1]
and Evelina Colacino[*4]

Full Research Paper

Address:
[1]Dipartimento di Scienze Chimiche e Geologiche, Università degli Studi di Cagliari, Cittadella Universitaria, SS 554 bivio per Sestu, 09042 Monserrato (Ca), Italy, [2]Dipartimento di Ingegneria Meccanica, Chimica e dei Materiali, Università degli Studi di Cagliari, via Marengo 2, 09123 Cagliari, Italy, [3]Dipartimento di Chimica e Farmacia, Università degli Studi di Sassari, via Vienna 2, 07100-Sassari, Italy and [4]Université de Montpellier & Institut Charles Gerhardt de Montpellier (ICGM), UMR 5253 CNRS – UM – ENSCM, 8 Rue de l'Ecole Normale, 34296 Montpellier, Cedex 5, France

Email:
Andrea Porcheddu[*] - porcheddu@unica.it; Evelina Colacino[*] - evelina.colacino@umontpellier.fr

* Corresponding author

Abstract

Aimed at eliminating or at least significantly reducing the use of solvents, sodium hypochlorite pentahydrate crystals (NaOCl·5H$_2$O) in the presence of a catalytic amount of a nitrosyl radical (TEMPO or AZADO) have been successfully used to induce mechanochemical oxidative processes on several structurally different primary and secondary alcohols. The proposed redox process is safe, inexpensive and performing effectively, especially on the macroscale. Herein, an Ertalyte® jar has been successfully used, for the first time, in a mechanochemical process.

Introduction

The conversion of primary and secondary alcohols to the corresponding carbonyl compounds (aldehydes and ketones, respectively) is of such importance in organic chemistry that it finds very few parallels in other synthetic organic processes [1,2]. These transformations can be achieved by using a wide range of oxidizing reagents [3], but most of them are difficult-to-handle and suffer from waste problems due to large amounts of by-products, thus decreasing the atom efficiency [4,5]. The

discovery of (2,2,6,6-tetramethylpiperidin-1-yl)oxyl, commonly known as TEMPO by Lebedev and Kazarnowskii in 1960 has been hailed as a significant breakthrough in the field of redox reactions, allowing the fast and selective oxidation of alcohols to the related carbonyl compounds under very mild conditions [6,7]. Initially used in a stoichiometric amount [8], over the last 20 years it has been exploited successfully in catalytic quantities in combination with other oxidants [9]. A

diverse range of co-oxidant agents (*N*-chlorosuccinimide, NaOCl, Oxone®, PhIO, PhICl₂, PhI(OAc)₂, I₂, CAN, etc.) has been intensively investigated with varying results in terms of yields, chemical selectivity, and environmental sustainability [10-18]. All oxidation procedures have their advantages and their flaws, so the search for efficient, selective, high-yielding, environmentally benign methods and atom-economical processes continues to be a pivotal challenge for chemists [19]. Stahl and many other researchers worked in this direction achieving noteworthy results by using air/oxygen as an oxidizing agent in the presence of a suitable metal complex [20-25]. However, even these recent methods suffer from serious drawbacks, such as the use of precious metals often combined with sophisticated organic ligands, which makes them expensive, especially if implemented on an industrial scale. In addition, increasingly restrictive legislation against residual metals in manufactured goods and active ingredients stimulates the ongoing search for new metal-free solutions to the problem making this challenge even topical [26,27]. Based on the considerations mentioned above, we focused on an alternative strategy to activate the oxidation process. In particular, in this study, we used sodium hypochlorite pentahydrate (NaOCl·5H₂O) in the presence of a catalytic amount of a nitrosyl radical (TEMPO or AZADO) to induce mechanochemical oxidation reactions on suitably selected primary and secondary alcohols. Performed in a high-energy ball mill and with the unprecedented utilization of Ertalyte® jars, the mechanical activation allows obtaining the oxidized products from a broad spectrum of initial substrates. We show that the proposed mechanochemical method is definitely safe, performing effectively and inexpensive, thus providing an interesting synthetic route that can be scaled up to pilot and industrial levels.
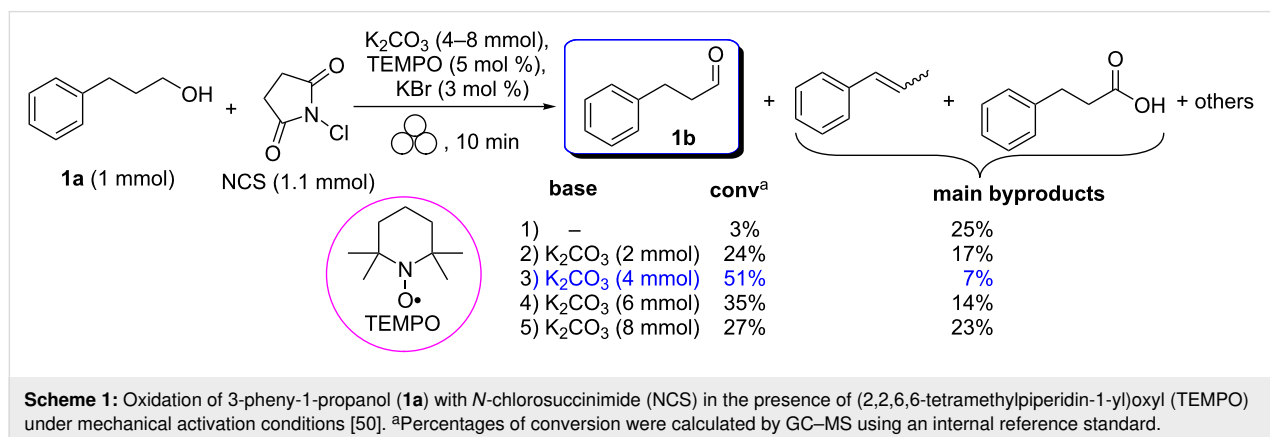
Results and Discussion

Since the most commonly employed oxidizing agents are solid reagents, we decided to develop an efficient and eco-friendly process for the selective oxidation of alcohols to the corresponding aldehydes/ketones based on a mechanochemical activation [28]. In comparison to solution-based techniques, ball-milling procedures provide an ideal solution for overcoming many of the drawbacks described above, due to the simplicity of use, shorter reaction times, large-scale production, low cost and sustainability of this methodology [28-39]. In addition, impact forces, that are generated by ball-milling media involve a very minimal fraction of reactive material mimicking the ideal behavior/trend of highly diluted reactive systems. This peculiar aspect of mechanochemical reactions, especially in redox processes conducted in no-metal reactors, could prevent excessive heating of the jar, avoid the decomposition of starting materials and therefore, limit the formation of byproducts [40]. Following our interest in mechanochemistry and the design of new cost-effective oxidation procedures, we have tried to combine both topics to the best [41-49]. In particular, we were mainly interested in developing a general, selective and versatile alcohol-to-aldehyde/ketone oxidative protocol applied to primary and secondary alcohols by using an oxidizing agent as cheap and eco-friendly as possible.

In order to optimize all the experimental conditions, we fine-tuned the reaction by using 3-phenyl-1-propanol as a model reagent and *N*-chlorosuccinimide (NCS) as an oxidizing agent. NCS is one of the most widely used co-oxidizing reagents in homogeneous-phase TEMPO-assisted oxidation reactions and, we have gained valuable experience in handling this reagent in several mechanochemical applications [45,46].

N-Chlorosuccinimide (1.1 mmol) and 3-pheny-1-propanol (1.0 mmol) were milled together in the presence of TEMPO (5 mol %), K₂CO₃ (4.0 mmol) and KBr (3.0 mol %) for 10 minutes in a zirconia jar containing 5 balls (5 mm Ø) of the same material (Scheme 1).

For all the experiments, we never observed a complete conversion of the alcohol into the aldehyde. Moreover, the first experi-

base	conv[a]	main byproducts
1) –	3%	25%
2) K₂CO₃ (2 mmol)	24%	17%
3) K₂CO₃ (4 mmol)	51%	7%
4) K₂CO₃ (6 mmol)	35%	14%
5) K₂CO₃ (8 mmol)	27%	23%

Scheme 1: Oxidation of 3-pheny-1-propanol (**1a**) with *N*-chlorosuccinimide (NCS) in the presence of (2,2,6,6-tetramethylpiperidin-1-yl)oxyl (TEMPO) under mechanical activation conditions [50]. [a]Percentages of conversion were calculated by GC–MS using an internal reference standard.

mental results showed the key role of the base in the conversion of an alcohol into an aldehyde: it fails in the absence of K_2CO_3, reaches a maximum of 51% with 4 equivalents and decreases (27%) for higher amounts (Scheme 1). This is mainly due to the fact that the concentration of the active oxidizing agent, HOCl is strongly dependent on the amount and strength of the base used in the grinding mixture [51].

Two different mechanisms have been postulated for similar reactions in homogeneous phase: one occurs under acidic conditions, while the other works better in a basic medium through a cyclic dipolar mechanism (Scheme 2) [52,53]. On the contrary, under ball-milling conditions, it is possible to hypothesize that only the cyclic dipolar mechanism, which operates mostly in basic conditions, allowed to gain access to the desired aldehyde.

Interestingly, the formation of a significant amount of over-oxidation [54] and elimination byproducts was observed for 3-pheny-1-propanol (**1a**) when increasing the reaction time (up to 20 min, Scheme 1). In contrast, comparable results were obtained when the milling time was reduced to 3 minutes, leading to an alcohol/aldehyde ratio very similar to that one obtained

after ten minutes. Any attempt to improve this conversion by varying other parameters such as the number (up to 15 balls, 5 mm Ø) and the diameter of balls (from 3 up to 10 mm Ø), or using a different base ($KHCO_3$ or Na_2CO_3) turned out to be unsuccessful.

The use of other solid oxidants such as trichloroisocyanuric acid (TCCA) did not bring any advantage to the process (Scheme 3), and the aldehyde was only detected in negligible amounts (GC–MS analyses). The (diacethoxyiodo)benzene acid (PIDA) allowed to further improve the alcohol-to-aldehyde conversion by a few percentage points (57%), but the formation of 2 equivalents of acetic acid makes it unsuitable for a mechanochemical process [55]. Also, Oxone® and $NH_2CONH_2·H_2O_2$ appeared to fail in the oxidation of 3-phenyl-1-propanol (**1a**) to the corresponding aldehyde.

Subsequently, we turned our attention to sodium hypochlorite (NaOCl), an inexpensive and widely used oxidizing reagent also applied as a disinfectant and household bleaching agent, usually sold as a 3–6% solution in water. Commercially available NaOCl is highly basic (pH ≈ 12.7) that dramatically slows down the oxidation process, and $NaHCO_3$ has to be added to
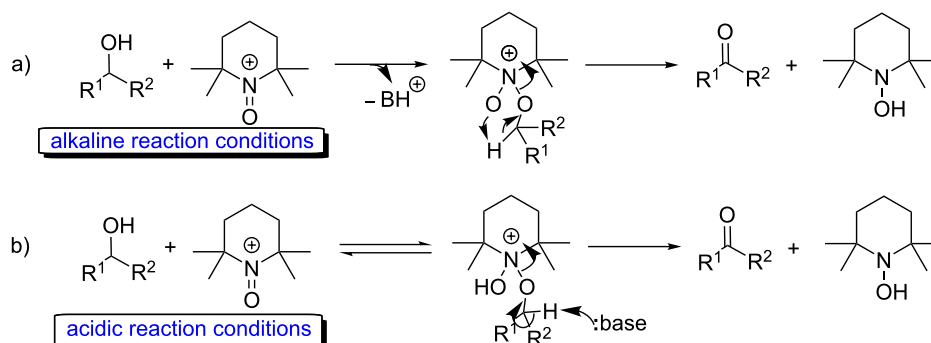
Scheme 2: Hypothesized pathways for the TEMPO-assisted oxidation of alcohols in a) basic or b) acidic reaction conditions.
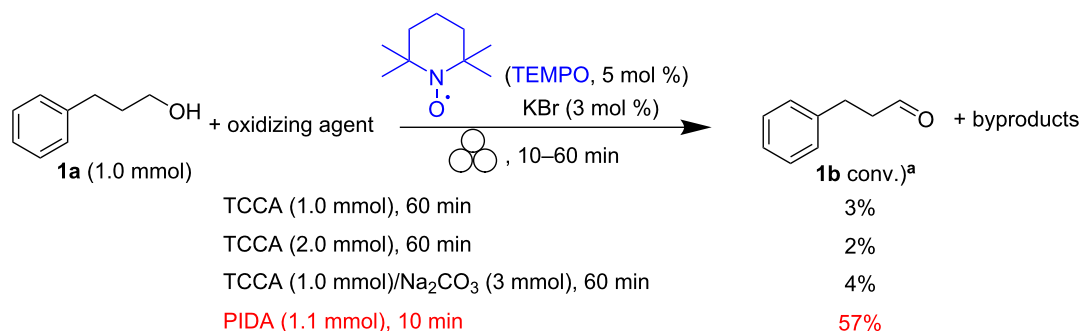
Scheme 3: TEMPO-assisted oxidation of 3-pheny-1-propanol (**1a**) under mechanical activation conditions. ªPercentages of conversion were calculated by GC–MS using an internal reference standard.

both maximize the concentration of the active oxidizing agent HOCl, and to absorb bleach [56]. The addition of a catalytic amount of KBr promotes the in situ generation of HOBr, which is a stronger oxidant than HOCl [57].

The results improved remarkably by using as oxidant a 6% aqueous solution of NaOCl (1.14 mL, 1.1 mmol) adsorbed on NaHCO$_3$ (6.5 g) in the presence of a catalytic amount of TEMPO (5.0 mol %) and KBr (3.0 mol %) (Table 1, entry 6). Within 20 minutes, the alcohol was completely and selectively oxidized into the corresponding aldehyde (as assessed by GC–MS analyses). The use of NaCl, alone or in combination with NaHCO$_3$, as an adsorbent [58] (Table 1, entries 1–5, 7) or bases (Na$_2$CO$_3$, Table 1, entries 7 and 8) other than NaHCO$_3$ significantly reduces the alcohol-to-aldehyde conversions.

Based on these preliminary results, we decided to replace aqueous NaOCl (bleach) with Ca(OCl)$_2$ that has been reported previously as a valid alternative to NaOCl aqueous solutions for mechanochemical chlorination reactions of hydantoins [41,59]. However, also using this oxidant, we observed low conversions (31%) and the formation of significant amounts of byproducts, mainly halides and olefins (elimination byproducts). The use of liquid-assisted grinding (LAG) procedures [60-62] by adding small quantities of water (250 µL) improved the performance of the reaction (alcohol-to-aldehyde conversion: 41%), but also raised the percentage of elimination products (38%). Solid NaOCl·5H$_2$O, which has been discovered over a century ago, represented a turning point in our search for a suitable reagent, avoiding some of the previously described shortcomings. As of 2013, this reagent is commercially available [63], inexpensive

and sufficiently stable and safe for potential applications in mechanochemistry (Figure S1a, Supporting Information File 1) [64-67].

Once the most promising oxidant was identified, NaOCl·5H$_2$O (1.1 mmol), 3-phenyl-1-propanol (1.0 mmol), NaHCO$_3$ (2.2 mmol), and KBr (3 mol %) were milled together in the presence of TEMPO (5 mol %) for 20 minutes in a zirconia jar containing 6 balls (5 mm Ø) of the same material. NaHCO$_3$ plays the double role of base and adsorbent for liquid alcohols (Table 2, entry 1). The first results were promising and showed a good alcohol-to-aldehyde conversion (75%). We have also used a Teflon jar, but we observed lower conversions (<50%). In addition, the reproducibility of data was often poor. In our ongoing efforts to develop mechanochemical reactions in jars manufactured from thermoplastic materials as alternatives to Teflon, having high mechanical resistance, rigidity, and hardness, we were pleased to find that Ertalyte® displayed an excellent performance in the mechanical process. All other parameters being equal, the conversion efficiency improved significantly by switching to an Ertalyte® jar (86%) [68] which could be further enhanced (93%) by slightly increasing the amount of the oxidant agent (1.5 equiv). Ertalyte® jars (Figure S1b, in Supporting Information File 1) are composed of polyethylene terephthalate (PET-P) and characterized by wear- and abrasion-, chemical and moderate acid resistance, with a low coefficient of friction and FDA approved [69].

In the absence of TEMPO, the oxidation reaction did not work anymore, while in the absence of KBr, the conversion rate was considerably reduced. The use of bases other than NaHCO$_3$

Table 1: Oxidation of 3-phenyl-1-propanol (**1a**) with aqueous NaOCl (6%, bleach) under mechanical activation conditions [50].

Entry	Base	NaCl (g)[a]	Time (min)	Aldehyde (%)[b]	Byproducts (%)[b]
1	NaHCO$_3$ (2.0 g)	3.5	15	73	16
2	NaHCO$_3$ (2.0 g)	3.0	15	77	22
3	NaHCO$_3$ (1.0 g)	5.0	15	78	8
4	NaHCO$_3$ (1.0 g)	5.0	30	78	6
5	NaHCO$_3$ (2.5 g)	2.5	15	88	4
6	**NaHCO$_3$ (6.5 g)**	**–**	**22**	**>99**	**–**
7	Na$_2$CO$_3$ (2.0 g)	3	22	61	37
8	Na$_2$CO$_3$ (6.0 g)	–	22	55	41

[a]NaCl was used as an adsorbent [58] in combination with NaHCO$_3$ or Na$_2$CO$_3$. [b]Percentages of conversion were calculated by GC using an internal reference standard.

Table 2: Oxidation of 3-phenyl-1-propanol (**1a**) with NaOCl·5H$_2$O crystals under mechanical activation conditions using ZrO$_2$ or Ertalyte® jars. Optimization of the reaction conditions.

Entry	NaOCl·5H$_2$O (mmol)	Jar	Aldehyde (%)[a]	Alcohol (%)[a]	Byproducts (%)[a]
1	1.1	Zirconia	75	19	6
2[b]	1.1	Zirconia	70	11	19
3	1.1	Ertalyte®	86	9	5
4	**1.5**	**Ertalyte®**	**93**	**5**	**2**
5[c]	1.5	Ertalyte®	69	27	4

[a]Percentages of conversion were calculated by GC using an internal reference standard. [b]The reaction time was extended to 40 min. [c]The amount of TEMPO was decreased from 5 to 3 mol %.

(Na$_2$CO$_3$ or sodium citrate) resulted in low alcohol-to-aldehyde conversions (<40%) and promoted, conversely, the formation of significant amounts of olefins (>25%) resulting from halide elimination. Any attempt to lower the amount of the nitrosyl catalyst resulted in a poor conversion (69%, Table 2, entry 5). Once the reaction conditions were fine-tuned, this procedure was applied to a range of alcohols to assess the scope of the reaction. The results are shown in Scheme 4.

Aliphatic alcohols **1a–5a** with carbon chains of different length were oxidized to give the corresponding aldehydes **1b–5b** in good yields and no carboxylic acid derivatives were observed in any sample. Similar results were obtained for alcohols containing an aliphatic carbon ring in their backbone, such as cyclohexylmethanol (**5a**). Interestingly, the oxidation reaction of benzylic alcohols proceeded smoothly to completeness in about 10 minutes even without need for TEMPO.
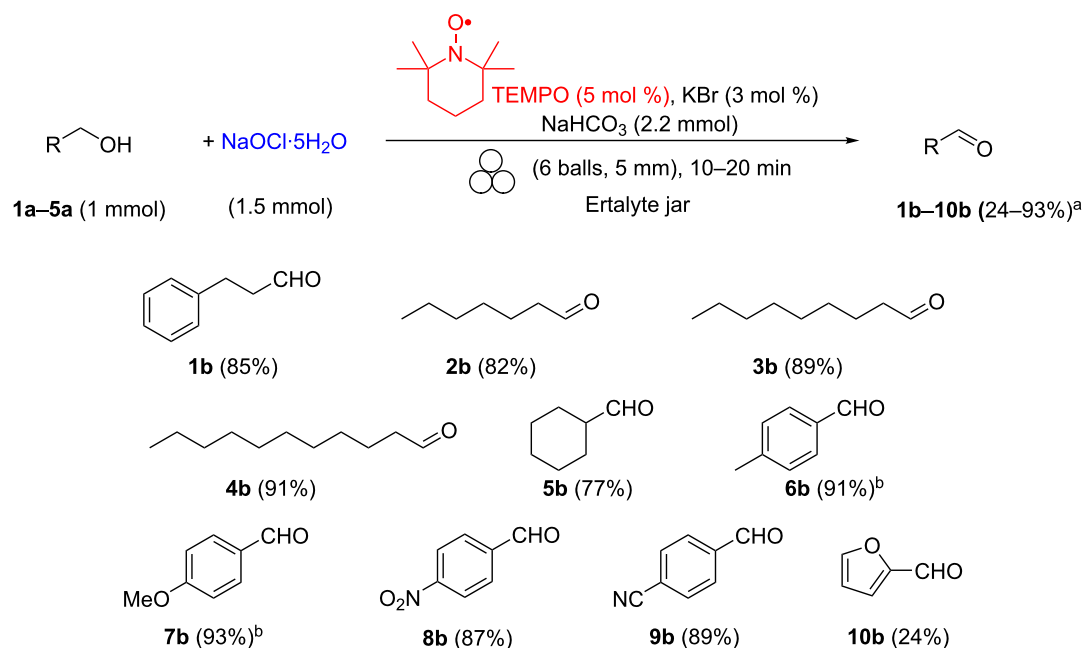
Scheme 4: Scope of primary alcohol oxidation under mechanical activation conditions. [a]All yields refer to isolated pure products. [b]The compound was prepared according to the general procedure A (see Supporting Information File 1) without adding TEMPO catalyst, and the reaction was completed within ten minutes.

The results changed significantly with benzylic alcohols decorated with an electron-withdrawing group in the aromatic ring such as 4-nitrobenzylalcohol (and 4-cyanobenzylalcohol), which required 5 mol % of TEMPO to be oxidized.

Based on these experimental results, we hypothesize that the reaction proceeded by a mechanism different from the classical solution-based TEMPO-assisted oxidation of alcohols, as illustrated in Scheme 5 [65]. In the first step of the reaction, potassium bromide, used as a co-catalyst, generates in situ sodium hypobromite, a more favorable oxidizing reagent than sodium hypochlorite. Ion metathesis due to the presence of KCl may lead to KOBr (Scheme 5, reaction 1). Subsequently, the species MOBr (M = Na, K) reacts with water to form HOBr, which is the active oxidizing agent (Scheme 5, reaction 2). Once the oxidizing agent formed, it reacts with the benzylic alcohols **6a** or **7a** to afford the corresponding intermediate benzyl hypobromites **6c** or **7c** (Scheme 5, reaction 3). In the final step, the base deprotonates the acidic benzylic proton leading to the corresponding benzaldehyde **6b** or **7b** (Scheme 5, reaction 4).

The oxidation of furfuryl alcohol gave furfural (**10b**), but in low and irreproducible yields together with significant amounts of byproducts. As expected, the reaction with conjugated alcohols (cinnamic alcohol, propargyl alcohol, etc.) was less successful due to the competing chlorination of the multiple bonds. Prompted by these findings, we further explored the efficacy of the protocol with a variety of secondary alcohols. Unfortunately, the oxidation reaction tested on 4-phenyl-2-butanol proceeded with low conversion yields (45%). An increase in both the amount of the oxidant (2 equiv) and the nitrosyl radical

(10 mol %), as well as longer reaction times (up to 1.5 h), did not lead to any significant improvement. However, we were pleased to find that the less hindered 2-aza-adamantane-*N*-oxyl (AZADO) was more effective than TEMPO in terms of conversion and yield with the model alcohol substrate, promoting an almost quantitative conversion of 4-phenyl-2-butanol into benzylacetone in only 30 min (Scheme 6, ketone **11b**). This protocol was successfully extended to other secondary alcohols to afford the corresponding ketones **11b–19b** in high conversions and yields.

The oxidation of sterically hindered secondary alcohols such as adamantan-2-ol (Scheme 4, alcohol **16a**) required doubling of the quantity of the nitrosyl catalyst (AZADO, 2 mol %) and longer reaction times (from 30 to 60 min) to achieve completion. Another useful feature of this protocol can be seen in the case of secondary benzyl alcohols, where the oxidation reaction to the corresponding ketones proceeded smoothly even without the necessity to use the nitrosyl catalyst (Scheme 6, ketones **17b–19b**). With all benzylic alcohols examined, the GC–MS analyses showed that the reactions were nearly complete in about 15 minutes, ketones **17b–19b** being isolated in high yields and purities. Finally, we investigated if this protocol could be potentially implemented on a larger scale. Pleasingly, we were able to scale-up the oxidation of **1a** and **11a** from a 1 mmol up to a 10 mmol scale without any significant drop in terms of purity and yield, thus confirming the method's potential adaptability to industrial settings.

The proposed mechanism for the TEMPO-based oxidative conversion of primary and secondary alcohols to the corre-
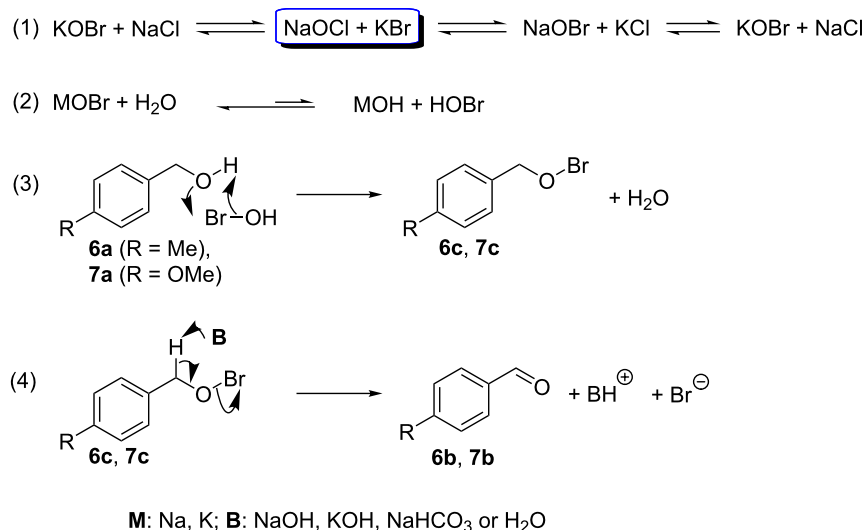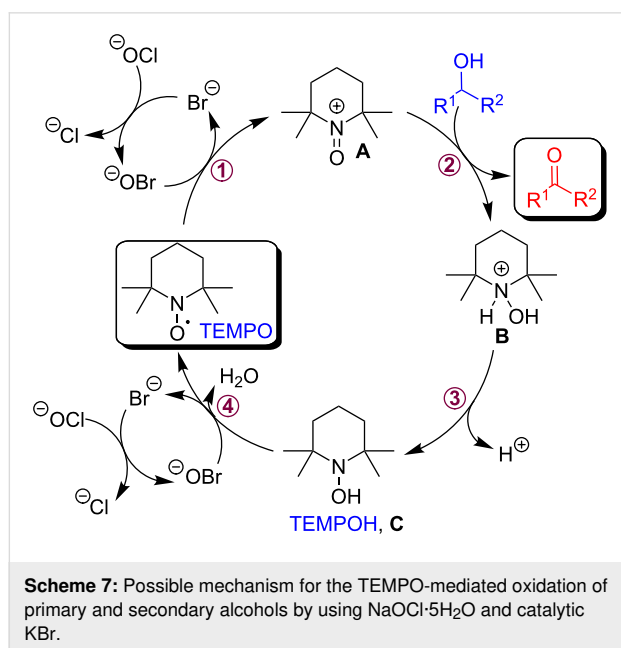

Scheme 5: Proposed mechanism for the oxidation of benzylic alcohols **6a** and **7a** under mechanochemical conditions and in the presence of KBr.
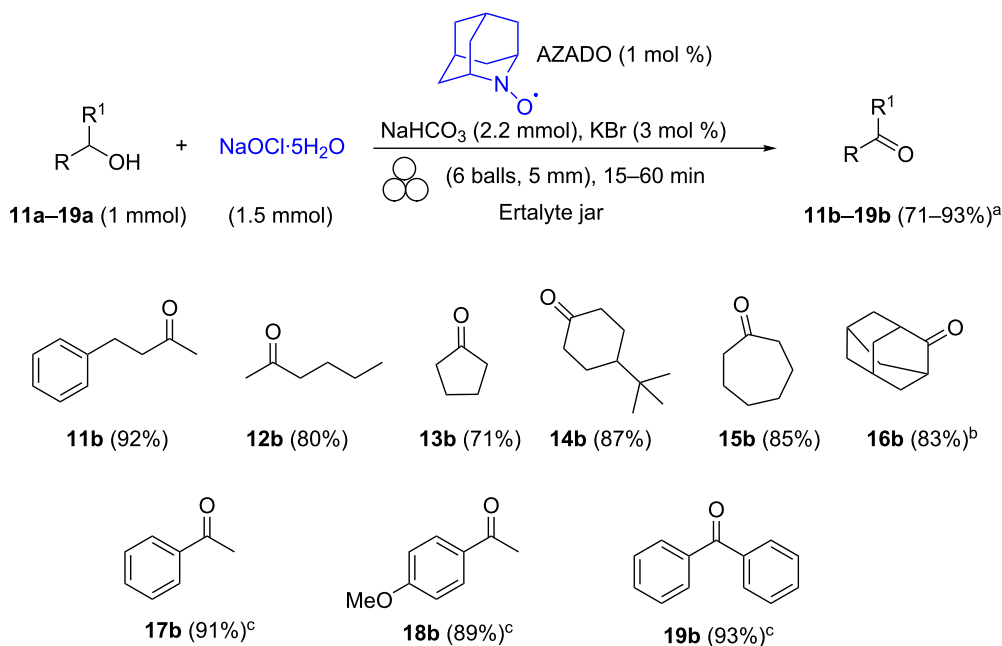
Scheme 6: Scope of secondary alcohols in the oxidation under mechanical activation conditions. [a]All yields refer to isolated pure products. [b]2-Aza-adamantane-*N*-oxyl (AZADO, 2 mol %), 60 min. [c]Oxidation carried out without AZADO catalyst, 15 min. The title compound was prepared according to the general procedure B (see Supporting Information File 1).

sponding carbonyl compounds is described in Scheme 7 and shares similarities with that postulated in other previous studies in solution.

Scheme 7: Possible mechanism for the TEMPO-mediated oxidation of primary and secondary alcohols by using NaOCl·5H$_2$O and catalytic KBr.

In general, NaOCl works as a co-oxidant agent, and in the catalytic cycle reacts with KBr generating in situ ⁻OBr, a stronger oxidizing species. Subsequently, a catalytic amount of ⁻OBr oxidizes the TEMPO radical to the *N*-oxo-ammonium ion **A**. The latter in turn rapidly oxidizes the alcohol to the corresponding carbonyl compound and gives the reduced form of TEMPO, the hydroxylamine **C**, TEMPOH. Then hydroxylamine **C** is reoxidized by ⁻OBr regenerating the starting TEMPO radical or directly the *N*-oxo-ammonium species **A**, thus closing the catalytic cycle (Scheme 7).

Conclusion

The conversion of primary and secondary alcohols to aldehydes and ketones, respectively, is one of the most important reactions in the panorama of organic chemistry. Although the literature describes a plethora of reagents and methodologies, most of them use toxic/harmful reagents that often cause serious environmental and public health concerns. Crystalline sodium hypochlorite (NaOCl·5H$_2$O) in the presence of a catalytic amount of a nitrosyl radical allowed developing a redox process without using any metal catalyst. With the aim to eliminate or at least reduce the use of solvents, NaOCl·5H$_2$O, among all the oxidants tested, was the one that best fitted with a general mechanochemical oxidative process of alcohols in Ertalyte® jars. The latter material never has been explored before in any of the mechanochemical transformations described in the literature and produced outperforming results compared to those obtained in zirconium oxide jars.

Supporting Information

Supporting Information File 1
Experimental procedures, characterization of new compounds and copies of ^{1}H and ^{13}C NMR spectra.
[https://www.beilstein-journals.org/bjoc/content/supplementary/1860-5397-15-172-S1.pdf]

Acknowledgements

ORCID® iDs

Andrea Porcheddu - https://orcid.org/0000-0001-7367-1102
Claudia Fattuoni - https://orcid.org/0000-0002-6956-7967
Evelina Colacino - https://orcid.org/0000-0002-1179-4913

References

1. Dubrovskiy, A. V.; Kesharwani, T.; Markina, N. A.; Pletnev, A. A.; Raminelli, C.; Yao, T.; Zeni, G.; Zhang, L.; Zhang, X.; Rozhkov, R.; Larock, R. C., Eds. *Comprehensive Organic Transformations: A Guide to Functional Group Preparations,* 3rd ed.; John Wiley and Sons: New York, U.S.A., 2018.

2. Smith, B. M. *March's Advanced Organic Chemistry: Reactions, Mechanisms, and Structure,* 7th ed.; John Wiley & Sons: New York, U.S.A., 2013.

3. Zhang, Z.; Gao, J.; Xia, J.-J.; Wang, G.-W. *Org. Biomol. Chem.* **2005,** *3,* 1617–1619. doi:10.1039/b502662h

4. Burke, S. D.; Danheiser, R. L. *Oxidizing and Reducing Agents;* John Willey & Sons: Chichester, UK, 1999.

5. Tojo, G.; Fernández, M. *Oxidation of Alcohol to Aldehyde and Ketones;* Springer: New York, U.S.A., 2006. doi:10.1007/b135954

6. Lebedev, O. A.; Kazarnovskii, S. N. T. *Khim. Tekhnol., Gorky* **1959,** *8,* 649.

7. Lebedev, O. L.; Kazarnovskii, S. N. T. *Zh. Obshch. Khim.* **1960,** *30,* 1631–1635.

8. Merbouh, N.; Bobbitt, J. M.; Brückner, C. *J. Org. Chem.* **2004,** *69,* 5116–5119. doi:10.1021/jo049461j

9. Beejapur, H. A.; Zhang, Q.; Hu, K.; Zhu, L.; Wang, J.; Ye, Z. *ACS Catal.* **2019,** *9,* 2777–2830. doi:10.1021/acscatal.8b05001 and references cited therein.

10. Anelli, P. L.; Biffi, C.; Montanari, F.; Quici, S. *J. Org. Chem.* **1987,** *52,* 2559–2562. doi:10.1021/jo00388a038

11. Bolm, C.; Magnus, A. S.; Hildebrand, J. P. *Org. Lett.* **2000,** *2,* 1173–1175. doi:10.1021/ol005792g

12. Dabral, S.; Wotruba, H.; Hernández, J. G.; Bolm, C. *ACS Sustainable Chem. Eng.* **2018,** *6,* 3242–3254. doi:10.1021/acssuschemeng.7b03418

13. Einhorn, J.; Einhorn, C.; Ratajczak, F.; Pierre, J.-L. *J. Org. Chem.* **1996,** *61,* 7452–7454. doi:10.1021/jo9609790

14. Jing, Y.; Daniliuc, C. G.; Studer, A. *Org. Lett.* **2014,** *16,* 4932–4935. doi:10.1021/ol5024568

15. Li, X.-Q.; Zhang, C. *Synthesis* **2009,** 1163–1169. doi:10.1055/s-0028-1087850

16. Miller, R. A.; Hoerrner, R. S. *Org. Lett.* **2003,** *5,* 285–287. doi:10.1021/ol0272444

17. Sahoo, P. K.; Bose, A.; Mal, P. *Eur. J. Org. Chem.* **2015,** 6994–6998. doi:10.1002/ejoc.201501039

18. Dabral, S.; Hernández, J. G.; Kamer, P. C. J.; Bolm, C. *ChemSusChem* **2017,** *10,* 2707–2713. doi:10.1002/cssc.201700703

19. Parmeggiani, C.; Cardona, F. *Green Chem.* **2012,** *14,* 547–564. doi:10.1039/c2gc16344f

20. Allen, S. E.; Walvoord, R. R.; Padilla-Salinas, R.; Kozlowski, M. C. *Chem. Rev.* **2013,** *113,* 6234–6458. doi:10.1021/cr300527g

21. Cao, Q.; Dornan, L. M.; Rogan, L.; Hughes, N. L.; Muldoon, M. J. *Chem. Commun.* **2014,** *50,* 4524–4543. doi:10.1039/c3cc47081d

22. Hoover, J. M.; Ryland, B. L.; Stahl, S. S. *J. Am. Chem. Soc.* **2013,** *135,* 2357–2367. doi:10.1021/ja3117203

23. Ochen, A.; Whitten, R.; Aylott, H. E.; Ruffell, K.; Williams, G. D.; Slater, F.; Roberts, A.; Evans, P.; Steves, J. E.; Sanganee, M. J. *Organometallics* **2019,** *38,* 176–184. doi:10.1021/acs.organomet.8b00546

24. Stahl, S. S.; Alsters, P. L., Eds. *Liquid Phase Aerobic Oxidation Catalysis: Industrial Applications and Academic Perspectives;* Wiley-VCH Verlag GmbH: Weinheim, Germany, 2016. doi:10.1002/9783527690121

25. Wang, L.; Shang, S.; Li, G.; Ren, L.; Lv, Y.; Gao, S. *J. Org. Chem.* **2016,** *81,* 2189–2193. doi:10.1021/acs.joc.6b00009

26. https://www.fda.gov/cosmetics/guidanceregulation/lawsregulations/ucm127406.htm (accessed June 16, 2019).

27. https://www.fda.gov/downloads/Drugs/Guidances/UCM509432.pdf (accessed June 16, 2019).

28. Cravotto, G.; Calcio Gaudino, E. Oxidation and Reduction by Solid Oxidants and Reducing Agents using Ball-Milling. In *Ball Milling Towards Green Synthesis: Applications, Projects, Challenges;* Ranu, B. C.; Stolle, A., Eds.; Royal Society of Chemistry: Cambridge, UK, 2015; pp 58–80. doi:10.1039/9781782621980-00058

29. Andersen, J.; Mack, J. *Green Chem.* **2018,** *20,* 1435–1443. doi:10.1039/c7gc03797j

30. Bolm, C.; Hernández, J. G. *Angew. Chem., Int. Ed.* **2019,** *58,* 3285–3299. doi:10.1002/anie.201810902

31. Do, J.-L.; Friščić, T. *ACS Cent. Sci.* **2017,** *3,* 13–19. doi:10.1021/acscentsci.6b00277

32. Užarević, K.; Ferdelji, N.; Mrla, T.; Julien, P. A.; Halasz, B.; Friščić, T.; Halasz, I. *Chem. Sci.* **2018,** *9,* 2525–2532. doi:10.1039/c7sc05312f

33. Margetić, D.; Štrukil, V. *Practical Considerations in Mechanochemical Organic Synthesis;* Mechanochemical Organic Synthesis; Elsevier: Amsterdam, Netherlands, 2016; pp 1–54. doi:10.1016/b978-0-12-802184-2.00001-7

34. Michalchuk, A. A. L.; Tumanov, I. A.; Boldyreva, E. V. *CrystEngComm* **2019,** *21,* 2174–2179. doi:10.1039/c8ce02109k

35. Piras, C. C.; Fernández-Prieto, S.; De Borggraeve, W. M. *Nanoscale Adv.* **2019,** *1,* 937–947. doi:10.1039/c8na00238j

36. Tan, D.; García, F. *Chem. Soc. Rev.* **2019,** *48,* 2274–2292. doi:10.1039/c7cs00813a

37. Tan, D.; Loots, L.; Friščić, T. *Chem. Commun.* **2016,** *52,* 7760–7781. doi:10.1039/c6cc02015a

38. Mack, J.; Fulmer, D.; Stofel, S.; Santos, N. *Green Chem.* **2007,** *9,* 1041–1043. doi:10.1039/b706167f

39. Li, A. Y.; Segalla, A.; Li, C.-J.; Moores, A.
    ACS Sustainable Chem. Eng. **2017,** *5,* 11752–11760.
    doi:10.1021/acssuschemeng.7b03298
40. Andersen, J.; Brunemann, J.; Mack, J. *React. Chem. Eng.* **2019,** *4,*
    1229–1236. doi:10.1039/c9re00027e
41. Colacino, E.; Porcheddu, A.; Charnay, C.; Delogu, F.
    React. Chem. Eng. **2019,** *4,* 1179–1188. doi:10.1039/c9re00069k
42. Colacino, E.; Carta, M.; Pia, G.; Porcheddu, A.; Ricci, P. C.; Delogu, F.
    ACS Omega **2018,** *3,* 9196–9209. doi:10.1021/acsomega.8b01431
43. Colacino, E.; Porcheddu, A.; Halasz, I.; Charnay, C.; Delogu, F.;
    Guerra, R.; Fullenwarth, J. *Green Chem.* **2018,** *20,* 2973–2977.
    doi:10.1039/c8gc01345d
44. Porcheddu, A.; Delogu, F.; De Luca, L.; Colacino, E.
    ACS Sustainable Chem. Eng. **2019,** *7,* 12044–12051.
    doi:10.1021/acssuschemeng.sc2019007099
45. De Luca, L.; Giacomelli, G.; Porcheddu, A. *Org. Lett.* **2001,** *3,*
    3041–3043. doi:10.1021/ol016501m
46. Gaspa, S.; Porcheddu, A.; Valentoni, A.; Garroni, S.; Enzo, S.;
    De Luca, L. *Eur. J. Org. Chem.* **2017,** 5519–5526.
    doi:10.1002/ejoc.201700689
47. Martina, K.; Rotolo, L.; Porcheddu, A.; Delogu, F.; Bysouth, S. R.;
    Cravotto, G.; Colacino, E. *Chem. Commun.* **2018,** *54,* 551–554.
    doi:10.1039/c7cc07758k
48. Mocci, R.; Luca, L. D.; Delogu, F.; Porcheddu, A. *Adv. Synth. Catal.*
    2016, *358,* 3135–3144. doi:10.1002/adsc.201600350
49. Porcheddu, A.; Colacino, E.; Cravotto, G.; Delogu, F.; De Luca, L.
    Beilstein J. Org. Chem. **2017,** *13,* 2049–2055. doi:10.3762/bjoc.13.202
50. Rightmire, N. R.; Hanusa, T. P. *Dalton Trans.* **2016,** *45,* 2352–2362.
    doi:10.1039/c5dt03866a
51. Gray, N. F. Free and Combined Chlorine. In *Microbiology of*
    Waterborne Diseases, 2nd ed.; Percival, S. L.; Yates, M. V.;
    Williams, D. W.; Chalmers, R. M.; Gray, N. F., Eds.; Academic Press,
    2014; pp 571–590. doi:10.1016/b978-0-12-415846-7.00031-7
52. de Nooy, A. E. J.; Besemer, A. C.; van Bekkum, H. *Tetrahedron* **1995,**
    51, 8023–8032. doi:10.1016/0040-4020(95)00417-7
53. Naik, N.; Braslau, R. *Tetrahedron* **1998,** *54,* 667–696.
    doi:10.1016/s0040-4020(97)10061-8
54. The over-oxidation product was mainly the corresponding carboxylic
    acid.
55. The resulting final crude reaction is a liquid, and the reaction takes
    place following an already known classical pathway for the solution
    phase.
56. In chemical methods based on solution-phase procedures, the pH
    lowering (ca. 8.6–9.5) usually accelerates the oxidation rate of this
    reaction.
57. Sheldon, R. A.; Arends, I. W. C. E.; ten Brink, G.-J.; Dijksman, A.
    Acc. Chem. Res. **2002,** *35,* 774–781. doi:10.1021/ar010075n
58. Konnert, L.; Gauliard, A.; Lamaty, F.; Martinez, J.; Colacino, E.
    ACS Sustainable Chem. Eng. **2013,** *1,* 1186–1191.
    doi:10.1021/sc4001115
59. Konnert, L.; Dimassi, M.; Gonnet, L.; Lamaty, F.; Martinez, J.;
    Colacino, E. *RSC Adv.* **2016,** *6,* 36978–36986.
    doi:10.1039/c6ra03222b
60. Tan, D.; Friščić, T. *Eur. J. Org. Chem.* **2018,** 18–33.
    doi:10.1002/ejoc.201700961
61. Cruz-Cabeza, A. J.; Karki, S.; Fábián, L.; Friščić, T.; Day, G. M.;
    Jones, W. *Chem. Commun.* **2010,** *46,* 2224–2226.
    doi:10.1039/b922955h
62. Friščić, T. *J. Mater. Chem.* **2010,** *20,* 7599–7605.
    doi:10.1039/c0jm00872a
63. Sodium hypochlorite pentahydrate (NaOCl·5H$_2$O, S0939) is
    commercially available from TCI chemicals.
    https://www.tcichemicals.com/eshop/en/it/catalog/list/search?searchWo
    rd=S0939&client=default_frontend&output=xml_no_dtd&proxystyleshe
    et=default_frontend&sort=date%3AD%3AL%3Ad1&oe=UTF-8&ie=UTF
    -8&ud=1&exclude_apps=1&site=en_it&mode=0 (accessed June 15,
    2019).
64. Hirashita, T.; Sugihara, Y.; Ishikawa, S.; Naito, Y.; Matsukawa, Y.;
    Araki, S. *Synlett* **2018,** *29,* 2404–2407. doi:10.1055/s-0037-1609629
65. Okada, T.; Asawa, T.; Sugiyama, Y.; Iwai, T.; Kirihara, M.; Kimura, Y.
    Tetrahedron **2016,** *72,* 2818–2827. doi:10.1016/j.tet.2016.03.064
66. Okada, T.; Asawa, T.; Sugiyama, Y.; Kirihara, M.; Iwai, T.; Kimura, Y.
    Synlett **2014,** *25,* 596–598. doi:10.1055/s-0033-1340483
67. Watanabe, A.; Miyamoto, K.; Okada, T.; Asawa, T.; Uchiyama, M.
    J. Org. Chem. **2018,** *83,* 14262–14268. doi:10.1021/acs.joc.8b02541
68. For more technical details about the Ertalyte®, see the following web
    site (Mitsubishi Chemical Advanced Materials):
    https://www.mcam.com/it/products/engineering-plastics/engineering-80
    -160-c/ertalyter-pet-p/?r=1, accessed April 6, 2019.
69. Wang, M.-L.; Huang, T.-H. *Chem. Eng. Commun.* **2007,** *194,* 618–634.
    doi:10.1080/00986440600992685

Halide metathesis in overdrive: mechanochemical synthesis of a heterometallic group 1 allyl complex

Ross F. Koby[1], Nicholas R. Rightmire[1], Nathan D. Schley[1], Timothy P. Hanusa[*1] and William W. Brennessel[2]

Abstract

As a synthesis technique, halide metathesis (n RM + M'X$_n$ → R$_n$M' + n MX) normally relies for its effectiveness on the favorable formation of a metal halide byproduct (MX), often aided by solubility equilibria in solution. Owing to the lack of significant thermodynamic driving forces, intra-alkali metal exchange is one of the most challenging metathetical exchanges to attempt, especially when conducted without solvent. Nevertheless, grinding together the bulky potassium allyl [KA']$_\infty$ (A' = [1,3-(SiMe$_3$)$_2$C$_3$H$_3$]$^-$) and CsI produces the heterometallic complex [CsKA'$_2$]$_\infty$ in low yield, which was crystallographically characterized as a coordination polymer that displays site disorder of the K$^+$ and Cs$^+$ ions. The entropic benefits of mixed Cs/K metal centers, but more importantly, the generation of multiple intermolecular K···CH$_3$ and Cs···CH$_3$ interactions in [CsKA'$_2$]$_\infty$, enable an otherwise unfavorable halide metathesis to proceed with mechanochemical assistance. From this result, we demonstrate that ball milling and unexpected solid-state effects can permit seemingly unfavored reactions to occur.

Introduction

Halide (or 'salt') metathesis is a broadly useful synthetic technique in organometallic chemistry, applicable to elements across the entire periodic table. A typical instance involves the reaction of a metal halide (M'X$_n$) with an organoalkali metal compound (RM; M = Li, Na, K) (Equation 1) [1].

$$n \text{ RM} + \text{M'X}_n \longrightarrow \text{R}_n\text{M'} + n \text{ MX} \qquad (1)$$
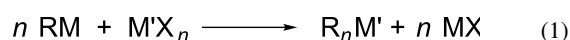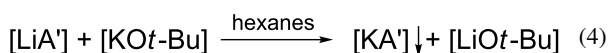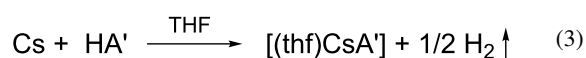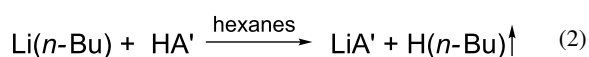
As the generation of MX normally provides a substantial portion of the energy for the exchange, M should be more electropositive than M', in order to maximize hard–soft acid–base

interactions [2]. The reaction will proceed without solvent, and mechanochemical activation, which promotes reactions through grinding or milling with no, or minimal, use of solvents, has been used in conjunction with halide metathesis to form organometallic compounds of the transition metals [3-7] and both s-[8,9] and p-block [10,11] main group elements.

The extent to which the exchange represented in Equation 1 is complete varies widely with the system. In general, the larger the value of *n*, and the correspondingly increased amount of MX that is formed, the greater the driving force. Consequently, exchange will be assisted with higher valent M'X$_n$ halides. Furthermore, although in general a solvent is not required, in solution environments the formation of products is assisted if the solubility of MX or R$_n$M' is limited, as their precipitation helps shift the equilibrium toward the product side. If ethers are used as solvents, for example, the low solubility of MX can be reduced further by choosing M to be potassium rather than lithium; as an added benefit, the resulting potassium halides are less likely to contaminate the desired product.

Without a solvent present and if M and M' are both univalent metals with similar electronegativity, complete exchange becomes difficult, and the extent of even partial exchange is hard to predict. For the alkali metals, all electronegativity scales indicate that caesium is the most electropositive, but they also indicate that there is comparatively little variation in this metric [12]. What happens when the energy difference between M'X and MX becomes particularly small? Here we describe the application of mechanochemistry in an organometallic context to examine alkali metal halide exchange unassisted by solvents. The organic group used is the bulky 1,3-bis(trimethylsilyl)allyl anion, [1,3-(SiMe$_3$)$_2$C$_3$H$_3$]$^-$ ([A']$^-$) [13,14], for which alkali metal complexes are known, including those of Li [15], Na [16], K [17,18], and Cs [18]. These have been formed via traditional solvent-based routes, by deprotonation of the substituted propene precursor with a metal alkyl or hydride (Equation 2) or with the metal itself (Equation 3) [18]. Intra-alkali metal exchange (although not specifically halide metathesis) has been conducted with the [A']$^-$ anion, but always in the presence of a solvent to help drive the process (Equation 4) [19].

$$\text{Li}(n\text{-Bu}) + \text{HA'} \xrightarrow{\text{hexanes}} \text{LiA'} + \text{H}(n\text{-Bu})\uparrow \quad (2)$$

$$\text{Cs} + \text{HA'} \xrightarrow{\text{THF}} [(\text{thf})\text{CsA'}] + 1/2\ \text{H}_2\uparrow \quad (3)$$

$$[\text{LiA'}] + [\text{KO}t\text{-Bu}] \xrightarrow{\text{hexanes}} [\text{KA'}]\downarrow + [\text{LiO}t\text{-Bu}] \quad (4)$$

Results and Discussion
Conditions for halide exchange

Apart from thermodynamic considerations, practical concerns place limits on the combinations of halides and alkali metals that could be feasibly studied in intra-alkali exchange experiments. For example, the fluorides have the largest heats of formation of the alkali halides, regardless of metal, but their high lattice energies make them typically unreactive, even under mechanochemical conditions [20]. The iodides, in contrast, have the smallest lattice energies and thus should be the most easily disrupted and liable to exchange. Although several metal compounds of the allyl anion [A']$^-$ were potential candidates for the present study, the need for a base-free, unsolvated complex that preferably had been crystallographically characterized limited the choice to the potassium complex [KA']$_\infty$. In that form [17], as well as when crystallized from THF [18], DME [21], or as described below, arenes, [KA']$_\infty$ retains the structure of an undulating or helical coordination polymer. Within these experimental parameters, the general reaction in Equation 5 was examined. When *n* = 1, a reaction carried to completion would result in full metal exchange, with partial exchange the outcome for any larger values of *n*.

$$n\ [\text{KA'}] + \text{M'I} \longrightarrow [\text{MK}_{n-1}\text{A'}_n] + \text{KI} \quad (5)$$
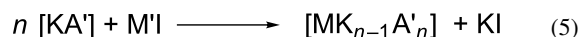
The experimental protocol involved grinding various ratios of [KA'] and alkali metal iodides, extracting the ground mixtures with hydrocarbon solvents, and then attempting crystallization of the extracts. This is necessarily an imperfect route to sampling the product space, as definitive characterization of any product(s) depended critically on the crystallizing process. In particular, NMR spectra were not expected to be highly diagnostic, as in all its group 1 complexes the resonances from the [A']$^-$ anion provide a characteristic spectrum of similar chemical shifts with singlet (-SiMe$_3$), doublet (C$_{1,3}$-H), and triplet (C$_2$-H) patterns that result from a π-bound allyl with *syn,syn*-trimethylsilyl arrangements [21].

Grinding [KA'] in a mixer or planetary mill in a 1:1 or 2:1 ratio with LiI, NaI, or RbI left the solids visibly unchanged. Only unreacted [KA'] could be extracted with toluene from the ground mixtures, and the allyl could be crystallized as its toluene solvate (see below). As a check on the consequences of halide identity, a 1:1 grind of [KA'] with LiCl was also investigated, but there was no evidence of reaction.

The grinds with CsI behaved differently from the others. A 1:1 grind for 5 min in a planetary mill left a pale orange solid that could be extracted with hexanes. When filtered and dried, the orange-brown residue displayed resonances in its ^{1}H NMR
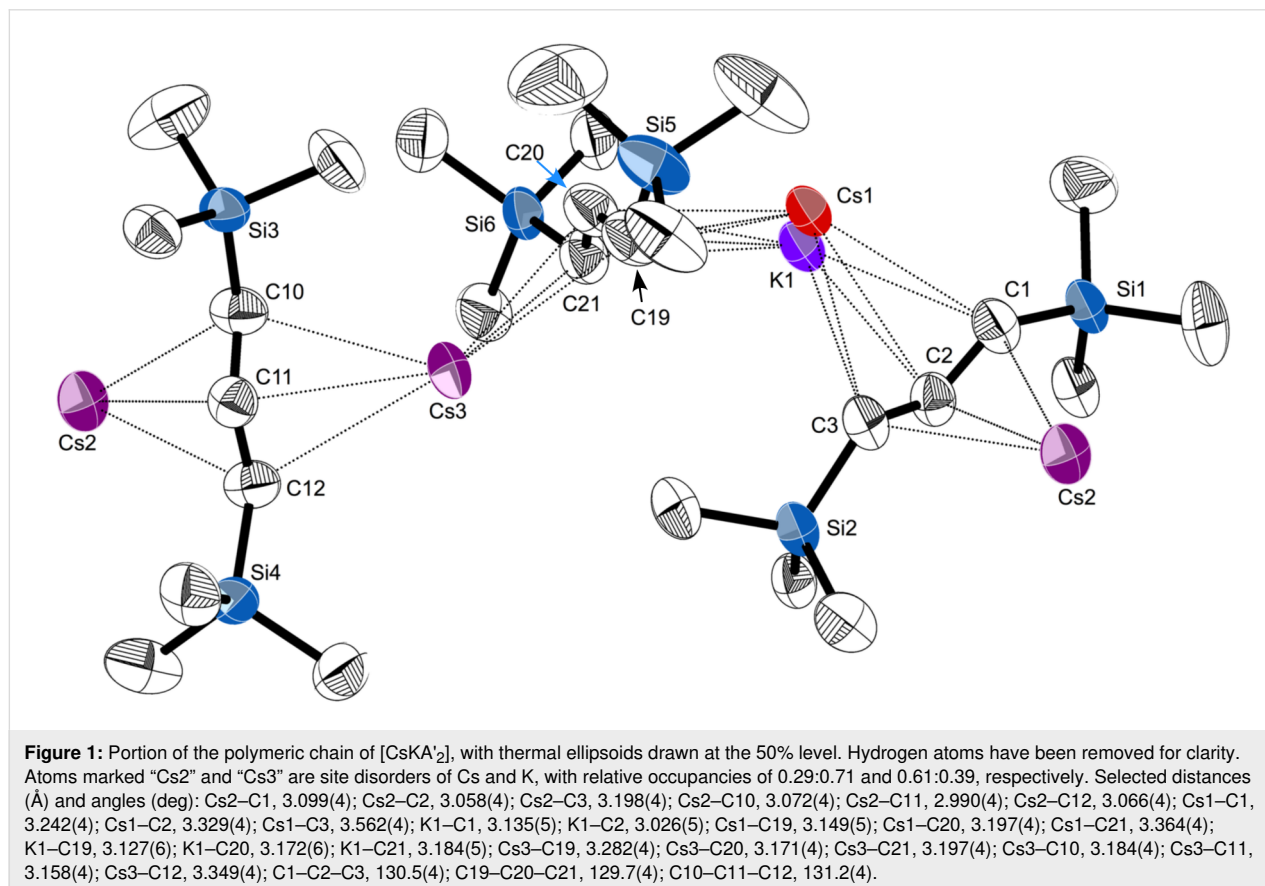
spectrum corresponding to a single type of π-bonded allyl ligand, all shifted slightly (by 0.09-0.4 ppm) from those for [KA'] [21]. The material could not be purified, and repeating the grind for 10 min did not help. After grinding a 3:1 mixture of [KA']:CsI for 15 min, however, a pale yellow-orange solid was generated that could be extracted with hexanes. After being filtered, the yellow filtrate was evaporated to yield a yellow solid in low yield. Recrystallization from hexanes produced crystals that were yellow-orange; they were highly soluble in C_6D_6, giving a bright red solution. Single crystal X-ray analysis identified the crystals as the heterometallic complex [KCsA'$_2$] (see below). The ^{1}H NMR spectrum of the products from the 1:1 and 3:1 grinds were identical. It should be noted that both [KA'] and CsI are insoluble in hexanes, and the grinding clearly initiated a reaction that occurred before the first hexanes extraction.
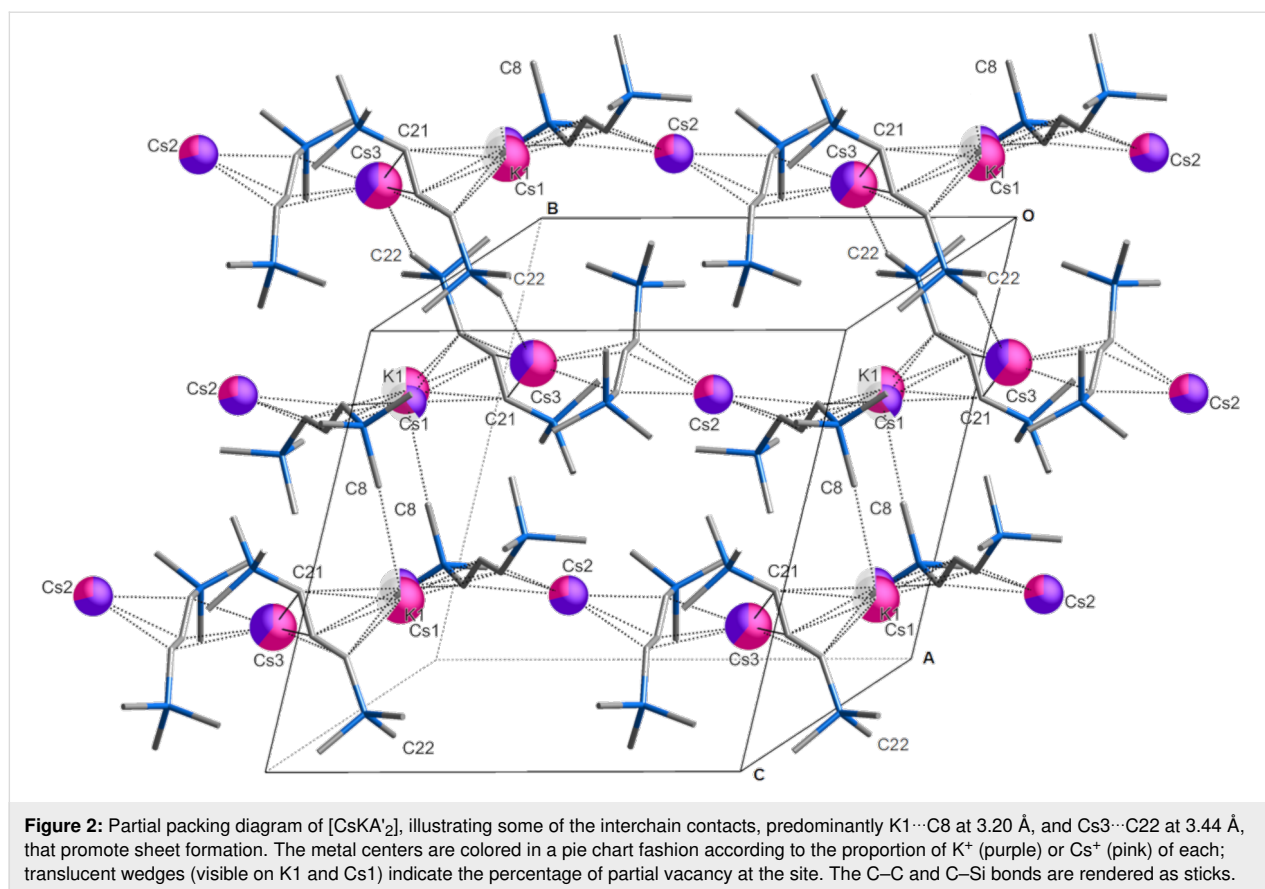
Structure of [CsKA'$_2$]

Small blocks grown from hexanes were identified from a single crystal X-ray study as the coordination polymer [CsKA'$_2$]$_∞$. A depiction of a single chain is provided in Figure 1, and a partial packing diagram is given in Figure 2. The asymmetric unit contains three alkali metal cations and three substituted allyl anions, all in general positions. Each of the three metal sites is modeled as a site disorder of atoms types K and Cs. Two distinct peaks were found in the difference Fourier map for the site containing atoms Cs1 and K1, and their positions were refined freely, but their anisotropic displacement parameters were constrained to be equivalent. For the other two site disorders (atom pairs Cs2/K2 and Cs3/K3), the atoms were constrained to be isopositional and their anisotropic displacement parameters were constrained to be equivalent. The ratios of Cs to K in the three sites refined to 0.60:0.40, 0.29:0.71, and 0.61:0.39 for atom pairs Cs1/K1, Cs2/K2, and Cs3/K3, respectively.

Although the metal–C(allyl) distances span a large range, they do so in a way that reflects the proportion of Cs and K in the metal to which they are bonded. For example, the average distance of Cs2 (0.29 Cs:0.71 K) to the allyl carbons C10–C12 is 3.04 Å. The same allyl is also bonded to Cs3, with a higher percentage of Cs (0.61 Cs:0.39 K), and the average M–C distance is correspondingly longer, at 3.22 Å. It is possible to extract consistent values from the M–C distances that can be assigned to the proportion of K and Cs, namely 2.95 Å and 3.40 Å, respectively (i.e., a hypothetical site that is 0.50 (K):0.50 (Cs) would be expected to exhibit an average M–C(allyl) bond distance of roughly 3.17 Å). These values do not recreate dis-

Figure 1: Portion of the polymeric chain of [CsKA'$_2$], with thermal ellipsoids drawn at the 50% level. Hydrogen atoms have been removed for clarity. Atoms marked "Cs2" and "Cs3" are site disorders of Cs and K, with relative occupancies of 0.29:0.71 and 0.61:0.39, respectively. Selected distances (Å) and angles (deg): Cs2–C1, 3.099(4); Cs2–C2, 3.058(4); Cs2–C3, 3.198(4); Cs2–C10, 3.072(4); Cs2–C11, 2.990(4); Cs2–C12, 3.066(4); Cs1–C1, 3.242(4); Cs1–C2, 3.329(4); Cs1–C3, 3.562(4); K1–C1, 3.135(5); K1–C2, 3.026(4); Cs1–C19, 3.149(5); Cs1–C20, 3.197(4); Cs1–C21, 3.364(4); K1–C19, 3.127(6); K1–C20, 3.172(6); K1–C21, 3.184(5); Cs3–C19, 3.282(4); Cs3–C20, 3.171(4); Cs3–C21, 3.197(4); Cs3–C10, 3.184(4); Cs3–C11, 3.158(4); Cs3–C12, 3.349(4); C1–C2–C3, 130.5(4); C19–C20–C21, 129.7(4); C10–C11–C12, 131.2(4).

Figure 2: Partial packing diagram of [CsKA'$_2$], illustrating some of the interchain contacts, predominantly K1···C8 at 3.20 Å, and Cs3···C22 at 3.44 Å, that promote sheet formation. The metal centers are colored in a pie chart fashion according to the proportion of K$^+$ (purple) or Cs$^+$ (pink) of each; translucent wedges (visible on K1 and Cs1) indicate the percentage of partial vacancy at the site. The C–C and C–Si bonds are rendered as sticks.

tances in the homometallic complexes exactly (i.e., the average K–C distance in [KA']$_\infty$ is 3.01 Å) [17], but they reflect the relative sizes of the K$^+$ and Cs$^+$ cations.

The structure is polymeric in two dimensions in the crystallographic *bc* plane; interchain K···CH$_3$ and Cs···CH$_3$ contacts are responsible for generating the 2D arrangement (Figure 2); this is discussed in more detail below.

Structure of [(C$_6$H$_6$)KA']$_\infty$

From all the grinds of [KA'] with the alkali metal iodides (excepting CsI), the potassium allyl was the only recoverable material; extracted with toluene, it crystallized from solution as the solvate. A single crystal X-ray study analysis reveals bent polymeric chains of alternating K$^+$ cations and [A']$^-$ anions. Each potassium is capped with a toluene molecule, bonded through cation–π interactions. The structure suffers from twinning, disorder in the toluene, and weak diffraction, and therefore its structural details are degraded (a depiction of the coordination polymer is available in Supporting Information File 1). Fortunately, when [KA'] is dissolved in benzene and the solution evaporated, an analogous solvate is obtained, and the resulting crystals are of higher quality than those from toluene. Single crystal X-ray analysis reveals that it has a structure that

is qualitatively the same as the toluene solvate, and only the benzene solvate is discussed here.

Like the unsolvated complex [KA']$_\infty$ [17] and the related DME and THF solvates [K(dme)A']$_\infty$ [21] and [K(thf)$_{3/2}$A']$_\infty$ [18], respectively, [(C$_6$H$_6$)KA']$_\infty$ is a coordination polymer with potassium ions linked by bridging π-allyl ligands. The polymer takes the form of bent chains running parallel to the *b* axis (Figure 3). There is only one crystallographically distinct potassium ion in the chains, and a single K···K'···K bending angle of 134.0°. This is different from the pattern found in [K(thf)$_{3/2}$A']$_\infty$, for example, (i.e., roughly linear K(1)···K(2)···K(1)' sections (170.2°) alternating with strongly bent K(2)···K(1)···K(2)' angles (103.3°)). The K–C$_6$H$_6$ ring centroid distance is 2.99 Å, which is typical for K$^+$···(arene) cation–π interactions [22,23]. The enthalpy of binding (Δ*H*°) of an isolated K···(benzene or toluene) unit is almost 80 kJ mol^{-1} (see calculated value in Table 1, entry 5); the energy is reduced by about 40% when the ring is bound to the neutral [KA'] fragment (entry 6).

In structurally characterized polymeric [L$_n$KA']$_\infty$ complexes, the average K–C(allyl) distances span a comparatively narrow range, regardless of coordinated ligands and the change in formal coordination number of the K$^+$ cation: i.e., 3.01 Å in
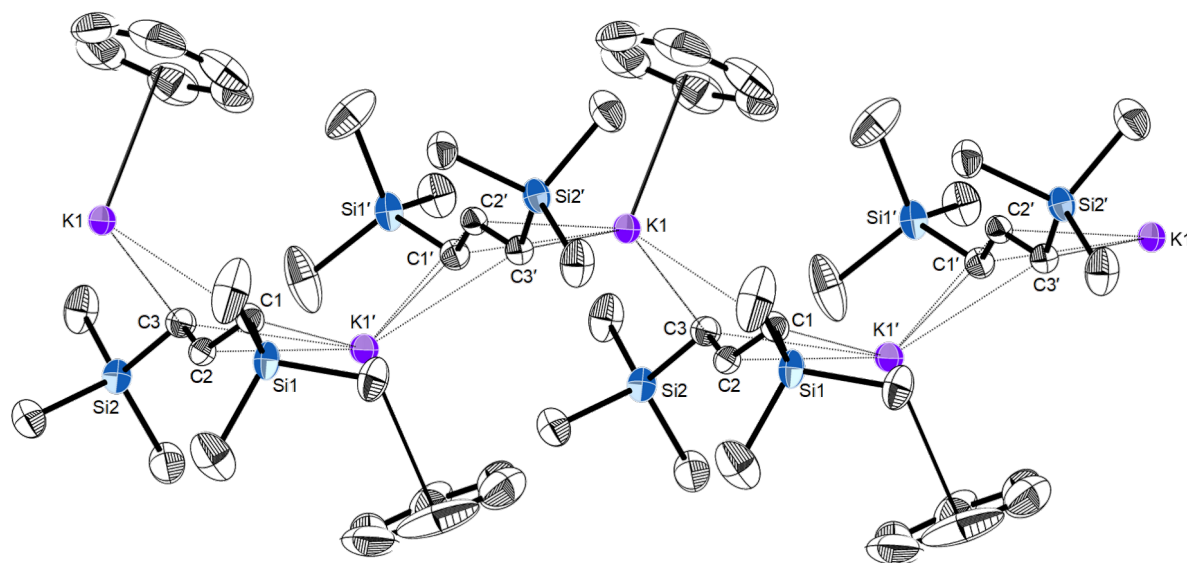
Figure 3: Portion of the polymeric chain of [(C₆H₆)KA']∞, with thermal ellipsoids drawn at the 50% level. Hydrogen atoms have been removed for clarity. Selected distances (Å) and angles (deg): K1–C1, 3.005(3); K1–C2, 2.963(3); K3–C3, 3.128(3); K1–C1', 2.959(3); K1–C2', 2.983(2); K3–C3', 3.140(3); K1⋯(C₆H₆ centroid), 2.99(1); K1⋯K1', 5.39; C1–C2–C3, 130.8(3); K1⋯K1'⋯K1, 134.0.

Table 1: Energies of reaction (B3PW91-D3BJ, kJ mol⁻¹).

Entry	Reaction[a]	Energy ($\Delta H°$, $\Delta G°$)
1	$K^+ + [C_3H_5]^- \rightarrow [K(C_3H_5)]$	−514.6, −481.5
2	$Cs^+ + [C_3H_5]^- \rightarrow [Cs(C_3H_5)]$	−484.9, −452.2
3	$K^+ + [A']^- \rightarrow [KA']$	−458.4, −426.5
4	$Cs^+ + [A']^- \rightarrow [CsA']$	−430.4, −398.1
5	$K^+ + toluene \rightarrow [(toluene)K]^+$	−78.9, −48.6
6	$[KA'] + toluene \rightarrow [(toluene)KA']$	−48.1, −13.1

[a]For entries 1–4, the def2-TZVPD basis set was used on all atoms. For entries 5 and 6, the def2-TZVP basis set was used on all atoms.

[KA']∞, 3.03 Å in [KA'(thf)₃/₂]∞ and [(C₆H₆)KA']∞ (3.04 Å in the poorer quality [(toluene)KA']∞ structure), and 3.06 Å in [KA'(dme)]∞ [24]. This suggests that the K⁺⋯[A'] interaction is a robust one, and its structure potentially capable of serving as a kind of template for inclusion (see below).

Formation of the heterometallic allyl complex

The net reaction that produced the clearest evidence for mechanochemically promoted alkali metal exchange is given by Equation 5 with *n* = 2 (i.e., Equation 6). Several features of it are noteworthy.

$$2[KA'] + CsI \xrightarrow{\text{⊗⊗}} [CsKA'_2] + KI \qquad (6)$$
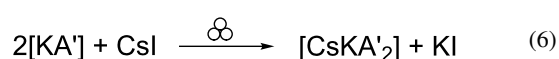
The ratio of [KA'] to CsI that yielded [CsKA'₂] was produced both from a 1:1 and a 3:1 ratio of [KA'] to CsI, and the predicted result from Equation 5, assuming complete reaction, would have been either pure [CsA'] or the heterometallic [CsK₂A'₃]. That neither of these outcomes was observed, and a non-stoichiometric product was obtained is actually not uncommon in mechanochemical synthesis, and can reflect the fact that products often do not have time to equilibrate or go from metastable to more stable products [9,11]. There can be multiple reasons for this, starting with the high energy environment of grinding that may be far from equilibrium [25], allowing the kinetic products to be the ones most likely to be isolated. The high concentration of reagents in a solid-state reaction may influence product formation as well. The possibility of partial exchange also needs to be considered. If the caesium iodide were insufficiently reactive, a starting ratio of 3:1 for [KA']:CsI could give rise to products with higher ratios of K to Cs than even [CsK₂A'₃], such as [CsK₃A'₄] or [CsK₄A'₅]. In this light, it is notable that CsI is the limiting reagent in the reaction, and the resulting 1:1 ratio of the metals in the allyl complex suggests that it is a favored composition.

Secondly, the relative free energies of formation of CsI and KI (−341 and −325 kJ mol⁻¹, respectively; $\Delta\Delta G$ = +16 kJ mol⁻¹) [26] means that the formation of the metal halide byproduct (KI) is non-spontaneous, and does not contribute to the driving force for the reaction. The relative free energies of the allyl complexes then must provide the difference. There are no experimental values available for the thermodynamic quantities

involving potassium and caesium allyls, however, although it would be expected that the smaller K^+ ion would interact more strongly with the allyl anion than would the larger, softer Cs^+ ion.

To explore this and several related points more quantitatively, various features of the K/Cs/[allyl]$^-$ system were modeled with DFT calculations, using the B3PW91 hybrid functional [27,28] with Grimme's -D3 dispersion corrections (GD3BJ) [29]. A calculation on the simple model systems $[K(C_3H_5)]$ and $[Cs(C_3H_5)]$ indicates that, consistent with the above rationale, $\Delta G°_f$ for the potassium complex is more negative than for the caesium complex (by 29.3 kJ mol^{-1}; Table 1, entries 1 and 2). The slightly greater realism provided by comparing the [KA'] and [CsA'] complexes does not meaningfully affect the difference (28.4 kJ mol^{-1}; Table 1, entries 3 and 4). Of course, these are calculations on isolated monomers, and the energetics of formation of the solid-state polymeric forms [30] would be expected to change these values, but not necessarily in a way that would clearly favor the formation of [CsA'] over [KA']. If so, there would consequently be no thermodynamic driving force for the metathesis reaction.

There are several ways that this simple analysis underestimates the energetics involved in the system. For example, full metal exchange does not occur, and the resulting heterometallic allyl complex has additional entropy provided by the two metal ions and the site disorder in the solid. Using a standard formula for the entropy of mixing two species (configurational entropy, $\Delta S_{mix} = -nR(X_A \ln X_A + X_B \ln X_B)$ [31], and with 3 atoms distributed randomly over the three crystallographically identified metal sites, the value of $\Delta S = +17$ J mol^{-1} K^{-1} is obtained. At 298 K, the $-T\Delta S$ value is -5.1 kJ mol^{-1}. As imperfect as this approximation is (e.g., the distribution of metal ions is not completely random, and the coordination environments are not exactly the same), it does suggest one source of driving force not present in the homometallic allyls.

A potentially much more important source of stability in [CsKA'$_2$] is the existence of multiple intermolecular M···CH$_3$ interactions, including Cs···CH$_3$ contacts, obviously energeti-

cally significant enough that they support the formation of two-dimensional sheets in the solid state. To appreciate the magnitude of this effect, the relative conformation of the known [L$_n$KA'] complexes are summarized by their (non-bonded) K···K'···K angles (Table 2).

Although the K···K'···K angles are only markers (there are no direct K···K' interactions in any of the complexes), it is notable that both [KA']$_\infty$ and [CsKA'$_2$] display three such angles, two of which are relatively similar at ca. 135–140°, and a third that is substantially more bent (<120°) (see the Supporting Information File 1, Figure S2, for a visualization of the similarity). The significance of this is that [KA'] can be viewed as a template into which Cs$^+$ are infused during the grinding. There are adjustments in M–C(allyl) bond distances (see above), but another consequence is the generation of multiple intermolecular M···CH$_3$ interactions. Both [KA'] and [CsKA'$_2$] possess K···CH$_3$ contacts at typical distances [32]; in [KA'], the two closest are both at 3.23 Å; the third is at 3.35 Å. In [CsKA'$_2$], the closest is at 3.20 Å, with the second at 3.38 Å.

The Cs···CH$_3$ interactions in [CsKA'$_2$], however, are especially noteworthy. The closest is at 3.44 Å (Cs3···C22), followed by four more at 3.56 Å, and farther ones at 3.67 and 3.74 Å. All these distances are substantially shorter than the sum of the van der Waal's radii of Cs (3.43 Å) and CH$_3$ (2.00 Å). Intermolecular Cs···CH$_3$ distances of ca. 3.6 Å and longer are not especially rare, and are strong enough to influence solid state structures. In the dme adduct of caesium [2,4,6-tri(*tert*-butyl)phenolate], for example, a Cs···CH$_3$ contact of 3.596(5) Å contributes to its form as a 1D coordination polymer [33]. In the caesium salt of the gallium metallate [Cs(toluene)$_2${CN(GaMe$_3$)$_2$}], multiple Cs···CH$_3$ interactions in the range from 3.54–3.64 Å help generate its three-dimensional network structure [34]. Intermolecular Cs···CH$_3$ distances below 3.5 Å, however, do not appear to have been previously reported [35]. The shortest distance in [CsKA'$_2$], at 3.44 Å, is 2.0 Å less than the sum of the appropriate van der Waal's radii (although less precisely located, the corresponding Cs···H distance (Cs3···H22B) is 3.05 Å, a third less than the sum of the van der Waal's radii (4.63 Å).

Table 2: Non-bonded intrachain K···K'···K angles in [L$_n$KA'] complexes.

Complex	K···K'···K (deg)	Reference
[KA']$_\infty$	135.1; 135.7; 118.2	[17]
[K(dme)A']$_\infty$	153.3, 141.9	[21]
[K(dme)A']$_\infty$	170.0, 103.3	[18]
[(C$_6$H$_6$)KA']$_\infty$	134.0	this work
[KCsA'$_2$]$_\infty$	140.3 (K1–Cs2–Cs3); 141.0 (K1–Cs3–Cs2); 107.3 (Cs2–K1–Cs3)	this work

Calculations on the model systems $[(CH_4)(K,Cs)A']$ and $[(HMe_2SiMe)(K,Cs)A']$ were used to place the energy of the M···methyl interactions in context (views of the optimized pairs are available in the Supporting Information File 1, Figure S3). Despite the gas-phase environment of the calculations, the distance between K^+ and CH_4 is 3.22 Å, a typical value for potassium–methyl interactions in the solid state, as is the $\Delta H°$ of almost 12 kJ mol^{-1}, in the range of hydrogen bonds (Table 3, entries 1 and 2) [32]. The distance of K^+ to Me_3SiH, chosen to represent somewhat more accurately the type of interactions occurring in $[KCsA'_2]$, is slightly shorter (3.14 Å) and stronger (30 kJ mol^{-1}), probably a result of the lower electronegativity of silicon compared to carbon and the correspondingly more negative methyl groups. The analogous calculations with Cs^+ (Table 3, entries 3 and 4) place the contact distance at 3.62 Å and 3.53 Å for CH_4 and Me_3SiH, respectively, with corresponding enthalpies of −3.9 and −23.6 kJ mol^{-1}. These distances are similar to those found in the solid state, and together with the potassium interactions, evidently help to drive the heterometallic complex formation.

Table 3: Energies of reaction (B3PW91-D3BJ, kJ mol^{-1})

Entry	Reaction[a]	Energy
1	$[KA'] + [CH_4] \rightarrow [(CH_4)']$	−11.9 ($\Delta H°$)
2	$[KA'] + HSiMe_3 \rightarrow [(HSiMe_3)KA']$	−30.0 ($\Delta H°$)
3	$[CsA'] + CH_4 \rightarrow [(CH_4)CsA']$	−3.9 ($\Delta H°$)
4	$[CsA'] + HSiMe_3 \rightarrow [(HSiMe_3)CsA']$	−23.6 ($\Delta H°$)

[a]The def2-TZVP basis set was used on all atoms.

Conclusion

Formally, halide metathesis as a synthetic technique depends strongly on the relative thermodynamic stabilities of the starting and final metal halide salts, M'X and MX. Practically, however, the reaction solvent is also a critical assistant in the process, as the insolubility of the MX product can strongly shift the position of equilibrium and drive the reaction. Mechanochemical techniques can be used to provide a driving force for a reaction that would be energetically unfavorable and has no solvent assistance. The formation of the heterometallic $[CsKA'_2]$ from the mixture of $[KA']$ and CsI, even though in low yield, owes its realization to the entropic benefit of a mixed metal system, but even more importantly to the formation of intermolecular M···CH_3 contacts, permitting the formation and stabilization of a sheet structure that ties the coordination polymer chains of M···A' units together. Recognition of this additional source of reaction energy has the potential to extend the usefulness of halide metathesis to systems previously considered too unpromising to explore.

Supporting Information

Crystallographic data for the structures reported in this paper have been deposited with the Cambridge Crystallographic Data Centre as CCDC 1897690 ($[KCsA'_2]$), 1897691 ($[(C_6H_6)KA']$), and 1897692 ($[(toluene)KA']$). Copies of the data can be obtained free of charge on application to CCDC, 12 Union Road, Cambridge CB2 1EZ, UK (fax: (+44)1223-336-033; email: deposit@ccdc.cam.ac.uk).

Supporting Information File 1
Experimental and computational details; crystal data and summary of X–ray data collection.
[https://www.beilstein-journals.org/bjoc/content/supplementary/1860-5397-15-181-S1.pdf]

Supporting Information File 2
Coordinates of DFT-optimized structures.
[https://www.beilstein-journals.org/bjoc/content/supplementary/1860-5397-15-181-S2.xyz]

ORCID® iDs

Ross F. Koby - https://orcid.org/0000-0001-5394-1160
Timothy P. Hanusa - https://orcid.org/0000-0002-7935-5968

References

1. Elschenbroich, C. *Organometallics,* 3rd ed.; VCH Publishers: Weinheim, 2006; p 28.
2. Pearson, R. G. *Hard and Soft Acids and Bases;* Dowden, Hutchinson & Ross: Stroudsburg, PA, 1973.
3. Borisov, A. P.; Makhaev, V. D.; Usyatinskii, A. Y.; Bregadze, V. I. *Izv. Akad. Nauk, Ser. Khim.* **1993,** 1715–1717.
4. Gomes, C. S. B.; Gomes, P. T.; Duarte, M. T. *J. Organomet. Chem.* **2014,** *760,* 101–107. doi:10.1016/j.jorganchem.2013.11.040
5. Makhaev, V. D.; Borisov, A. P.; Petrova, L. A. *J. Organomet. Chem.* **1999,** *590,* 222–226. doi:10.1016/s0022-328x(99)00460-x
6. Boyde, N. C.; Rightmire, N. R.; Bierschenk, E. J.; Steelman, G. W.; Hanusa, T. P.; Brennessel, W. W. *Dalton Trans.* **2016,** *45,* 18635–18642. doi:10.1039/c6dt03199d
7. Boyde, N. C.; Steelman, G. W.; Hanusa, T. P. *ACS Omega* **2018,** *3,* 8149–8159. doi:10.1021/acsomega.8b00943
8. Peters, D. W.; Blair, R. G. *Faraday Discuss.* **2014,** *170,* 83–91. doi:10.1039/c3fd00157a
9. Boyde, N.; Rightmire, N.; Hanusa, T.; Brennessel, W. *Inorganics* **2017,** *5,* 36. doi:10.3390/inorganics5020036

10. Rightmire, N. R.; Hanusa, T. P.; Rheingold, A. L. *Organometallics* **2014,** *33,* 5952–5955. doi:10.1021/om5009204

11. Koby, R. F.; Hanusa, T. P.; Schley, N. D. *J. Am. Chem. Soc.* **2018,** *140,* 15934–15942. doi:10.1021/jacs.8b09862

12. Allred, A. L.; Rochow, E. G. *J. Inorg. Nucl. Chem.* **1958,** *5,* 264–268. doi:10.1016/0022-1902(58)80003-2
    The Allred-Rochow electronegativities of the alkali metals, for example, vary only over a range of 0.86–1.01.

13. Chmely, S. C.; Hanusa, T. P. *Eur. J. Inorg. Chem.* **2010,** 1321–1337. doi:10.1002/ejic.200900813

14. Solomon, S. A.; Layfield, R. A. *Dalton Trans.* **2010,** *39,* 2469–2483. doi:10.1039/b918619k

15. Boche, G.; Fraenkel, G.; Cabral, J.; Harms, K.; Van Eikema Hommes, N. J. R.; Lohrenz, J.; Marsch, M.; Schleyer, P. v. R. *J. Am. Chem. Soc.* **1992,** *114,* 1562–1565. doi:10.1021/ja00031a004

16. McMillen, C. H.; Gren, C. K.; Hanusa, T. P.; Rheingold, A. L. *Inorg. Chim. Acta* **2010,** *364,* 61–68. doi:10.1016/j.ica.2010.07.079

17. Gren, C. K.; Hanusa, T. P.; Rheingold, A. L. *Main Group Chem.* **2009,** *8,* 225–235. doi:10.1080/10241220903065235

18. Quisenberry, K. T.; Gren, C. K.; White, R. E.; Hanusa, T. P.; Brennessel, W. W. *Organometallics* **2007,** *26,* 4354–4356. doi:10.1021/om700410a

19. Harvey, M. J.; Hanusa, T. P.; Young, Jr., V. G. *Angew. Chem., Int. Ed.* **1999,** *38,* 217–219. doi:10.1002/(sici)1521-3773(19990115)38:1/2<217::aid-anie217>3.3.co;2-h

20. Speight, I. R.; Chmely, S. C.; Hanusa, T. P.; Rheingold, A. L. *Chem. Commun.* **2019,** *55,* 2202–2205. doi:10.1039/c8cc10155h
    Alkali metal fluorides can be useful as reagents if the thermodynamics of the system are appropriately configured, however. For example, the reaction of [LiN(SiMe$_3$)$_2$] with CsF works to produce the products [CsN(SiMe$_3$)$_2$] with LiF in high yield because the relative heats of formation ($\Delta H°_f$) of CsF and LiF (−554 and −616 kJ mol^{-1}, respectively) provide a net driving force of −62 kJ mol^{-1}. See: Ojeda-Amador, A. I.; Martínez-Martínez, A. J.; Kennedy, A. R.; O'Hara, C. T. *Inorg. Chem.* **2016,** *55,* 5719–5728. doi:10.1021/acs.inorgchem.6b00839

21. Simpson, C. K.; White, R. E.; Carlson, C. N.; Wrobleski, D. A.; Kuehl, C. J.; Croce, T. A.; Steele, I. M.; Scott, B. L.; Young,, V. G.; Hanusa, T. P.; Sattelberger, A. P.; John, K. D. *Organometallics* **2005,** *24,* 3685–3691. doi:10.1021/om050098w

22. Ma, J. C.; Dougherty, D. A. *Chem. Rev.* **1997,** *97,* 1303–1324. doi:10.1021/cr9603744

23. Ojeda-Amador, A. I.; Martínez-Martínez, A. J.; Robertson, G. M.; Robertson, S. D.; Kennedy, A. R.; O'Hara, C. T. *Dalton Trans.* **2017,** *46,* 6392–6403. doi:10.1039/c7dt01118k

24. Solomon, S. A.; Muryn, C. A.; Layfield, R. A. *Chem. Commun.* **2008,** 3142–3144. doi:10.1039/b803364a

25. Shi, Y. X.; Xu, K.; Clegg, J. K.; Ganguly, R.; Hirao, H.; Friščić, T.; García, F. *Angew. Chem., Int. Ed.* **2016,** *55,* 12736–12740. doi:10.1002/anie.201605936

26. Wagman, D. D.; Evans, W. H.; Parker, V. B.; Schumm, R. H.; Halow, I. *The NBS Tables of Chemical Thermodynamic Properties;* American Chemical Society and the American Institute of Physics for the National Bureau of Standards, 1982; p 392.

27. Becke, A. D. *Phys. Rev. A* **1988,** *38,* 3098–3100. doi:10.1103/physreva.38.3098

28. Perdew, J. P.; Wang, Y. *Phys. Rev. B* **1992,** *45,* 13244–13249. doi:10.1103/physrevb.45.13244

29. Grimme, S.; Antony, J.; Ehrlich, S.; Krieg, H. *J. Chem. Phys.* **2010,** *132,* 154104. doi:10.1063/1.3382344

30. The structure of unsolvated [CsAʹ] is unknown, but it is presumed to be a coordination polymer, in the manner of its THF-solvate, [(thf)CsAʹ]$_∞$. See ref. [18].

31. Garcés, J. *Appl. Phys. Lett.* **2010,** *96,* 161904. doi:10.1063/1.3400221

32. Kleeberg, C.; Grunenberg, J.; Xie, X. *Inorg. Chem.* **2014,** *53,* 4400–4410. doi:10.1021/ic500065s

33. Westerhausen, M.; Oßberger, M. W.; Alexander, J. S.; Ruhlandt-Senge, K. *Z. Anorg. Allg. Chem.* **2005,** *631,* 2836–2841. doi:10.1002/zaac.200500165

34. Kopp, M. R.; Neumüller, B. *Z. Anorg. Allg. Chem.* **1998,** *624,* 1642–1646. doi:10.1002/(sici)1521-3749(199810)624:10<1642::aid-zaac1642>3.0.co;2-y

35. *Cambridge Structural Database;* 2018. Release Nov. 2018.

License and Terms